



## UvA-DARE (Digital Academic Repository)

### Oncogenic signaling and mechanisms of immune evasion in aggressive B-cell lymphomas

Minderman, M.

**Publication date**

2024

**Document Version**

Final published version

[Link to publication](#)

**Citation for published version (APA):**

Minderman, M. (2024). *Oncogenic signaling and mechanisms of immune evasion in aggressive B-cell lymphomas*. [Thesis, fully internal, Universiteit van Amsterdam].

**General rights**

It is not permitted to download or to forward/distribute the text or part of it without the consent of the author(s) and/or copyright holder(s), other than for strictly personal, individual use, unless the work is under an open content license (like Creative Commons).

**Disclaimer/Complaints regulations**

If you believe that digital publication of certain material infringes any of your rights or (privacy) interests, please let the Library know, stating your reasons. In case of a legitimate complaint, the Library will make the material inaccessible and/or remove it from the website. Please Ask the Library: <https://uba.uva.nl/en/contact>, or a letter to: Library of the University of Amsterdam, Secretariat, Singel 425, 1012 WP Amsterdam, The Netherlands. You will be contacted as soon as possible.

**ONCOGENIC SIGNALING AND  
MECHANISMS OF IMMUNE  
EVASION IN AGGRESSIVE  
B-CELL LYMPHOMAS**

Marthe Minderman

**ONCOGENIC SIGNALING AND MECHANISMS OF IMMUNE  
EVASION IN AGGRESSIVE B-CELL LYMPHOMAS**

Marthe Minderman

**ONCOGENIC SIGNALING AND  
MECHANISMS OF IMMUNE EVASION IN  
AGGRESSIVE B-CELL LYMPHOMAS**

Marthe Minderman

Cover image: Marielle van de Wiel  
Cover: Ilse Modder ([www.ilsemodder.nl](http://www.ilsemodder.nl))  
Layout: Ilse Modder ([www.ilsemodder.nl](http://www.ilsemodder.nl))  
Printed by: Gildeprint Enschede ([www.gildeprint.nl](http://www.gildeprint.nl))

This work was financially supported by the Lymph&Co foundation.

ISBN: 978-94-6496-095-2

Copyright © 2024 M. Minderman. All rights are reserved. No part of this book may be reproduced, distributed, stored in a retrieval system, or transmitted in any form or by any means, without written permission of the author. The copyright of the publications remains with the publishers.

# Oncogenic signaling and mechanisms of immune evasion in aggressive B-cell lymphomas

## ACADEMISCH PROEFSCHRIFT

ter verkrijging van de graad van doctor  
aan de Universiteit van Amsterdam  
op gezag van de Rector Magnificus  
prof. dr. ir. P.P.C.C. Verbeek  
ten overstaan van een door het College voor Promoties ingestelde commissie,  
in het openbaar te verdedigen in de Agnietenkapel  
op donderdag 16 mei 2024, te 10.00 uur

door

**Marthe Minderman**  
geboren te Eindhoven

## Promotiecommissie

<b>Promotores:</b>	prof. dr. S.T. Pals	AMC-UvA
	prof. dr. M.J. Kersten	AMC-UvA
<b>Copromotor:</b>	dr. M. Spaargaren	AMC-UvA
<b>Overige leden:</b>	prof. dr. E.F. Eldering	AMC-UvA
	dr. J.E.J. Guikema	AMC-UvA
	prof. dr. M.D. Hazenberg	AMC-UvA
	dr. J.S.P. Vermaat	LUMC
	dr. A. Amir	Radboudumc
	prof. dr. C.J.M. van Noesel	AMC-UvA

## Faculteit der Geneeskunde

# TABLE OF CONTENTS

<b>Chapter 1</b>	General introduction	9
<b>Chapter 2</b>	MALT1-dependent cleavage of CYLD promotes NF- $\kappa$ B signaling and growth of aggressive B-cell receptor-dependent lymphomas <i>Blood Cancer J. 2023 Mar 15;13(1):37.</i>	33
<b>Chapter 3</b>	Identification of the SRC-family tyrosine kinase HCK as a therapeutic target in mantle cell lymphoma <i>Leukemia. 2021 Mar;35(3):881-886</i>	69
<b>Chapter 4</b>	The oncogenic L265P mutation genocopies the activating effects of MYD88 serine 257 phosphorylation in B cells <i>Blood Cancer J. 2023 Aug 18;13(1):125.</i>	89
<b>Chapter 5</b>	Prevalence and prognostic value of MYD88 and CD79B mutations in ocular adnexal large B-cell lymphoma: a reclassification of ocular adnexal large B-cell lymphoma <i>Br J Ophthalmol. 2023 Apr;107(4):576-581</i>	115
<b>Chapter 6</b>	Sinonasal diffuse large B-cell lymphoma: molecular profiling identifies subtypes with distinctive prognosis and targetable genetic features <i>Blood Adv. 2024 Feb 7; Online ahead of print.</i>	129
<b>Chapter 7</b>	Immune evasion in primary testicular and central nervous system lymphomas: HLA loss rather than 9p24.1/PD-L1/PD-L2 alterations <i>Blood. 2021 Sep 30;138(13):1194-1197.</i>	167
<b>Chapter 8</b>	General discussion	177
<b>Appendix</b>	Summary	206
	Nederlandse samenvatting	208
	PhD portfolio	210
	Curriculum Vitae	212
	Publications with author contributions	213
	Acknowledgements	215



# 1

General introduction

# GENERAL INTRODUCTION

## The immune system

The immune system is a highly complex biological system that protects the human body against different threats. Proper functioning of the immune system is of the utmost importance for the elimination of harmful pathogens, foreign substances or cancer cells. In order to properly defend the body from infections and disease, many different cell types have to work together in a strictly coordinated manner.

When a pathogen is able to successfully penetrate through the mechanical, chemical and microbiological barriers of the skin and mucosal surfaces, the innate immune system is triggered. Cells of the innate immune system do not recognize specific antigens but are able to recognize different microbial ligands or cell damage associated molecular motifs via their pattern recognition receptors (PRRs). These germ line-encoded receptors can recognize pathogen-associated molecular patterns (PAMPs), such as  $\beta$ -glucan or lipopolysaccharide (LPS), or detect damage-associated molecular patterns (DAMPs), endogenous molecules released from damaged or dying cells. Often, the innate immune system is able to successfully eliminate a pathogen. However, when the innate immune system fails to clear an infection the adaptive immune system is triggered and builds on the innate immune response.

Cells of the adaptive immune system, T and B cells, are, unlike cells of the innate immune system, able to specifically recognize antigens and provide immunological memory for these antigens. Both T and B cells express receptors with specific antigen-binding properties, but the types of antigens they recognize are very different. The T-cell receptor (TCR) can only recognize small degraded antigen fragments (peptides) presented by antigen presenting cells (APCs) in the context of a major histocompatibility complex (MHC) molecule, sometimes also referred to as human leukocyte antigen (HLA) in humans. In contrast, the B-cell receptor (BCR) is a membrane-bound immunoglobulin molecule that can recognize native macromolecules. Immunoglobulin molecules of the same antigen specificity are secreted as antibodies by terminally differentiated B cells, also known as plasma cells. The antibody-mediated immune response is often referred to as humoral immunity and contributes to clearance of pathogens by neutralization, opsonization and activation of the complement system.

## B-cell development

B cells originate from the multipotent hematopoietic stem cells (HSCs) in the bone marrow, where they acquire functional antigen receptors via gene rearrangements. During early B-cell development, the gene loci encoding the immunoglobulin heavy (IgH) and light (IgL) chains of the BCR undergo stepwise, random rearrangements resulting in

a highly diverse BCR repertoire. This process, called V(D)J recombination, is mediated by the recombination activating genes (RAGs) which introduce DNA double-strand breaks at specific recombination signal sequences (RSSs) adjacent to each V, D, and J gene segment (1). Joining of the generated gene segments is carried out by the error-prone non-homologous end joining (NHEJ) machinery and is accompanied by (random) addition or removal of nucleotides (2). The imprecise joining of gene segments is referred to as junctional diversity and further contributes to the generation of enormous diversity within the antibody repertoire (3).

V(D)J recombination starts at the early pro-B cell stage with the joining of one D and one J gene segment of the heavy chain locus followed by the joining of one V gene segment during the late pro-B cell stage (4). During the pre-B cell stage, B cells start to express a so-called pre-BCR: two rearranged immunoglobulin heavy chains covalently bound to two immunoglobulin light chain-like molecules called surrogate light chains (5). Pre-BCR signaling results in a few rounds of proliferation, accompanied by reduced RAG1/2 expression and eventually loss of surface pre-BCR expression. During the late pre-B cell stage, re-expression of RAG1/2 allows initiation of immunoglobulin light chain rearrangements (6). Expression of a successfully rearranged light chain allows for assembly of the BCR on the cell surface. Immature B cells showing reactivity towards self-antigen presented by bone marrow stromal cells will continue to rearrange light chain gene segments and eventually undergo apoptosis if the new BCR remains self-reactive (7). IgM<sup>+</sup> immature B cells will exit the bone marrow to continue maturation in the circulation and secondary lymphoid organs, including the spleen, lymph nodes, Peyer's patches and tonsils. First, immature B cells enter the spleen as transitional B cells, where they develop into marginal zone B cells or follicular B cells (8, 9). Subsequently, antigen-induced activation of follicular B cells is continued in germinal centers and leads to the generation of memory B cells and high-affinity antibody secreting plasma cells (Figure 1).

### **Germinal centers**

Germinal centers (GC) are specialized areas in secondary lymphoid tissues where follicular B cells undergo clonal expansion, somatic hypermutation (SHM), immunoglobulin isotype switching and affinity-based selection (Figure 1). Follicular B cells acquire antigen from follicular dendritic cells (FDCs), specialized stromal cells that present and maintain large amounts of intact antigen on their surface. In addition to antigen presentation, FDCs express adhesion molecules, cytokines and chemokines that mediate the recruitment and retention of B cells and helper T-cell subsets (10). Following antigen recognition, B cells upregulate CCR7 expression and migrate to the border between the B-cell follicle and the T-cell zone (T:B border), where they receive co-stimulatory signals from CD4<sup>+</sup> T follicular helper (Tfh) cells (11). The activated B cells can differentiate into short-lived

plasma cells or memory B cells. Alternatively, the B cells will migrate towards the center of the follicle where they rapidly proliferate, giving rise to an early GC (12). The GC can be divided into two distinct compartments: the dark zone and the light zone. In order to achieve optimal affinity-based selection, the GC B cells must cycle between the two compartments (13). The GC dark zone contains CXCL12-expressing reticular cells, which mediate the attraction of rapidly dividing, CXCR4-expressing B cells, named centroblasts (14). Within the GC dark zone, centroblasts undergo SHM of the genes encoding their BCR (15). During SHM, random point mutations are introduced in the variable regions of immunoglobulin genes further diversifying the BCR repertoire. This process is initiated by activation-induced cytidine deaminase (AID), an enzyme mediating deamination of cytosine bases turning them into uracils (16, 17). Subsequently, the resulting U:G mismatch is repaired by a number of different mutagenic DNA damage response pathways possibly resulting in changes in the amino acid sequence. Centroblasts express high levels of BCL6, a transcriptional repressor, which is essential in protecting the cells against DNA-damage-induced apoptosis. Moreover, BCL6 is crucial for the migration of GC B cells towards the center of the follicle. Following SHM, GC centroblasts transition to a centrocyte phenotype through expression of CXCR5 and downregulation of CXCR4, allowing them to migrate towards CXCL13 expressing FDCs in the light zone (14, 18). Within the light zone, centrocytes capture and process antigen presented by FDCs and subsequently present this antigen to Tfh cells in order to undergo positive selection. Centrocytes expressing BCRs with low affinity towards antigen do not receive (sufficient) survival signals, such as CD40L-CD40 engagement, from Tfh cells and go into apoptosis (19). Then, the selected B cells either exit the GC and differentiate into memory B cells or plasma cells or re-enter into the dark zone where they undergo more cycles of clonal expansion and SHM (20). As B cells go through multiple rounds of SHM and clonal selection, the surviving B cells will gradually accumulate affinity-enhancing mutations since they will outcompete B cells with lower affinity BCRs. This process is called affinity maturation and results in generation of antibodies with increased affinity for a particular antigen during the course of an immune response. Further diversification of the antibody repertoire is mediated by class switch recombination (CSR), which results in a change from IgM and IgD expression by naive B cells to expression of respectively IgG, IgA or IgE (21). This process requires generation of DNA double-strand breaks within the switch (S) regions that lie upstream and downstream of the various immunoglobulin heavy chain constant regions. Similar to SHM, this process depends crucially on recruitment and activity of AID (22). Antibody isotype switching does not affect the antigen specificity, but greatly affects the biological function of the antibody by determining its tissue distribution, interaction with other immune cells and ability to activate the complement system. Positively selected GC B cells eventually exit the germinal center and differentiate into long-lived memory B cells or plasma cells. The three most important transcription factors driving plasma cell differentiation are interferon regulatory factor 4 (IRF4), B

lymphocyte-induced maturation protein 1 (BLIMP1) and X-box binding protein 1 (XBP1) (23). In addition, downregulation of BCL6 is essential for plasma cell differentiation since BCL6 directly represses expression of BLIMP1 (24). The mechanism underlying the differentiation of GC B cells towards the memory compartment is incompletely understood, but was shown to involve B cells expressing lower affinity BCRs compared to cells entering the plasma cell compartment (25).

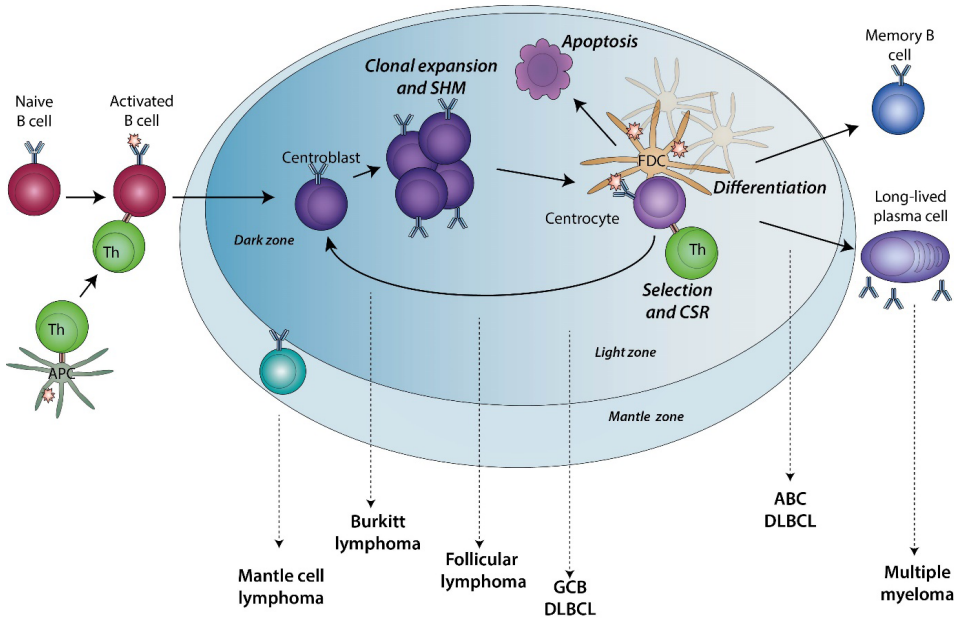


**Figure 1. The origin of germinal center-derived B-cell lymphomas.** Naive antigen-activated B cells are driven into B-cell follicles in secondary lymphoid organs where they can form germinal centers (GCs). The GC is a transient and dynamic structure consisting of a dark zone, light zone and a surrounding mantle zone. In the dark zone GC B cells (centroblasts) rapidly proliferate and undergo SHM to mutate their immunoglobulin genes. In the light zone, the GC B cells (centrocytes) interact with follicular dendritic cells and follicular T-helper cells and are selected based on the highest antigen affinity. GC B cells that are not selected in the light zone undergo apoptosis. Cyclic re-entry into the dark zone allows GC B cells to increase their affinity towards a specific antigen. Positively selected cells can exit the germinal center and differentiate into memory B cells or long-lived plasma cells. The putative relation of GC-derived B-cell lymphomas with their respective healthy GC counterpart is shown. Abbreviations: APC, antigen presenting cell; SHM, somatic hyper mutation; FDC, follicular dendritic cells; CSR, class switch recombination; Th, T (follicular) helper cells; GCB DLBCL, germinal-center B-cell-like diffuse large B-cell lymphoma; ABC DLBCL, activated B-cell-like diffuse large B-cell lymphoma.

### Germinal center reaction and lymphomagenesis

The antibody diversification mechanisms that take place during the GC reaction are of the utmost importance for generating B cells expressing a diverse repertoire of high-affinity BCRs, but bear an inherent risk for inducing mutations and chromosomal

translocations. Well known examples include immunoglobulin-*MYC* translocations in Burkitt lymphoma (BL) and *BCL6* translocations in diffuse large B cell lymphoma (DLBCL) (26, 27). In addition, aberrant SHM of genes outside of the immunoglobulin locus frequently introduces mutations in the proto-oncogenes *BCL6*, *FAS*, *PIM1* and *cMYC* in DLBCL (28). Since the molecular mechanisms involved in regulating the normal GC reaction can be hijacked during malignant transformation, the majority of mature B cell non-Hodgkin lymphomas (B-NHLs) originate from GC B cells. These GC-derived lymphomas reflect the normal counterparts of GC B cells that are blocked at different stages of maturation (Figure 1). BL originates from dark zone B cells, while FL and germinal center B cell-like (GCB) DLBCL both originate from light zone B cells. The activated B cell-like (ABC) type of DLBCL resembles late stage GC B cells, which are arrested at the plasmablast stage (29). In contrast, mantle cell lymphoma (MCL) is believed to be derived from naïve CD5<sup>+</sup> B cells present in the mantle zone that surrounds the GC follicle (30). Intriguingly, approximately 20% of MCL cases do show somatic hypermutation of their V-region genes, suggesting that they originate from a GC-derived B cell (31). MCL is often characterized by translocation of *CCND1* (cyclin D1) to the immunoglobulin heavy chain locus (32). In contrast to the CSR-mediated translocations occurring in GC-derived malignancies, the *CCND1-IGH* translocation in MCL takes place during an error in VDJ recombination in the course of the pre-B cell stage (33). On the other hand, *CCND1-IGH* translocations resulting from errors in isotype switching are frequently detected in multiple myeloma (MM), a malignant expansion of post-germinal center plasma cells that home to the bone marrow (34). The following paragraphs will further zoom into the pathogenesis, genetic aberrations and key pathways that are dysregulated in distinct types of B-NHL, specifically focusing on MCL and DLBCL.

## MCL

MCL is an aggressive, mature B-cell malignancy, comprising approximately 3-6% of all B-NHL cases and hence is a relatively rare disease (35). Most MCL cases are characterized by an aggressive clinical course and a poor prognosis. Standard immunochemotherapy, with the incorporation of high dose cytarabine, followed by autologous stem cell transplantation has led to an increase in median overall survival (OS) from 2.5 to approximately 5 years, but most patients still relapse and frequently develop chemoresistance (36, 37). There is a high need for novel treatment options to combat relapsed/refractory disease as well as for more tolerable treatment alternatives for elderly patients. Recent insights into the molecular pathogenesis of MCL led to the discovery of new potential drug targets. Promising new agents include the proteasome inhibitor bortezomib, the immunomodulatory compound lenalidomide, inhibitors of the BCR signaling cascade, such as ibrutinib, and the BCL2 inhibitor venetoclax (38-41).

The genetic hallmark of MCL is the chromosomal translocation t(11;14)(q13;q32),

juxtaposing the cyclin D1 gene to the immunoglobulin heavy chain gene enhancers, leading to constitutive overexpression of Cyclin D1. Cyclin D1 assembles with the cyclin-dependent kinases CDK4 or CDK6, resulting in accelerated cell cycle progression (42). In 2016, the World Health Organization (WHO) acknowledged that MCL likely develops along two distinct molecular pathways. The most common type of MCL is named 'classical MCL' and originates from B cells that did not go through the germinal center reaction and harbor no or very few *IGHV* somatic mutations (43). These lymphomas display expression of transcription factor SOX11 and usually involve lymph nodes and extranodal sites. These tumors are genetically unstable and acquire many secondary genetic aberrations, including mutations in cell-cycle regulators, DNA damage-associated proteins as well as in components of the BCR signaling cascade (44). Leukemic, non-nodal MCL is less common and originates from B cells that underwent *IGHV* somatic hypermutation, do not express SOX11 and are genetically more stable. These lymphomas preferentially disseminate to the peripheral blood, bone marrow and spleen and are associated with a more indolent clinical course (45, 46).

Next to the Cyclin D1 translocation, the majority of MCL cases harbor a large number of secondary genetic aberrations. The most frequently mutated or deleted gene in MCL is the *ataxia-telangiectasia mutated (ATM)* gene, which encodes a kinase that initiates activation of the cellular response to DNA double-strand breaks (47). These mutations and deletions frequently affect the phosphatidylinositol-3 kinase domain or lead to a truncated and rapidly degraded protein (48). These aberrations usually result in inactivation of both alleles of the *ATM* gene. ATM can phosphorylate the tumor suppressor p53, which is also frequently mutated or deleted in MCL patients (49, 50). Interestingly, genetic aberrations of *ATM* and *TP53* are almost completely mutually exclusive, but only disruption of *TP53* is associated with poor progression-free and overall survival (51, 52). Likewise, genetic aberrations of *KMT2D* (lysine methyltransferase 2D), also known as *MLL2*, are frequently detected in MCL (14%) and associated with poor clinical outcome (52). Also the chromatin modifying enzymes *WHSC1* and *MEF2B* are frequently mutated in MCL (10% and 3% of MCL cases, respectively) (50). Intriguingly, almost all mutations in *MLL2*, *WHSC1* and *MEF2B* are detected in the SOX11 positive/*IGHV*-unmated subgroup of MCL. In contrast, activating mutations in Toll-like receptor (*TLR2*) were only detected in a small fraction of the SOX11-negative/*IGHV*-mutated subgroup of MCL (50).

Contrary to ABC DLBCL, which is characterized by frequent mutations in the canonical NF- $\kappa$ B signaling pathway (see below), MCL cases show frequent mutations in genes involved in the non-canonical (alternative) NF- $\kappa$ B signaling pathway, such as *BIRC3* (also known as cellular IAP2; c-IAP2), *TRAF2* and *MAP3K14* (also known as NIK; NF- $\kappa$ B-inducing kinase) (50, 53, 54). The non-canonical pathway is triggered by, among others, the TNF (tumor necrosis factor) cytokine family, CD40 ligand (CD40L) and B cell-activating

factor (BAFF). In the non-canonical pathway, NIK activates the downstream I $\kappa$ B kinase- $\alpha$  (IKK $\alpha$ ) which then promotes the processing of p100 into the active p52 isoform through phosphorylation and subsequent proteosomal degradation (55, 56). TRAF2 and BIRC3 (also known as cIAP2) are part of a degradation complex which mediates ubiquitination of NIK, promoting its rapid proteosomal degradation and are therefore negative regulators of alternative NF- $\kappa$ B signaling (Figure 2) (53, 57). Notably, mutations in *TRAF2* or *BIRC3* were shown to be associated with resistance to ibrutinib (53). Ibrutinib is FDA-approved for the treatment of MCL, based on a phase 2 clinical trial that showed an overall response rate of 68% in patients with relapsed or refractory MCL (40). In contrast to ABC DLBCL, where BCR signaling is propagated by activating *CD79B* mutations, and CLL, where BCR signaling is stimulated by the lymph node microenvironment, the molecular basis for ibrutinib sensitivity in MCL remains incompletely understood (58, 59). However, despite the absence of activating *CD79B* mutations, several studies have shown phosphorylation of proximal BCR signaling components in MCL tumor tissue, suggesting activation of the BCR pathway (60, 61). Intriguingly, MCL is characterized by a highly restricted *IGHV* repertoire as well as stereotyped VH CDR3 sequences and specific SHM patterns, strongly pointing towards a role for antigen-based selection, but the putative antigenic targets are unknown (62).

## DLBCL

DLBCL is the most common type of B-NHL, accounting for 30 to 50% of newly diagnosed B-NHL cases, and is a highly heterogeneous disease that can be classified into distinct subtypes based on phenotypical, molecular and clinical features. DLBCL is often associated with an aggressive clinical course, with a median survival of less than one year in untreated patients (63). For many years the standard treatment regimen for DLBCL consisted of cyclophosphamide, doxorubicin, vincristine, and prednisone (CHOP), which cured approximately 40 percent of patients (64). The addition of rituximab, a monoclonal antibody against the CD20 B-cell antigen, to the CHOP regimen greatly improved event-free and overall survival in DLBCL patients (65). Based on gene expression profiling according to the cell-of-origin (COO) classification, DLBCL can be classified into GCB DLBCL, ABC DLBCL, primary mediastinal B-cell lymphoma (PMBCL), or an “unclassifiable” subtype (66-68). Genes that define GCB-like DLBCL highly resemble genes expressed in normal germinal center B cells, such as CD10 and BCL6 (66). Most genes defining ABC-like DLBCL are upregulated in *in vitro* activated peripheral blood B cells and include the IRF4 (MUM1) gene, which is transiently expressed during normal lymphocyte activation and is required for the generation of antibody-secreting plasma cells (69). PMBCL accounts for approximately 6 to 10% of DLBCL cases and originates from thymic medulla B cells. PMBCL often presents as a bulky, fast-growing anterior mediastinal mass, mostly affecting young (female) adults (70). Clinically and molecularly, PMBCL has striking similarities with the nodular sclerosis subtype of classical Hodgkin lymphoma (CHL) (71).

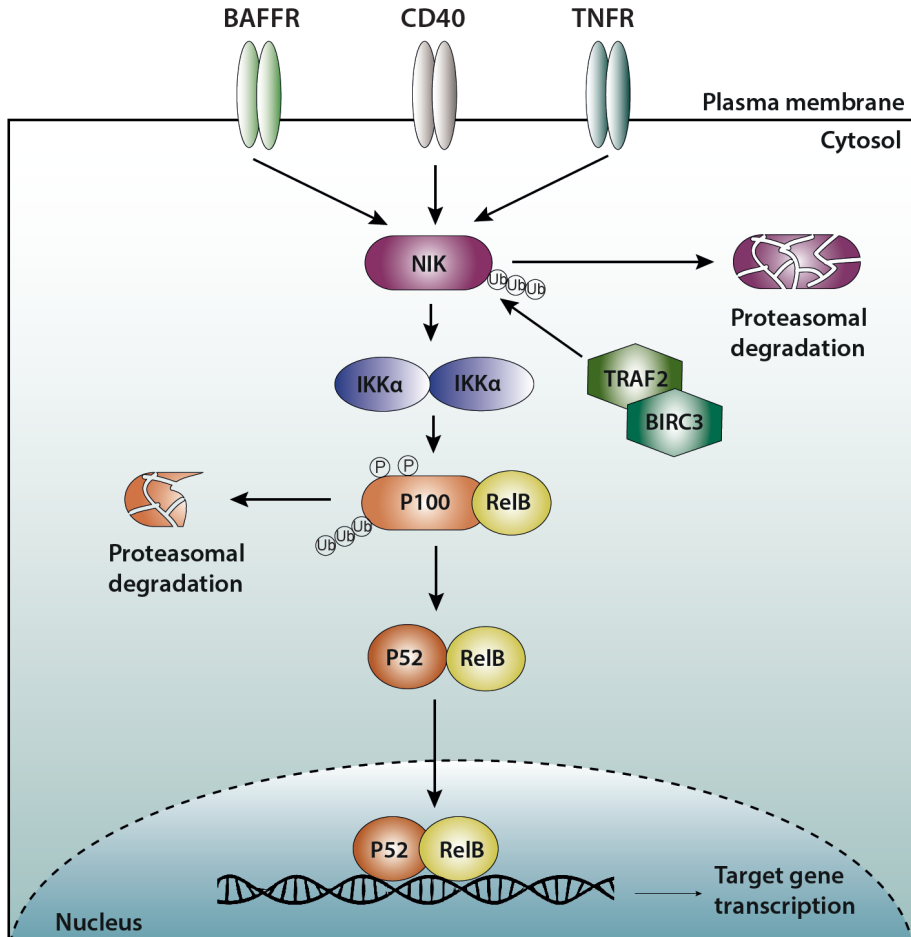


**Figure 2. Schematic representation of non-canonical NF- $\kappa$ B signaling.** The non-canonical pathway is activated by various receptors including, TNFR, CD40 and BAFFR. NIK, a central component of the non-canonical pathway, activates the downstream kinase IKK $\alpha$ . Thereafter, IKK $\alpha$  phosphorylates p100, resulting in its processing into the active p52 isoform. This eventually allows the p52/RelB NF- $\kappa$ B complex to be released into the nucleus to induce target gene expression. In absence of a ligand, NIK is continuously degraded by a TRAF2-BIRC (also known as cIAP) destruction complex. Abbreviations: BAFFR, B-cell activating factor receptor; TNFR, tumor necrosis factor receptor; NIK, NF-kappa-B-inducing kinase; TRAF2, TNF receptor associated factor 2; IKK $\alpha$ , I $\kappa$ B kinase  $\alpha$ ; BIRC3, Baculoviral IAP repeat-containing protein 3; Ub, ubiquitin; P, phosphate group.

PMBCL has been suggested to be of germinal center or post-germinal center origin, which is supported by mutational analysis of *IGHV* and *BCL6* genes showing a high load of somatic mutations (72, 73). The COO-classification was shown to better predict outcome to conventional immunochemotherapy independent of the international prognostic index (IPI). PMBCL patients have a relatively favorable clinical outcome after

chemotherapy with a five-year survival rate of 64% compared to 59% for GCB DLBCL and 30% for ABC DLBCL patients (67, 74). When treated with R-CHOP therapy, GCB DLBCL patients showed a three-year overall survival rate of 80%, compared to 45% in ABC DLBCL patients (75).

Beside the COO-classification, double-hit (DHL) and triple-hit lymphoma (THL) represent a particularly aggressive subset of DLBCL, characterized by rearrangement of the *MYC* gene concurrent with rearrangements of the *BCL2* and/or *BCL6* gene. Although most of these lymphomas are of the GCB subtype, they have a very poor prognosis when treated with standard immunochemotherapy. This implies that within the ABC and GCB subgroups, there still is great heterogeneity when it comes to prognosis and molecular pathogenesis. To address this issue, Chapuy *et al.* and Schmitz *et al.* performed a multiplatform analysis, which integrates gene expression data with the detection of somatic mutations, copy number alterations and structural variants (76, 77). In 2020, Wright *et al.* unified these data to develop the 'LymphGen' algorithm, which classifies a DLBCL biopsy into one of seven genetic subtypes: MCD, N1, A53, B2N, ST2 and EZB (with or without *MYC* rearrangements)(78).

These newly defined genetic subtypes show marked differences in their outcomes after immunochemotherapy and can help to further stratify ABC and GCB DLBCL patients into different risk groups. Patients with the MCD subtype of DLBCL showed less favorable outcomes compared to other ABC DLBCL patients and patients with the EZB subtype had a less favorable outcome when compared to other GCB DLBCL patients. Importantly, this new classification system will strongly support the development of novel targeted therapies. For example, several studies have indicated that (extranodal) lymphomas with mutations in MCD-defining genes are highly sensitive to the BTK inhibitor ibrutinib (79-81). Similarly, patients with the EZB subtype of DLBCL, which is characterized by *EZH2* mutations and *BCL2* translocations, can likely benefit from treatment with *EZH2* inhibitors or *BCL2* inhibitors, such as venetoclax. Indeed, an interim analysis of the CAVALLI clinical trial, shows that addition of venetoclax to R-CHOP therapy is beneficial for DLBCL patients displaying *BCL2* protein overexpression by immunohistochemistry (82). Moreover, results of the GUIDANCE-01 phase II trial demonstrate that genetic subtype-guided targeted agents plus R-CHOP (R-CHOP-X) can significantly improve progression-free survival in newly diagnosed DLBCL (83). In this study MCD-like and B2N-like DLBCL were treated with the BTK inhibitor ibrutinib, N1-like DLBCL and unclassified DLBCL with the immunomodulatory agent lenalidomide, A53-like DLBCL with the demethylating agent decitabine and EZB-like DLBCL cases with the HDAC inhibitor tucidinostat.

The EZB subtype of DLBCL is the largest subset, accounting for approximately one third of total DLBCL cases and is highly enriched for cases classified as GCB type DLBCL.

This subtype is characterized by mutational activation of *EZH2*, inactivating mutations of chromatin modifiers, such as *CREBBP*, *EP300* and *KMT2D*, and translocations of *BCL2*. The somewhat smaller ST2 subtype also predominantly consists of GCB DLBCL cases and is named for its recurrent *SGK1* and *TET2* mutations. The second largest subset, B2N, is characterized by translocations of *BCL6* and mutations in *NOTCH2* and consists of a mix of ABC, GCB and unclassified DLBCL cases. In contrast, the A53 subtype (characterized by *TP53* mutations and deletions) and N1 subtype (characterized by gain-of-function *NOTCH1* mutations) almost exclusively consists of ABC DLBCL cases. The same holds true for the MCD subtype of DLBCL, which is defined by a high prevalence of (co-occurring) MYD88 L265P and CD79B mutations, which collaboratively activate the canonical NF- $\kappa$ B signaling pathway. The prevalence of the different subtypes and the most frequent genetic alterations within each subtype are summarized in Figure 3.

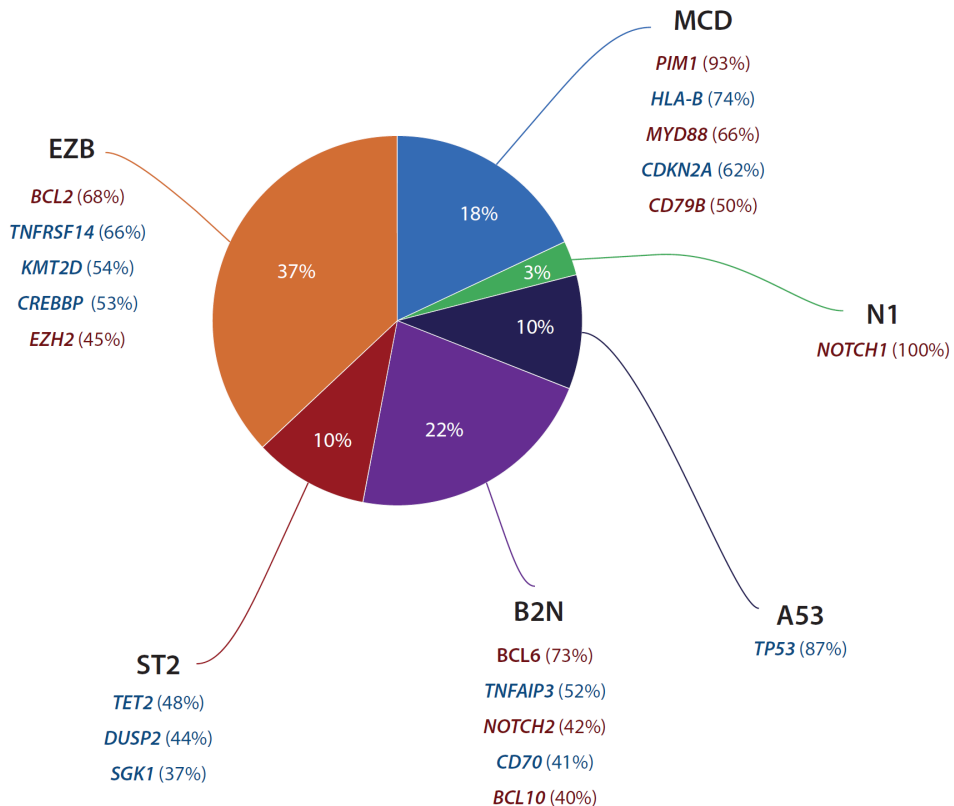


**Figure 3. The most frequently affected genes for each molecular subtype of DLBCL.** Copy number gains/amplifications or gain-of-function mutations are visualized in red. Deletions or loss-of-function mutations are visualized in blue. The percentages within the pie chart represent the prevalence of each molecular subtype.

## Molecular characteristics of MCD DLBCL

Next to *MYD88* and *CD79B* mutations, lymphomas belonging to the MCD subtype frequently harbor loss of the *CDKN2A* locus, gain or amplification of the *BCL2* and *MALT1* gene loci (located on *18q*) and mutations in *PIM1* (84). MCD DLBCL display frequent gains or amplifications of *SPIB*, a transcription factor that promotes plasmacytic differentiation, while full plasmacytic differentiation is blocked by inactivating mutations in *PRDM1* (BLIMP1) (76). In addition, these lymphomas frequently harbor mutations in the tumor suppressor genes *ETV6*, *BTG1*, and *BTG2*. Intriguingly, MCD-type lymphomas are often associated with extranodal involvement. While DLBCLs typically present in lymph nodes and other professional lymphoid tissues, primary extranodal lymphomas present at different types of non-lymphoid organs, such as the central nervous system (CNS), breast, testis and vitreoretinal compartment. Interestingly, extranodal lymphomas are often of the MCD subtype with frequent mutations of *MYD88*, *CD79B*, *PIM1* and *PRMD1*. Moreover, both MCD DLBCL and primary extranodal lymphomas prevalently harbor genetic aberrations of immune surveillance genes, including the major histocompatibility complex class I (*HLA-A*, *B* and *C*) loci as well as inactivating mutations of *CD58*, a ligand for the CD2 receptor on T and NK cells (85).

## Signaling pathways in MCD DLBCL

Mutations in TLR adaptor molecule *MYD88* and BCR-associated protein *CD79* drive constitutive NF- $\kappa$ B pathway activation, promoting lymphoma cell proliferation and survival. MYD88 is the key signaling adaptor molecule for IL-1R and IL-18R as well as for all TLRs, except for TLR3 and certain TLR4 derived signals. MYD88 consists of a C-terminal TIR domain, a short intermediary domain, and a N-terminal death domain (DD). Upon binding of IL-1/IL-18 or a TLR ligand, MYD88 is able to recruit the serine–threonine kinase IL-1-receptor associated kinase 4 (IRAK4) through interactions of their DD domains. In turn, IRAK2 or IRAK1 is recruited to the complex and phosphorylated by IRAK4. This large signaling complex consisting of MYD88, IRAK4 and IRAK2 or IRAK1 is also known as the Myddosome (86). IRAK2 does not have intrinsic kinase activity, and kinase activity of IRAK1 seems irrelevant for downstream activation of NF- $\kappa$ B (87). Following phosphorylation by IRAK4, IRAK2 and IRAK1 are able to interact with tumor necrosis factor receptor (TNFR)-associated factor 6 (TRAF6) through their C-terminal domains (88). TRAF6 is a E3 ubiquitin ligase able to catalyze Lys 63-linked polyubiquitination of TGF $\beta$ -activated kinase 1 (TAK1) resulting in its activation and autophosphorylation (89). Supported by two adaptor proteins, TAB1 and TAB2, TAK1 phosphorylates both mitogen-activated protein (MAP) kinases and I $\kappa$ B kinase  $\beta$  (IKK $\beta$ ). In turn, IKK $\beta$  phosphorylates the inhibitory I $\kappa$ B $\alpha$  protein leading to its ubiquitination and subsequent proteosomal degradation (90–92). Dissociation of I $\kappa$ B $\alpha$  allows translocation of nuclear factor (NF)- $\kappa$ B dimers to the nucleus ultimately causing enhanced expression of NF- $\kappa$ B target genes (Figure 4).

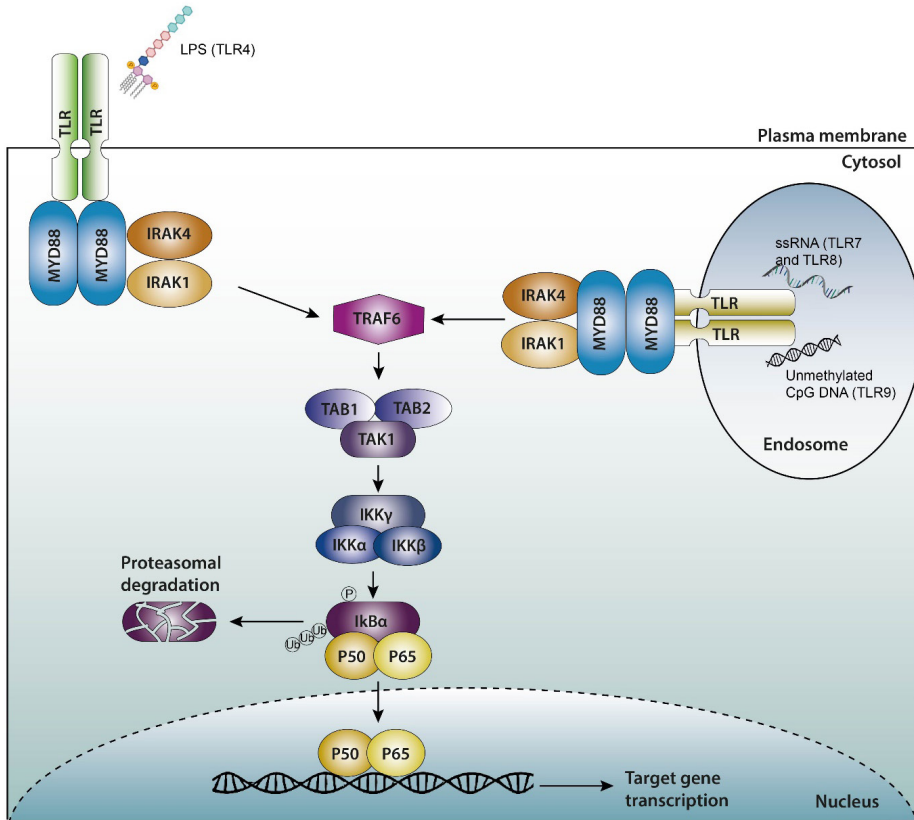


**Figure 4. Schematic representation of TLR/MyD88 signaling.** Upon binding of a TLR ligand (e.g. LPS, ssRNA or CpG DNA), MyD88 recruits IRAK4 and, in turn, IRAK1, which is phosphorylated by IRAK4. Subsequently, phosphorylated IRAK1 interacts with E3 ubiquitin ligase TRAF6, which mediates Lys 63-linked polyubiquitination of TAK1 resulting in its recruitment and autophosphorylation. Then, activated TAK1 phosphorylates IKKβ. In turn, IKKβ phosphorylates the inhibitory IκBα protein leading to its ubiquitination and subsequent proteasomal degradation. This allows translocation of NF-κB dimers to the nucleus causing target gene expression. Abbreviations: LPS, lipopolysaccharide; TLR, toll-like receptor; MyD88, myeloid differentiation primary response 88; IRAK4/1, interleukin-1 receptor (IL-1R) associated kinase 4/1; TRAF6, TNF receptor associated factor 6; TAB1/2, TGF-β-activated kinase 1 binding protein 1/2; TAK1, TGF-β-activated kinase 1; IKKα/β, IκB kinase α/β; IκBα, Inhibitor kappa B-α; Ub, ubiquitin; P, phosphate group.

TLR/MyD88 signaling is not the only cause of constitutive NF-κB activity in DLBCL. In 2010 a genetic RNA interference library screen demonstrated that the vast majority of ABC DLBCL cell lines is dependent on both proximal BCR components as well as downstream signaling proteins for their survival (59). The BCR is a membrane bound immunoglobulin molecule consisting of a heavy (IgH) and light (IgL) chain. Most ABC DLBCL cases express IgM on their cell surface, in contrast to GC DLBCL, which predominantly express IgG (93). The membrane bound BCR interacts through disulfide bridges with the CD79 heterodimer, which is composed of Ig-α (CD79A) and Ig-β (CD79B). The cytoplasmic domains of both

CD79A and CD79B contain an immunoreceptor tyrosine-based activation motif (ITAM), which is critical for BCR-mediated signal transduction. Next to propagating BCR signaling, the CD79 heterodimer plays a key role in regulating BCR internalization and trafficking (94). Following ligation of the BCR, tyrosine residues within the ITAM motifs of CD79 are phosphorylated by members of the Src-family of cytoplasmic protein-tyrosine kinases (SFKs), including LYN, FYN, and BLK. This in turn leads to the recruitment, autophosphorylation and activation of spleen tyrosine kinase (SYK). SYK can then phosphorylate B cell linker protein (BLNK), a scaffold protein which is able to recruit phospholipase C $\gamma$  (PLC $\gamma$ ) and Bruton's tyrosine kinase (BTK) through their respective Src Homology 2 (SH2) domains (95). In parallel, phosphorylation of CD19 by SFKs mediates activation of phosphoinositide 3-kinase  $\delta$  (PI3K $\delta$ ), which via production of phosphatidylinositol (3,4,5)-trisphosphate (PIP3), further facilitates recruitment of BTK and PLC $\gamma$  to the cell membrane through their Pleckstrin homology (PH) domains (96). Subsequently, BTK is activated through transphosphorylation by LYN or SYK at tyrosine residue 551 in the activation loop, followed by autophosphorylation at tyrosine residue 223 in the SH3 domain (97). Activated BTK can then phosphorylate PLC $\gamma$ 2 at multiple tyrosine residues leading to its activation (98). PLC $\gamma$ 2 catalyzes the hydrolysis of phosphatidylinositol 4,5-bisphosphate (PIP2) resulting in the formation of inositol trisphosphate (IP3) and diacylglycerol (DAG) which function as second messengers mediating several important downstream signaling events including activation of Protein kinase C (PKC) isoforms, predominantly being PKC $\beta$  in B cells (99, 100). One of the direct downstream targets of PKC $\beta$  is constitutive caspase recruitment domain-containing protein 11 (CARD11) (101). PKC $\beta$  phosphorylates key serine residues in the PKC-regulated domain (PRD) of CARD11 provoking a conformational change and allowing CARD11 to interact with B-cell lymphoma 10 (BCL10), which subsequently associates with mucosa-associated-lymphoid-tissue lymphoma-translocation gene 1 (MALT1) (102). The formation of this CARD11/BCL10/MALT1 (CBM) complex enables the function of MALT1 as a scaffolding protein allowing recruitment of the E3 ubiquitin ligase TRAF6. This subsequently propagates ubiquitin-mediated recruitment and activation of TAK1 and IKK complexes eventually resulting in canonical NF- $\kappa$ B signaling (Figure 5).

### **Immune evasion in DLBCL**

The ability of cancer cells to evade attack and elimination by host immune cells is considered one of the emerging hallmarks of cancer (103). Accordingly, next to mutations in oncogenic driver pathways, DLBCL cases frequently harbor genetic alterations in immune surveillance genes (104). In DLBCL these genetic alterations mostly result in decreased or absent expression of molecules involved in antigen presentation or increased expression of immunosuppressive ligands (105). Activation of CD8<sup>+</sup> effector T cells requires recognition of a tumor antigen presented in the context of MHC class I molecules. In addition, an effective antitumor immune response requires MHC class II-dependent antigen presentation to CD4<sup>+</sup> effector cells. In DLBCL, loss of surface MHC

class I and II expression is the most common mechanism employed by tumor cells to evade immune surveillance (85, 106, 107). Next to loss of function mutations in *HLA* genes, loss of MHC surface expression frequently results from mutations in *B2M* in case of MHC class I and *CIITA* in case of MHC class II (85, 108). Additionally, several studies reported increased expression of Programmed death-ligand 1 (PD-L1) in DLBCL as a result of copy number gains, amplifications, and translocations (109-111). PD-L1 belongs to the B7 family and promotes T cell exhaustion through ligation to the inhibitory PD-1 receptor (112).

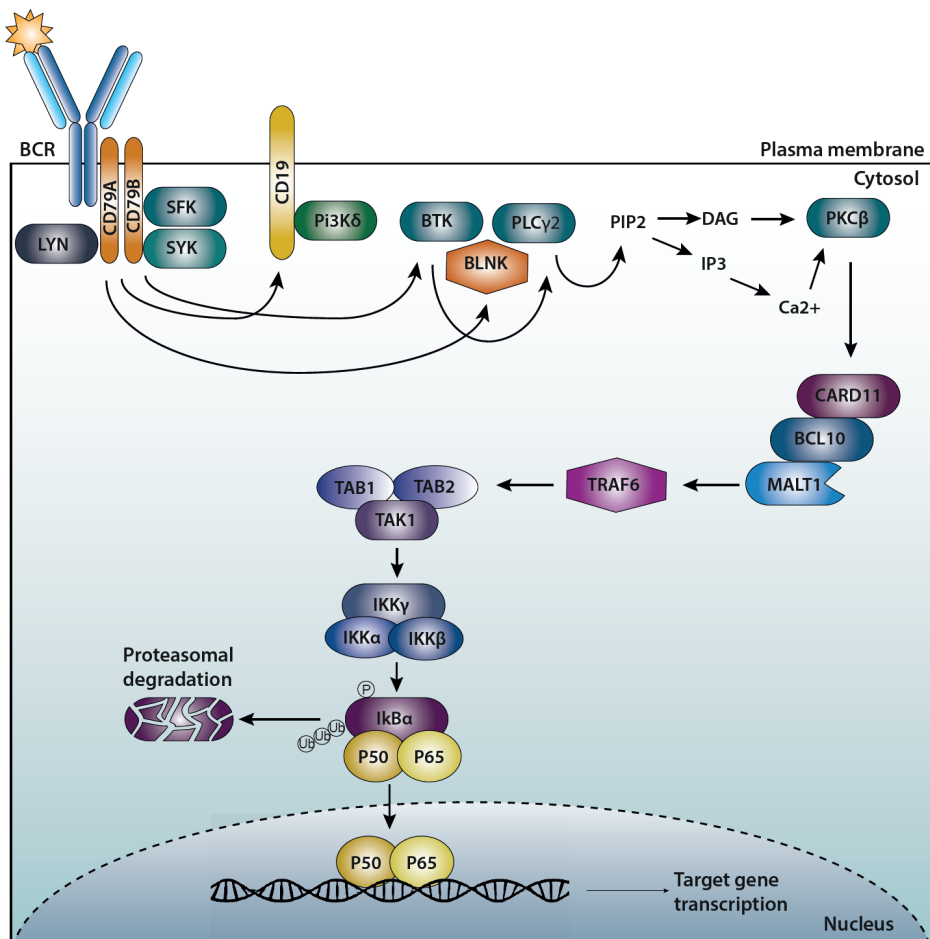


**Figure 5. Schematic representation of B-cell receptor (BCR) signaling.** Upon ligation of the BCR, tyrosine residues within the ITAM motifs of CD79 are phosphorylated by the src-family kinase LYN. This in turn leads to recruitment, autophosphorylation and activation of cytoplasmic tyrosine kinase SYK. SYK can then phosphorylate BLNK, a scaffold protein which is able to recruit PLC $\gamma$  and BTK. In parallel, phosphorylation of CD19 by SFKs mediates activation of PI3K $\delta$ , which, via production of PIP3, induces membrane translocation of BTK and PLC $\gamma$ . Subsequently, BTK is activated and can then phosphorylate PLC $\gamma$ 2, which catalyzes hydrolysis of PIP2 resulting in the formation of IP3 and DAG, second messengers mediating activation

of PKC $\beta$ . PKC $\beta$  phosphorylates CARD11, allowing CARD11 to interact with BCL10, which subsequently associates with MALT1. The formation of this complex mediates recruitment of the E3 ubiquitin ligase TRAF6. This subsequently propagates ubiquitin-mediated recruitment and activation of TAK1 and IKK complexes eventually resulting in canonical NF- $\kappa$ B signaling. Abbreviations: SYK, spleen tyrosine kinase; PI3K $\delta$ , Phosphoinositide-3-kinase  $\delta$ ; BTK, Bruton's tyrosine kinase; BLNK, B-cell linker; PLC $\gamma$ 2, Phospholipase  $\gamma$ 2; PIP2, Phosphatidylinositol 4,5-bisphosphate; IP3, Inositol trisphosphate; DAG, diacylglycerol; PKC $\beta$ , Protein kinase  $\beta$ ; CARD11, Caspase activation and recruitment domain 11; BCL10, B-cell lymphoma 10; MALT1, Mucosa-associated lymphoid tissue lymphoma translocation protein 1; TRAF6, TNF receptor associated factor 6; TAB1/2, TGF- $\beta$ -activated kinase 1 binding protein 1/2; TAK1, TGF- $\beta$ -activated kinase 1; IKK $\alpha/\beta/\gamma$ , IkB kinase  $\alpha/\beta/\gamma$ ; I $\kappa$ B $\alpha$ , Inhibitor kappa B- $\alpha$ ; Ub, ubiquitin; P, phosphate group.

## AIM AND OUTLINE OF THIS THESIS

Signaling through the BCR and TLRs is essential for development and maturation of healthy B cells. Deregulation of these pathways promotes growth and survival in various lymphoma types, including (MCD) DLBCL and MCL. In MCD DLBCL, there is accumulating evidence for synergistic cooperation of BCR and TLR signaling. In the current studies we sought to further elucidate the role of TLR and BCR signaling in the pathogenesis of DLBCL and MCL. In addition, we studied immune evasion mechanisms in different types of extranodal (MCD) DLBCL.

Mutations affecting the BCR CD79A/B subunit have been identified in approximately 10% of ABC DLBCL. Although these mutations are rare in MCL, there is accumulating evidence for BCR activation in a subset of MCL patients. In **chapter 2**, we show that BCR signaling propagates MALT1-mediated cleavage and, consequently, inactivation of CYLD in a subset of DLBCL and MCL cases. In addition, we demonstrate that silencing of CYLD expression rendered BCR-dependent lymphoma cell lines less sensitive to inhibition of NF- $\kappa$ B signaling and cell proliferation by BCR pathway inhibitors indicating that these effects are partially mediated by CYLD.

The MYD88 L265P hotspot mutation is frequently detected in ABC DLBCL, but the prevalence greatly varies depending on the location of the tumor. In DLBCL, mutant MYD88 promotes expression of the SRC-family tyrosine kinase hematopoietic cell kinase (HCK). In **chapter 3**, we demonstrate that in MCL, HCK is aberrantly expressed in a MYD88-dependent fashion, irrespective of oncogenic mutations in MYD88. Therefore, the aberrant HCK expression in primary MCL cells may result from presence of TLR ligands in the tumor microenvironment. In **chapter 4**, we further studied MYD88 activation in B cells without *MYD88* mutations. In this study, we propose a model in which the oncogenic L265P mutant promotes MYD88 TIR domain homodimerization and NF- $\kappa$ B activation in a similar manner as phosphorylation of MYD88 at serine 257.

The MYD88 L265P mutation frequently co-occurs with mutations in CD79B, especially in extranodal lymphomas arising in immune privileged sites, such as the CNS, testis and vitreoretinal compartment. In **chapter 5**, we demonstrate that also in ocular adnexal large B-cell lymphomas, *MYD88* mutations are important drivers of lymphomagenesis and frequently co-occur with mutations in *CD79B*. In **chapter 6**, we demonstrate that primary sinonasal DLBCL, a rare subtype of extranodal lymphoma, consists of two distinct subtypes. When stratified based upon COO, ABC-like sinonasal DLBCL was associated with inferior five-year progression-free survival, a high prevalence of *MYD88* and *CD79B* mutations and loss of MHC class II expression. In **chapter 7**, we studied immune evasion mechanisms in extranodal primary central nervous system (PCNSL) and primary testis lymphomas (PTL), which display a remarkably high prevalence of activating somatic *MYD88* mutations. We show that PTLs and PCNSLs hardly use the programmed death-ligand 1/2 (PD-L1/2) checkpoint, but instead use loss of MHC expression as the major mechanism of immune evasion. Lastly, in **chapter 8**, we discuss the mechanisms behind the oncogenic cooperation of MYD88 and CD79 mutations in immune-privileged site associated (MCD) DLBCL and review therapeutic options for these aggressive lymphomas.

## REFERENCES

1. McBlane JF, van Gent DC, Ramsden DA, Romeo C, Cuomo CA, Gellert M, Oettinger MA. Cleavage at a V(D)J recombination signal requires only RAG1 and RAG2 proteins and occurs in two steps. *Cell*. 1995;83(3):387-95.
2. Ma Y, Pannicke U, Schwarz K, Lieber MR. Hairpin opening and overhang processing by an Artemis/DNA-dependent protein kinase complex in nonhomologous end joining and V(D)J recombination. *Cell*. 2002;108(6):781-94.
3. Komori T, Okada A, Stewart V, Alt FW. Lack of N regions in antigen receptor variable region genes of TdT-deficient lymphocytes. *Science*. 1993;261(5125):1171-5.
4. Bassing CH, Swat W, Alt FW. The mechanism and regulation of chromosomal V(D)J recombination. *Cell*. 2002;109 Suppl:S45-55.
5. Karasuyama H, Rolink A, Shinkai Y, Young F, Alt FW, Melchers F. The expression of Vpre-B/lambda 5 surrogate light chain in early bone marrow precursor B cells of normal and B cell-deficient mutant mice. *Cell*. 1994;77(1):133-43.
6. Burrows PD, Stephan RP, Wang YH, Lassoued K, Zhang Z, Cooper MD. The transient expression of pre-B cell receptors governs B cell development. *Semin Immunol*. 2002;14(5):343-9.
7. Retter MW, Nemazee D. Receptor editing occurs frequently during normal B cell development. *J Exp Med*. 1998;188(7):1231-8.
8. Saito T, Chiba S, Ichikawa M, Kunisato A, Asai T, Shimizu K, et al. Notch2 is preferentially expressed in mature B cells and indispensable for marginal zone B lineage development. *Immunity*. 2003;18(5):675-85.
9. Wen L, Brill-Dashoff J, Shinton SA, Asano M, Hardy RR, Hayakawa K. Evidence of marginal-zone B cell-positive selection in spleen. *Immunity*. 2005;23(3):297-308.
10. Liu YJ, Grouard G, de Bouteiller O, Banchereau J. Follicular dendritic cells and germinal centers. *Int Rev Cytol*. 1996;166:139-79.
11. Reif K, Ekland EH, Ohl L, Nakano H, Lipp M, Forster R, Cyster JG. Balanced responsiveness to chemoattractants from adjacent zones determines B-cell position. *Nature*. 2002;416(6876):94-9.
12. Green JA, Suzuki K, Cho B, Willison LD, Palmer D, Allen CD, et al. The sphingosine 1-phosphate receptor S1P(2) maintains the homeostasis of germinal center B cells and promotes niche confinement. *Nat Immunol*. 2011;12(7):672-80.
13. Allen CD, Okada T, Cyster JG. Germinal-center organization and cellular dynamics. *Immunity*. 2007;27(2):190-202.
14. Allen CD, Ansel KM, Low C, Lesley R, Tamamura H, Fujii N, Cyster JG. Germinal center dark and light zone organization is mediated by CXCR4 and CXCR5. *Nat Immunol*. 2004;5(9):943-52.
15. Wilson PC, de Bouteiller O, Liu YJ, Potter K, Banchereau J, Capra JD, Pascual V. Somatic hypermutation introduces insertions and deletions into immunoglobulin V genes. *J Exp Med*. 1998;187(1):59-70.
16. Muramatsu M, Kinoshita K, Fagarasan S, Yamada S, Shinkai Y, Honjo T. Class switch recombination and hypermutation require activation-induced cytidine deaminase (AID), a potential RNA editing enzyme. *Cell*. 2000;102(5):553-63.
17. Revy P, Muto T, Levy Y, Geissmann F, Plebani A, Sanal O, et al. Activation-induced cytidine deaminase (AID) deficiency causes the autosomal recessive form of the Hyper-IgM syndrome (HIGM2). *Cell*. 2000;102(5):565-75.
18. Bannard O, Horton RM, Allen CD, An J, Nagasawa T, Cyster JG. Germinal center centroblasts transition to a centrocyte phenotype according to a timed program and depend on the dark zone for effective selection. *Immunity*. 2013;39(5):912-24.
19. Luo W, Weisel F, Shlomchik MJ. B Cell Receptor and CD40 Signaling Are Rewired for Synergistic Induction of the c-Myc Transcription Factor in Germinal Center B Cells. *Immunity*. 2018;48(2):313-26 e5.
20. Victora GD, Schwickert TA, Fooksman DR, Kamphorst AO, Meyer-Hermann M, Dustin ML, Nussenzweig MC. Germinal center dynamics revealed by multiphoton microscopy with a photoactivatable fluorescent reporter. *Cell*. 2010;143(4):592-605.
21. Stavnezer J, Guikema JE, Schrader CE. Mechanism and regulation of class switch recombination. *Annu Rev Immunol*. 2008;26:261-92.
22. Chaudhuri J, Tian M, Khuong C, Chua K, Pinaud E, Alt FW. Transcription-targeted DNA deamination by the AID antibody diversification enzyme. *Nature*. 2003;422(6933):726-30.
23. Minnich M, Tagoh H, Bonelt P, Axelsson E, Fischer M, Cebolla B, et al. Multifunctional role of the transcription factor Blimp-1 in coordinating plasma cell differentiation. *Nat Immunol*. 2016;17(3):331-43.
24. Ochiai K, Muto A, Tanaka H, Takahashi S, Igarashi K. Regulation of the plasma cell transcription factor Blimp-1 gene by Bach2 and Bcl6. *Int Immunol*. 2008;20(3):453-60.
25. Shinnakasu R, Inoue T, Kometani K, Moriyama S, Adachi Y, Nakayama M, et al. Regulated selection of germinal-center cells into the memory B cell compartment. *Nat Immunol*. 2016;17(7):861-9.
26. Gelmann EP, Psallidopoulos MC, Papas TS, Dalla-Favera R. Identification of reciprocal translocation sites within

- the c-myc oncogene and immunoglobulin mu locus in a Burkitt lymphoma. *Nature*. 1983;306(5945):799-803.
27. Salam D, Thit EE, Teoh SH, Tan SY, Peh SC, Cheah SC. C-MYC, BCL2 and BCL6 Translocation in B-cell Non-Hodgkin Lymphoma Cases. *J Cancer*. 2020;11(1):190-8.
  28. Pasqualucci L, Neumeister P, Goossens T, Nanjangud G, Chaganti RS, Kuppers R, Dalla-Favera R. Hypermutation of multiple proto-oncogenes in B-cell diffuse large-cell lymphomas. *Nature*. 2001;412(6844):341-6.
  29. Kuppers R. Mechanisms of B-cell lymphoma pathogenesis. *Nat Rev Cancer*. 2005;5(4):251-62.
  30. Bertoni F, Ponzoni M. The cellular origin of mantle cell lymphoma. *Int J Biochem Cell Biol*. 2007;39(10):1747-53.
  31. Walsh SH, Thorselius M, Johnson A, Soderberg O, Jerkeman M, Bjorck E, et al. Mutated VH genes and preferential VH3-21 use define new subsets of mantle cell lymphoma. *Blood*. 2003;101(10):4047-54.
  32. Rimokh R, Berger F, Delsol G, Digonnet I, Rouault JP, Tigaud JD, et al. Detection of the chromosomal translocation t(11;14) by polymerase chain reaction in mantle cell lymphomas. *Blood*. 1994;83(7):1871-5.
  33. Weizel N, Le T, Marculescu R, Mitterbauer G, Chott A, Pott C, et al. Templated nucleotide addition and immunoglobulin JH-gene utilization in t(11;14) junctions: implications for the mechanism of translocation and the origin of mantle cell lymphoma. *Cancer Res*. 2001;61(4):1629-36.
  34. Chesi M, Bergsagel PL, Brents LA, Smith CM, Gerhard DS, Kuehl WM. Dysregulation of cyclin D1 by translocation into an IgH gamma switch region in two multiple myeloma cell lines. *Blood*. 1996;88(2):674-81.
  35. Swerdlow SH, Campo E, Pileri SA, Harris NL, Stein H, Siebert R, et al. The 2016 revision of the World Health Organization classification of lymphoid neoplasms. *Blood*. 2016;127(20):2375-90.
  36. Ogura M, Yamamoto K, Morishima Y, Wakabayashi M, Tobinai K, Ando K, et al. R-High-CHOP/CHASER/LEED with autologous stem cell transplantation in newly diagnosed mantle cell lymphoma: JCOG0406 STUDY. *Cancer Sci*. 2018;109(9):2830-40.
  37. Hermine O, Hoster E, Walewski J, Bosly A, Stilgenbauer S, Thieblemont C, et al. Addition of high-dose cytarabine to immunochemotherapy before autologous stem-cell transplantation in patients aged 65 years or younger with mantle cell lymphoma (MCL Younger): a randomised, open-label, phase 3 trial of the European Mantle Cell Lymphoma Network. *Lancet*. 2016;388(10044):565-75.
  38. Robak T, Huang H, Jin J, Zhu J, Liu T, Samoilo O, et al. Bortezomib-based therapy for newly diagnosed mantle-cell lymphoma. *N Engl J Med*. 2015;372(10):944-53.
  39. Wang M, Fayad L, Wagner-Bartak N, Zhang L, Hagemeister F, Neelapu SS, et al. Lenalidomide in combination with rituximab for patients with relapsed or refractory mantle-cell lymphoma: a phase 1/2 clinical trial. *Lancet Oncol*. 2012;13(7):716-23.
  40. Wang ML, Rule S, Martin P, Goy A, Auer R, Kahl BS, et al. Targeting BTK with ibrutinib in relapsed or refractory mantle-cell lymphoma. *N Engl J Med*. 2013;369(6):507-16.
  41. Zhao S, Kanagal-Shamanna R, Navsaria L, Ok CY, Zhang S, Nomie K, et al. Efficacy of venetoclax in high risk relapsed mantle cell lymphoma (MCL) - outcomes and mutation profile from venetoclax resistant MCL patients. *Am J Hematol*. 2020;95(6):623-9.
  42. Fernandez V, Hartmann E, Ott G, Campo E, Rosenwald A. Pathogenesis of mantle-cell lymphoma: all oncogenic roads lead to dysregulation of cell cycle and DNA damage response pathways. *J Clin Oncol*. 2005;23(26):6364-9.
  43. Navarro A, Clot G, Royo C, Jares P, Hadzidimitriou A, Agathangelidis A, et al. Molecular subsets of mantle cell lymphoma defined by the IGHV mutational status and SOX11 expression have distinct biologic and clinical features. *Cancer Res*. 2012;72(20):5307-16.
  44. Perez-Galan P, Dreyling M, Wiestner A. Mantle cell lymphoma: biology, pathogenesis, and the molecular basis of treatment in the genomic era. *Blood*. 2011;117(1):26-38.
  45. Fernandez V, Salamer O, Espinet B, Sole F, Royo C, Navarro A, et al. Genomic and gene expression profiling defines indolent forms of mantle cell lymphoma. *Cancer Res*. 2010;70(4):1408-18.
  46. Orchard J, Garand R, Davis Z, Babbage G, Sahota S, Matutes E, et al. A subset of t(11;14) lymphoma with mantle cell features displays mutated IgVH genes and includes patients with good prognosis, nonnodal disease. *Blood*. 2003;101(12):4975-81.
  47. Schaffner C, Idler I, Stilgenbauer S, Dohner H, Lichter P. Mantle cell lymphoma is characterized by inactivation of the ATM gene. *Proc Natl Acad Sci U S A*. 2000;97(6):2773-8.
  48. Camacho E, Hernandez L, Hernandez S, Tort F, Bellosillo B, Bea S, et al. ATM gene inactivation in mantle cell lymphoma mainly occurs by truncating mutations and missense mutations involving the phosphatidylinositol-3 kinase domain and is associated with increasing numbers of chromosomal imbalances. *Blood*. 2002;99(1):238-44.
  49. Banin S, Moyal L, Shieh S, Taya Y, Anderson CW, Chessa L, et al. Enhanced phosphorylation of p53 by ATM in response to DNA damage. *Science*. 1998;281(5383):1674-7.
  50. Bea S, Valdes-Mas R, Navarro A, Salaverria I, Martin-Garcia D, Jares P, et al. Landscape of somatic mutations and clonal evolution in mantle cell lymphoma. *Proc Natl Acad Sci U S A*. 2013;110(45):18250-5.
  51. Mareckova A, Malcikova J, Tom N, Pal K, Radova L, Salek D, et al. ATM and TP53 mutations show mutual exclusivity but distinct clinical impact in mantle cell lymphoma patients. *Leuk Lymphoma*. 2019;60(6):1420-

- 8.
52. Ferrero S, Rossi D, Rinaldi A, Brusca G, Spina V, Eskelund CW, et al. KMT2D mutations and TP53 disruptions are poor prognostic biomarkers in mantle cell lymphoma receiving high-dose therapy: a FIL study. *Haematologica*. 2020;105(6):1604-12.
53. Rahal R, Frick M, Romero R, Korn JM, Kridel R, Chan FC, et al. Pharmacological and genomic profiling identifies NF-kappaB-targeted treatment strategies for mantle cell lymphoma. *Nat Med*. 2014;20(1):87-92.
54. Zhang J, Jima D, Moffitt AB, Liu Q, Czader M, Hsi ED, et al. The genomic landscape of mantle cell lymphoma is related to the epigenetically determined chromatin state of normal B cells. *Blood*. 2014;123(19):2988-96.
55. Sun SC. The non-canonical NF-kappaB pathway in immunity and inflammation. *Nat Rev Immunol*. 2017;17(9):545-58.
56. Balaji S, Ahmed M, Lorence E, Yan F, Nomie K, Wang M. NF-kappaB signaling and its relevance to the treatment of mantle cell lymphoma. *J Hematol Oncol*. 2018;11(1):83.
57. Zarnegar BJ, Wang Y, Mahoney DJ, Dempsey PW, Cheung HH, He J, et al. Noncanonical NF-kappaB activation requires coordinated assembly of a regulatory complex of the adaptors cIAP1, cIAP2, TRAF2 and TRAF3 and the kinase NIK. *Nat Immunol*. 2008;9(12):1371-8.
58. Herishanu Y, Perez-Galan P, Liu D, Biancotto A, Pittaluga S, Vire B, et al. The lymph node microenvironment promotes B-cell receptor signaling, NF-kappaB activation, and tumor proliferation in chronic lymphocytic leukemia. *Blood*. 2011;117(2):563-74.
59. Davis RE, Ngo VN, Lenz G, Tolar P, Young RM, Romesser PB, et al. Chronic active B-cell-receptor signalling in diffuse large B-cell lymphoma. *Nature*. 2010;463(7277):88-92.
60. Saba NS, Liu D, Herman SE, Underbayev C, Tian X, Behrend D, et al. Pathogenic role of B-cell receptor signaling and canonical NF-kappaB activation in mantle cell lymphoma. *Blood*. 2016;128(1):82-92.
61. Pighi C, Gu TL, Dalai I, Barbi S, Parolini C, Bertolaso A, et al. Phospho-proteomic analysis of mantle cell lymphoma cells suggests a pro-survival role of B-cell receptor signaling. *Cell Oncol (Dordr)*. 2011;34(2):141-53.
62. Gemenetzi K, Agathangelidis A, Zaragoza-Infante L, Sofou E, Papaioannou M, Chatzidimitriou A, Stamatopoulos K. B Cell Receptor Immunogenetics in B Cell Lymphomas: Immunoglobulin Genes as Key to Ontogeny and Clinical Decision Making. *Front Oncol*. 2020;10:67.
63. Fisher RI, Miller TP, O'Connor OA. Diffuse aggressive lymphoma. *Hematology Am Soc Hematol Educ Program*. 2004;221-36.
64. Fisher RI, Gaynor ER, Dahlborg S, Oken MM, Grogan TM, Mize EM, et al. Comparison of a standard regimen (CHOP) with three intensive chemotherapy regimens for advanced non-Hodgkin's lymphoma. *N Engl J Med*. 1993;328(14):1002-6.
65. Coiffier B, Lepage E, Briere J, Herbrecht R, Tilly H, Bouabdallah R, et al. CHOP chemotherapy plus rituximab compared with CHOP alone in elderly patients with diffuse large-B-cell lymphoma. *N Engl J Med*. 2002;346(4):235-42.
66. Alizadeh AA, Eisen MB, Davis RE, Ma C, Lossos IS, Rosenwald A, et al. Distinct types of diffuse large B-cell lymphoma identified by gene expression profiling. *Nature*. 2000;403(6769):503-11.
67. Rosenwald A, Wright G, Leroy K, Yu X, Gaulard P, Gascoyne RD, et al. Molecular diagnosis of primary mediastinal B cell lymphoma identifies a clinically favorable subgroup of diffuse large B cell lymphoma related to Hodgkin lymphoma. *J Exp Med*. 2003;198(6):851-62.
68. Rosenwald A, Wright G, Chan WC, Connors JM, Campo E, Fisher RI, et al. The use of molecular profiling to predict survival after chemotherapy for diffuse large-B-cell lymphoma. *N Engl J Med*. 2002;346(25):1937-47.
69. Klein U, Casola S, Cattoretti G, Shen Q, Lia M, Mo T, et al. Transcription factor IRF4 controls plasma cell differentiation and class-switch recombination. *Nat Immunol*. 2006;7(7):773-82.
70. Dabrowska-Iwanicka A, Walewski JA. Primary mediastinal large B-cell lymphoma. *Curr Hematol Malig Rep*. 2014;9(3):273-83.
71. Savage KJ, Monti S, Kutok JL, Cattoretti G, Neuberg D, De Leval L, et al. The molecular signature of mediastinal large B-cell lymphoma differs from that of other diffuse large B-cell lymphomas and shares features with classical Hodgkin lymphoma. *Blood*. 2003;102(12):3871-9.
72. Csernus B, Timar B, Fulop Z, Bognar A, Szepesti A, Laszlo T, et al. Mutational analysis of IgVH and BCL-6 genes suggests thymic B-cells origin of mediastinal (thymic) B-cell lymphoma. *Leuk Lymphoma*. 2004;45(10):2105-10.
73. Leithauser F, Bauerle M, Huynh MQ, Moller P. Isotype-switched immunoglobulin genes with a high load of somatic hypermutation and lack of ongoing mutational activity are prevalent in mediastinal B-cell lymphoma. *Blood*. 2001;98(9):2762-70.
74. Wright G, Tan B, Rosenwald A, Hurt EH, Wiestner A, Staudt LM. A gene expression-based method to diagnose clinically distinct subgroups of diffuse large B cell lymphoma. *Proc Natl Acad Sci U S A*. 2003;100(17):9991-6.
75. Lenz G, Wright G, Dave SS, Xiao W, Powell J, Zhao H, et al. Stromal gene signatures in large-B-cell lymphomas. *N Engl J Med*. 2008;359(22):2313-23.
76. Schmitz R, Wright GW, Huang DW, Johnson CA, Phelan JD, Wang JQ, et al. Genetics and Pathogenesis of Diffuse Large B-Cell Lymphoma. *N Engl J Med*. 2018;378(15):1396-407.

77. Chapuy B, Stewart C, Dunford AJ, Kim J, Kamburov A, Redd RA, et al. Molecular subtypes of diffuse large B cell lymphoma are associated with distinct pathogenic mechanisms and outcomes. *Nat Med.* 2018;24(5):679-90.
78. Wright GW, Huang DW, Phelan JD, Coulibaly ZA, Roulland S, Young RM, et al. A Probabilistic Classification Tool for Genetic Subtypes of Diffuse Large B Cell Lymphoma with Therapeutic Implications. *Cancer Cell.* 2020;37(4):551-68 e14.
79. Wilson WH, Young RM, Schmitz R, Yang Y, Pittaluga S, Wright G, et al. Targeting B cell receptor signaling with ibrutinib in diffuse large B cell lymphoma. *Nat Med.* 2015;21(8):922-6.
80. Lionakis MS, Dunleavy K, Roschewski M, Widemann BC, Butman JA, Schmitz R, et al. Inhibition of B Cell Receptor Signaling by Ibrutinib in Primary CNS Lymphoma. *Cancer Cell.* 2017;31(6):833-43 e5.
81. Grommes C, Pastore A, Palaskas N, Tang SS, Campos C, Schartz D, et al. Ibrutinib Unmasks Critical Role of Bruton Tyrosine Kinase in Primary CNS Lymphoma. *Cancer Discov.* 2017;7(9):1018-29.
82. Morschhauser F, Feugier P, Flinn IW, Gasiorowski R, Greil R, Illes A, et al. A phase II study of venetoclax plus R-CHOP as first-line treatment for patients with diffuse large B-cell lymphoma. *Blood.* 2020.
83. Zhang MC, Tian S, Fu D, Wang L, Cheng S, Yi HM, et al. Genetic subtype-guided immunochemotherapy in diffuse large B cell lymphoma: The randomized GUIDANCE-01 trial. *Cancer Cell.* 2023;41(10):1705-16 e5.
84. Dierlamm J, Murga Penas EM, Bentink S, Wessendorf S, Berger H, Hummel M, et al. Gain of chromosome region 18q21 including the MALT1 gene is associated with the activated B-cell-like gene expression subtype and increased BCL2 gene dosage and protein expression in diffuse large B-cell lymphoma. *Haematologica.* 2008;93(5):688-96.
85. Challa-Malladi M, Lieu YK, Califano O, Holmes AB, Bhagat G, Murty VV, et al. Combined genetic inactivation of beta2-Microglobulin and CD58 reveals frequent escape from immune recognition in diffuse large B cell lymphoma. *Cancer Cell.* 2011;20(6):728-40.
86. Lin SC, Lo YC, Wu H. Helical assembly in the MyD88-IRAK4-IRAK2 complex in TLR/IL-1R signalling. *Nature.* 2010;465(7300):885-90.
87. Janssens S, Beyaert R. Functional diversity and regulation of different interleukin-1 receptor-associated kinase (IRAK) family members. *Mol Cell.* 2003;11(2):293-302.
88. Ye H, Arron JR, Lamothe B, Cirilli M, Kobayashi T, Shevde NK, et al. Distinct molecular mechanism for initiating TRAF6 signalling. *Nature.* 2002;418(6896):443-7.
89. Xia ZP, Sun L, Chen X, Pineda G, Jiang X, Adhikari A, et al. Direct activation of protein kinases by unanchored polyubiquitin chains. *Nature.* 2009;461(7260):114-9.
90. Kim SI, Kwak JH, Zachariah M, He Y, Wang L, Choi ME. TGF-beta-activated kinase 1 and TAK1-binding protein 1 cooperate to mediate TGF-beta1-induced MKK3-p38 MAPK activation and stimulation of type I collagen. *Am J Physiol Renal Physiol.* 2007;292(5):F1471-8.
91. Takaesu G, Kishida S, Hiyama A, Yamaguchi K, Shibuya H, Irie K, et al. TAB2, a novel adaptor protein, mediates activation of TAK1 MAPKKK by linking TAK1 to TRAF6 in the IL-1 signal transduction pathway. *Mol Cell.* 2000;5(4):649-58.
92. Takaesu G, Surabhi RM, Park KJ, Ninomiya-Tsuji J, Matsumoto K, Gaynor RB. TAK1 is critical for I kappa B kinase-mediated activation of the NF-kappaB pathway. *J Mol Biol.* 2003;326(1):105-15.
93. Lenz G, Nagel I, Siebert R, Roschke AV, Sanger W, Wright GW, et al. Aberrant immunoglobulin class switch recombination and switch translocations in activated B cell-like diffuse large B cell lymphoma. *J Exp Med.* 2007;204(3):633-43.
94. Cassard S, Salamero J, Hanau D, Spehner D, Davoust J, Fridman WH, Bonnerot C. A tyrosine-based signal present in Ig alpha mediates B cell receptor constitutive internalization. *J Immunol.* 1998;160(4):1767-73.
95. Geahlen RL. Syk and pTyr<sup>d</sup>: Signaling through the B cell antigen receptor. *Biochim Biophys Acta.* 2009;1793(7):1115-27.
96. Li Z, Wahl MI, Eguinoa A, Stephens LR, Hawkins PT, Witte ON. Phosphatidylinositol 3-kinase-gamma activates Bruton's tyrosine kinase in concert with Src family kinases. *Proc Natl Acad Sci U S A.* 1997;94(25):13820-5.
97. Rawlings DJ, Scharenberg AM, Park H, Wahl MI, Lin S, Kato RM, et al. Activation of BTK by a phosphorylation mechanism initiated by SRC family kinases. *Science.* 1996;271(5250):822-5.
98. Watanabe D, Hashimoto S, Ishiai M, Matsushita M, Baba Y, Kishimoto T, et al. Four tyrosine residues in phospholipase C-gamma 2, identified as Btk-dependent phosphorylation sites, are required for B cell antigen receptor-coupled calcium signaling. *J Biol Chem.* 2001;276(42):38595-601.
99. Barbazuk SM, Gold MR. Protein kinase C-delta is a target of B-cell antigen receptor signaling. *Immunol Lett.* 1999;69(2):259-67.
100. Su TT, Guo B, Kawakami Y, Sommer K, Chae K, Humphries LA, et al. PKC-beta controls I kappa B kinase lipid raft recruitment and activation in response to BCR signaling. *Nat Immunol.* 2002;3(8):780-6.
101. Sommer K, Guo B, Pomerantz JL, Bandaranayake AD, Moreno-Garcia ME, Ovechkina YL, Rawlings DJ. Phosphorylation of the CARMA1 linker controls NF-kappaB activation. *Immunity.* 2005;23(6):561-74.
102. Ruefli-Brasse AA, French DM, Dixit VM. Regulation of NF-kappaB-dependent lymphocyte activation and development by paracaspase. *Science.* 2003;302(5650):1581-4.
103. Hanahan D, Weinberg RA. Hallmarks of cancer: the next generation. *Cell.* 2011;144(5):646-74.

104. Nestic M, Sonderkaer M, Brondum RF, El-Galaly TC, Pedersen IS, Bogsted M, Dybkaer K. The mutational profile of immune surveillance genes in diagnostic and refractory/relapsed DLBCLs. *BMC Cancer*. 2021;21(1):829.
105. de Charette M, Houot R. Hide or defend, the two strategies of lymphoma immune evasion: potential implications for immunotherapy. *Haematologica*. 2018;103(8):1256-68.
106. Brown PJ, Wong KK, Felce SL, Lyne L, Spearman H, Soilleux EJ, et al. FOXP1 suppresses immune response signatures and MHC class II expression in activated B-cell-like diffuse large B-cell lymphomas. *Leukemia*. 2016;30(3):605-16.
107. Fangazio M, Ladewig E, Gomez K, Garcia-Ibanez L, Kumar R, Teruya-Feldstein J, et al. Genetic mechanisms of HLA-I loss and immune escape in diffuse large B cell lymphoma. *Proc Natl Acad Sci U S A*. 2021;118(22).
108. Cycon KA, Rimsza LM, Murphy SP. Alterations in CIITA constitute a common mechanism accounting for downregulation of MHC class II expression in diffuse large B-cell lymphoma (DLBCL). *Exp Hematol*. 2009;37(2):184-94.
109. Chapuy B, Roemer MG, Stewart C, Tan Y, Abo RP, Zhang L, et al. Targetable genetic features of primary testicular and primary central nervous system lymphomas. *Blood*. 2016;127(7):869-81.
110. Georgiou K, Chen L, Berglund M, Ren W, de Miranda NF, Lisboa S, et al. Genetic basis of PD-L1 overexpression in diffuse large B-cell lymphomas. *Blood*. 2016;127(24):3026-34.
111. Godfrey J, Tumuluru S, Bao R, Leukam M, Venkataraman G, Phillip J, et al. PD-L1 gene alterations identify a subset of diffuse large B-cell lymphoma harboring a T-cell-inflamed phenotype. *Blood*. 2019;133(21):2279-90.
112. Xu-Monette ZY, Zhou J, Young KH. PD-1 expression and clinical PD-1 blockade in B-cell lymphomas. *Blood*. 2018;131(1):68-83.





# 2

## MALT1-dependent cleavage of CYLD promotes NF- $\kappa$ B signaling and growth of aggressive B-cell receptor-dependent lymphomas

Marthe Minderman<sup>1,2,3</sup>, Hildo C. Lantermans<sup>1,2,3</sup>, Leonie J. Grüneberg<sup>1,2,3</sup>,  
Saskia A. G. M. Cillessen<sup>1,4</sup>, Richard J. Bende<sup>1,2,3</sup>, Carel J. M. van Noesel<sup>1,2,3</sup>,  
Marie José Kersten<sup>2,5</sup>, Steven T. Pals<sup>1,2,3,6</sup>, Marcel Spaargaren<sup>1,2,3,6</sup>

<sup>1</sup>Department of Pathology, Amsterdam UMC, location University of Amsterdam, Amsterdam, The Netherlands;

<sup>2</sup>Lymphoma and Myeloma Center Amsterdam (LYMMCARE), Amsterdam, The Netherlands; <sup>3</sup>Cancer Center Amsterdam (CCA), Cancer Biology and Immunology, Target & Therapy Discovery, Amsterdam, The Netherlands;

<sup>4</sup>Department of Pathology, Amsterdam UMC, location VU University, Amsterdam, Netherlands; <sup>5</sup>Department of Hematology, Amsterdam UMC, location University of Amsterdam, Amsterdam, The Netherlands; <sup>6</sup>The authors share last authorship

## ABSTRACT

The paracaspase mucosa-associated lymphoid tissue 1 (MALT1) is a protease and scaffold protein essential in propagating B-cell receptor (BCR) signaling to NF- $\kappa$ B. The deubiquitinating enzyme cylindromatosis (CYLD) is a recently discovered MALT1 target that can negatively regulate NF- $\kappa$ B activation. Here, we show that low expression of CYLD is associated with inferior prognosis of diffuse large B-cell lymphoma (DLBCL) and mantle cell lymphoma (MCL) patients, and that chronic BCR signaling propagates MALT1-mediated cleavage and, consequently, inactivation and rapid proteasomal degradation of CYLD. Ectopic overexpression of WT CYLD or a MALT1-cleavage resistant mutant of CYLD reduced phosphorylation of I $\kappa$ B $\alpha$ , repressed transcription of canonical NF- $\kappa$ B target genes and impaired growth of BCR-dependent lymphoma cell lines. Furthermore, silencing of CYLD expression rendered BCR-dependent lymphoma cell lines less sensitive to inhibition of NF- $\kappa$ B signaling and cell proliferation by BCR pathway inhibitors, *e.g.*, the BTK inhibitor ibrutinib, indicating that these effects are partially mediated by CYLD. Taken together, our findings identify an important role for MALT1-mediated CYLD cleavage in BCR signaling, NF- $\kappa$ B activation and cell proliferation, which provides novel insights into the underlying molecular mechanisms and clinical potential of inhibitors of MALT1 and ubiquitination enzymes as promising therapeutics for DLBCL, MCL and potentially other B-cell malignancies.

## INTRODUCTION

Diffuse large B-cell lymphoma (DLBCL) and mantle cell lymphoma (MCL) are aggressive subtypes of B-cell non-Hodgkin lymphoma (B-NHL) characterized by a poor prognosis. The NF- $\kappa$ B signaling pathway is constitutively active in activated B-cell-like (ABC) DLBCL as a result of oncogenic mutations in the Toll-like receptor (TLR) signaling pathway and the B-cell antigen receptor (BCR) signaling pathway (1-3). Although these mutations are rare in MCL, a subset of MCL cell lines was also demonstrated to be dependent on BCR-mediated, chronic activation of canonical NF- $\kappa$ B signaling (4, 5). Intriguingly, analysis of the immunoglobulin heavy chain (*IGHV*) gene repertoire points towards a possible role for chronic (super) antigen-dependent BCR activation in a subset of ABC DLBCL and MCL patients (6, 7). Promising single-agent efficacy of the Bruton's tyrosine kinase (BTK) inhibitor ibrutinib supports the notion that BCR signaling is essential in the pathogenesis of ABC DLBCL and MCL (8, 9).

Formation of the caspase recruitment domain family member 11 (CARD11)—B-cell lymphoma 10 (BCL10)—mucosa-associated lymphoid tissue lymphoma translocation gene 1 (MALT1) complex (CBM complex) is a key event in linking BCR antigen recognition to canonical NF- $\kappa$ B activation (reviewed by Thome *et al.* (10)). MALT1 functions as a scaffolding protein allowing recruitment and activation of the E3-ubiquitin ligase tumor necrosis factor receptor (TNFR)-associated factor 6 (TRAF6). TRAF6 mediates Lys-63-linked polyubiquitination of various targets including the regulatory gamma subunit of the inhibitor of I $\kappa$ B kinase (IKK) complex (IKK- $\gamma$  or NEMO), allowing full activation of the IKK complex (11, 12). Next to its function as scaffold protein, MALT1 possesses protease activity and is able to cleave and inactivate negative regulators of NF- $\kappa$ B signaling, *e.g.* RelB and A20 (13-15). Inhibition of MALT1 proteolytic activity impairs survival in a subset of MCL and ABC DLBCL cell lines as well as in *ex vivo* cultured primary DLBCL, suggesting that cleavage of these substrates is essential for lymphomagenesis (16-22).

Another negative regulator of NF- $\kappa$ B is the deubiquitinating enzyme cylindromatosis (CYLD), which can hydrolyze Lys-63-linked ubiquitin chains of various targets, including TRAF2, TRAF6 and IKK- $\gamma$  (23-25). Whereas deletion or mutation of the gene encoding CYLD is a frequently occurring genomic aberration in multiple myeloma (MM), these events are extremely uncommon in DLBCL and MCL (26, 27). Previous studies have indicated that CYLD deubiquitinase activity can be repressed by IKK-mediated phosphorylation as well as by (para)caspase-mediated cleavage, including, at least in T-cells, by MALT1 (28-31). This prompted us to investigate if in DLBCL and MCL similar, non-genetic, mechanisms contribute to inactivation of CYLD. Here, we demonstrate that low expression of CYLD is associated with a poor prognosis of (ABC) DLBCL and MCL patients, and that chronic BCR signaling controls cleavage-mediated inactivation of

CYLD by the paracaspase MALT1, followed by rapid proteasomal degradation. Ectopic overexpression of WT CYLD or a MALT1-cleavage resistant mutant of CYLD reduced NF- $\kappa$ B activity and growth of BCR-dependent lymphoma cell lines. Furthermore, silencing of CYLD renders BCR-dependent cell lines less sensitive to BCR signalosome inhibitors, indicating that their inhibitory effects on cell proliferation and NF- $\kappa$ B activity are partially CYLD dependent.

## MATERIALS AND METHODS

### Cell culture and primary cell isolation

DLBCL and MCL cell lines were cultured as previously described (32). Primary DLBCL and peripheral blood derived MCL cells were obtained after routine diagnostics or follow-up procedures at the Amsterdam University Medical Centers, the Netherlands. DLBCLs were purified using Ficoll and B cell isolation kit (Miltenyi Biotec, Bergisch Gladbach, Germany). MCLs were sorted on a BD-FACS-Aria IIu to obtain CD5+/CD19+ cells. DLBCLs were classified as either GCB- or non-GCB like, using the immunohistochemical algorithm of Hans *et al.* (33). This study was approved by the AMC Medical Committee on Human Experimentation. Informed consent was obtained in accordance with the revised Declaration of Helsinki 2008.

### Cell viability and cell cycle analyses

For growth assays,  $10\text{--}50 \times 10^3$  cells were plated in 96-well plates and treated as indicated. Cells were analyzed on a FACSCanto II flow cytometer (BD Biosciences, Franklin Lakes, New Jersey, USA) and viability was determined using 7-AAD viability staining solution (Thermo Fisher Scientific, Waltham, Massachusetts, USA). For long-term competition assays, cells were passaged every 3-4 days at a density of  $0.3 \times 10^6$  cells/ml. For cell cycle analysis, cells were incubated for 1 hour with  $20 \mu\text{M}$  BrdU (Sigma Aldrich, Saint Louis, Missouri, USA) and subsequently stained with anti-BrdU FITC (clone B44, BD Biosciences) and  $100 \text{ nM}$  To-pro 3 Iodide (Invitrogen Life Technologies, Carlsbad, California, USA).

### Statistical analysis

Survival analysis was performed using the Kaplan–Meier method and log-rank test. Data is presented as mean  $\pm$  SD of at least three independently performed experiments. Experimental data were analyzed using one-way ANOVA followed by Tukey's multiple comparisons test or two-way ANOVA followed by Sidak's multiple comparisons test. The Brown-Forsythe test was used to check for equal variances. Differences were considered significant when  $p < 0.05$ .

Please see Supplementary Methods for additional materials and methods.

## RESULTS

### Low *CYLD* expression is associated with inferior overall survival in DLBCL and MCL

Analysis of gene expression microarray data shows that *CYLD* is expressed in normal B-cell subsets and all analyzed B-cell malignancies (Figure 1A). In line with previous studies, the microarray data show that *CYLD* expression is lost in 3.3% (18/542) of MM. In contrast, *CYLD* expression was lost in only 0.6% (2/350) of DLBCL.

Interestingly, in line with its potential function as a tumor suppressor, low *CYLD* expression significantly correlates with poor overall survival in DLBCL and MCL. If DLBCL patients were separated into groups of low and high mRNA expression with average *CYLD* expression as cutoff, the median overall survival was below 6 years in the *CYLD* low patients, while it was over 10 years in the *CYLD* high patients (Figure 1B). Of relevance, given the worse prognosis of ABC versus GCB DLBCL patients, no differential (i.e., lower) expression of *CYLD* was observed in ABC versus GCB DLBCL (Figure 1A). When classified into ABC or GCB DLBCL, ABC DLBCL patients with low *CYLD* expression showed a trend towards worse overall survival ( $p=0.085$ ), while this was not the case for GCB DLBCL patients (Supplemental figure 1A). In MCL patients, the median overall survival was only 1,5 years in the *CYLD* low patients, compared to almost 4 years in the *CYLD* high patients (Figure 1B). Taken together, our findings suggest that, although loss of *CYLD* is an uncommon mechanism in DLBCL and MCL, low *CYLD* expression is associated with inferior overall survival in DLBCL and MCL patients.

### Cleavage of *CYLD* is dependent on MALT1 protease activity

To further explore the potential role of *CYLD* as a tumor suppressor, we assessed *CYLD* mRNA and protein levels in a panel of DLBCL and MCL cell lines. In line with the primary lymphoma cases, we observed variable levels of *CYLD* mRNA expression in DLBCL and MCL cell lines (Figure 1C). Interestingly, using an antibody raised against a C-terminal epitope of *CYLD*, we detected a ~110 kDa protein corresponding with the anticipated molecular weight of *CYLD* in all cell DLBCL lines, but exclusively in the ABC DLBCL cell lines also a prominent protein of ~70 kDa was observed (Figure 1D). This C-terminal *CYLD* fragment was also present in the MCL cell lines Jeko, Mino and Rec1, but was absent in Z138, Maver and Granta. In cell lines expressing only full-length *CYLD*, a strong correlation between *CYLD* mRNA expression and *CYLD* protein expression was observed (Supplemental Figure 1B). Interestingly, in a panel of primary DLBCL and MCL cases we detected *CYLD* protein expression in all samples and a ~70 kDa cleaved *CYLD* fragment was observed in 1/5 GCB DLBCL (20%), 4/7 ABC DLBCL (57%) and 6/7 MCL cases (86%) (Figure 1E).

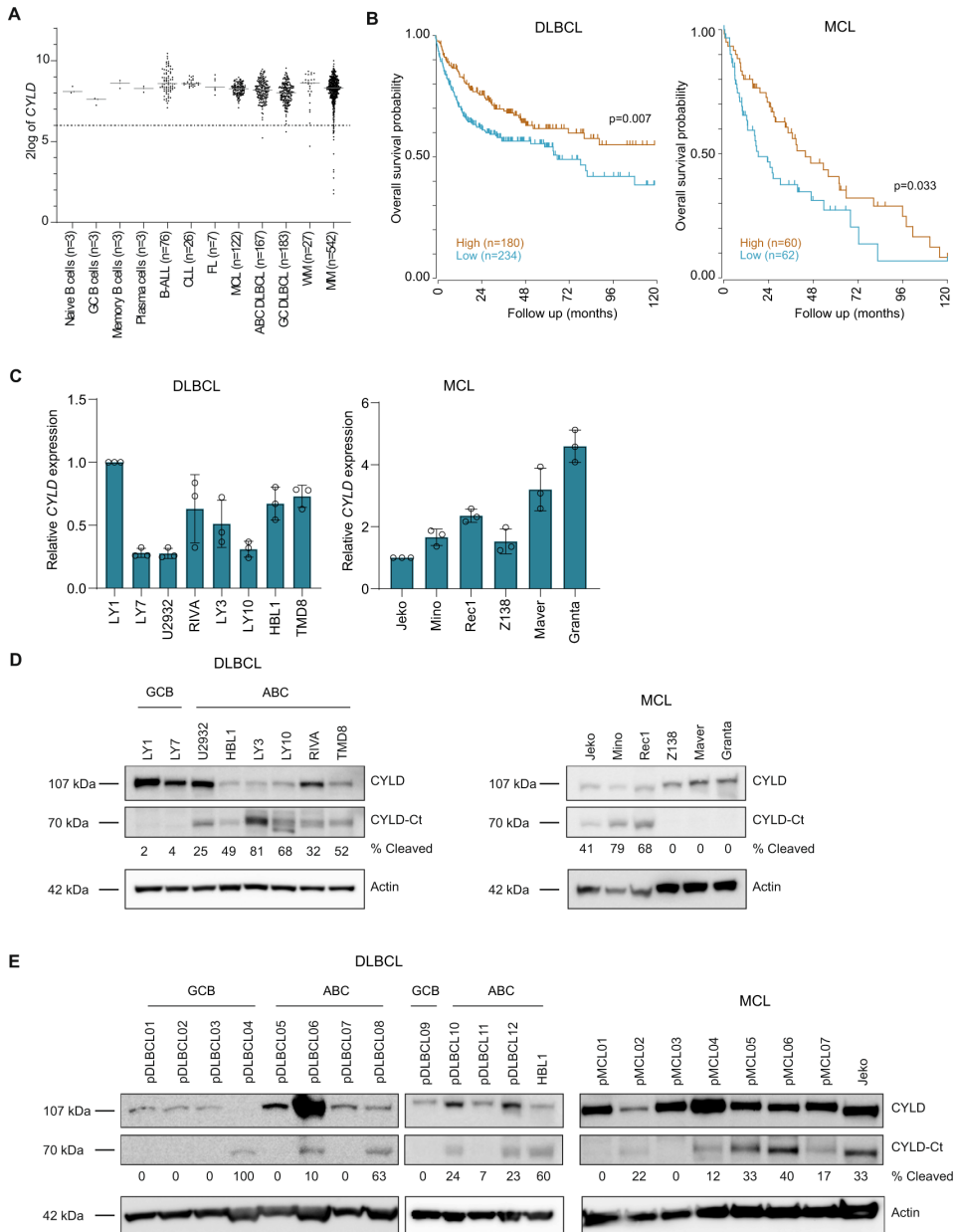


**Figure 1. CYLD is variably expressed in B-cell non-Hodgkin lymphomas (B-NHLs).** **A** CYLD mRNA expression analysis of publicly available micro-array datasets of naïve B cells, GC (germinal center) B cells, memory B cells, plasma cells, B-cell acute lymphoblastic leukemia (B-ALL), chronic lymphocytic leukemia (CLL), follicular lymphoma (FL), mantle cell lymphoma (MCL), germinal center B-cell-like diffuse large B-cell lymphoma (GCB-DLBCL), activated B-cell-like diffuse large B-cell lymphoma (ABC-DLBCL), Waldenström's macroglobulinemia (WM) and multiple myeloma (MM). The gray line represents the median expression value within each group. The dotted black line shows the threshold value (i.e., log-transformed probe intensity values of <math><26</math>). **B** Kaplan-Meier survival curve showing overall survival probability in CYLD high versus CYLD low expressing DLBCL and MCL patients. The cut off was based on the average CYLD expression within each cohort. The log-rank test was used to compare the survival distributions of the two

groups. **C** RT-qPCR analysis of CYLD mRNA expression in DLBCL and MCL cell lines. RPLP0 was used as an input control and data are normalized to CYLD expression in LY1 for DLBCL cell lines and Jeko for MCL cell lines. The mean  $\pm$  SD of three independent experiments performed in triplicate is shown. **D** Immunoblot analysis of CYLD expression in DLBCL and MCL cell lines using an antibody raised against a C-terminal epitope which detects full-length CYLD and a C-terminal fragment of CYLD (CYLD-Ct).  $\beta$ -actin was used as a loading control. **E** Immunoblot analysis of CYLD expression in primary DLBCL and MCL samples.  $\beta$ -actin was used as a loading control.

Previously, Staal *et al.* demonstrated that CYLD can be cleaved in T-cells by MALT1 at arginine 324 generating an N-terminal fragment of 40 kDa and a C-terminal fragment of 70 kDa (31). To assess whether BCR signaling results in MALT1-mediated CYLD cleavage, we treated cell lines with phorbol myristate acetate (PMA) and ionomycin, which activate protein kinase C (PKC), a key intermediate of BCR-controlled MALT1 activation. In line with increased NF- $\kappa$ B activation, phosphorylation of I $\kappa$ B- $\alpha$  at serine 32 was increased in all cell lines and accordingly, total I $\kappa$ B- $\alpha$  levels were reduced as a consequence of proteasomal degradation. Moreover, in all cell lines treatment with PMA/ionomycin resulted in decreased levels of the 110 kDa full-length CYLD protein accompanied by increased levels of the 70 kDa C-terminal fragment (Figure 2A). Importantly, pre-treatment with the MALT1 tetrapeptide protease inhibitor z-VRPR-fmk inhibits formation of the 70 kDa C-terminal fragment upon PMA/ionomycin treatment, demonstrating that CYLD cleavage is dependent on MALT1 proteolytic activity (Figure 2B). The observation that CYLD is spontaneously cleaved in a subset of cell lines suggests that MALT1 is constitutively active in these cells (Figure 1D). Since differences in MALT1 protein expression do not account for the observed differences in cleaved CYLD levels (Figure 2C), this suggests that post-translational regulation of MALT1 activity, not MALT1 expression as such, determines CYLD cleavage in lymphoma cell lines.

### **CYLD is constitutively cleaved in cell lines dependent on chronic BCR signaling**

ABC DLBCL tumors frequently harbor activating mutations in *CD79A/B* and *CARD11* which propagate 'chronic' BCR signaling (1, 3). Cell lines harboring mutations in *CD79A* (LY10) or *CD79B* (HBL1 and TMD8) were highly sensitive to inhibition of BTK through treatment with ibrutinib and to inhibition of PKC through treatment with sotrastaurin, whereas LY3 cells harboring an activating mutation in *CARD11* downstream of BTK and PKC were resistant (Figure 3A). In addition, blocking BCR signaling downstream of *CARD11* by the MALT1 inhibitory peptide z-VRPR-fmk strongly reduced cell growth in all cell lines with *CARD11* or *CD79A/B* mutations (Figure 3A).

Since MALT1 is a key signaling protein downstream of the BCR, we hypothesized that chronic BCR signaling contributes to CYLD cleavage in ABC DLBCL cell lines. Indeed, upon treatment with ibrutinib, sotrastaurin or z-VRPR-fmk, we observed a strong reduction in the 70 kDa cleavage product of CYLD in LY10, which was accompanied

by accumulation of full-length CYLD (Figure 3B). Similar results were obtained in ABC DLBCL cell lines U2932, HBL1 and TMD8 (Supplementary Figure 2). Notably, in line with harboring an oncogenic *CARD11* mutation, LY3 only showed a reduction in CYLD cleavage upon incubation with z-VRPR-fmk but not with sotrastaurin or ibrutinib (Figure 3B). In addition, except for ibrutinib and sotrastaurin treatment of LY3 (as expected), treatment with these BCR signalosome inhibitors substantially reduced expression of the NF- $\kappa$ B target and pro-survival protein BCL-XL in the ABC-DLBCL cell lines (Figure 3B and Supplementary Figure 2).

Recent studies showed that knockdown or pharmacological inhibition of central components of the BCR cascade was also toxic to a subset of MCL cell lines (4, 17). In line with these studies, we confirmed that MCL cell lines Jeko, Mino and Rec1 strongly respond to treatment with ibrutinib, sotrastaurin or Z-VRPR-fmk (Figure 3C). Moreover, inhibition of the BCR signaling cascade resulted in a substantial reduction of cleaved CYLD levels, accompanied by accumulation of full-length CYLD and downregulation of BCL-XL expression (Figure 3D). In contrast, Z138, Maver and Granta were relatively resistant to inhibition of BTK, PKC or MALT1 suggesting that these cell lines do not depend on BCR signaling for their survival (Figure 3C). Indeed, these cell lines did not show cleavage of CYLD, indicating a lack of MALT1 proteolytic activity (Figure 1D). Hence, these data indicate that BCR signaling mediates survival as well as CYLD cleavage in BCR-dependent ABC DLBCL and MCL cell lines.

### **CYLD represses cell growth and NF- $\kappa$ B activity**

To assess whether MALT1-mediated CYLD cleavage directly contributes to growth of BCR-dependent lymphoma cell lines, we generated a CYLD mutant that can no longer be cleaved by MALT1 (CYLD R324A) (31). Using a retroviral overexpression system, we expressed either wild type CYLD or CYLD R324A in a panel of lymphoma cell lines. CYLD expression clearly led to reduced survival in ABC DBCL cell lines LY10 and RIVA as well as the BCR-dependent MCL cell line Mino (Figure 4A). A similar effect was observed for CYLD R324A, demonstrating that MALT1-mediated cleavage of CYLD is not required for the observed growth repression. Interestingly, in LY10 the inhibitory effect of CYLD expression was more pronounced upon overexpression of CYLD R324A, which is fully resistant to MALT1-mediated cleavage. Immunoblot analysis demonstrates that these cell lines lack sufficient MALT1 activity to effectively cleave all ectopically overexpressed wild type CYLD, explaining why ectopic expression of wild type CYLD also confers a prominent growth disadvantage (Figure 4B). In the BCR-independent cell lines LY1 and Z138, CYLD expression did not affect cell survival (Figure 4C). Moreover, immunoblot analysis shows that these cell lines indeed lack MALT1 protease activity as we only detected full-length CYLD upon expression of the wild type CYLD construct (Figure 4D).

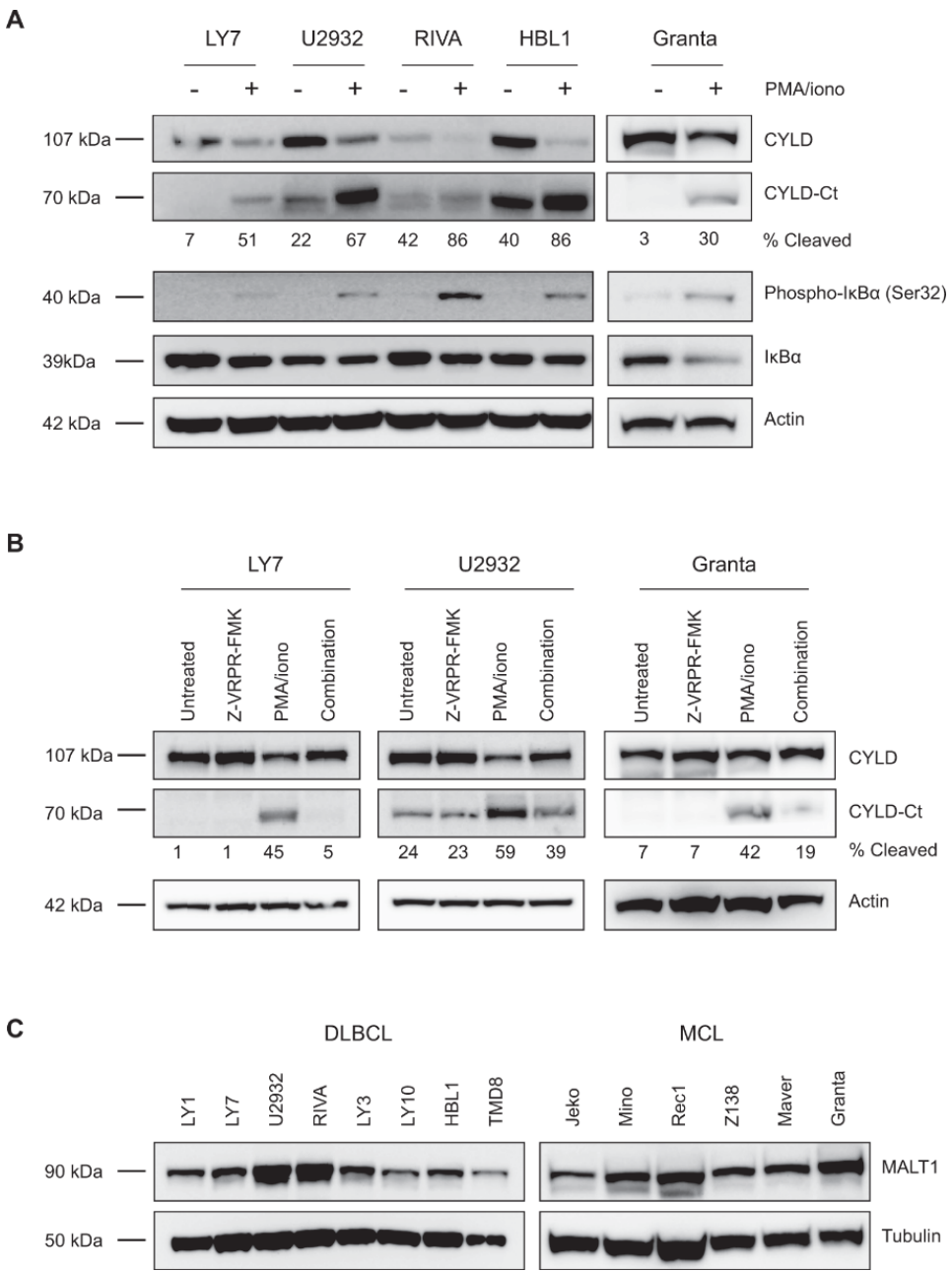


**Figure 2. CYLD is cleaved by MALT1 protease.** **A** Immunoblot analysis of CYLD cleavage following treatment with phorbol myristate acetate (PMA) and ionomycin. Cells were treated for 1 h with PMA (50 ng/ml) and ionomycin (1 µg/ml) as indicated. Phosphorylated IκBα (Ser32) and total IκBα were used as positive controls for PMA/ionomycin stimulation; β-actin was used as a loading control. **B** Immunoblot analysis of CYLD cleavage following treatment with PMA/ionomycin and/or MALT1 inhibitor Z-VRPR-FMK. Cells were pre-treated for 1 h with 75 µM Z-VRPR-fmk before incubation for 1 h with PMA (50 ng/ml) and ionomycin (1 µg/ml) as indicated. β-actin was used as a loading control. **C** Immunoblot analysis of MALT1 expression in DLBCL and MCL cell lines. β-tubulin was used as a loading control.

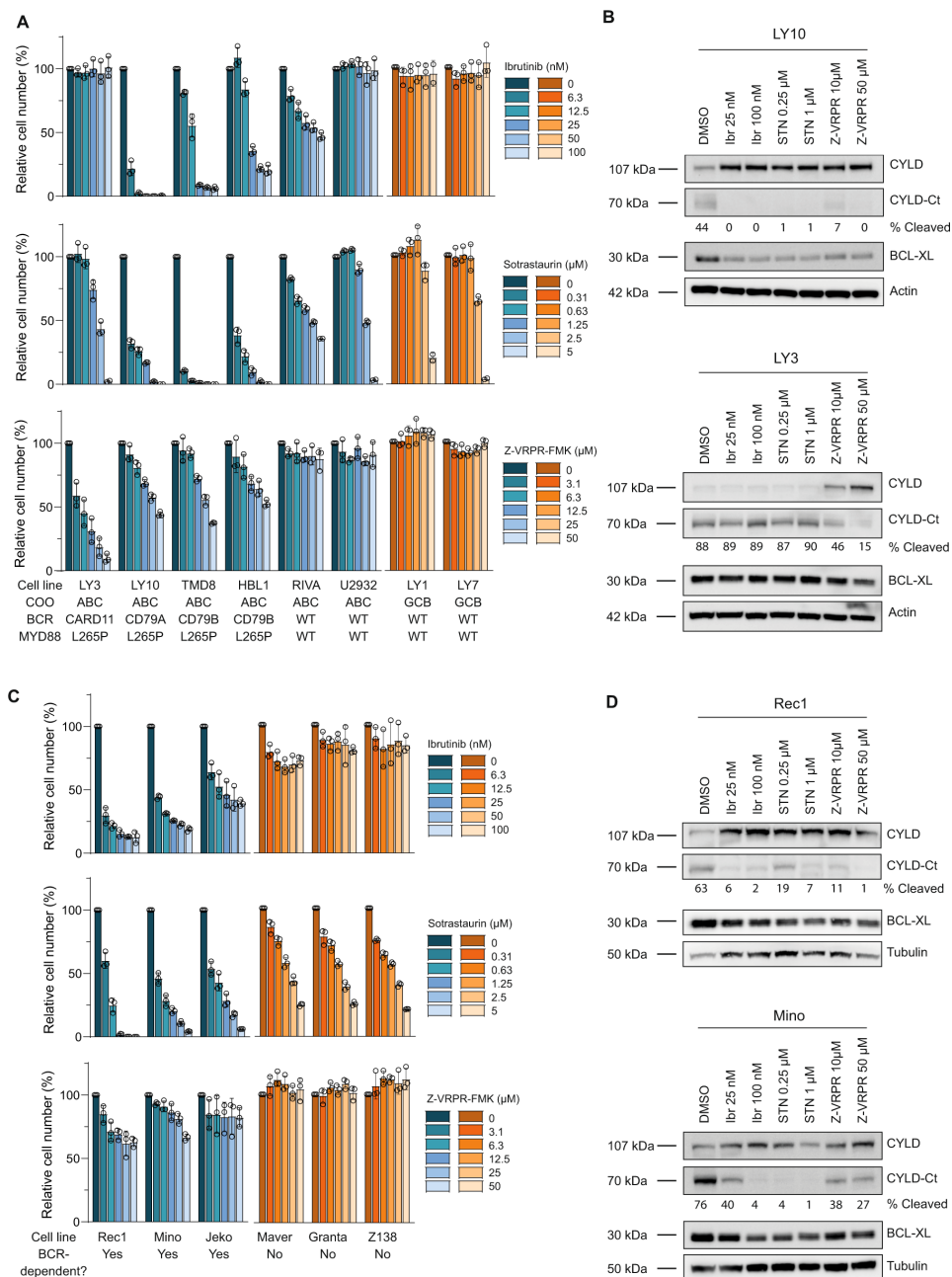


**Figure 3. CYLD is constitutively cleaved in ABC DLBCL and BCR-dependent MCL cell lines.** **A** Flow cytometric analysis of the number of viable cells, as determined by 7-AAD staining, after 5 days of treatment with indicated concentrations of BTK inhibitor Ibrutinib, PKC inhibitor Sotrastaurin or MALT1 inhibitor Z-VRPR-FMK. The number of viable cells was normalized to the vehicle-treated condition. Data are presented as mean  $\pm$  SD of three independent experiments. **B** Immunoblot analysis of CYLD cleavage in DLBCL cell lines LY3 and LY10 using an antibody raised against a C-terminal epitope which detects full-length CYLD and a C-terminal fragment of CYLD (CYLD-Ct). Cells were incubated with indicated concentrations of the different BCR signalosome inhibitors for 48 h. BCL-XL protein levels were determined

as a positive control for efficacy of the inhibitors;  $\beta$ -actin was used as loading control. **C** Flow cytometric analysis of the number of viable cells, as determined by 7-AAD staining, after 7 days of treatment with indicated concentrations of BTK inhibitor Ibrutinib, PKC inhibitor Sotrastaurin or MALT1 inhibitor Z-VRPR-FMK. The number of viable cells was normalized to the vehicle-treated condition. Data are presented as mean  $\pm$  SD of three independent experiments. **D** Immunoblot analysis of CYLD cleavage in MCL cell lines Rec1 and Mino using an antibody raised against a C-terminal epitope which detects full-length CYLD and a C-terminal fragment of CYLD (CYLD-Ct). Cells were incubated with indicated concentrations of the different BCR signalosome inhibitors for 72 h. BCL-XL protein levels were determined as a positive control for efficacy of the inhibitors;  $\beta$ -tubulin was used as loading control.

To study whether the CYLD-dependent growth inhibition is associated with reduced NF- $\kappa$ B activation, we performed immunoblot analysis to assess I $\kappa$ B- $\alpha$  phosphorylation. Since phosphorylation of I $\kappa$ B- $\alpha$  at serine 32 leads to its rapid proteasomal degradation, cells were co-incubated with proteasome inhibitor MG132. Indeed, we observed strong accumulation of phosphorylated I $\kappa$ B- $\alpha$  in LY10 and Mino incubated with MG132 (Figure 4E). Intriguingly, phosphorylated I $\kappa$ B- $\alpha$  was strongly reduced in cells expressing CYLD (WT or R324A mutant), suggesting that CYLD represses NF- $\kappa$ B signaling upstream of the IKK complex. Analysis of *CYLD* mRNA ensured equal expression of wild type and mutated CYLD (Supplemental Figure 3A). In addition, we performed RT-qPCR to determine expression of a panel of established NF- $\kappa$ B target genes, most of which are also implicated in lymphomagenesis (34). In LY10, a ABC DLBCL cell line characterized by constitutive MALT1 activity, ectopic expression of CYLD reduced expression of *IL6*, *IL10*, *CXCL10*, *CCR7*, *NFKBIA*, *CD80* and *ICAM1* (Figure 4F). In Mino, *IL6*, *IL10* and *CXCL10* were not expressed, but we did observe downregulation of *TNFAIP3*, *NFKBIA*, *CD80* and *ICAM1* upon expression of CYLD (WT or R324A mutant). Furthermore, in line with down regulation of *IL-6* and *IL-10*, we observed reduced phosphorylated STAT3 and total STAT3 levels in LY10 cells expressing CYLD (WT or R324A mutant). In accordance with a lack of *IL-6* and *IL-10* expression, we did not detect basal levels of phosphorylated STAT3 in Mino (Supplemental Figure 3B).

CYLD has also been reported to act as a negative regulator of Wnt/ $\beta$ -catenin signaling in MM (35); however, in DLBCL cell lines LY10 and RIVA, we hardly detected nuclear beta-catenin and in Mino nuclear beta-catenin levels were not affected by ectopic CYLD expression (Supplemental Figure 3C). In addition, CYLD was previously shown to be involved in TCR-induced JNK phosphorylation (31); however, we did not detect altered JNK phosphorylation upon ectopic expression of CYLD (Supplemental Figure 3D). Altogether, our findings indicate that full-length CYLD represses growth of BCR-dependent cell lines, not by affecting Wnt/ $\beta$ -catenin or JNK signaling, but through suppression of NF- $\kappa$ B activity.

### **MALT1-dependent cleavage suppresses activity of CYLD and promotes its proteosomal degradation**

To assess the functionality of the CYLD fragments produced by MALT1-mediated cleavage, we ectopically expressed the resulting N-terminal or C-terminal fragment of CYLD, and for comparison also wild type CYLD or CYLD R324A (Figure 5A and Supplemental Figure 4A). Expression of the N-terminal CYLD fragment did not affect cell growth, while expression of the C-terminal CYLD fragment did reduce cell growth, albeit in LY10 to a lesser extent than expression of full-length CYLD. Likewise, expression of the N-terminal fragment in LY10 did not result in suppression of I $\kappa$ B- $\alpha$  phosphorylation, whereas I $\kappa$ B- $\alpha$  phosphorylation was slightly reduced in cells expressing the C-terminal fragment (Figure 5C).

To further explore the functional implications of proteolytic cleavage of CYLD, we examined the fate of the endogenous C-terminal and N-terminal cleavage products. In both Mino and LY10, the C-terminal and N-terminal CYLD fragment were no longer detectable following 16 hours of ibrutinib treatment, suggesting that these fragments are unstable (Figure 5D). Addition of proteasome inhibitor MG132 to the ibrutinib-treated cells resulted in stabilization of both the C-terminal and N-terminal CYLD fragment (Figure 5E). These data indicate that, following MALT1-mediated cleavage, the C-terminal and N-terminal CYLD fragment undergo subsequent degradation by the proteasome. In accordance, we observed accumulation of both the C-terminal and N-terminal CYLD fragment in LY10 and Mino solely incubated with the proteasome inhibitor MG132 (Supplemental Figure 4C). Thus, after MALT1-mediated cleavage, the resulting CYLD fragments are quickly degraded by the proteasome.

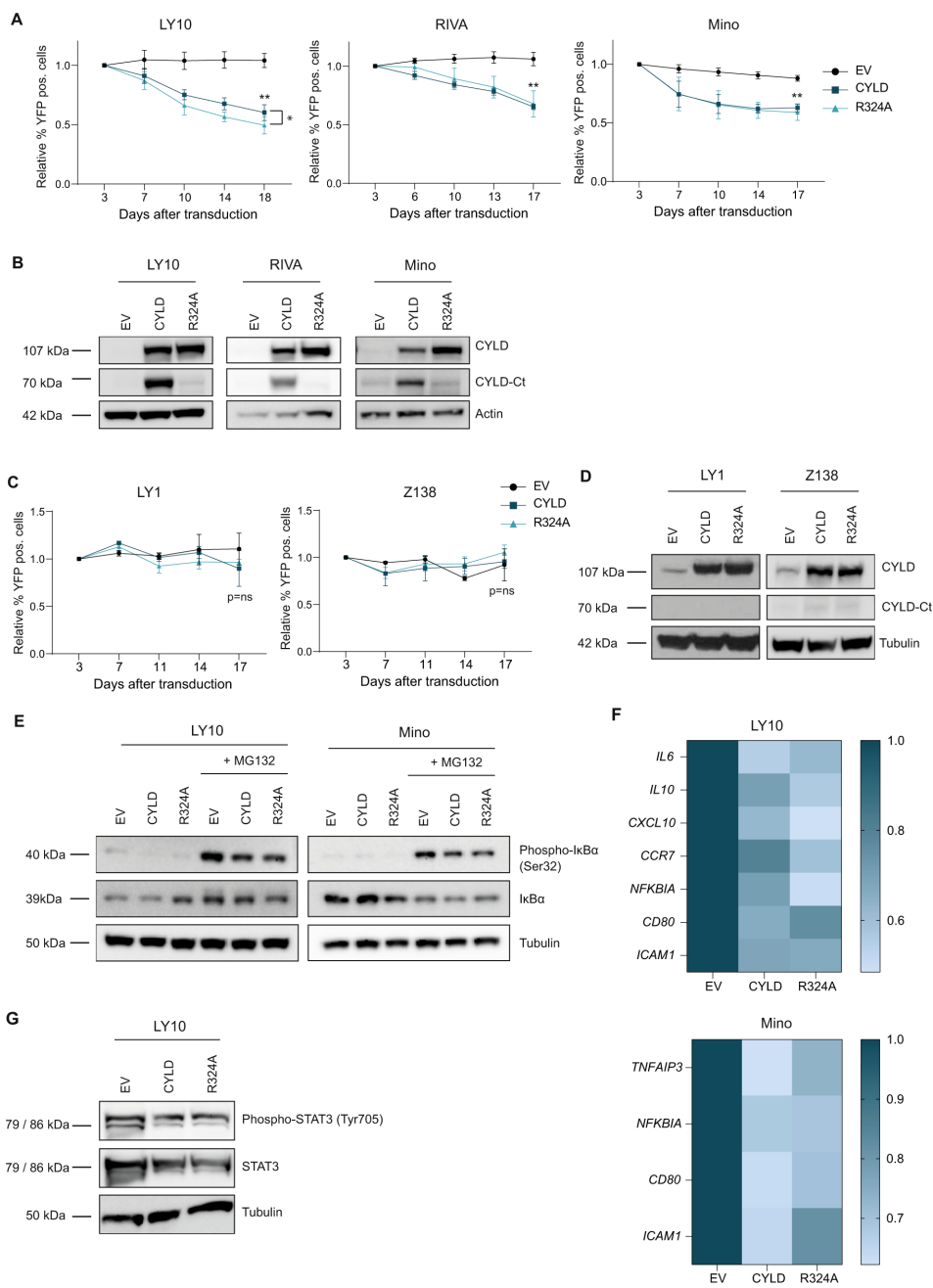


**Figure 4. Ectopic expression of non-cleavable CYLD inhibits cell growth and NF-κB pathway activity.** **A** Flow cytometric analysis of LY10, RIVA and Mino cells transduced with an empty vector (EV) or a CYLD (wildtype or R324A mutant) containing bicistronic vector co-expressed with YFP. The percentage of YFP positive cells was followed in time and plotted as the percentage of YFP+ cells, normalized to the value at day 3 following retroviral transduction. The mean ± SD of at least three independent transductions is shown. \*P < 0.05; \*\*P < 0.01 using 1-way ANOVA with Tukey's multiple comparisons test. **B** Immunoblot

analysis of CYLD in LY10, RIVA and Mino using an antibody raised against a C-terminal epitope which detects full-length CYLD and a C-terminal fragment of CYLD (CYLD-Ct). Cells were transduced with an empty vector (EV) or an expression vector for CYLD (WT or non-cleavable R324A mutant) and sorted for YFP expression.  $\beta$ -actin was used as loading control. **C** Flow cytometric analysis of LY1 and Z138 cells transduced with an empty vector (EV) or a CYLD (wildtype or R324A mutant) containing bicistronic vector co-expressed with YFP. The percentage of YFP positive cells was followed in time and plotted as the percentage of YFP+ cells, normalized to the value at day 3 or day 4 following retroviral transduction. The mean  $\pm$  SD of three independent transductions is shown.  $P > 0.05$ ; ns (non-significant) using 1-way ANOVA with Tukey's multiple comparisons test. **D** Immunoblot analysis of CYLD in LY1 and Z138 using an antibody raised against a C-terminal epitope which detects full-length CYLD and a C-terminal fragment of CYLD (CYLD-Ct). Cells were transduced with an empty vector (EV) or an expression vector for CYLD (WT or non-cleavable R324A mutant) and sorted for YFP expression.  $\beta$ -tubulin was used as loading control. **E** Immunoblot analysis of (phosphorylated) I $\kappa$ B $\alpha$  in LY10 and Mino transduced with an empty vector (EV) or a CYLD (wildtype or R324A mutant) expressing vector. Three days after sorting cells were incubated with or without 5  $\mu$ M proteasome inhibitor MG132 for 3 h before harvesting.  $\beta$ -tubulin was used as loading control. **F** Heatmap representing the RT-qPCR analysis of NF- $\kappa$ B target gene expression in LY10 and Mino transduced with an empty vector (EV) or an expression vector for CYLD (WT or non-cleavable R324A mutant). Cells were sorted for YFP expression and allowed to recover for 48 h before RNA isolation. RPLP0 was used as an input control and data are normalized to the EV control expression levels. The mean of three independent experiments performed in triplicate is shown. **G** Immunoblot analysis of (phosphorylated) STAT3 in LY10 transduced with an empty vector (EV) or an expression vector for CYLD (WT or non-cleavable R324A mutant).  $\beta$ -tubulin was used as loading control.

### **CYLD-deficient cells are less sensitive to BCR signalosome inhibitors**

Given the previously described function of CYLD as a negative regulator of NF- $\kappa$ B signaling (23-25), we investigated if loss of CYLD would be sufficient to augment NF- $\kappa$ B activity. For this purpose, we generated CYLD-deficient HBL1, LY10 and Mino cell lines using the CRISPR-Cas9 system. Considering that NF- $\kappa$ B is constitutively activated and that CYLD is partially cleaved in these cell lines, we treated the cells with BCR signalosome inhibitors to repress NF- $\kappa$ B activity and promote full-length CYLD accumulation. In line with our previous results (see Figure 3B and 3D), treatment with ibrutinib and sotrastaurin strongly induced accumulation of full-length CYLD (Figure 6A). This was largely impaired in CYLD-deficient cells, indicating efficient silencing of CYLD. Interestingly, whereas treatment with ibrutinib and sotrastaurin strongly repressed cell growth, as anticipated (see also Figure 3A and 3C), this growth-inhibitory effect was significantly reduced in CYLD-deficient cells (Figure 6B). Ensuring that the observed effects are on-target, similar effects were observed with a second CYLD gRNA (Supplementary Figure 5A and B).

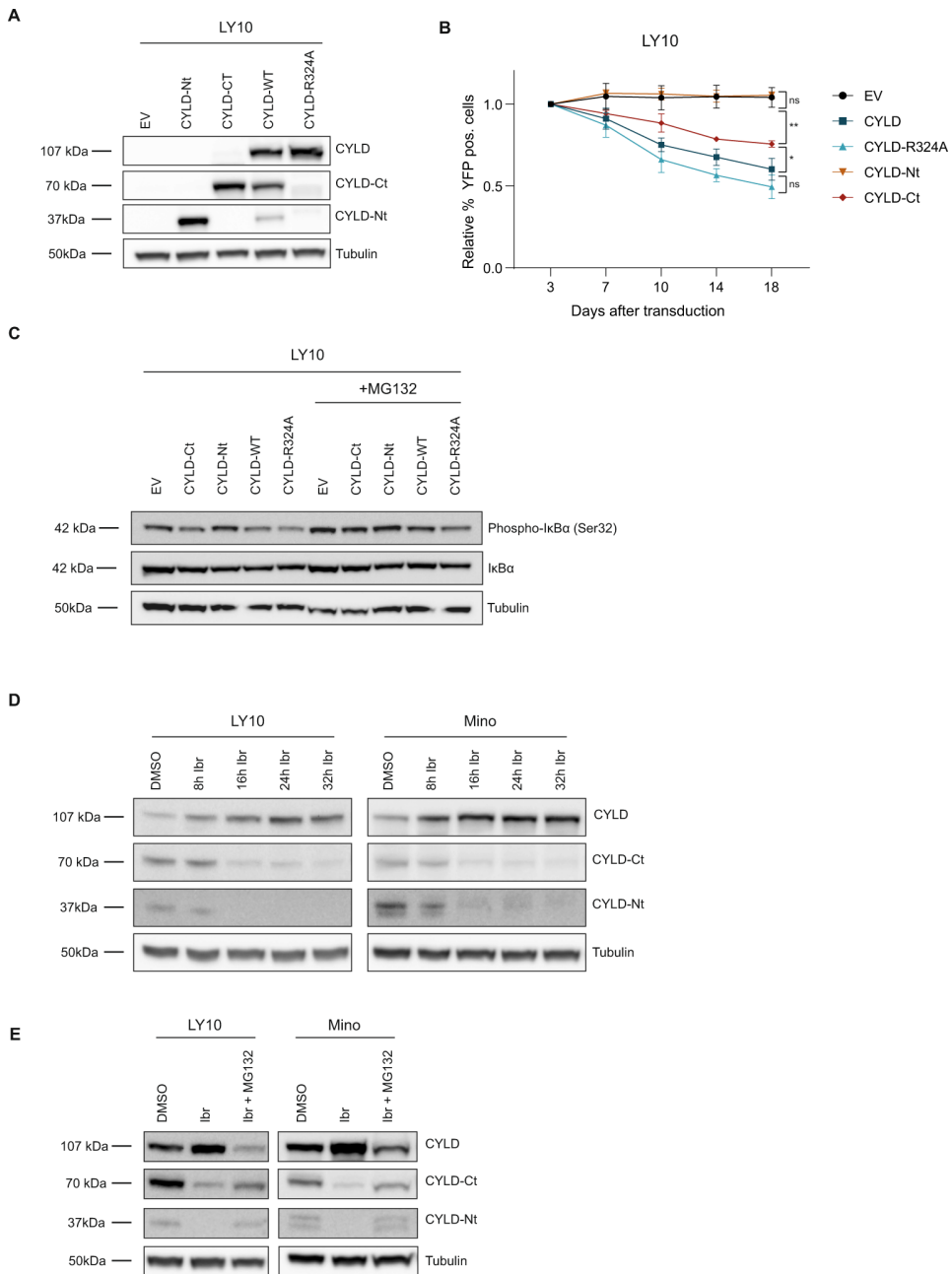


**Figure 5. MALT1-dependent proteolytic cleavage inhibits activity and promotes proteasomal degradation of CYLD.** **A** Immunoblot analysis of CYLD variants in LY10. Cells were transduced with an empty vector (EV) or an expression vector for CYLD (N-terminal fragment, C-terminal fragment, WT or non-cleavable R324A mutant) and sorted for YFP expression. CYLD was detected using an antibody raised against a C-terminal epitope which detects full-length CYLD and a C-terminal fragment of CYLD (CYLD-Ct), or an antibody against an N-terminal epitope for detection of the N-terminal fragment (CYLD-Nt).  $\beta$ -tubulin was used as loading control. **B** Flow cytometric analysis of LY10 cells transduced with an empty vector (EV)

or a bicistronic expression vector for CYLD (N-terminal fragment, C-terminal fragment, WT or non-cleavable R324A mutant) co-expressing YFP. The percentage of YFP positive cells was followed in time and plotted as the percentage of YFP+ cells, normalized to the value at day 3 following retroviral transduction. The mean  $\pm$  SD of four independent transductions is shown.  $P > 0.05$ ; ns (non-significant); \* $P < 0.05$ ; \*\* $P < 0.01$  using 1-way ANOVA with Tukey's multiple comparisons test. **C** Immunoblot analysis of (phosphorylated) I $\kappa$ B $\alpha$  in LY10 transduced with an empty vector (EV) or an expression vector for CYLD (N-terminal fragment, C-terminal fragment, WT or non-cleavable R324A mutant) expressing vector. Three days after sorting cells were incubated with or without 5  $\mu$ M proteasome inhibitor MG132 for 3 h before harvesting.  $\beta$ -tubulin was used as loading control. **D** Immunoblot analysis of CYLD cleavage in LY10 and Mino. Cells were incubated with 100 nM ibrutinib for the indicated time points.  $\beta$ -tubulin was used as loading control. **E** Immunoblot analysis of endogenous CYLD cleavage in LY10 and Mino. Cells were incubated with 100 nM ibrutinib for 24 h in the presence or absence of 10  $\mu$ M MG132. To prevent apoptosis, cell lines were co-incubated with 10  $\mu$ M Q-VD-OPh (QVD).  $\beta$ -tubulin was used as loading control.

Notably, in HBL1, LY10 and Mino, ibrutinib and sotrastaurin induced a strong G1-arrest, which was partially restored in CYLD-deficient cells (Supplemental Figure 6A and 6B), whereas cell viability was hardly affected, indicating that these inhibitors mainly arrest cell proliferation (Supplemental Figure 6C and 6D).

To determine whether the enhanced cell proliferation in CYLD-deficient cells results from augmented NF- $\kappa$ B signaling, we next assessed I $\kappa$ B- $\alpha$  phosphorylation. Treatment with ibrutinib and sotrastaurin markedly reduced I $\kappa$ B- $\alpha$  phosphorylation, which was partially restored in CYLD-deficient cells (Figure 6C and Supplemental Figure 7). In line with the observed effects on NF- $\kappa$ B signaling, treatment with ibrutinib and sotrastaurin strongly reduced STAT3 phosphorylation, and this was partially overcome in CYLD-deficient cells (Figure 6D). Since *STAT3* itself is a target gene of phosphorylated STAT3, these effects are also reflected by changes in total STAT3 protein. In accordance to Supplemental Figure 3B, we did not observe basal levels of phosphorylated STAT3 in Mino (data not shown). Collectively, our findings demonstrate that loss of CYLD renders BCR-dependent lymphoma cell lines less sensitive to BCR pathway inhibition by ibrutinib and sotrastaurin, indicating that their inhibitory effects on proliferation and signaling are at least partially dependent upon CYLD.

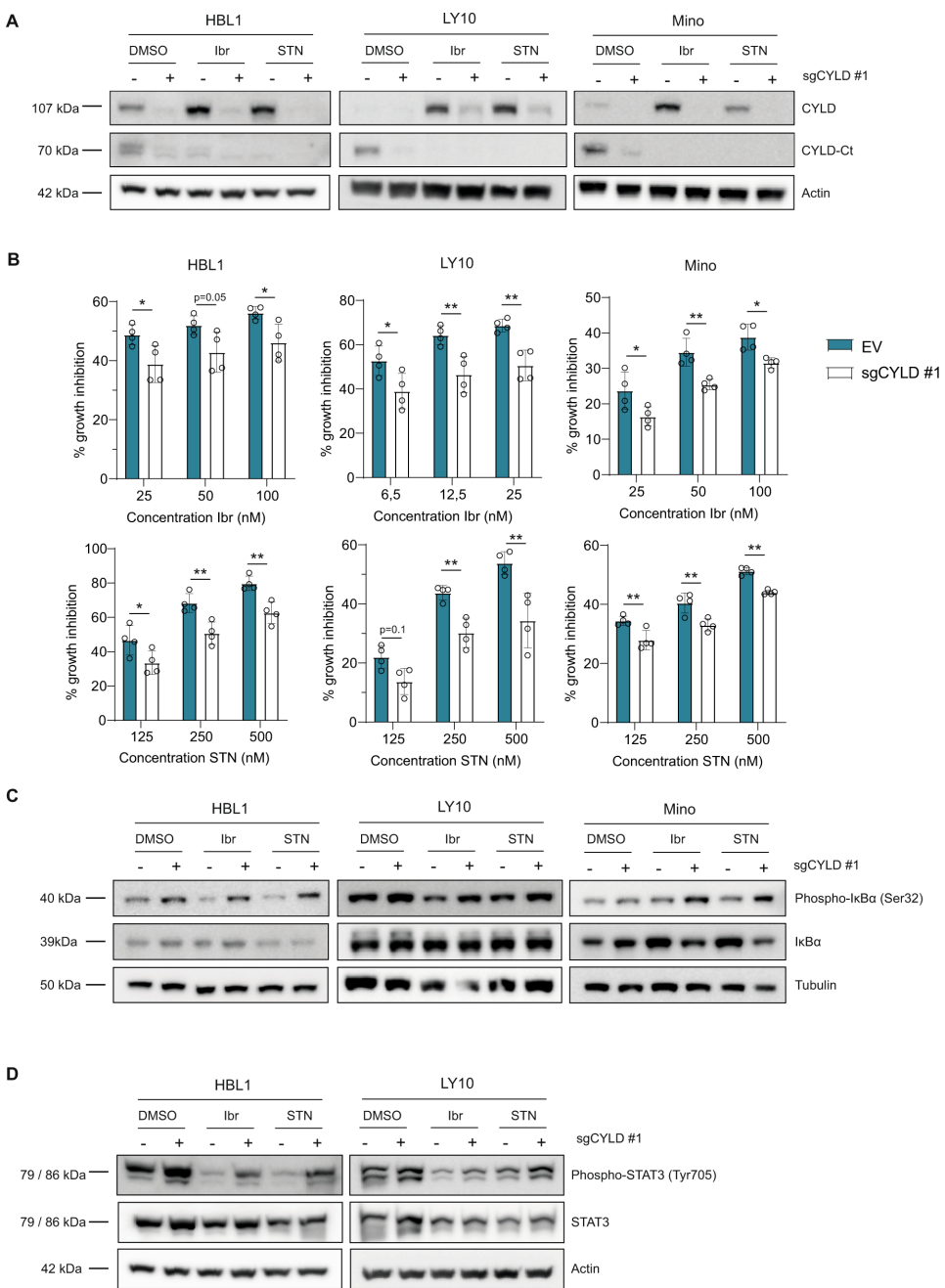


**Figure 6. CYLD knockdown promotes cell growth and NF-κB activation.** **A** Immunoblot analysis of CYLD in HBL1, LY10 and Mino transduced with lentiCRISPR-Cas9 (±sgCYLD) using an antibody raised against a C-terminal epitope which detects full-length CYLD and a C-terminal fragment of CYLD (CYLD-Ct). Cells were treated with 50 nM BTK inhibitor Ibrutinib or 500 nM PKC inhibitor Sotrastaurin for 48 h as indicated. β-tubulin was used as loading control. **B** HBL1, LY10 and Mino transduced with lentiCRISPR-Cas9 without gRNA (empty vector; EV) or with sgCYLD were treated for 3 days with indicated concentrations of Ibrutinib or Sotrastaurin. The number of viable cells, as determined by 7-AAD staining, was normalized

to the untreated condition. The mean  $\pm$  SD of four independent experiments performed in triplicate is shown. \* $P < 0.05$ ; \*\* $P < 0.01$  using 2-way ANOVA with Sidak's multiple comparisons test. **C** Immunoblot analysis of (phosphorylated) I $\kappa$ B $\alpha$  in HBL1, LY10 and Mino transduced with lentiCRISPR-Cas9 ( $\pm$ sgCYLD) treated for 48 h with 50 nM Ibrutinib or 500 nM Sotrastaurin as indicated. Cells were incubated with 5  $\mu$ M proteasome inhibitor MG132 for 3 h before harvesting.  $\beta$ -tubulin was used as loading control. **D** Immunoblot analysis of (phosphorylated) STAT3 in LY10, HBL1 and Mino transduced with lentiCRISPR-Cas9 ( $\pm$ sgCYLD) treated 48 h with 50 nM Ibrutinib or 500 nM Sotrastaurin as indicated.  $\beta$ -actin was used as loading control.

## DISCUSSION

CYLD has been implicated in the pathogenesis of many malignancies, including breast, colon, liver and skin cancers (28, 36-38). Our study reveals a tumor suppressive function of CYLD in the pathogenesis of DLBCL and MCL. First, our microarray analysis showed that high *CYLD* expression correlates with improved overall survival in both DLBCL and MCL patients. Previous studies have established that high *CYLD* expression is also associated with improved overall survival in CLL and MM (35, 39). Interestingly, in MM, a malignancy of plasma cells, *CYLD* expression is frequently lost through deletions or inactivating mutations (26, 40). These genomic aberrations hardly occur in DLBCL and MCL, suggesting an important role for other post-translational or transcriptional control mechanisms (27). At the post-translational level, phosphorylation of CYLD at serine 418 by IKK has been demonstrated to reduce its deubiquitinase activity (28, 29, 41). In addition, CYLD can be cleaved by caspase 8 at aspartate 215 promoting its degradation, as well as by (para)caspase MALT1 at arginine 324 resulting in its proteolytic inactivation (30, 31). In various *in vitro* models, CYLD has been demonstrated to negatively regulate NF- $\kappa$ B activation and interact with many proteins that are essential in the signal transduction cascade mediating NF- $\kappa$ B activation (23-25, 35, 37). This is in accordance with our findings showing that silencing of CYLD promotes NF- $\kappa$ B activation and cell growth and, conversely, ectopic expression of CYLD represses NF- $\kappa$ B signaling and cell growth in BCR-dependent lymphoma cell lines. In addition, our data demonstrate that MALT1-dependent cleavage of CYLD substantially reduces its functionality and, moreover, initiates its proteosomal degradation. Taken together, our data revealed that 1) CYLD is cleaved by MALT1, 2) these MALT1-mediated cleavage products of CYLD undergo rapid proteasomal degradation (inactivation), and 3) CYLD represses NF- $\kappa$ B activity and cell growth; hence, MALT-mediated cleavage of CYLD promotes NF- $\kappa$ B activity and growth of aggressive B-cell receptor-dependent lymphomas. Notably, this may also affect NF- $\kappa$ B activity controlled by, *e.g.*, TLR/MyD88-signaling (summarized in Figure 7).

CYLD consists of three conserved cytoskeleton-associated protein glycine-rich (CAP-Gly) domains and a C-terminal catalytic ubiquitin-specific protease (USP) domain that is able to hydrolyze lysine 63-linked ubiquitin chains (Figure 7). The first and second CAP-Gly

domains bind to microtubules, which might be required for optimal localization and interaction of CYLD with its interaction partners such as TRAF2, TRAF6 or TAK1 (23-25, 42), whereas the third CAP-Gly domain interacts with NEMO/IKK $\gamma$  (43, 44). Furthermore, Elliot *et al.* recently demonstrated that both the second and third CAP-Gly domain contain ubiquitin-binding domains and can therefore contribute to CYLD deubiquitinase activity (45). As anticipated, our data show that the N-terminal fragment (lacking the third CAP-Gly and USP domain) is unable to repress cell growth. The observed ability of the C-terminal fragment to partially repress growth of LY10 cells suggests that, whereas the first and/or second CAP-Gly domain are required for optimal deubiquitinase activity, ectopic (high) overexpression of the C-terminal fragment may to some extent overcome the dependence upon the localization domains. Importantly, however, in addition to reduced functionality, our current findings demonstrate that the MALT1-produced endogenous CYLD fragments are rapidly degraded by the proteasome. Previous studies demonstrated that the E3 ubiquitin ligases TRIM47 and MIB2 are involved in proteasomal degradation of full-length CYLD (46, 47). Interestingly, TRIM47 predominantly interacts with the N-terminal CAP-Gly domains, whereas MIB2 preferentially interacts with the third CAP-Gly domain, suggesting that these ligases could be involved in degradation of the CYLD fragments generated upon MALT1-mediated cleavage.

Next to CYLD, several other MALT1 substrates have been identified, but the complete role of the MALT1 protease activity in lymphomagenesis remains incompletely understood. MALT1-dependent cleavage of A20 and RelB, as well as MALT1 auto-proteolysis, have been implicated in fine-tuning NF- $\kappa$ B activation (13, 15, 48). Since CYLD and A20 are both MALT1 targets which negatively regulate NF- $\kappa$ B signaling by deconjugating ubiquitin chains of largely overlapping substrates, it is remarkable that genetic aberrations in *CYLD* are rare, while deletions/mutations of *TNFAIP3/A20* occur in over 30% of various B-cell malignancies (27, 49, 50). This suggests that CYLD may have non-redundant, essential functions other than NF- $\kappa$ B suppression. Interestingly, Stegmeier *et al.*, demonstrated that CYLD deubiquitinase activity is required for efficient mitotic entry, independent of its role in canonical NF- $\kappa$ B signaling (51). Later studies showed that CYLD directly interacts with microtubules promoting their assembly and stability, which is essential for cell division (43, 52). In line with an important role in cell cycle progression, CYLD is constitutively expressed in most cell types, albeit at a low level (53). In contrast, A20 expression is mostly low/absent under basal conditions, but can be strongly upregulated in response to various stimuli (53-55). The complex role of CYLD in cell cycle regulation and how this relates to its tumor suppressive functions remains to be fully elucidated.

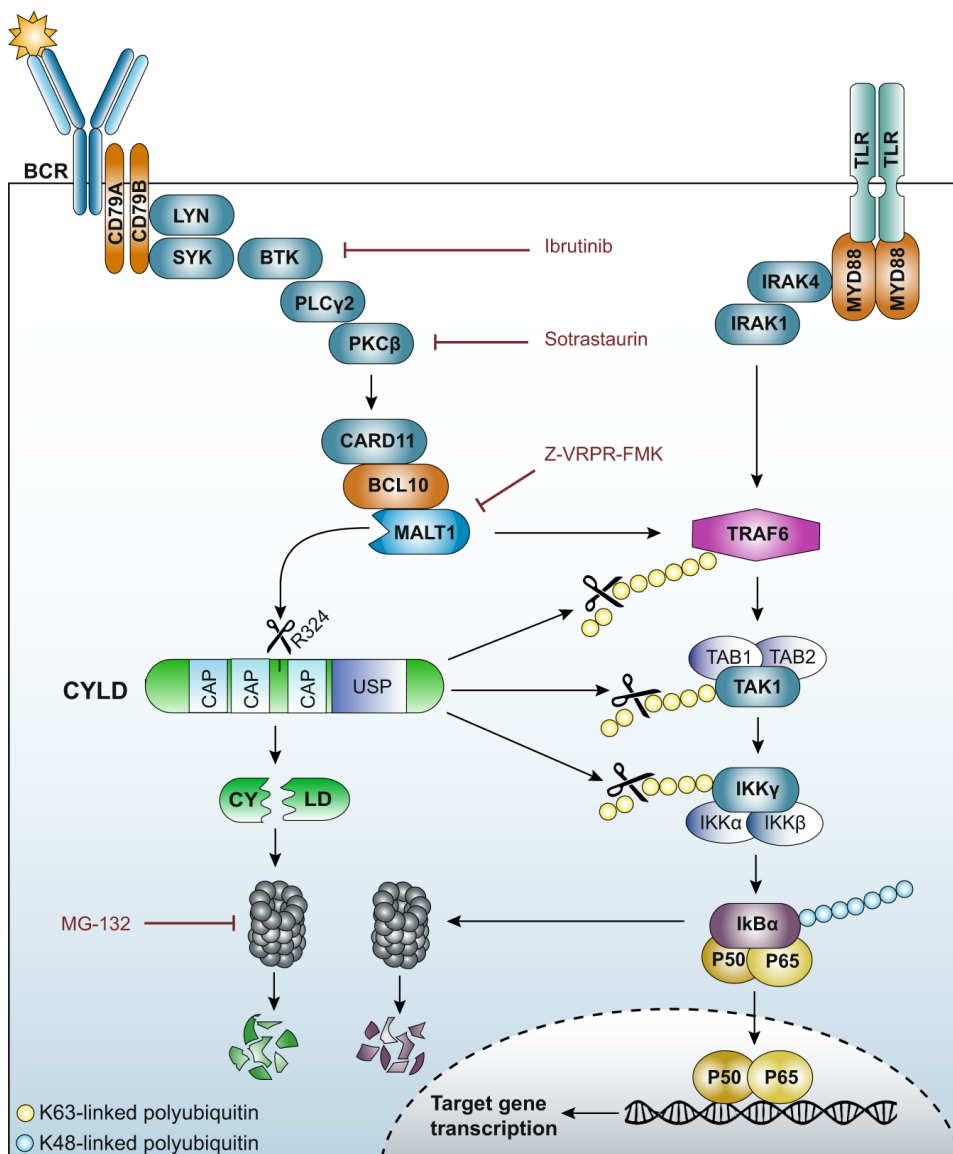


**Figure 7. Model of the role of CYLD in NF-κB activation in B-cell lymphomas.** Upon B-cell receptor (BCR) ligation, tyrosine residues within the ITAM motifs of CD79 are phosphorylated by the Src-family tyrosine kinase LYN leading to activation of spleen tyrosine kinase (SYK). Subsequently, Bruton's tyrosine kinase (BTK) is activated and can then phosphorylate phospholipase Cy2 (PLCγ2). PLCγ2 mediates the formation of second messengers that activate protein kinase Cβ (PKCβ). PKCβ phosphorylates caspase recruitment domain-containing protein 11 (CARD11) provoking a conformational change and allowing CARD11 to interact with B-cell lymphoma 10 (BCL10), and subsequently MALT1. MALT1 is a protease that cleaves various target proteins, including CYLD. In addition, oligomerized MALT1 functions as a scaffolding protein allowing recruitment of the E3 ubiquitin ligase tumor necrosis factor receptor-associated factor 6 (TRAF6). In parallel, Toll-like receptor (TLR) engagement results in MyD88-dependent recruitment of IL-1 receptor-associated kinase-4 (IRAK4) and subsequently IRAK1. IRAK4 phosphorylates IRAK1, which then can associate with TRAF6. BCR/TLR-activated TRAF6 promotes Lys-63-linked ubiquitination of TRAF6

itself as well as transforming growth factor beta-activated kinase 1 (TAK1) and NEMO/IKK- $\gamma$ . Ubiquitinated TRAF6 binds to adaptor proteins TAB1/2/3, leading to the recruitment and auto-phosphorylation of TAK1. Ubiquitination of NEMO/IKK- $\gamma$  mediates the recruitment of the IKK subunits to the TAK1/TAB complex, thereby facilitating the phosphorylation of IKK- $\beta$  by TAK1. IKK- $\beta$  then phosphorylates I $\kappa$ B $\alpha$  resulting in Lys-48-polyubiquitination and subsequent proteasomal degradation which allows NF- $\kappa$ B dimers to translocate to the nucleus. The deubiquinating enzyme CYLD consists of three conserved cytoskeleton-associated protein glycine-rich (CAP-Gly) domains and a C-terminal catalytic ubiquitin-specific protease (USP) domain that is able to hydrolyze lysine 63-linked ubiquitin chains. CYLD can hydrolyze Lys-63-linked polyubiquitin chains of TRAF6, TAK1 and/or NEMO/IKK- $\gamma$ , thereby suppressing NF- $\kappa$ B activation. Accordingly, MALT1-dependent cleavage of CYLD substantially reduces its functionality and initiates its proteasomal degradation, thereby promoting cell growth and NF- $\kappa$ B activation.

Our current findings underline that MALT1 inhibitors are promising therapeutic agents for B-cell lymphomas that are dependent on chronic BCR signaling. The MALT1 inhibitor z-VRPR-fmk effectively inhibits ABC DLBCL growth *in vitro* and *in vivo*, but is presumably unsuitable for clinical applications as a consequence of its large size and relatively poor cell permeability (16, 18). The first small molecule inhibitor irreversibly targeting MALT1, MI-2, showed both safety and efficacy in mouse models (18). In addition, phenothiazine derivatives, which reversibly inhibit MALT1, were shown to strongly represses ABC DLBCL growth *in vitro* and *in vivo* (21, 56). The first clinical trials using the MALT1 inhibitor JNJ-67856633 are currently ongoing in patients with non-Hodgkin's Lymphoma and CLL (Clinical trials.gov; NCT03900598 and NCT04876092). In addition, ONO-7018 (formerly known as CTX-177) was demonstrated to be effective in ABC DLBCL and MCL models *in vitro* and *in vivo* and will soon enter clinical trials (57, 58) (Clinical trials.gov; NCT05515406).

In addition, our findings suggest that inhibition of MALT1-mediated CYLD cleavage, through other BCR signalosome inhibitors such as ibrutinib and sotrastaurin, contributes to the anti-tumor effects of these drugs. These findings are of great interest in the context of (pre-)clinical studies showing that ibrutinib and sotrastaurin are highly effective in ABC DLBCL cases harboring mutations that promote chronic BCR signaling (9, 59-62).

Altogether, our findings establish an important role for MALT1-mediated CYLD cleavage in BCR signaling, canonical NF- $\kappa$ B activity, and consequently cell growth of BCR-dependent lymphomas, thereby providing novel insights into targeting MALT1 protease activity and ubiquitination enzymes as a promising therapeutic approach for these aggressive lymphomas.

**ACKNOWLEDGMENTS**

This work is supported by grants from Lymph&Co to M.K., S.T.P. and M.S.

**AUTHORSHIP CONTRIBUTIONS**

M.M. designed the research, performed experiments, analyzed the data and wrote the paper; H.C.L. and L.J.G. performed experiments and analyzed the data. S.A.G.M.C, R.J.B. and C.J.M.N. provided patient material. M.K., S.T.P. and M.S. supervised the study, designed the research and analyzed the data. M.S. and S.T.P wrote the paper.

**COMPETING INTERESTS**

The authors declare no competing interests.

**DATA AVAILABILITY STATEMENT**

The datasets generated during and/or analysed during the current study are available from the corresponding author on reasonable request.

## REFERENCES

- Davis RE, Ngo VN, Lenz G, Tolar P, Young RM, Romesser PB, et al. Chronic active B-cell-receptor signalling in diffuse large B-cell lymphoma. *Nature*. 2010;463(7277):88-92.
- Ngo VN, Young RM, Schmitz R, Jhavar S, Xiao W, Lim KH, et al. Oncogenically active MYD88 mutations in human lymphoma. *Nature*. 2011;470(7332):115-9.
- Lenz G, Davis RE, Ngo VN, Lam L, George TC, Wright GW, et al. Oncogenic CARD11 mutations in human diffuse large B cell lymphoma. *Science*. 2008;319(5870):1676-9.
- Rahal R, Frick M, Romero R, Korn JM, Kridel R, Chan FC, et al. Pharmacological and genomic profiling identifies NF-kappaB-targeted treatment strategies for mantle cell lymphoma. *Nat Med*. 2014;20(1):87-92.
- Bea S, Valdes-Mas R, Navarro A, Salaverria I, Martin-Garcia D, Jares P, et al. Landscape of somatic mutations and clonal evolution in mantle cell lymphoma. *Proc Natl Acad Sci U S A*. 2013;110(45):18250-5.
- Hadzidimitriou A, Agathangelidis A, Darzentas N, Murray F, Delfau-Larue MH, Pedersen LB, et al. Is there a role for antigen selection in mantle cell lymphoma? Immunogenetic support from a series of 807 cases. *Blood*. 2011;118(11):3088-95.
- Young RM, Wu T, Schmitz R, Dawood M, Xiao W, Phelan JD, et al. Survival of human lymphoma cells requires B-cell receptor engagement by self-antigens. *Proc Natl Acad Sci U S A*. 2015;112(44):13447-54.
- Wang ML, Rule S, Martin P, Goy A, Auer R, Kahl BS, et al. Targeting BTK with ibrutinib in relapsed or refractory mantle-cell lymphoma. *N Engl J Med*. 2013;369(6):507-16.
- Wilson WH, Young RM, Schmitz R, Yang Y, Pittaluga S, Wright G, et al. Targeting B cell receptor signaling with ibrutinib in diffuse large B cell lymphoma. *Nat Med*. 2015;21(8):922-6.
- Thome M, Charton JE, Pelzer C, Hailfinger S. Antigen receptor signaling to NF-kappaB via CARMA1, BCL10, and MALT1. *Cold Spring Harb Perspect Biol*. 2010;2(9):a003004.
- Sun L, Deng L, Ea CK, Xia ZP, Chen ZJ. The TRAF6 ubiquitin ligase and TAK1 kinase mediate IKK activation by BCL10 and MALT1 in T lymphocytes. *Mol Cell*. 2004;14(3):289-301.
- Deng L, Wang C, Spencer E, Yang L, Braun A, You J, et al. Activation of the IkkappaB kinase complex by TRAF6 requires a dimeric ubiquitin-conjugating enzyme complex and a unique polyubiquitin chain. *Cell*. 2000;103(2):351-61.
- Coornaert B, Baens M, Heynincx K, Bekaert T, Haegman M, Staal J, et al. T cell antigen receptor stimulation induces MALT1 paracaspase-mediated cleavage of the NF-kappaB inhibitor A20. *Nat Immunol*. 2008;9(3):263-71.
- Rebeaud F, Hailfinger S, Posevitz-Fejfar A, Tapernoux M, Moser R, Rueda D, et al. The proteolytic activity of the paracaspase MALT1 is key in T cell activation. *Nat Immunol*. 2008;9(3):272-81.
- Hailfinger S, Nogai H, Pelzer C, Jaworski M, Cabalzar K, Charton JE, et al. Malt1-dependent RelB cleavage promotes canonical NF-kappaB activation in lymphocytes and lymphoma cell lines. *Proc Natl Acad Sci U S A*. 2011;108(35):14596-601.
- Ferch U, Kloo B, Gewies A, Pfander V, Duwel M, Peschel C, et al. Inhibition of MALT1 protease activity is selectively toxic for activated B cell-like diffuse large B cell lymphoma cells. *J Exp Med*. 2009;206(11):2313-20.
- Dai B, Grau M, Juillard M, Kleiner P, Horing E, Molinsky J, et al. B-cell receptor-driven MALT1 activity regulates MYC signaling in mantle cell lymphoma. *Blood*. 2017;129(3):333-46.
- Fontan L, Yang C, Kabaleeswaran V, Volpon L, Osborne MJ, Beltran E, et al. MALT1 small molecule inhibitors specifically suppress ABC-DLBCL in vitro and in vivo. *Cancer Cell*. 2012;22(6):812-24.
- Fontan L, Qiao Q, Hatcher JM, Casalena G, Us I, Teater M, et al. Specific covalent inhibition of MALT1 paracaspase suppresses B cell lymphoma growth. *J Clin Invest*. 2018;128(10):4397-412.
- Fontan L, Goldstein R, Casalena G, Durant M, Teater MR, Wilson J, et al. Identification of MALT1 feedback mechanisms enables rational design of potent antilymphoma regimens for ABC-DLBCL. *Blood*. 2021;137(6):788-800.
- Nagel D, Spranger S, Vincendeau M, Grau M, Raffegerst S, Kloo B, et al. Pharmacologic inhibition of MALT1 protease by phenothiazines as a therapeutic approach for the treatment of aggressive ABC-DLBCL. *Cancer Cell*. 2012;22(6):825-37.
- Hailfinger S, Lenz G, Ngo V, Posvitz-Fejfar A, Rebeaud F, Guzzardi M, et al. Essential role of MALT1 protease activity in activated B cell-like diffuse large B-cell lymphoma. *Proc Natl Acad Sci U S A*. 2009;106(47):19946-51.
- Kovalenko A, Chable-Bessia C, Cantarella G, Israel A, Wallach D, Courtois G. The tumour suppressor CYLD negatively regulates NF-kappaB signalling by deubiquitination. *Nature*. 2003;424(6950):801-5.
- Brummelkamp TR, Nijman SM, Dirac AM, Bernards R. Loss of the cylindromatosis tumour suppressor inhibits apoptosis by activating NF-kappaB. *Nature*. 2003;424(6950):797-801.
- Trompouki E, Hatzivassiliou E, Tschirritzis T, Farmer H, Ashworth A, Mosialos G. CYLD is a deubiquitinating enzyme that negatively regulates NF-kappaB activation by TNFR family members. *Nature*. 2003;424(6950):793-6.

26. Annunziata CM, Davis RE, Demchenko Y, Bellamy W, Gabrea A, Zhan F, et al. Frequent engagement of the classical and alternative NF-kappaB pathways by diverse genetic abnormalities in multiple myeloma. *Cancer Cell*. 2007;12(2):115-30.
27. Schmitz R, Wright GW, Huang DW, Johnson CA, Phelan JD, Wang JQ, et al. Genetics and Pathogenesis of Diffuse Large B-Cell Lymphoma. *N Engl J Med*. 2018;378(15):1396-407.
28. Hutti JE, Shen RR, Abbott DW, Zhou AY, Sprott KM, Asara JM, et al. Phosphorylation of the tumor suppressor CYLD by the breast cancer oncogene IKKepsilon promotes cell transformation. *Mol Cell*. 2009;34(4):461-72.
29. Reiley W, Zhang M, Wu X, Granger E, Sun SC. Regulation of the deubiquitinating enzyme CYLD by IkkappaB kinase gamma-dependent phosphorylation. *Mol Cell Biol*. 2005;25(10):3886-95.
30. O'Donnell MA, Perez-Jimenez E, Oberst A, Ng A, Massoumi R, Xavier R, et al. Caspase 8 inhibits programmed necrosis by processing CYLD. *Nat Cell Biol*. 2011;13(12):1437-42.
31. Staal J, Driege Y, Bekaert T, Demeyer A, Muylaert D, Van Damme P, et al. T-cell receptor-induced JNK activation requires proteolytic inactivation of CYLD by MALT1. *EMBO J*. 2011;30(9):1742-52.
32. Lantermans HC, Minderman M, Kuil A, Kersten MJ, Pals ST, Spaargaren M. Identification of the SRC-family tyrosine kinase HCK as a therapeutic target in mantle cell lymphoma. *Leukemia*. 2021;35(3):881-6.
33. Hans CP, Weisenburger DD, Greiner TC, Gascoyne RD, Delabie J, Ott G, et al. Confirmation of the molecular classification of diffuse large B-cell lymphoma by immunohistochemistry using a tissue microarray. *Blood*. 2004;103(1):275-82.
34. Compagno M, Lim WK, Grunn A, Nandula SV, Brahmachary M, Shen Q, et al. Mutations of multiple genes cause deregulation of NF-kappaB in diffuse large B-cell lymphoma. *Nature*. 2009;459(7247):717-21.
35. van Andel H, Kocemba KA, de Haan-Kramer A, Mellink CH, Piwowar M, Broijl A, et al. Loss of CYLD expression unleashes Wnt signaling in multiple myeloma and is associated with aggressive disease. *Oncogene*. 2017;36(15):2105-15.
36. Massoumi R, Kuphal S, Hellerbrand C, Haas B, Wild P, Spruss T, et al. Down-regulation of CYLD expression by Snail promotes tumor progression in malignant melanoma. *J Exp Med*. 2009;206(1):221-32.
37. Hellerbrand C, Bumès E, Bataille F, Dietmaier W, Massoumi R, Bosserhoff AK. Reduced expression of CYLD in human colon and hepatocellular carcinomas. *Carcinogenesis*. 2007;28(1):21-7.
38. Miliani de Marval P, Lutfekali S, Jin JY, Leshin B, Selim MA, Zhang JY. CYLD inhibits tumorigenesis and metastasis by blocking JNK/AP1 signaling at multiple levels. *Cancer Prev Res (Phila)*. 2011;4(6):851-9.
39. Wu W, Zhu H, Fu Y, Shen W, Xu J, Miao K, et al. Clinical significance of down-regulated cylindromatosis gene in chronic lymphocytic leukemia. *Leuk Lymphoma*. 2014;55(3):588-94.
40. Keats JJ, Fonseca R, Chesi M, Schop R, Baker A, Chng WJ, et al. Promiscuous mutations activate the noncanonical NF-kappaB pathway in multiple myeloma. *Cancer Cell*. 2007;12(2):131-44.
41. Xu X, Wei T, Zhong W, Ang R, Lei Y, Zhang H, et al. Down-regulation of cylindromatosis protein phosphorylation by BTK inhibitor promotes apoptosis of non-GCB-diffuse large B-cell lymphoma. *Cancer Cell Int*. 2021;21(1):195.
42. Reiley WW, Jin W, Lee AJ, Wright A, Wu X, Tewalt EF, et al. Deubiquitinating enzyme CYLD negatively regulates the ubiquitin-dependent kinase Tak1 and prevents abnormal T cell responses. *J Exp Med*. 2007;204(6):1475-85.
43. Gao J, Huo L, Sun X, Liu M, Li D, Dong JT, et al. The tumor suppressor CYLD regulates microtubule dynamics and plays a role in cell migration. *J Biol Chem*. 2008;283(14):8802-9.
44. Saito K, Kigawa T, Koshiha S, Sato K, Matsuo Y, Sakamoto A, et al. The CAP-Gly domain of CYLD associates with the proline-rich sequence in NEMO/IKKgamma. *Structure*. 2004;12(9):1719-28.
45. Elliott PR, Leske D, Wagstaff J, Schlicher L, Berridge G, Maslen S, et al. Regulation of CYLD activity and specificity by phosphorylation and ubiquitin-binding CAP-Gly domains. *Cell Rep*. 2021;37(1):109777.
46. Ji YX, Huang Z, Yang X, Wang X, Zhao LP, Wang PX, et al. The deubiquitinating enzyme cylindromatosis mitigates nonalcoholic steatohepatitis. *Nat Med*. 2018;24(2):213-23.
47. Uematsu A, Kido K, Takahashi H, Takahashi C, Yanagihara Y, Saeki N, et al. The E3 ubiquitin ligase MIB2 enhances inflammation by degrading the deubiquitinating enzyme CYLD. *J Biol Chem*. 2019;294(38):14135-48.
48. Baens M, Bonsignore L, Somers R, Vanderheydt C, Weeks SD, Gunnarsson J, et al. MALT1 auto-proteolysis is essential for NF-kappaB-dependent gene transcription in activated lymphocytes. *PLoS One*. 2014;9(8):e103774.
49. Kato M, Sanada M, Kato I, Sato Y, Takita J, Takeuchi K, et al. Frequent inactivation of A20 in B-cell lymphomas. *Nature*. 2009;459(7247):712-6.
50. Honma K, Tsuzuki S, Nakagawa M, Tagawa H, Nakamura S, Morishima Y, et al. TNFAIP3/A20 functions as a novel tumor suppressor gene in several subtypes of non-Hodgkin lymphomas. *Blood*. 2009;114(12):2467-75.
51. Stegmeier F, Sowa ME, Nalepa G, Gygi SP, Harper JW, Elledge SJ. The tumor suppressor CYLD regulates entry into mitosis. *Proc Natl Acad Sci U S A*. 2007;104(21):8869-74.
52. Klei LR, Hu D, Panek R, Alfano DN, Bridwell RE, Bailey KM, et al. MALT1 Protease Activation Triggers Acute Disruption of Endothelial Barrier Integrity via CYLD Cleavage. *Cell Rep*. 2016;17(1):221-32.

53. Uhlen M, Fagerberg L, Hallstrom BM, Lindskog C, Oksvold P, Mardinoglu A, et al. Proteomics. Tissue-based map of the human proteome. *Science*. 2015;347(6220):1260419.
54. Verstrepren L, Verhelst K, van Loo G, Carpentier I, Ley SC, Beyaert R. Expression, biological activities and mechanisms of action of A20 (TNFAIP3). *Biochem Pharmacol*. 2010;80(12):2009-20.
55. Krikos A, Laherty CD, Dixit VM. Transcriptional activation of the tumor necrosis factor alpha-inducible zinc finger protein, A20, is mediated by kappa B elements. *J Biol Chem*. 1992;267(25):17971-6.
56. Schlauderer F, Lammens K, Nagel D, Vincendeau M, Eitelhuber AC, Verhelst SH, et al. Structural analysis of phenothiazine derivatives as allosteric inhibitors of the MALT1 paracaspase. *Angew Chem Int Ed Engl*. 2013;52(39):10384-7.
57. Morishita D, Mizutani A, Tozaki H, Arikawa Y, Kameda T, Kamiunten A, et al. Preclinical Evaluation of a Novel MALT1 Inhibitor CTX-177 for Relapse/Refractory Lymphomas. *Blood*. 2020;136:3-4.
58. Morishita D, Mizutani A, Yamakawa H, Arikawa Y, Tozaki H, Kameda T, et al. Preclinical Translational Research Suggests a Clinical Trial Strategy for a Novel MALT1 Inhibitor ONO-7018/CTX-177 Against Malignant Lymphomas. *Blood*. 2022;140(Supplement 1):8874-5.
59. Wilson WH, Wright GW, Huang DW, Hodgkinson B, Balasubramanian S, Fan Y, et al. Effect of ibrutinib with R-CHOP chemotherapy in genetic subtypes of DLBCL. *Cancer Cell*. 2021;39(12):1643-53 e3.
60. Naylor TL, Tang H, Ratsch BA, Enns A, Loo A, Chen L, et al. Protein kinase C inhibitor sotrastaurin selectively inhibits the growth of CD79 mutant diffuse large B-cell lymphomas. *Cancer Res*. 2011;71(7):2643-53.
61. Grommes C, Pastore A, Palaskas N, Tang SS, Campos C, Schartz D, et al. Ibrutinib Unmasks Critical Role of Bruton Tyrosine Kinase in Primary CNS Lymphoma. *Cancer Discov*. 2017;7(9):1018-29.
62. Lionakis MS, Dunleavy K, Roschewski M, Widemann BC, Butman JA, Schmitz R, et al. Inhibition of B Cell Receptor Signaling by Ibrutinib in Primary CNS Lymphoma. *Cancer Cell*. 2017;31(6):833-43 e5.

## SUPPLEMENTAL METHODS AND SUPPLEMENTAL FIGURES

### Microarray analyses

All microarray datasets were generated using the Affymetrix Human Genome U133 Plus 2.0 Array and are publically available through the NCBI Gene Expression Omnibus. Datasets analyzed were: GSE12366 (B-cell subsets), GSE11877 (B-ALL), GSE21029 (CLL), GSE16024 (FL), GSE93291 (MCL), GSE10846 (DLBCL), GSE9656 (WM) and GSE2658 (MM). Data analysis and visualization was performed using R2: Genomics Analysis and Visualization Platform (<http://r2.amc.nl>).

### Cell lines and reagents

The MCL cell lines JeKo-1, Granta-519, Maver-1, Z-138, Rec-1 and Mino and the DLBCL cell lines OCI-LY1, OCI-LY3 and OCI-LY7 were cultured in IMDM supplemented with 10% FCS. OCI-LY10 was cultured in IMDM supplemented with 20% human serum (Sigma Aldrich). U2932 and RIVA were cultured in RPMI-1640 supplemented with 10% FCS. HBL1 and TMD8 were cultured in RPMI-1640 supplemented with 20% FCS. Cell Line authentication was routinely performed using Short Tandem Repeat DNA profiling (PowerPlex 16, Promega) and cell lines were frequently tested for mycoplasma contamination using RT-qPCR.

The small molecule inhibitors Ibrutinib and Sotrastaurin and proteasome inhibitor MG132 were purchased from Selleckchem; the MALT1 inhibitor Z-VRPR-FMK was purchased from Enzo Life Sciences. Phorbol myristate acetate (PMA) and ionomycin were both purchased from Sigma Aldrich. Q-VD-OPh was purchased from MedChemExpress.

### Transfection and transduction

To generate CYLD knockout cell lines, we inserted a single guide RNA targeting CYLD (sgRNA1: ATGGGAAGGACGATTCTGCC, sgRNA2: TGAGACTGAATGGTAAAGAG) into pL-CRISPR.EFS.GFP (Addgene plasmid #57818). For retroviral overexpression of CYLD we subcloned CYLD (NM\_015247) from Flag-HA-CYLD (Addgene plasmid #22544) into LZRS-IRES-YFP, which was kindly provided by Dr. H. Spits. We employed the QuikChange II Site-Directed Mutagenesis Kit (Agilent) to generate a CYLD R324A mutant construct according to the manufacturer's instructions.

### Immunoblotting antibodies

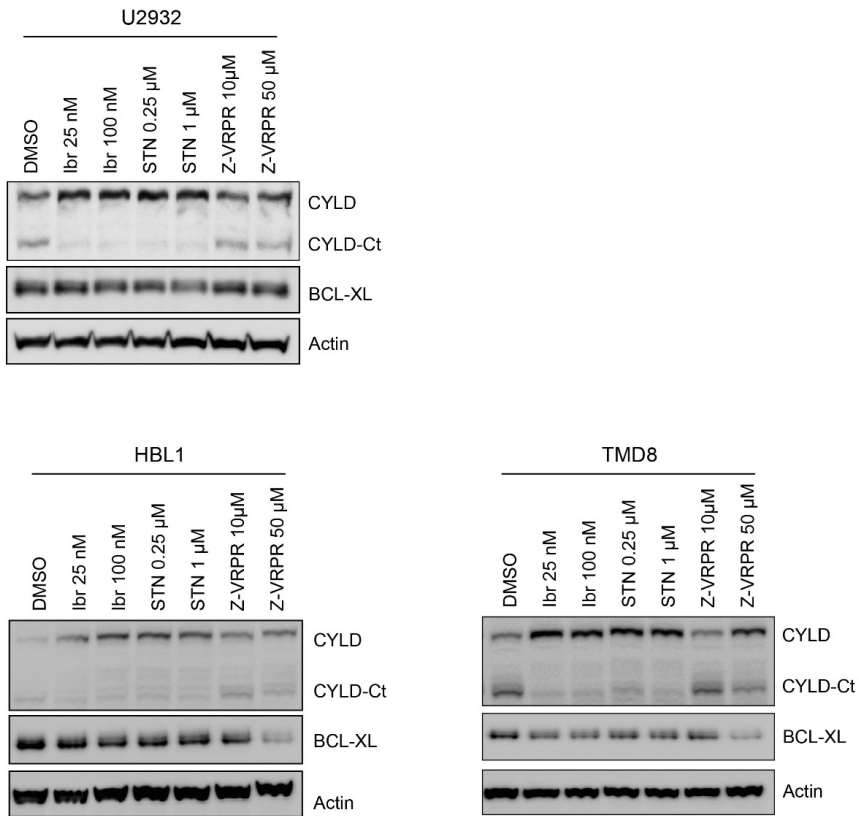
The primary antibodies used were: mouse anti- $\beta$ -tubulin (clone D66, Sigma Aldrich), mouse anti- $\beta$ -actin (clone AC-15, Sigma-Aldrich), mouse anti-CYLD (clone E-10, Santa Cruz), mouse anti-MALT1 (clone B-12, Santa Cruz), rabbit anti-BCL XL (clone 54H6, Cell Signaling Technology), rabbit anti-phospho-I $\kappa$ B $\alpha$  (Ser32) (clone 14D4, Cell Signaling Technology), rabbit anti-I $\kappa$ B $\alpha$  (clone 44D4, Cell Signaling Technology), rabbit anti-

phospho-STAT3 (Tyr705) (Cell Signaling Technology), mouse-anti-STAT3 (clone 124H6, Cell Signaling Technology), rabbit anti-CYLD (clone D1A10, Cell Signaling Technology), mouse anti-beta-catenin (clone 14, BD Biosciences), rabbit anti-TBP (Abcam) and rabbit anti-phospho-SAPK/JNK (Thr183/Tyr185) (Cell Signaling Technology). Secondary antibodies used were anti-mouse-HRP or anti-rabbit-HRP (both DAKO).

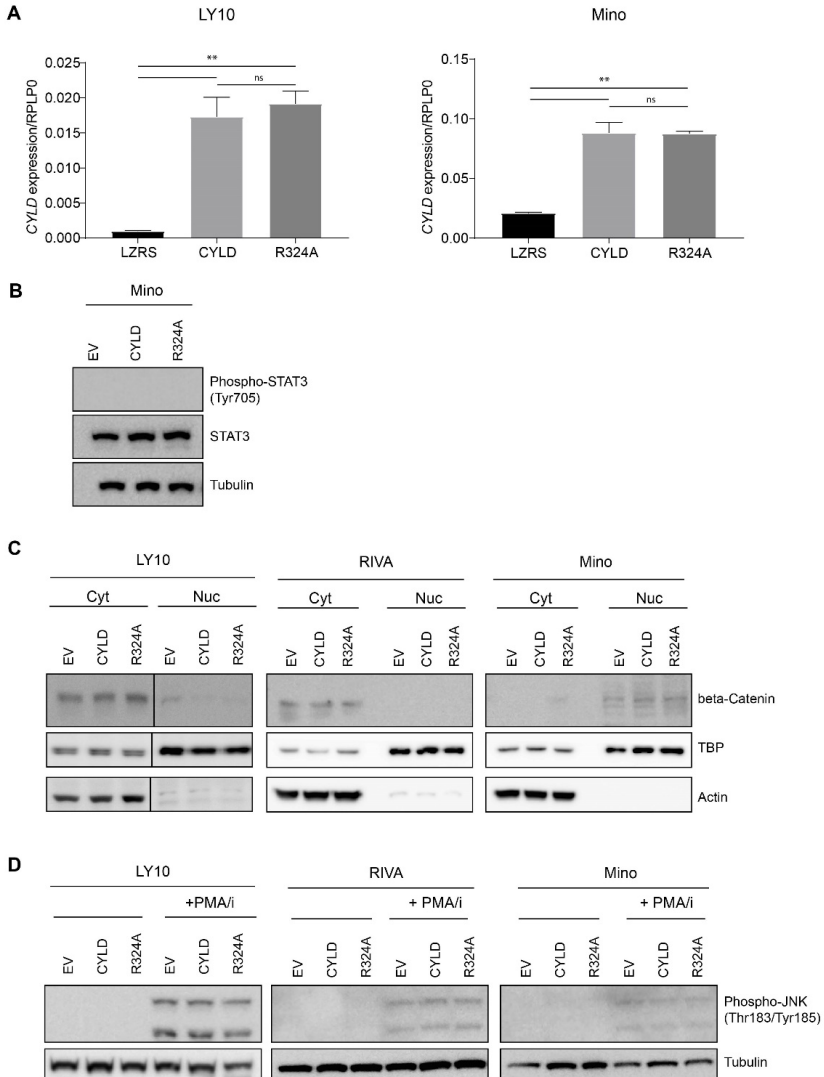
### RNA isolation, cDNA synthesis and RT-qPCR

Total RNA was isolated using TRI-reagent according to the manufacturer's protocol (Sigma Aldrich). RNA was converted to cDNA using oligo(dT) primers for 1 hour at 37 °C. RT-qPCRs were performed using Sensifast (Bioline) on a Lightcycler 480 (Roche). Expression levels were normalized relative to expression of control gene *RPLP0*. The following primer pairs were used: CYLD forward (5'- TGCAGGCTGTACGGATGGAACCT -3'); CYLD reverse (5'-TCCTGATGCAGCCTCCACCT -3'); IL6 forward (5'- GACTTGCCTGGTGAAAATCATCACTG -3'); IL6 reverse (5'- GGGTCAGGGGTGGTTATTGCATC -3'); IL10 forward (5'- TTACCTGGAGGAGGTGATGC -3'); IL10 reverse (5'- GGCCTTGCTCTTGTTTTTCAC -3'); CXCL10 forward (5'- GTGGCATTCAAGGAGTACCTC -3'); CXCL10 reverse (5'- TGATGGCCTTCGATTCTGGATT -3'); TNF forward (5'- CTCTTCTGCCTGCTGCACTTTG -3'); TNF reverse (5'- ATGGGCTACAGGCTTGCTACTC -3'); CCR7 forward (5'- CAACATCACCAGTAGCACCTGTG -3'); CCR7 reverse (5'- TGCGGAACCTTGACGCCGATGAA -3'); ICAM1 forward (5'- CATCTACAGCTTCCGGCGCCC -3'); ICAM1 reverse (5'- AGAAGCTGCGCCCCTTGTCC -3'); CD80 forward (5'- TAGATGCGAGTTTGTGCCAG -3'); CD80 reverse (5'- GCTGGCTGGTCTTTCTCACT -3'); RPLP0 forward (5'- GCTTCCTGGAGGGTGTCCGC -3'); RPLP0 reverse (5'- TCCGTCTCCACAGACAAGGCCA -3').

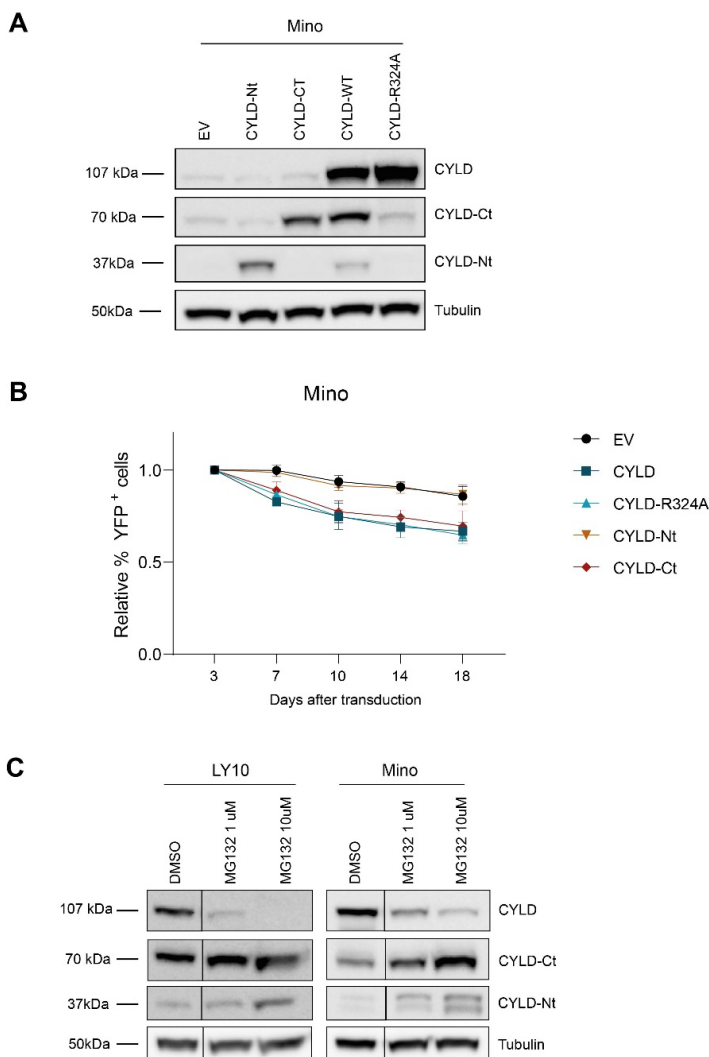




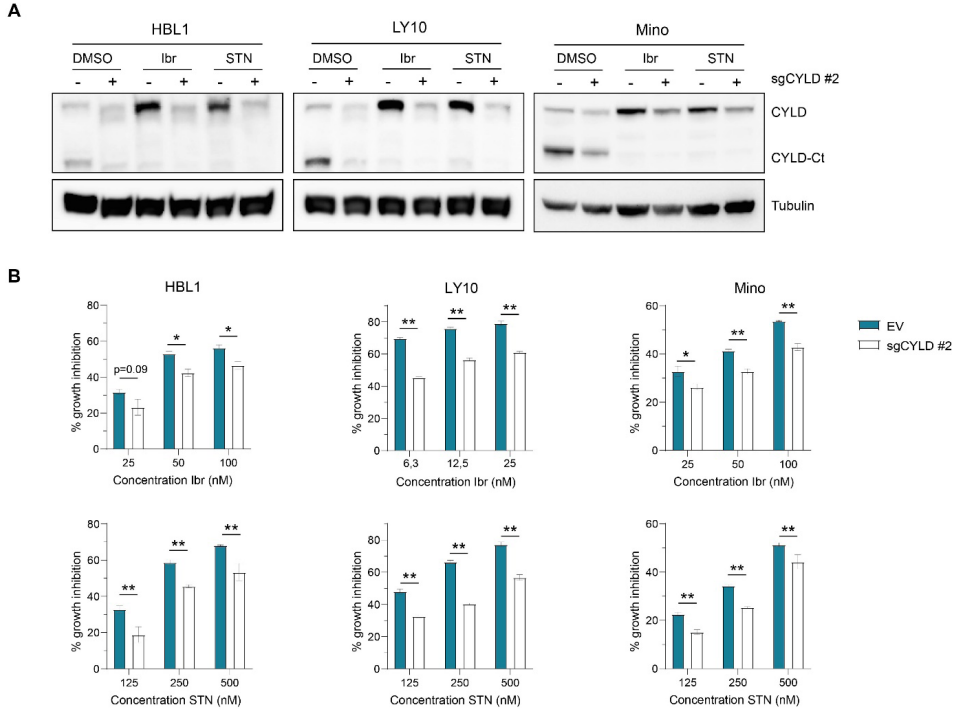
**Supplementary Figure 2.** Immunoblot analysis of CYLD cleavage in DLBCL cell lines U2932, HBL1 and TMD8 using an antibody raised against a C-terminal epitope which detects full-length CYLD and a C-terminal fragment of CYLD (CYLD-Ct). Cells were incubated with indicated concentrations of the different BCR signalosome inhibitors for 48 hours. BCL-XL protein levels were determined as a positive control for efficacy of the inhibitors;  $\beta$ -actin was used as loading control.



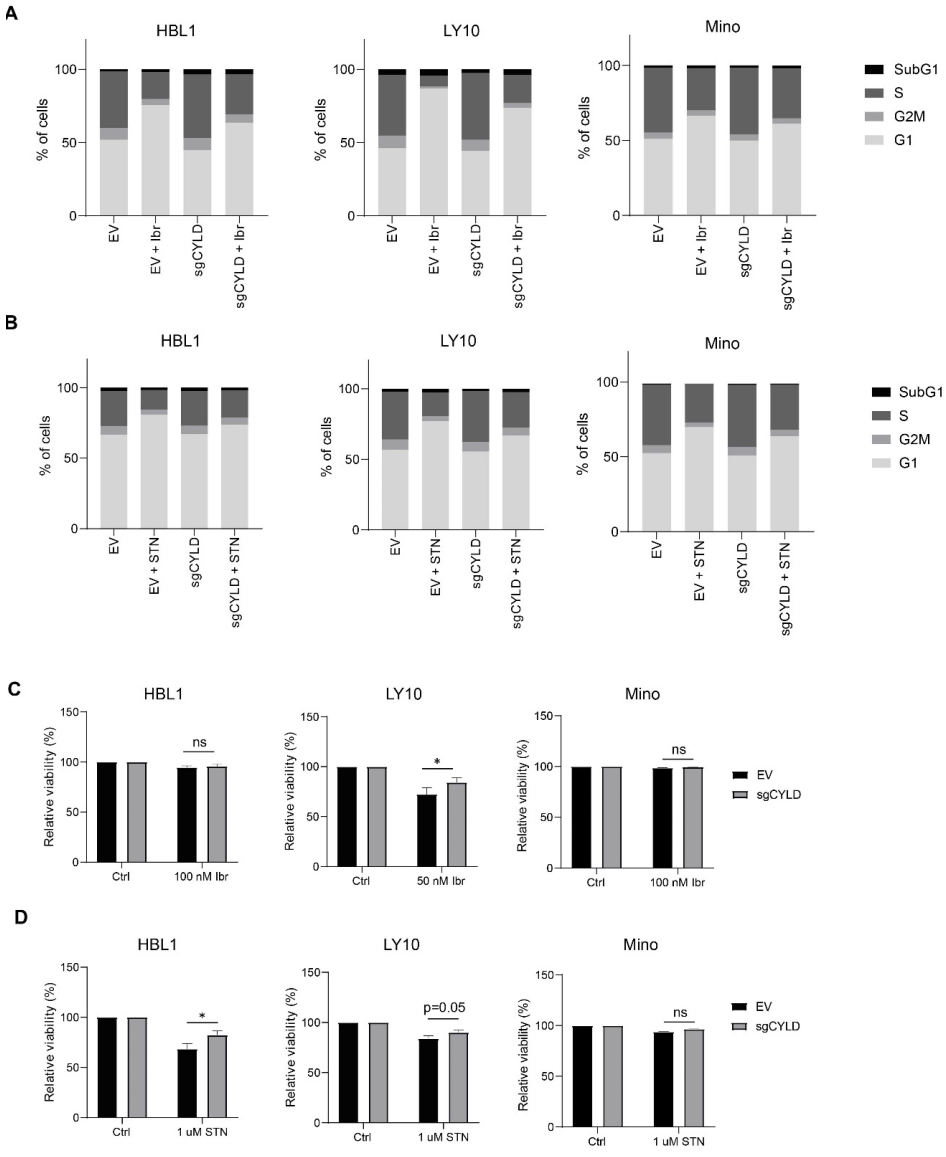
**Supplementary Figure 3.** (A) RT-qPCR analysis of CYLD expression in LY10 and Mino transduced with an empty vector (LZRS) or an expression vector for CYLD (WT or non-cleavable R324A mutant). Cells were sorted for YFP expression and allowed to recover for 48 hours before RNA isolation. RPLP0 was used as an input control. The mean  $\pm$  SD of one representative experiment is shown. (B) Immunoblot analysis of (phosphorylated) STAT3 in Mino transduced with an empty vector (EV) or an expression vector for CYLD (WT or non-cleavable R324A mutant)  $\beta$ -tubulin was used as loading control. (C) Immunoblot analysis of beta-catenin levels following nuclear fractionation in LY10, RIVA and Mino transduced with an empty vector (EV) or a CYLD (wildtype or R324A mutant) expressing vector. TBP was used as a loading control for the nuclear fraction;  $\beta$ -actin was used as loading control for the cytosolic fraction. (D) Immunoblot analysis of phosphorylated JNK (Thr183/Tyr185) levels following stimulation of 1 hour with PMA (50 ng/ml) and ionomycin (1  $\mu$ g/ml) in LY10, RIVA and Mino transduced with an empty vector (EV) or a CYLD (wildtype or R324A mutant) expressing vector.  $\beta$ -tubulin was used as loading control.



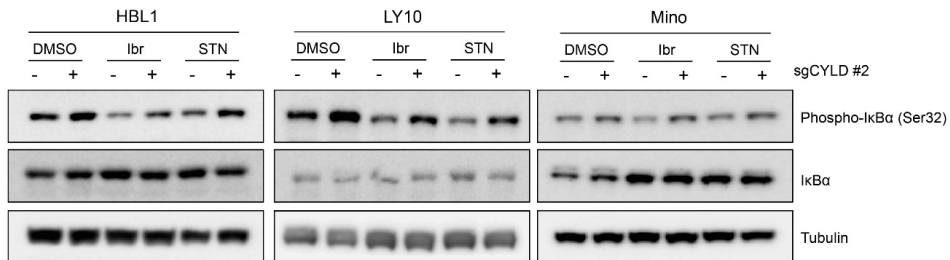
**Supplementary Figure 4.** (A) Immunoblot analysis of CYLD variants in Mino. Cells were transduced with an empty vector (EV) or an expression vector for CYLD (N-terminal fragment, C-terminal fragment, WT or non-cleavable R324A mutant) and sorted for YFP expression. CYLD was detected using an antibody raised against a C-terminal epitope which detects full-length CYLD and a C-terminal fragment of CYLD (CYLD-Ct), or an antibody against an N-terminal epitope for detection of the N-terminal fragment (CYLD-Nt).  $\beta$ -tubulin was used as loading control. (B) Flow cytometric analysis of Mino transduced with an empty vector (EV) or a bicistronic expression vector for CYLD (N-terminal fragment, C-terminal fragment, WT or non-cleavable R324A mutant) co-expressing YFP. The percentage of YFP positive cells was followed in time and plotted as the percentage of YFP+ cells, normalized to the value at day 3 following retroviral transduction. The mean  $\pm$  S.E.M. of three independent transductions is shown. (C) Immunoblot analysis of CYLD cleavage in LY10 and Mino. Cells were incubated with indicated concentrations of MG132 for 24 hours. To prevent apoptosis, cell lines were co-incubated with  $10\mu\text{M}$  Q-VD-OPH (QVD). CYLD was detected using an antibody raised against a C-terminal epitope which detects full-length CYLD and a C-terminal fragment of CYLD (CYLD-Ct). A second antibody raised against an N-terminal epitope was used for detection of the N-terminal fragment (CYLD-Nt).  $\beta$ -tubulin was used as loading control.



**Supplementary Figure 5.** (A) Immunoblot analysis of CYLD in HBL1, LY10 and Mino transduced with lentiCRISPR-Cas9 (+/- sgCYLD) using an antibody raised against a C-terminal epitope which detects full-length CYLD and a C-terminal fragment of CYLD (CYLD-Ct). Cells were treated with 50 nM BTK inhibitor Ibrutinib or 500 nM PKC inhibitor Sotrastaurin for 48 hours as indicated.  $\beta$ -tubulin was used as loading control. (B) HBL1, LY10 and Mino transduced with lentiCRISPR-Cas9 without gRNA (empty vector; EV) or with sgCYLD were treated for 3 days with indicated concentrations of Ibrutinib or Sotrastaurin. The number of viable cells, as determined by 7-AAD staining, was normalized to the untreated condition. The mean  $\pm$  SD of one representative experiment is shown.



**Supplementary Figure 6.** (A-B) Flow cytometric analysis of the percentage of cells in Sub-G1 (BrdU-, <To-Pro-3-), G1 (BrdU-,To-Pro-3-), S (BrdU+) and G2/M (BrdU-, To-Pro-3+) after 48 hours of treatment with 50 nM Ibrutinib (A) or 500 nM Sotrastaurin (B) in HBL1, LY10 and Mino transduced with pLC-GFP-sgCYLD or empty vector control (EV). One representative experiment of three independent experiments is shown. (C-D) Viability assay in LY10, HBL1 and Mino transduced with lentiCRISPR-Cas9 without gRNA (empty vector; EV) or with sgCYLD treated for 3 days with indicated concentrations of Ibrutinib (C) or Sotrastaurin (D). The percentage of viable cells was defined as the percentage of cells being 7AAD negative. The mean  $\pm$  S.E.M. of at least two independent experiments performed in triplicate is shown. \*P<0.05 using 2-way ANOVA with Bonferroni's multiple comparisons test.



**Supplementary Figure 7.** Immunoblot analysis of (phosphorylated) IκBα in HBL1, LY10 and Mino transduced with lentiCRISPR-Cas9 (+/- sgCYLD) treated for 48 hours with 50 nM Ibrutinib or 500 nM Sotrastaurin as indicated. Cells were incubated with 5 μM proteasome inhibitor MG132 for 3 hours before harvesting. β-tubulin was used as loading control.





# 3

## Identification of the SRC-family tyrosine kinase HCK as a therapeutic target in mantle cell lymphoma

Hildo Lantermans<sup>1,2</sup>, Marthe Minderman<sup>1,2</sup>, Annemieke Kuil<sup>1,2</sup>,  
Marie-José Kersten<sup>2,3</sup>, Steven T. Pals<sup>1,2,4</sup>, Marcel Spaargaren<sup>1,2,4</sup>

<sup>1</sup>Department of Pathology, Cancer Center Amsterdam, Amsterdam UMC, University of Amsterdam, The Netherlands; <sup>2</sup>Lymphoma and Myeloma Center Amsterdam – LYMMCARE, The Netherlands; <sup>3</sup>Department of Hematology, Amsterdam UMC, University of Amsterdam, the Netherlands; <sup>4</sup>The authors share last authorship

## ABSTRACT

Mantle cell lymphoma (MCL) is an aggressive non-Hodgkin lymphoma subtype arising from naïve B cells. Although novel therapeutics have improved patient prognosis, drug resistance remains a key problem. Here, we show that the SRC-family tyrosine kinase hematopoietic cell kinase (HCK), which is primarily expressed in the hematopoietic lineage but not in mature B cells, is aberrantly expressed in MCL, and that high expression of HCK is associated with inferior prognosis of MCL patients. HCK expression is controlled by the toll-like receptor (TLR) adaptor protein MYD88 and can be enhanced by TLR agonists in MCL cell lines and primary MCL. In line with this, primary MCL with high HCK expression are enriched for a TLR-signaling pathway gene set. Silencing of HCK expression results in cell cycle arrest and apoptosis. Furthermore, HCK controls integrin-mediated adhesion of MCL cells to extracellular matrix and stromal cells. Taken together, our data indicate that TLR/MYD88-controlled aberrant expression of HCK plays a critical role in MCL proliferation and survival as well as in retention of the malignant cells in the growth- and survival-supporting lymphoid organ microenvironment, thereby contributing to lymphomagenesis. These novel insights provide a strong rationale for therapeutic targeting of HCK in MCL.

## INTRODUCTION

Mantle cell lymphoma (MCL) is an aggressive lymphoma subtype with poor clinical outcome, characterized by the t(11;14)(q13;q32) translocation, resulting in overexpression of Cyclin D1. Advances in MCL therapy have improved patient prognosis, but due to primary and secondary resistance there is a high clinical need for novel therapeutic targets [1].

The SRC-family tyrosine kinase hematopoietic cell kinase (HCK), which is predominantly expressed in the hematopoietic lineage, has been implicated in various cellular processes including chemokine signaling, proliferation, apoptosis, and immune cell activation [2,3,4,5]. Furthermore, HCK has been shown to be deregulated in hematological and solid malignancies, and plays a role in tumor cell survival [6,7,8]. In Waldenström's Macroglobulinemia (WM) and activated B-cell type diffuse large B-cell lymphoma (ABC-DLBCL) cells harboring the pathogenic MYD88-L265P mutation, mutant MYD88-dependent HCK expression was observed and HCK knockdown reduces cell viability, implying that HCK targeting could be beneficial in patients with lymphomas with mutant MYD88 [8]. Although no MYD88 mutations have been reported in MCL, MYD88-regulatory toll-like receptors (TLRs) are upregulated and TLR stimulation supports cell proliferation and survival [9,10,11]. Here, we show that HCK is aberrantly expressed in MCL in a TLR- and MYD88-dependent fashion and that high HCK expression correlates with poor prognosis. Furthermore, HCK controls proliferation and survival as well as integrin-mediated adhesion of MCL cells. Our results indicate that HCK inhibition has therapeutic potential in MCL, and possibly also in other lymphomas that do not harbor MYD88 mutations.

## METHODS

For information about shRNA cloning, cell-culture, transductions, stimulations, immunoblotting, primary cell isolation, RT-qPCR, cell-cycle analysis, Annexin-V staining, integrin staining, and Gene Set Enrichment Analysis (GSEA) see Supplementary "Materials and Methods".

For adhesion experiments, JeKo-1 cells expressing inducible shRNA's were pre-treated with doxycycline and allowed to adhere to 96-well-plates, coated with fibronectin or the stromal cell line HS-27a expressing GFP, in the absence/presence of phorbol-12-myristate 13-acetate (PMA). To quantify adhesion to HS-27a, cells were trypsinized and quantified by flow cytometric analysis. As indicated, JeKo-1 or primary MCL cells were treated for 30 min at 37 °C (A419259) or 4 °C (HP2/1, TS1/22) prior to allowing cells to

adhere to fibronectin-coated plates or the stromal cell line HS-27a-GFP, For further details see Supplementary “Materials and Methods”.

## RESULTS AND DISCUSSION

To evaluate HCK mRNA expression across various lymphoid malignancies, we analyzed publicly available microarray data. In germinal center B-cells and normal plasma cells HCK was below the detection-threshold, whereas it was weakly expressed in memory B-cells (Fig. 1a). In tumor biopsies of ABC- and Germinal Center (GC)-DLBCL HCK was expressed, with higher levels of HCK in ABC-DLBCL (Fig. 1a). Expression of HCK in MCL was comparable to GC-DLBCL and higher than in WM, multiple myeloma (MM), or chronic lymphocytic leukemia samples (Fig. 1a). Importantly, high HCK expression was found to correlate with poor overall survival in MCL patients. The median overall survival was 17 months in HCK-high vs. 40 months in HCK-low patients and the 5 year survival was 14% in HCK-high vs. 41% in HCK-low patients (Fig. 1b).

Next, we analyzed HCK protein expression in a panel of WM, DLBCL and MCL cell lines. In the MCL cell lines Maver-1, Granta-519, JeKo-1, Rec-1, and Mino HCK levels were similar to ABC-DLBCLs without MYD88 mutations, whereas in Z-138 HCK was barely detectable (Fig. 1c). Notably, Z-138 represents an atypical MCL cell line, with blastoid transformation in the terminal phase of disease. In GC-DLBCL cell lines HCK was hardly detectable, whereas it was expressed in all ABC-DLBCL cell lines independent of the presence of a MYD88 mutation, although the levels were higher when MYD88 was mutated (Fig. 1c). Notably, the WM cell lines, expressing mutant MYD88, contained less HCK than most MCL lines (Fig. 1c). Higher expression of HCK was observed in the WM cell line MWCL-1 than in BCWM.1, in accordance with a previous study [8]. In addition, we also analyzed HCK expression in primary MCLs alongside healthy B-cell subsets. Whereas HCK mRNA and protein were hardly detectable in naïve, GC and memory B-cells, or in plasmablasts (Fig. 1d & Supplementary Fig. 1), high expression of HCK mRNA (Fig. 1a, Supplementary Fig. 1) and protein (Fig. 1d) was observed in 6 out of 7 primary MCLs, at similar levels as in Granta-519 (Fig. 1d). Taken together, HCK is aberrantly upregulated in MCL, high HCK expression correlates with poor patient survival, and enhanced HCK expression in B-cell malignancies is not dependent upon oncogenic MYD88 mutations.

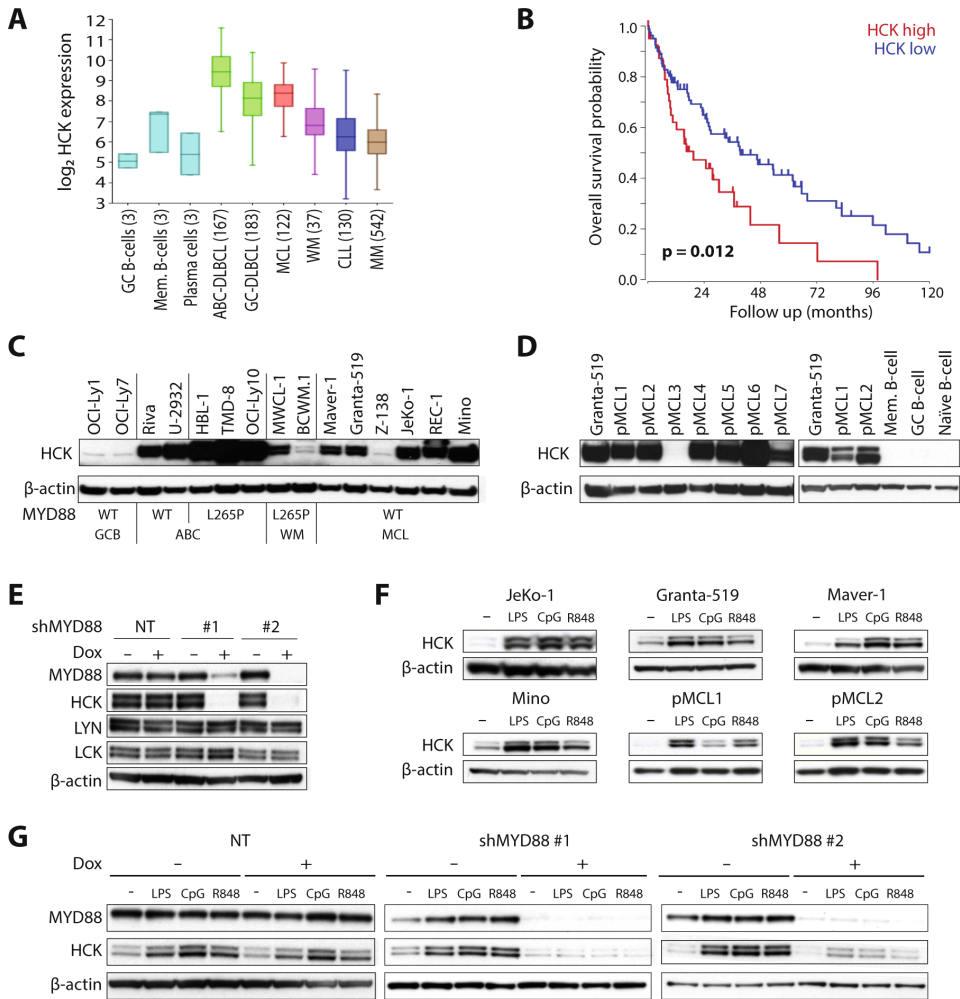


**Figure 1. Aberrant HCK expression in MCL is associated with poor patient survival and controlled by TLR/MyD88-signaling.** **a** *HCK* mRNA expression in MCL patients. Publicly available micro-array datasets of normal B-cell subsets and various B-cell malignancies were analyzed for *HCK* expression. In MCL, *HCK* mRNA is upregulated in comparison to normal B-cell subsets, WM, CLL, and MM. *HCK* expression levels in MCL are similar to those in GC-DLBCL. Between brackets the number of patients per dataset. **b** High *HCK* mRNA expression is correlated with poor MCL patient prognosis. The GSE93291 micro-array dataset containing 122 MCL patients was used to evaluate the prognostic value of *HCK* expression for the tertile of patients with the highest *HCK* expression (HCK high,  $n = 41$ ) versus the rest (HCK low,  $n = 81$ ). Kaplan-Meier curves for overall survival probability are shown,  $p = 0.012$  by the log-rank test. **c** *HCK* protein expression across a panel of various B-cell malignancies. Immunoblot,  $\beta$ -actin was used as a loading control. MYD88 status indicates whether MYD88 is wildtype (WT) or mutated in each cell line. GCB = GC-DLBCL, ABC = ABC-DLBCL **(d)** *HCK* protein expression in primary MCLs and normal B-cells subsets. Immunoblot,  $\beta$ -actin was used as a loading control. **e** *HCK*, *LYN*, and *LCK* protein expression of JeKo-1 cells transduced with pLKO-TET-puro plasmids encoding two shRNA's targeting MYD88 or a scrambled shRNA (NT). Cells were treated with doxycycline (dox) for 7 days. Immunoblot,  $\beta$ -actin was used as a loading control. **f** *HCK* protein expression in MCL cell lines and primary patient cells stimulated with TLR-ligands LPS, CpG, or R848 for 48 h. Immunoblot,  $\beta$ -actin was used as a loading control. **g** *HCK* protein expression in JeKo-1 cells expressing two shRNAs targeting MYD88 or a scrambled shRNA (NT). Cells were treated with doxycycline (dox) for 3 days, followed by stimulation for 48 h with LPS, CpG, or R848 in the absence or presence of doxycycline. Immunoblot,  $\beta$ -actin was used as a loading control.

To investigate whether HCK expression depends on (wild type) MYD88, we transduced JeKo-1 with doxycycline-inducible MYD88 shRNAs. MYD88 knockdown strongly reduced HCK protein and RNA levels, indicating that MYD88-mediated signaling drives HCK transcription in JeKo-1 (Fig. 1e, Supplementary Fig. 2). In contrast, underlining the specificity of this effect, expression of the Src family kinases Lyn, Lck, and Fyn was not affected (Fig. 1e and data not shown). Notably, HCK expression was not reduced upon serum deprivation of the cells, indicating a cell intrinsic mechanism for MYD88-dependent HCK expression (data not shown). Since MYD88 plays a prominent role in TLR-signaling and TLR agonists from necrotic cells are abundantly present in the tumor microenvironment, we stimulated MCL cells with TLR agonists and analyzed HCK levels. Stimulation of JeKo-1, Granta-519, Maver-1, Mino, and primary MCL with TLR agonists enhanced HCK mRNA (Supplementary Fig. 3) and HCK protein levels (Fig. 1f), in a MYD88-dependent manner (Fig. 1g). Hence, HCK expression in MCL depends on constitutive MYD88 signaling and can be further enhanced by TLR stimulation. In line with these findings, GSEA of MCL patients with high versus low HCK expression showed enrichment of the KEGG TLR signaling pathway gene set (Supplementary Table 1 and Supplementary Fig. 4).

Since HCK has been identified as a pro-survival kinase in MYD88-mutated ABC-DLBCL and WM cell lines [8], we investigated if HCK is involved in MCL cell survival. JeKo-1 and Granta-519 were transduced with doxycycline-inducible HCK shRNAs and in both cell lines knockdown of HCK resulted in a significant decrease in the number of viable cells (Fig. 2a, b). To discriminate between effects on cell proliferation and apoptosis, we performed BrdU cell proliferation and Annexin-V apoptosis assays following HCK knockdown. In both cell lines HCK knockdown increased the percentage of cells in G1 and decreased the percentage of cells in S-phase (Fig. 2c). Furthermore, an increase in the amount of Annexin-V positive cells was observed after HCK knockdown (Fig. 2d). These data demonstrate that HCK regulates proliferation, i.e., G1/S transition, and survival of MCL cells.

As illustrated by the molecular mechanism underlying the clinical efficacy of the BTK inhibitor ibrutinib in MCL patients, MCL cells are critically dependent upon the interaction with their tumor microenvironment for *in vivo* survival and growth, and integrin-mediated adhesion is crucial for retention of the MCL cells in their protective lymphoid organ niche [12,13,14]. Interestingly, the integrin-mediated adhesion of MCL cells to fibronectin and the bone marrow stromal cell line HS-27a was significantly impaired after HCK knockdown (Fig. 2e, f). Notably, integrin activation by stimulation of PKC with PMA rescued this effect (Fig. 2e), demonstrating that the impaired adhesion upon HCK silencing does not reflect reduced cell viability or integrin expression (Supplementary Fig. 5a) and that PKC controls integrin activity independent or downstream of HCK. Pretreatment of MCL

cells with the integrin  $\alpha 4$  blocking antibody HP2/1 completely abrogated the adhesion to fibronectin and diminished the adhesion to the bone marrow stromal cell line HS-27a by more than 85% (Supplementary Fig. 5b), demonstrating the involvement of integrin  $\alpha 4\beta 1$ , also in the interaction with stromal cells. Finally, to assess a possible role for HCK in adhesion of primary MCL, we employed a potent inhibitor of HCK, the pan-Src family kinase inhibitor A419259 [15]. Both primary MCL tested, as well as JeKo-1 cells, showed a strong dose-dependent reduction in the adhesion to fibronectin upon treatment with A419259 (Fig. 2g & Supplementary Fig. 5c), and stimulation of PKC with PMA rescued this effect (Supplementary Fig. 5c). Although inhibition of other SFKs may also contribute to the observed reduction in adhesion, these data support a potential involvement of HCK in regulation of integrin-mediated adhesion of primary MCL cells as well.

Taken together, we demonstrate that HCK is aberrantly upregulated in MCL cell lines and primary patient samples, and high expression of HCK correlates with inferior prognosis. In MCL, HCK expression is MYD88-dependent, but not driven by mutant MYD88. Furthermore, TLR/MYD88-signaling transcriptionally regulates HCK levels. Thus, the aberrant HCK expression in primary MCL cells may reflect local TLR stimulation in the tumor microenvironment. This notion is supported by the GSEA, showing enrichment of a TLR signaling pathway gene set in MCL patients with high expression of HCK. Functionally, HCK knockdown results in G1/S arrest and impaired cell viability. In addition, we established that HCK regulates integrin-mediated adhesion of MCL cells to the extracellular matrix and stromal cells. By analogy to our studies on the mechanism of action underlying the clinical efficacy of ibrutinib [12,13,14], this implies that HCK inhibition could mobilize MCL cells from their protective lymphoid organ niche into the circulation, thereby depriving them from critical growth- and survival-factors. Combined with the restricted expression of HCK in hematopoietic cells, enhancing the likelihood of clinical safety, our results provide a strong rationale for clinical studies exploring the efficacy of targeted therapy with HCK inhibitors in MCL.

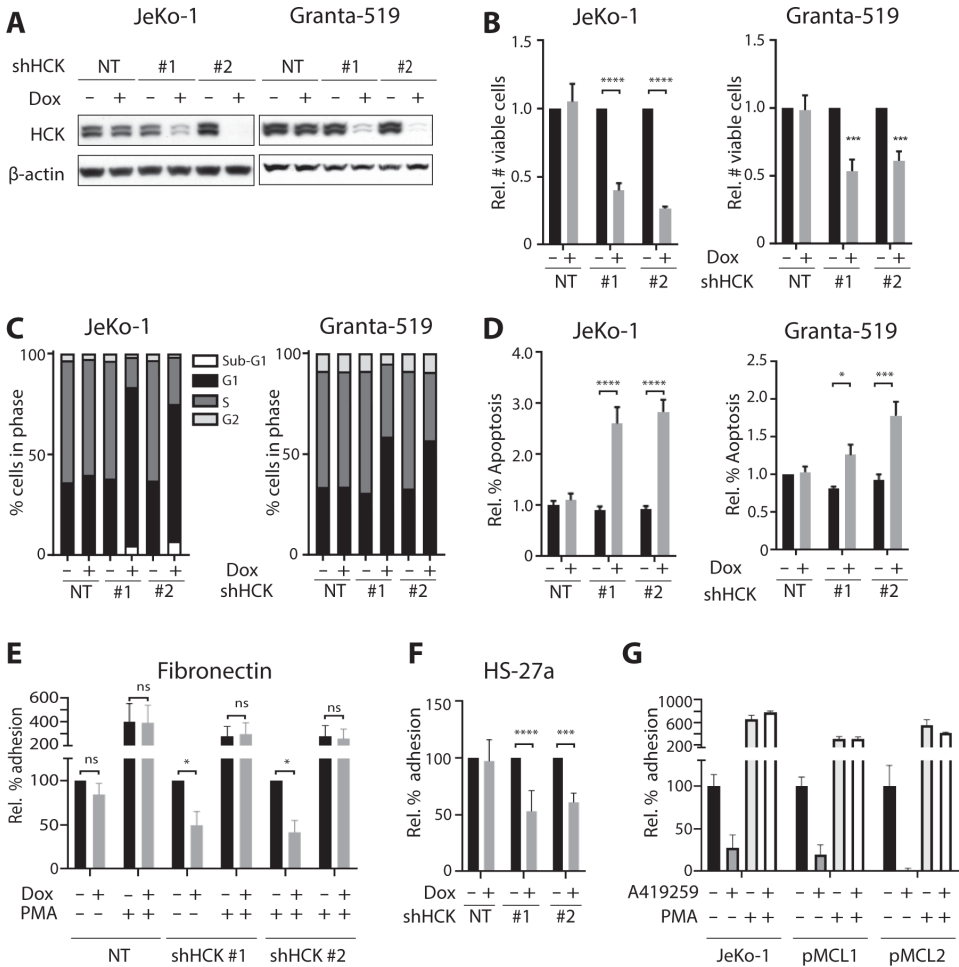


**Figure 2. HCK is critical for proliferation, survival and integrin-mediated adhesion of MCL cells.** **a-f** JeKo-1 and Granta-519 cells were transduced with pLKO-TET-puro plasmids encoding two shRNA's targeting HCK or a scrambled shRNA (NT). **a** HCK protein expression in MCL cell lines after 3 days of doxycycline treatment. Immunoblot,  $\beta$ -actin was used as a loading control. **b** Number of viable cells after HCK knockdown, determined by flow cytometric analysis and 7-AAD staining after 7 days of doxycycline treatment. Number of viable cells was normalized to the untreated condition. Data are presented as mean  $\pm$  S.E.M. of four independent experiments performed in triplicate. **c** Cell cycle analysis after HCK knockdown. The percentage of cells in Sub-G1 (BrdU-, <To-Pro-3-), G1 (BrdU-, To-Pro-3-), S (BrdU+), and G2 (BrdU+, To-Pro-3+) were determined by flow cytometric analysis after 7 days of doxycycline treatment. The graphs are representative for 3 individual experiments. **d** Apoptosis after HCK knockdown, defined as the percentage of Annexin-V positive cells after 7 days of doxycycline treatment. Percentage of Annexin-V positive cells were normalized to the untreated condition. Data are presented as mean  $\pm$  S.E.M. of three independent experiments. **e** Integrin-mediated adhesion of JeKo-1 cells after HCK knockdown. Cells were treated with doxycycline for 4 days and allowed to adhere to fibronectin-coated plates for 30 min in the presence or absence of PMA. Non-adherent cells were removed by extensive washing, and adherent cells were quantified. Percentage of adherent cells were normalized to the untreated condition. Data are presented as mean  $\pm$  S.E.M. of two independent experiments performed in triplicate. **f** Stromal cell adhesion of JeKo-1 cells after HCK knockdown. JeKo-1 cells were treated with doxycycline for 5 days and allowed to adhere to a monolayer of HS-27a-GFP stromal cells for 30 min. Non-adherent cells were removed by extensive washing, and adherent cells were quantified by flow cytometric analysis to

separate HS-27a-GFP from JeKo-1 cells. Percentage of adherent cells were normalized to the untreated condition. Data are presented as mean  $\pm$  S.E.M. of four independent experiments performed in triplicate. **g** Integrin-mediated adhesion of primary MCL or JeKo-1 cells treated for 30 min with 100 nM A419259 and allowed to adhere to fibronectin-coated plates for 30 min. Non-adherent cells were removed by extensive washing, and adherent cells were quantified. Percentage of adherent cells were normalized to the untreated condition. \*P < 0.05; \*\*P < 0.01; \*\*\*P < 0.001; \*\*\*\*P < 0.0001 using two-way ANOVA with Sidak multiple comparison test.

## **ACKNOWLEDGEMENTS**

This work is supported by grants from Lymph&Co, the IWMMF, and the Dutch Cancer Society (KWF).

## **CONTRIBUTIONS**

HCL designed the research, performed experiments, analyzed the data, designed the figures, and wrote the paper; MM and AK performed experiments; MK supervised the study and provided primary patient material; STP and MS supervised the study, designed the research, analyzed the data, and wrote the paper.

## **CONFLICT OF INTEREST**

The authors declare that they have no conflict of interest.

## REFERENCES

1. Martin P, Maddocks K, Leonard JP, Ruan J, Goy A, Wagner-Johnston N, et al. Postibrutinib outcomes in patients with mantle cell lymphoma. *Blood*. 2016;127:1559–63. doi: 10.1182/blood-2015-10-673145.
2. Ziegler SF, Marth JD, Lewis DB, Perlmutter RM. Novel protein-tyrosine kinase gene (hck) preferentially expressed in cells of hematopoietic origin. *Mol Cell Biol*. 1987;7:2276–85. doi: 10.1128/MCB.7.6.2276.
3. El-Shazly A, Yamaguchi N, Masuyama K, Suda T, Ishikawa T. Novel association of the Src family kinases, Hck and c-Fgr, with CCR3 receptor stimulation: A possible mechanism for eotaxin-induced human eosinophil chemotaxis. *Biochem Biophys Res Commun*. 1999;264:163–70. doi: 10.1006/bbrc.1999.1379.
4. Scholz G, Cartledge K, Dunn AR. Hck enhances the adherence of lipopolysaccharide-stimulated macrophages via Cbl and phosphatidylinositol 3-kinase. *J Biol Chem*. 2000;275:14615–23. doi: 10.1074/jbc.275.19.14615.
5. Podar K, Mostoslavsky G, Sattler M, Tai YT, Hayashi T, Catley LP, et al. Critical role for hematopoietic cell kinase (Hck)-mediated phosphorylation of Gab1 and Gab2 docking proteins in interleukin 6-induced proliferation and survival of multiple myeloma cells. *J Biol Chem*. 2004;279:21658–65. doi: 10.1074/jbc.M305783200.
6. Kubo T, Kuroda Y, Shimizu H, Kokubu A, Okada N, Hosoda F, et al. Resequencing and copy number analysis of the human tyrosine kinase gene family in poorly differentiated gastric cancer. *Carcinogenesis*. 2009;30:1857–64. doi: 10.1093/carcin/bgp206.
7. Roversi FM, Pericole FV, Machado-Neto JA, da Silva Santos Duarte A, Longhini AL, Corrocher FA, et al. Hematopoietic cell kinase (HCK) is a potential therapeutic target for dysplastic and leukemic cells due to integration of erythropoietin/PI3K pathway and regulation of erythropoiesis: HCK in erythropoietin/PI3K pathway. *Biochim Biophys Acta Mol Basis Dis*. 2017;1863:450–61. doi: 10.1016/j.bbadis.2016.11.013.
8. Yang G, Buhrlage SJ, Tan L, Liu X, Chen J, Xu L, et al. HCK is a survival determinant transactivated by mutated MYD88, and a direct target of ibrutinib. *Blood*. 2016;127:3237–52. doi: 10.1182/blood-2016-01-695098.
9. Akhter A, Street L, Ghosh S, Burns BF, Elyamany G, Shabani-Rad MT, et al. Concomitant high expression of Toll-like receptor (TLR) and B-cell receptor (BCR) signalling molecules has clinical implications in mantle cell lymphoma. *Hematol Oncol*. 2017;35:79–86. doi: 10.1002/hon.2251.
10. Wang L, Zhao Y, Qian J, Sun L, Lu Y, Li H, et al. Toll-like receptor-4 signaling in mantle cell lymphoma: effects on tumor growth and immune evasion. *Cancer*. 2013;119:782–91. doi: 10.1002/cncr.27792.
11. Mastorci K, Muraro E, Pasini E, Furlan C, Sigalotti L, Cinco M, et al. Toll-like receptor 1/2 and 5 ligands enhance the expression of cyclin D1 and D3 and induce proliferation in mantle cell lymphoma. *PLoS One*. 2016;11:e0153823. doi: 10.1371/journal.pone.0153823.
12. Chang BY, Francesco M, De Rooij MF, Magadala P, Steggerda SM, Huang MM, et al. Egress of CD19(+)CD5(+) cells into peripheral blood following treatment with the Bruton tyrosine kinase inhibitor ibrutinib in mantle cell lymphoma patients. *Blood*. 2013;122:2412–24. doi: 10.1182/blood-2013-02-482125.
13. de Rooij MF, Kuil A, Kater AP, Kersten MJ, Pals ST, Spaargaren M. Ibrutinib and idelalisib synergistically target BCR-controlled adhesion in MCL and CLL: a rationale for combination therapy. *Blood*. 2015;125:2306–9. doi: 10.1182/blood-2014-12-619163.
14. de Rooij MF, Kuil A, Geest CR, Eldering E, Chang BY, Buggy JJ, et al. The clinically active BTK inhibitor PCI-32765 targets B-cell receptor- and chemokine-controlled adhesion and migration in chronic lymphocytic leukemia. *Blood*. 2012;119:2590–4. doi: 10.1182/blood-2011-11-390989.
15. Saito Y, Yuki H, Kuratani M, Hashizume Y, Takagi S, Honma T, et al. A pyrrolo-pyrimidine derivative targets human primary AML stem cells in vivo. *Sci Transl Med*. 2013;5:181ra52. doi: 10.1126/scitranslmed.3004387.

## SUPPLEMENTARY METHODS AND FIGURES

### Cell culture and treatments

The MCL cell lines JeKo-1, Granta-519, Maver-1, Z-138, Rec-1 and Mino; the DLBCL cell lines OCI-Ly1, OCI-Ly7; and the WM cell lines BCWM.1 and MWCL-1 (both kindly provided by Dr. Zachary Hunter) were cultured in IMDM medium supplemented with 10 % fetal calf serum. The DLBCL cell lines Riva and U2932 were cultured in RPMI-1640 medium supplemented with 10 % fetal calf serum, HBL-1 and TMD8 supplemented with 20 % fetal calf serum and OCI-Ly10 supplemented with 20 % human serum (Sigma-Aldrich). The stromal cell line HS-27a was cultured in DMEM supplemented with 10 % fetal calf serum. All cells were cultured with supplement of 2 mM L-glutamine, 100 units/mL penicillin and 100 µg/mL streptomycin. Cell lines were routinely authenticated by STR profiling (Promega, Madison, Wisconsin, USA) and monitored for contaminations with mycoplasmas. Peripheral blood derived MCL cells were obtained after routine diagnostics or follow-up procedures at the department of Hematology of the Amsterdam University Medical Centers, location AMC, the Netherlands, and were purified using Ficoll and B cell isolation kit (Milteny Biotec.) Purified MCL samples were sorted on a BD-FACS-Aria IIu to obtain CD5+/CD19+ cells and were cultured in IMDM supplemented with 20 % fetal calf serum, 2 mM L-glutamine, 100 units/ml penicillin and 100 µg/ml streptomycin. This study was approved by the AMC Medical Committee on Human Experimentation. Informed consent was obtained in accordance with the revised Declaration of Helsinki 2008.

Naïve B-cells (CD19+/IgD-/CD38-), germinal center B-cells (CD19+/IgD-/CD38+), memory B-cells (CD19+/IgD-/CD38-) and plasmablasts (CD19+/IgD-/Cd38hi) were isolated from tonsil and sorted on a BD FACS-Aria IIu (BD Biosciences).

For inducible shRNA-mediated knockdown, cells were incubated with 3 µg/ml doxycycline for 3-7 days as indicated. MCL cell were stimulated with 1 µg/ml LPS (Sigma-Aldrich), 0.05 µM CPG (Invivogen) or 1 µg/ml R848 (Invivogen) for 3 hours (RNA) or 48 hours (immunoblot).

### Transfection and transduction

shRNA's against HCK #1 (CCAGGTCGGAGGCAATACATT), #2 (CAGGGAGATACCGTGAAACAT) and against MYD88 #1 (CCTGTCTCTGTTCTTGAACGT) and #2 (GCAGAGCAAGGAATGTGACTT) were inserted in Tet-pLKO-puro (Gift from Dmitri Wiederschain, Addgene #21915) as previously described<sup>1</sup>. Lentiviral particles were generated by cotransfection of pMD2.G (Gift from Didier Trono, Addgene #12259), pPAX2 (Gift from Didier Trono, Addgene #12260) and the lentiviral shRNA encoding vector in a 1:2:4 ratio with Genius DNA transfection reagent (Westburg) according to

the manufacturer's instructions. Forty-eight hours after transfection, lentiviral particles were harvested and MCL cells were spinofected for 60 minutes at 1800 x g at 33° C in the presence of 8 µg/ml polybrene (Sigma-Aldrich). Three days after transduction the cells were selected with increasing concentrations of puromycin (Invivogen) for 10-14 days (JeKo-1) or 18-21 days (Granta-519). Similarly, HS-27a was transduced with pLKO-GFP, with the exception that transduced GFP positive cells were sorted on a Sony SH800s cell sorter.

### Immunoblotting

Protein lysates (whole-cell extracts in RIPA-buffer) were separated on Bolt™ 4-12% Bis-Tris Plus gels (Invitrogen) and subsequently blotted to a PVDF-membrane. The antibodies used were: mouse anti-β-actin (AC-15, Sigma-Aldrich), rabbit anti-HCK (E117F, Cell Signaling Technology), rabbit anti-MYD88 (D80F5, Cell Signaling Technology), rabbit anti-LYN (44, Santa Cruz Biotechnology) and rabbit anti-LCK (2102, Santa Cruz Biotechnology). Primary antibodies were detected with anti-mouse-HRP or anti-rabbit-HRP (both DAKO), followed by detection using Pierce™ ECL Western Blotting Substrate (Thermo Scientific).

### RT-qPCR

Total RNA was isolated using TRI-reagent (Sigma-Aldrich), according to the manufacturer's protocol. RNA was converted to cDNA using oligo-DT. PCRs were performed using Sensifast (Bioline) on a CFX-384 RT-PCR detection system (Bio-Rad) and obtained Ct values were normalized to those of the input control RPLP0. Primers used were: HCK forward (TGGCAGTGAAGACGATGAAG), HCK reverse (GTAGATGGGCTCCTTGGTGA), RPLP0 forward (GCTTCCTGGAGGGTGCCGC) and RPLP0 reverse (TCCGTCTCCACAGACAAGGCCA)

### Adhesion assay

The adhesion assays were essentially performed as previously described 2.3. In detail, adhesion assays were performed in triplicate on Microlon® high binding plates (Greiner) coated overnight with PBS containing 10 µg/ml fibronectin (Sigma-Aldrich) or 4 % BSA (Sigma-Aldrich) at 4° C overnight or with 1 mg/ml poly-L-lysine (PLL, Sigma-Aldrich) for 15 minutes at 37° C. On the day of the experiment plates were blocked for 1h at 37° C with IMDM/4 % BSA. In the case of adhesion to the stromal cell line HS-27a-GFP, 15.000 cells were seeded the day prior to the experiment in order to form a confluent cell monolayer. As indicated, cells were treated for 30 minutes with A419259 at 37° C or Hp2/1 (Millipore) and TS1/22 (Invitrogen) at 4° C. Per well 1,5\*10<sup>5</sup> JeKo-1 or 5\*10<sup>5</sup> primary MCL cells were plated and incubated with or without PMA (50 ng/ml) at 37° C for 30 minutes. After extensive washing of the plate with IMDM/0,5 % BSA to remove non-adherent cells, the cells were fixed for 10 minutes with 10 %

glutaraldehyde/PBS (Millipore) and subsequently stained with 0,4 % crystalviolet/20 % ethanol for 45 minutes. After thorough washing with ddH<sub>2</sub>O, ethanol was added for 30 minutes to elute the dye and quantified by measuring the absorbance at 570 nm on a spectrophotometer (Clariostar, BMG Labtech). In the case of adhesion to stromal cell line HS-27a-GFP, cells were not fixed but trypsinised and subsequently quantified by flow cytometric analysis (FACS Cantoll, BD Biosciences). When analyzing adhesion to fibronectin, absorbance due to nonspecific adhesion, as determined in wells coated with 4% BSA, was subtracted. Maximal adhesion (100%) was determined by applying the cells to wells coated with PLL, without washing the wells before fixation or, in the case of adhesion to HS-27a, by counting the number of input cells.

### **Annexin-V staining**

Annexin-V staining was essentially performed as previously described 4. Briefly, cells were stained with Annexin-V-FITC in Annexin binding buffer followed by staining with To-Pro-3 and analysis on a FACS Cantoll. Apoptotic cells were defined as Annexin-V+. Typically JeKo-1 cells showed approximately 7 % Annexin-V+ cells at baseline and Granta-519 13 % respectively.

### **BrdU cell-cycle analysis**

For cell-cycle analysis, cells were incubated for 1 hour with 20  $\mu$ M BrdU (Sigma-Aldrich), washed once with PBS/0,1 % BSA and subsequently fixed in ice-cold 75 % ethanol/PBS. After washing, the cells were incubated with 0,4 mg/ml pepsin in 0.2 mM HCl for 30 minutes at room temperature and subsequently with 2 N HCl for 25 minutes at 37° C. Cells were washed once with PBT (PBS/0,05 % Tween-20) and once with PBTB (PBT/2 % BSA) and stained for 30 minutes with anti-BrdU-FITC (clone B44, BD Biosciences) in PBTB. After washing with PBT and PBTB, cells were treated with 500  $\mu$ g/ml RNAse A (Bioke) and stained with 0,1  $\mu$ M To-Pro-3 (Invitrogen) in PBS/1 % BSA/0,05 % NaN<sub>3</sub> for 15 minutes at 37° C followed by analysis on a FACS Canto II (BD Biosciences).

### **Flow Cytometric analysis**

105 cells were stained with anti- $\alpha$ 4-integrin ( HP2/1, Millipore), anti- $\alpha$ 4 $\beta$ 7-integrin 5, anti- $\beta$ 1-integrin (4B4, Coulter Immunology), or control mouse anti-IgG1, followed by staining with PE-conjugated anti-mouse IgG1. Cell surface staining was analyzed on a FACSCantoll (BD Biosciences).

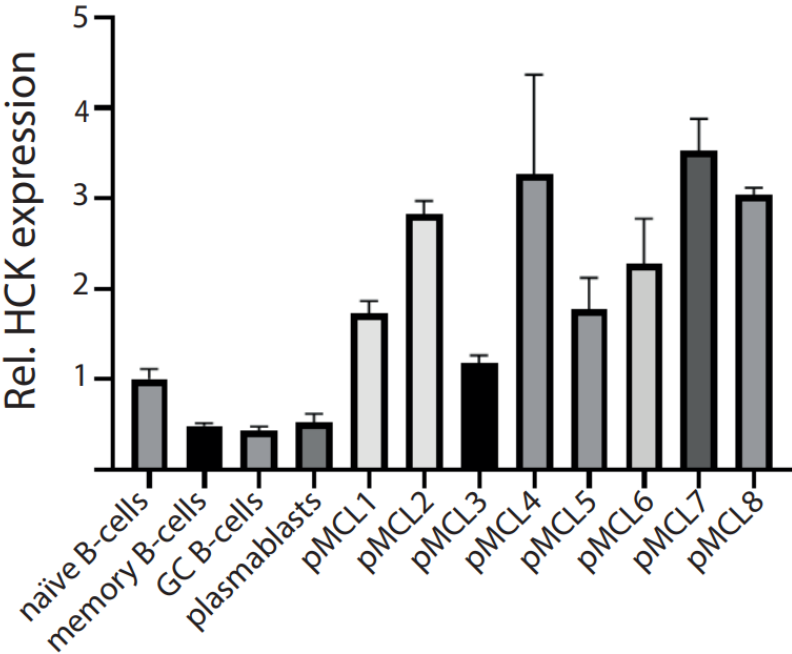
### **Microarray analysis**

The following gene expression data, publically available and deposited in the NIH Gene Expression Omnibus database, were analyzed using the R2 Genomics Analysis and Visualization Platform (r2.amc.nl): GSE12366 (healthy B-cells, excluding undefined B-cells), GSE10846 (DLBCL, excluding unclassified subtypes), GSE93921 (MCL), GSE9656

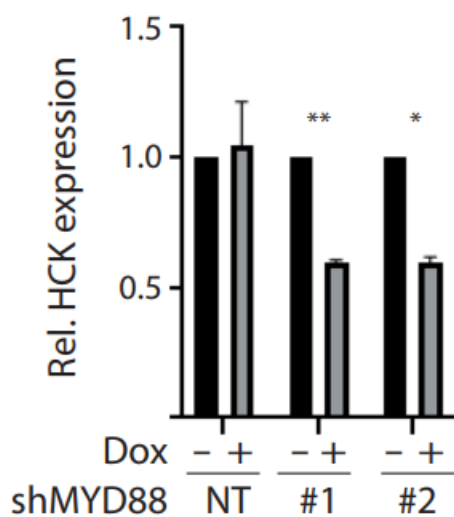
(WM), GSE39671 (CLL) and GSE2658 (MM). The overall survival of the tertile of MCL patients (GSE93921) with the highest HCK expression (HCK high) was compared to the rest (HCK low). All datasets were obtained with the Affymetrix U133p2 array and normalized using the MAS 5.0 algorithm to allow comparison between datasets.

### Gene Set Enrichment Analysis

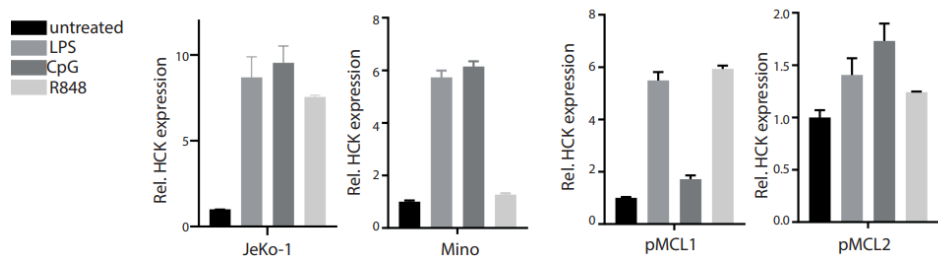
Gene Set Enrichment Analysis (GSEA) was performed using the GSEA application (version 4.0.3) on microarray data comparing the HCK high versus HCK low MCL patients on the curated KEGG pathway gene sets. GSEA plots were redrawn using the replotGSEA function from the Rtoolbox package (<https://github.com/PepperLab/Rtoolbox>).



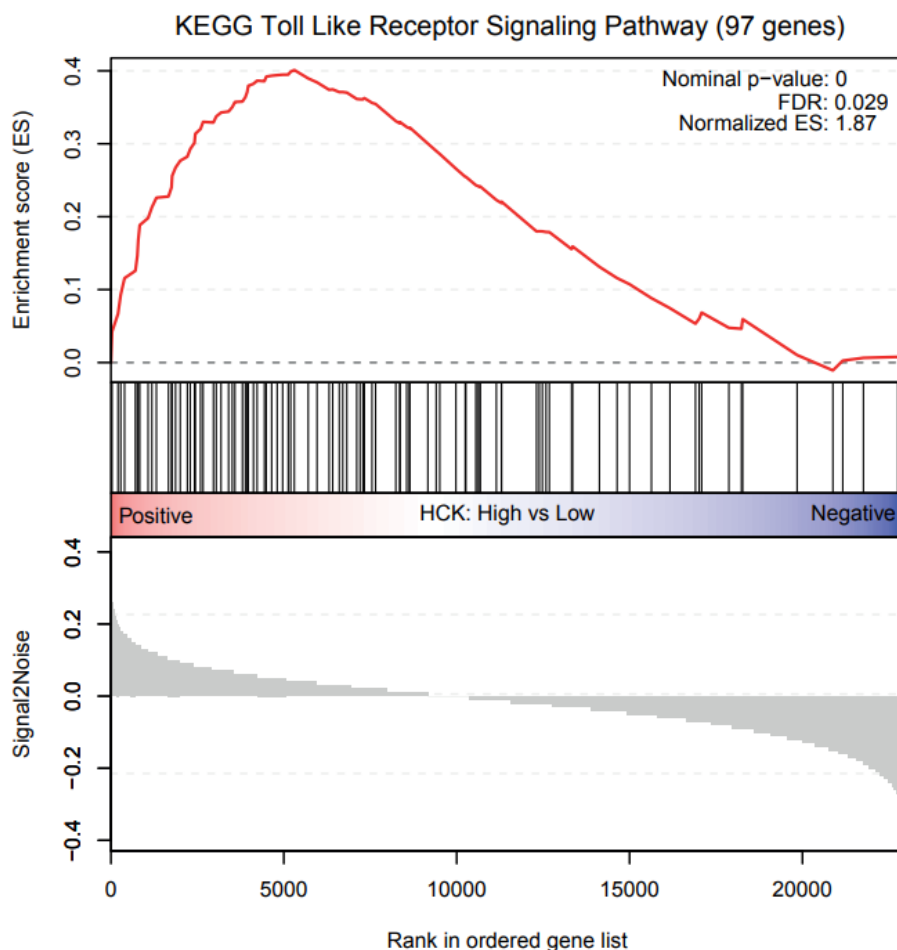
**Supplemental Figure 1.** HCK mRNA expression in normal B-cells or primary MCL material determined by RT-qPCR. RPLP0 was used as an input control. Data were normalized to the value of naïve B-cells.



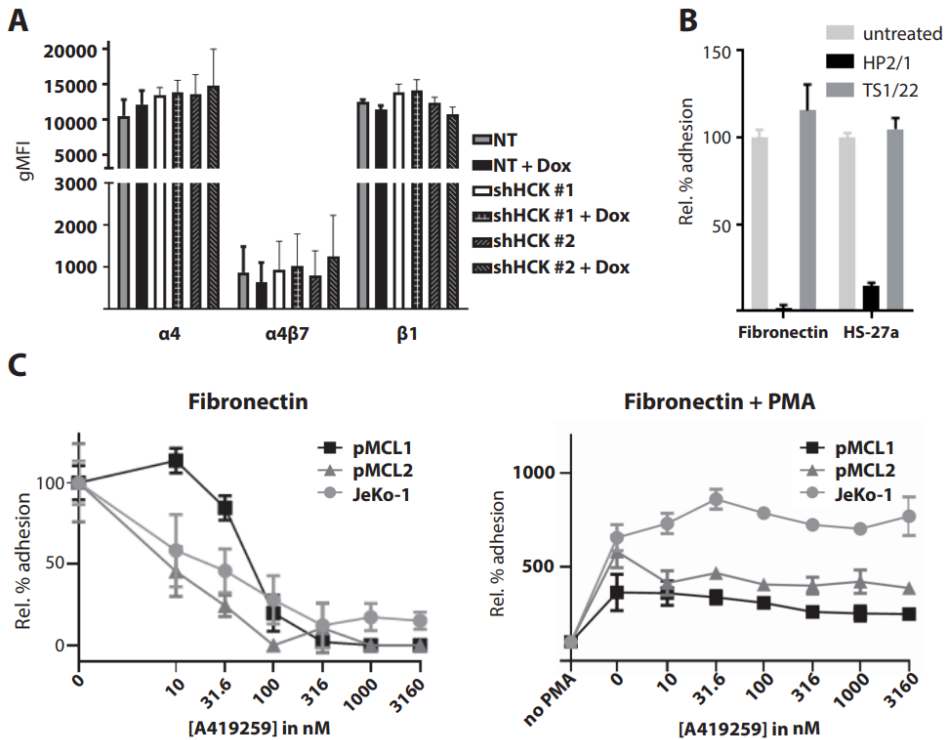
**Supplemental Figure 2.** HCK mRNA expression after MYD88 knockdown determined by RT-qPCR. Jeko-1 cells expressing two doxycycline-inducible shRNA targeting MYD88 or a non-targeting shRNA (NT) were treated for 7 days with doxycycline. Data were normalized to the value of untreated cells. RPLP0 was used as an input control. Data are presented as mean  $\pm$  S.E.M of three independent experiments performed in triplicate.



**Supplemental Figure 3.** HCK mRNA expression in primary MCL material and cell lines stimulated for 3 hours with LPS, CpG or R848 determined by RT-qPCR. RPLP0 was used as an input control. Different y-axis scales were used in order to visualize the various stimuli in each cell type. Data were normalized to the value of untreated cells.



**Supplemental Figure 4.** Enrichment plot of HCK High (n=41) versus Low (n=81) patients on the curated KEGG geneset Toll Like Receptor Signaling Pathway. FDR = False Discovery Rate, ES = Enrichment Score.



**Supplemental Figure 5.** (A) Expression of various integrin subtypes after HCK knockdown in JeKo-1 cells transduced with pLKO-TET-puro plasmids encoding two shRNA's targeting HCK, as determined by flow cytometric analysis after 4 days of doxycycline treatment. Data are presented as mean  $\pm$  S.E.M. of three independent experiments. (B) Integrin-mediated adhesion of JeKo-1 cells after treatment with blocking antibodies against integrin- $\alpha 4$  (HP2/1) or integrin- $\alpha L$  (TS1/22). Cells were treated for 30 minutes at 4 °C and then allowed to adhere to fibronectin-coated plates or a monolayer of HS-27a-GFP stromal cells for 30 minutes. Non-adherent cells were removed by extensive washing, and adherent cells were quantified. Percentages of adherent cells were normalized to the untreated condition. Data are presented as mean  $\pm$  S.D. (C) Integrin-mediated adhesion of primary MCL or JeKo-1 cells after treatment with A419259 with or without PMA. Cells were treated for 30 minutes with various concentrations of A419259 in the absence (left panel) or presence (right panel) of PMA and allowed to adhere to fibronectin-coated plates for 30 minutes. Non-adherent cells were removed by extensive washing, and adherent cells were quantified. Percentages of adherent cells were normalized to the untreated condition without PMA.

### Supplementary Table 1

Ten most enriched KEGG pathway gene sets when comparing MCL patients with high HCK (41) compared to low HCK (81) using the GSEA software.

Rank	Geneset (size)	NES	NOM p-val	FDR
1	KEGG Cell Cycle (121)	2,43	0	0
2	KEGG DNA Replication (33)	2,4	0	0
3	KEGG Base Excision Repair (30)	2,15	0	0,003
4	KEGG Leishmania Infection (68)	2,14	0	0,004
5	KEGG P53 Signaling Pathway (68)	2,1	0	0,004
6	KEGG Homologous Recombination (24)	1,9	0,005	0,017
7	KEGG Fructose and Mannose Metabolism (32)	1,89	0,005	0,017
8	KEGG Pyrimidine Metabolism (89)	1,88	0	0,016
9	KEGG Toll Like Receptor Signaling Pathway (97)	1,87	0	0,029
10	KEGG Nucleotide Excision Repair (42)	1,78	0	0,03

NES = Normalised Enrichment Score, NOM p-val = nominal p-value, FDR = False Discovery Rate

## SUPPLEMENTARY REFERENCES

1. Wiederschain D, Wee S, Chen L, et al. Single-vector inducible lentiviral RNAi system for oncology target validation. *Cell Cycle*. 2009;8(3):498-504.
2. Spaargaren M, Beuling EA, Rurup ML, et al. The B cell antigen receptor controls integrin activity through Btk and PLCgamma2. *J Exp Med*. 2003;198(10):1539-1550.
3. de Rooij MF, Kuil A, Geest CR, et al. The clinically active BTK inhibitor PCI-32765 targets B-cell receptor- and chemokine-controlled adhesion and migration in chronic lymphocytic leukemia. *Blood*. 2012;119(11):2590-2594.
4. Koopman G, Reutelingsperger CP, Kuijten GA, Keehnen RM, Pals ST, van Oers MH. Annexin V for flow cytometric detection of phosphatidylserine expression on B cells undergoing apoptosis. *Blood*. 1994;84(5):1415-1420.
5. Lazarovits AI, Moscicki RA, Kurnick JT, et al. Lymphocyte activation antigens. I. A monoclonal antibody, anti-Act I, defines a new late lymphocyte activation antigen. *J Immunol*. 1984;133(4):1857-1862.



# 4

## The oncogenic human B-cell lymphoma MYD88 L265P mutation genocopies activation by phosphorylation at the Toll/interleukin-1 receptor (TIR) domain

Marthe Minderman<sup>1,2</sup>, Hildo Lantermans<sup>1,2</sup>, Carmen van der Zwaan<sup>3</sup>,  
Arjan J. Hoogendijk<sup>3</sup>, Maartje van den Biggelaar<sup>3</sup>, Marie José Kersten<sup>2,4</sup>,  
Marcel Spaargaren<sup>1,2,5</sup>, Steven T. Pals<sup>1,2,5</sup>.

<sup>1</sup>Department of Pathology, Cancer Center Amsterdam, Amsterdam UMC, Location University of Amsterdam, The Netherlands; <sup>2</sup>Lymphoma and Myeloma Center Amsterdam – LYMMCARE, The Netherlands; <sup>3</sup>Department of Molecular Hematology, Sanquin Research, Amsterdam, The Netherlands. <sup>4</sup>Department of Hematology, Cancer Center Amsterdam, Amsterdam UMC, Location University of Amsterdam, the Netherlands. <sup>5</sup>The authors share last authorship

## ABSTRACT

MYD88 is the key signaling adaptor-protein for Toll-like and interleukin-1 receptors. A somatic L265P mutation within the Toll/interleukin-1 receptor(TIR) domain of MYD88 is found in 90% of Waldenström macroglobulinemia cases and in a significant subset of diffuse large B-cell lymphomas. MYD88-L265P strongly promotes NF- $\kappa$ B pathway activation, JAK-STAT signaling and lymphoma cell survival. Previous studies have identified other residues of the TIR-domain crucially involved in NF- $\kappa$ B activation, including serine 257 (S257), indicating a potentially important physiological role in the regulation of MYD88 activation. Here, we demonstrate that MYD88 S257 is phosphorylated in B-cell lymphoma cells and that this phosphorylation is required for optimal TLR-induced NF- $\kappa$ B activation. Furthermore, we demonstrate that a phosphomimetic MYD88-S257D mutant promotes MYD88 aggregation, IRAK1 phosphorylation, NF- $\kappa$ B activation and cell growth to a similar extent as the oncogenic L265P mutant. Lastly, we show that expression of MYD88-S257D can rescue cell growth, upon silencing of endogenous MYD88-L265P expression, in lymphoma cells addicted to oncogenic MYD88 signaling. Our data suggest that the L265P mutation promotes TIR domain homodimerization and NF- $\kappa$ B activation by copying the effect of MY88 phosphorylation at S257, thus providing novel insights into the molecular mechanism underlying the oncogenic activity of MYD88-L265P in B-cell malignancies.

## INTRODUCTION

B cells can detect antigen-specific signals through their B-cell antigen receptor (BCR) and damage- or pathogen-associated signals by the expression of Toll-like receptors (TLRs). Myeloid differentiation primary-response gene 88 (MYD88) is the key signaling adaptor molecule for both interleukin-1 receptors (IL-1Rs) and TLR-derived signals. Activating *MYD88* mutations are found in 10-20% of activated B-cell-like diffuse large B-cell lymphoma (ABC-DLBCL) cases, but are rare in germinal center-like DLBCL (GCB-DLBCL) and most other B cell non-Hodgkin lymphomas (1). Remarkably, *MYD88* mutations are present in approximately 70% of primary testis lymphomas (PTLs), primary central nervous system lymphomas (PCNSLs) and primary vitreoretinal lymphomas (PVRLs) and in over 90% of Waldenström macroglobulinemia (WM) cases (2-7). The vast majority of *MYD88* mutations involve the same amino acid substitution, *i.e.*, a leucine to proline at position 265 (L265P), within the MYD88 Toll/interleukin-1 receptor (TIR) domain. This mutation strongly enhances NF- $\kappa$ B and JAK-STAT3 signaling and thereby promotes the survival of these lymphoma cells (1). In DLBCL but not in WM, the *MYD88* L265P mutation frequently co-occurs with mutations in *CD79B*, an essential BCR complex-associated protein, suggesting that BCR and TLR signaling cooperate to optimally promote NF- $\kappa$ B signaling and tumor cell survival (2, 3, 8).

The regulation of TLR/MYD88 signaling in lymphomas without *MYD88* mutations, as well as in healthy B cells, is incompletely understood. Using mutagenesis assays in HEK293T cells, Vyncke *et al.* identified MYD88 residues essential for MYD88 TIR domain interactions and NF- $\kappa$ B activation. Interestingly, they demonstrated that phosphomimetic S255D and S257D mutations, which mimic physiological phosphorylation at these positions, have opposing effects on NF- $\kappa$ B activation: whereas the S257D mutant promotes hyperactivation of NF- $\kappa$ B, the S255D mutant has an inhibitory effect (9). In line with these findings, previous studies have shown that an alanine substitution at position S257, but not at S255, impairs MYD88 TIR domain interactions and downstream NF- $\kappa$ B activation (10). Importantly, both serine 255 and 257 were shown to be phosphorylated in TLR4-expressing HEK293T cells (11).

The above findings indicate a potentially important physiological role for serine 255 and 257 in the regulation of MYD88 activation, a role that might greatly impact B cell biology and lymphomagenesis. In support of this hypothesis, molecular dynamics simulation revealed that the phosphomimetic MYD88 S257D and the oncogenic L265P mutations provoke a similar conformational change in the MYD88 TIR domain (9). These findings prompted us to directly explore the presence and functional consequences of MYD88 S257 phosphorylation in the cells of interest, *i.e.*, in B lymphoma cells. In the current study, we demonstrate that MYD88 S257 indeed is phosphorylated in B lymphoma cells

and that cells expressing a S257A mutant, impeding phosphorylation, display reduced NF- $\kappa$ B activation upon stimulation with TLR ligands. In addition, we demonstrate that the MYD88 S257D mutant, which mimics constitutive S257 phosphorylation, induces strong MYD88 aggregation, IRAK1 phosphorylation, NF- $\kappa$ B activity and proliferation in DLBCL cells, similar to the L265P mutant, and, moreover, rescues lymphoma cells addicted to MYD88 L265P upon silencing of this oncogene.

## MATERIALS AND METHODS

### Cell lines

OCI-LY1 and OCI-LY7 were cultured in IMDM (Thermo Fisher Scientific, Waltham, Massachusetts, USA) supplemented with 10% FCS. U2932 and RIVA were cultured in RPMI-1640 (Thermo Fisher Scientific) supplemented with 10% FCS and HBL1 and TMD8 were cultured in RPMI-1640 supplemented with 20% FCS. OCI-LY10 was cultured in IMDM supplemented with 20% human serum (Sigma Aldrich, Saint Louis, Missouri, USA). OCI-LY1 and OCI-LY7 were kindly provided by Dr. U. Klein (University of Leeds, Leeds, United Kingdom). OCI-LY10, RIVA and TMD8 were kindly provided by Dr. G. Lenz (University Hospital Münster, Münster, Germany). All cell lines were frequently tested for mycoplasma contamination using RT-qPCR and cell line authentication was routinely performed using Short Tandem Repeat DNA profiling (PowerPlex 16, Promega, Madison, Wisconsin, USA).

### Cloning, transfection and transduction

The MYD88 coding sequence was subcloned into LZRS-IRES-GFP (Addgene plasmid #21961). Subsequently, the QuikChange II Site-Directed Mutagenesis Kit (Agilent, Santa Clara, California, USA) was utilized to generate the MYD88 mutant constructs according to the manufacturer's instructions. Mutants were confirmed by Sanger sequencing. To generate doxycycline-inducible MYD88 knockdown cell lines, we inserted an shRNA targeting MYD88 (GCAGAGCAAGGAATGTGACTT or GACCCAATGTACCAGTATT) into Tet-pLKO-puro (Addgene plasmid #21915). To generate MYD88 knockout cells, we inserted a single guide RNA targeting MYD88 (CTGCTCTCAACATGCGAGTG or CTCGAGCAGTCGGCCTACAG) into pL-CRISPR.EFS.GFP (Addgene plasmid #57818). For generation of stable Cas9 expressing cell lines, we used lentiCas9-Blast (Addgene plasmid #52962). MSCV-CA-IKK2-IRES-GFP was kindly provided by Dr J. Schuringa (University of Groningen, Groningen, The Netherlands).

### RNA isolation, cDNA synthesis and RT-qPCR

Total RNA was extracted using TRI-reagent according to the manufacturer's instructions (Sigma Aldrich) and converted to cDNA using oligo(dT) primers for 1 hour at 37 °C. RT-

qPCRs were executed using Sensifast (Bioline, London, UK) on a on a Lightcycler 480 (Roche, Basel, Switzerland). Expression levels were normalized to expression of RPLP0. Primers used were: MYD88 fw (5'- GAGGCTGAGAAGCCTTACAGG -3'); MYD88 rv (5'- GCAGATGAAGGCATCGAAACGC -3'); HCK fw (5'- TGGCAGTGAAGACGATGAAG -3'); HCK rv (5'- GTAGATGGGCTCCTTGGTGA -3'); CD80 fw (5'- TAGATGCGAGTTTGTGCCAG -3'); CD80 rv (5'- GCTGGCTGGTCTTCTCACT-3'); RPLP0 fw (5'- GCTTCCTGGAGGGTGTCCGC -3'); RPLP0 rv (5'- TCCGTCTCCACAGACAAGGCCA-3').

### **Flow cytometry and viability assays**

Cells were fixed with 4% PFA and subsequently permeabilized with permeabilization buffer (PBS, 1% BSA, 0.1% Saponin) for 15 minutes on ice. Subsequently, cells were incubated with anti-phospho-IRAK1 (Thr209) antibody for 30 minutes on ice (ab218130, Abcam, Cambridge, UK) followed by goat anti-rabbit IgG -DyLight® 650 (ab96886, Abcam) for another 30 minutes. For cell surface staining, cells were incubated with anti-CD80-PE (clone 2D10.4, eBioscience, San Diego, California, USA) for 30 minutes at 4 degrees.

Cell viability was assessed using 7-AAD viability staining solution (Thermo Fisher Scientific). For Annexin-V viability assays (12), cells were incubated with anti-Annexin V-APC (BioLegend, San Diego, California) for 30 minutes at 4 degrees followed by 5 minutes with propidium iodide (PI) (Thermo Fisher Scientific), both diluted in Annexin-V binding buffer (0.1M Hepes (pH 7.4), 1.4M NaCl, and 25 mM CaCl<sub>2</sub>). To assess proliferation, cells were stained with eFluor 660 dye according to manufacturer's instructions (Thermo Fisher Scientific). All flow cytometric measurements were performed on a FACSCanto II flow cytometer (BD Biosciences, San Jose, California, USA).

### **Immunoblotting**

Cells were lysed in RIPA buffer (20 mM Tris-HCl pH 7.4, 150 mM NaCl, 1% NP-40, 0.5% Sodium deoxycholate, 0.1% SDS, 5 mM EDTA, 10% glycerol). Primary antibodies used were: mouse anti-β-tubulin (clone D66, Sigma Aldrich), mouse anti-β-actin (clone AC-15, Sigma-Aldrich), rabbit anti-MYD88 (clone D80F5, Cell Signaling Technology, Danvers, Massachusetts, USA), rabbit anti-HCK (clone E117F, Cell Signaling Technology), rabbit anti-phospho-NF-κB p65 (Ser536) (clone 93H1, Cell Signaling Technology) and mouse anti-p65 (clone F-6, Santa Cruz Biotechnology). Secondary antibodies used were anti-mouse-HRP and anti-rabbit-HRP (both from DAKO, Santa Clara, California, USA). Images were acquired on a ImageQuant LAS 4000 (GE Healthcare Life Sciences) and quantification of immunoblot membranes was performed using Image Lab software (Bio-Rad Laboratories, Hercules, California, USA).

## Statistical analysis

Data is presented as mean  $\pm$  SD of at least three independently performed experiments. Experimental data were analyzed using one-way ANOVA followed by Tukey's multiple comparisons test or two-way ANOVA followed by Sidak's multiple comparisons test. The differences were considered significant when  $p < 0.05$ .

For further details and other methods, see "Supplemental Methods".

# RESULTS

## MYD88 TIR domain serine 257 mediates TLR-induced NF- $\kappa$ B activation in DLBCL cells

Phosphorylation of MYD88 at S257 has been previously described in various cell line models, including HEK293T cells, HeLa cells and K562 leukemia cells (11, 13-15). In B cells, however, phosphorylation has not yet been reported. By employing label-free quantitative mass spectrometry (MS), we detected MYD88 S257 phosphorylation in the DLBCL cell line U2932, which contains unmutated (wildtype) MYD88 (Supplemental Figure 1A). Please note that, to align with the annotation of the oncogenic MYD88 L265P mutant first described by Ngo et al., amino acid positions in the current study are shown according to protein accession NCBI NP\_002459.2 (Figure 1A). MYD88 S257 and L265 correspond to S244 and L252, respectively, annotated according to the canonical sequence (NP\_002459.3).

To establish whether MYD88 phosphorylation at S257 is involved in TLR-mediated NF- $\kappa$ B signaling in B lymphoma, we generated an alanine mutant at position 257 (S257A), disabling phosphorylation. Subsequently, either this S257A mutant or wildtype MYD88 was introduced in the ABC DLBCL cell lines U2932 and RIVA in which the endogenous (wild type) MYD88 protein had been deleted using CRISPR technology (Figure 1B), to rule out signaling via endogenous MYD88. TLR-induced NF- $\kappa$ B activation was effectively abrogated in MYD88 KO U2932 and RIVA cells, confirming functional knockout (Figure 1C, Figure 1D and Supplemental Figure 1B). Equal levels of ectopically expressed wildtype and mutant MYD88 S257A were confirmed by immunoblotting (Figure 1C and Supplemental Figure 1B). Interestingly, TLR-induced NF- $\kappa$ B activation was substantially repressed in cells expressing the MYD88 S257A mutant compared to wildtype MYD88. These results were observed for stimulation with the TLR9 ligand CpG (Figure 1C and Figure 1D) as well as for the TLR1/2 ligand Pam3CSK4 (Supplemental Figure 1B). Both U2932 and RIVA showed a stronger response to CpG stimulation as compared to stimulation with Pam3CSK4. The reduction in NF- $\kappa$ B activation in MYD88 S257A expressing cells was observed after 15, 30 and 60 minutes of TLR stimulation (Figure

1D). These findings indicate that MYD88 S257 phosphorylation is required for optimal TLR-mediated NF- $\kappa$ B activation.

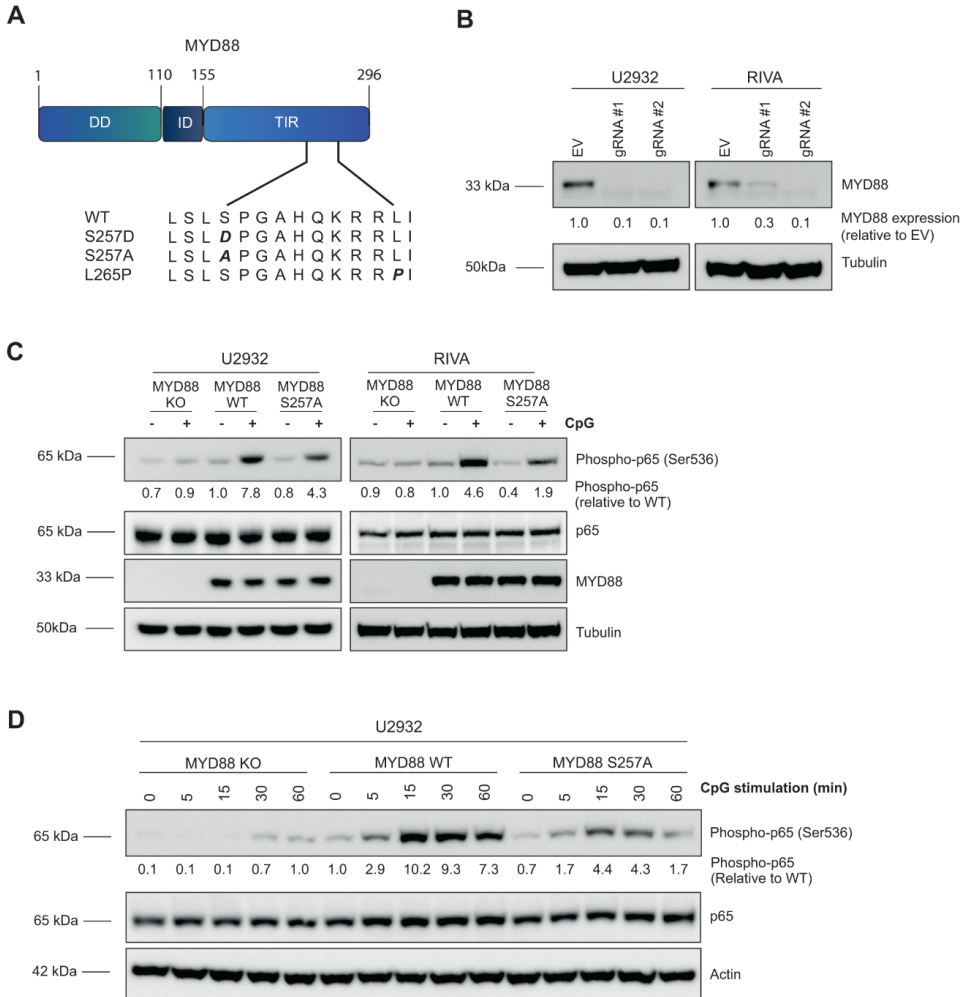


**Figure 1. TLR-induced NF- $\kappa$ B activation is repressed in cells expressing the MYD88 S257A mutant. A**

A schematic diagram of wild-type and mutant MYD88 proteins. Amino acid positions are shown according to protein accession NCBI NP\_002459.2. **B** Immunoblot analysis of MYD88 in U2932 and RIVA transduced lentiCas9-Blast and subsequently transfected with pLentiGuide-GFP containing two different single guide RNAs (sgRNA) targeting MYD88. Cells were allowed to recover for 48 h after transfection before the GFP positive cells were sorted.  $\beta$ -tubulin was used as loading control. **C** Immunoblot analysis of phosphorylated p65 (Ser536) and MYD88 in U2932 and RIVA expressing MYD88 WT or MYD88 S257A. Cells were serum starved for 1 h at 37 °C before stimulation for 15 min with 500 ng/ml CpG. Total p65 and  $\beta$ -tubulin were used as loading controls. **D** Immunoblot analysis of phosphorylated p65 (Ser536) and MYD88 in U2932 expressing MYD88 WT or MYD88 S257A. Cells were serum starved for 1 h at 37 °C before stimulation for 5, 15, 30 or 60 min with 500 ng/ml CpG. Total p65,  $\beta$ -actin and  $\beta$ -tubulin were used as loading controls.

### **The phosphomimetic MYD88 S257D and oncogenic MYD88 L265P mutants both promote molecular aggregation of MYD88**

To further elucidate the role of serine phosphorylation in MYD88 signaling, we generated expression constructs encoding the activating MYD88 S257D phosphomimetic mutant and the oncogenic L265P mutant (Figure 1A). Next, we retrovirally introduced all MYD88 variants in DLBCL cell lines OCI-LY1 and OCI-LY7, which endogenously express wildtype MYD88 and display very weak basal NF- $\kappa$ B activation. Immunoblot analysis shows that we achieved increased MYD88 expression levels, compared to empty vector (EV) transduced cells (Figure 2A). Surprisingly, protein expression of the phosphomimetic MYD88 S257D and oncogenic MYD88 L265P was remarkably lower as compared to wildtype MYD88. RT-PCR analysis shows that these differences in protein level were not caused by differential expression at the transcriptional level (Figure 2B).

Interestingly, using confocal microscopy Avbelj et al. previously demonstrated that MYD88 L265P, as well as other lymphoma-associated mutants, strongly promote aggregation of MYD88 (16). Moreover, these authors established that this aggregation renders the MYD88 protein less soluble, causing it to end up in the pellet fraction of a protein lysate. Using immunofluorescence (IF) microscopy, we confirmed that MYD88 L265P indeed strongly promotes aggregation of MYD88 (Figure 2C and 2D). Interestingly, the phosphomimetic MYD88 S257D mutant similarly showed strong aggregation, while aggregation was hardly observed for wildtype MYD88 or MYD88 S257A. Using immunoblot analysis, we demonstrated that MYD88 S257D and L265P levels were significantly enriched in the insoluble/pellet fraction, further supporting the presence of molecular aggregation (Figure 2E).

### **The phosphomimetic MYD88 S257D is equally potent as the MYD88 L265P oncogenic mutant in NF- $\kappa$ B pathway activation**

To assess whether the MYD88 aggregation caused by MYD88 S257D or L265P expression, correlates to enhanced signaling, we studied TLR/MYD88/NF- $\kappa$ B pathway activation. Ligand recognition by TLRs promotes the recruitment of MYD88 to the TIR domain of TLRs. This triggers recruitment of IRAK4 and IRAK1 to the receptor complex via their respective death-domains (DD) (17). The subsequent activation of IRAK1 is a multistep process, which first requires phosphorylation of threonine 209, resulting in a conformational change of the kinase domain, allowing further phosphorylation steps to occur (18).

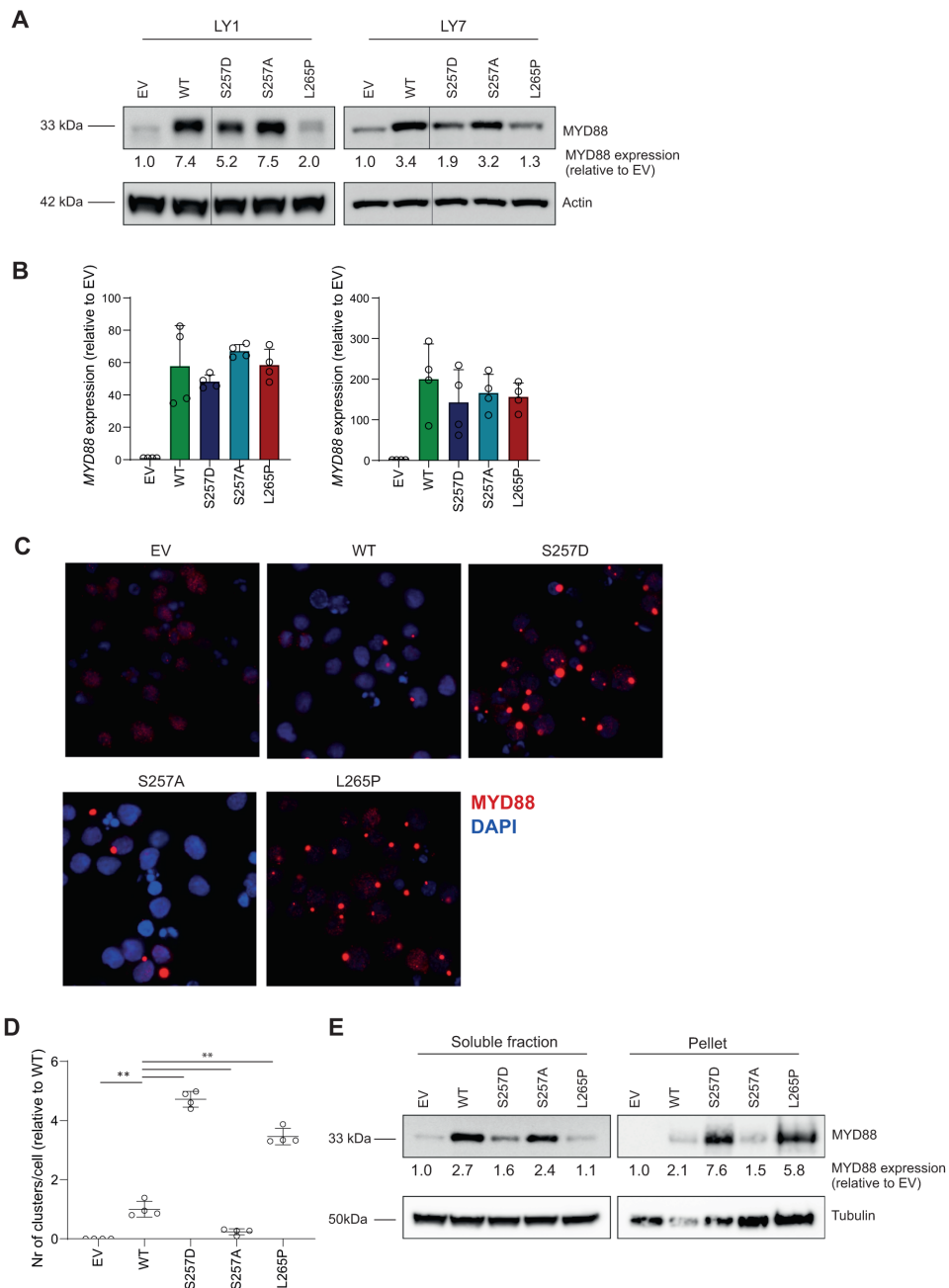


**Figure 2. Expression of MYD88 S257D and L265P induces molecular aggregation.** **A** Immunoblot analysis for MYD88 in OCI-LY1 and OCI-LY7 transduced with different MYD88 mutants. Cells were transduced with an empty vector (EV) or an expression vector for MYD88 (WT, S257D, S257A or L265P) and sorted for GFP expression.  $\beta$ -actin was used as loading control. **B** RT-qPCR analysis of MYD88 expression in OCI-LY1 and OCI-LY7 transduced with different MYD88 mutants. Cells were allowed to

recover for 72 h before RNA isolation. RPLP0 was used as an input control and data are normalized to the EV control expression levels. The mean  $\pm$  SD of four independent experiments performed in triplicate is shown. **C** Immunofluorescence analysis of MYD88 in OCI-LY7 cells. Cells were fixed and stained with an anti-MYD88 antibody followed by goat-anti-mouse IgG-AF594 antibody (red) and nuclei were counterstained with DAPI (blue). **D** Quantification of the number of clusters per cell determined using ImageJ software. Values are normalized to the number of clusters per cell for cells expressing WT MYD88. The mean  $\pm$  SD of four independent experiments performed is shown. **E** Immunoblot analysis comparing MYD88 expression in the soluble fraction versus the pellet fraction in OCI-LY7 transduced with different MYD88 mutants. Cell lysates were fractionated by centrifugation.  $\beta$ -tubulin was used as loading control.

By employing phosflow analysis, we established that both MYD88 S257D and MYD88 L265P promote IRAK1 phosphorylation at threonine 209 in both OCI-LY1 and OCI-LY7 (Figure 3A). Expression of wildtype MYD88 and MYD88 S257A resulted in a small increase in IRAK1 phosphorylation compared to empty vector (EV) transduced cells. To confirm that increased IRAK1 phosphorylation indeed results in enhanced downstream NF- $\kappa$ B pathway activation, we performed NF- $\kappa$ B luciferase assays. These assays demonstrated that both MYD88 S257D and L265P strongly promote NF- $\kappa$ B pathway activation in both DLBCL cell lines (Figure 3B). Introduction of both wildtype MYD88 and MYD88 S257A weakly stimulated NF- $\kappa$ B pathway activation compared to cells expressing only endogenous MYD88. In addition, MYD88 S257D and L265P greatly enhanced the expression of the NF- $\kappa$ B target genes CD80 and HCK (Figure 3C and 3E). A similar upregulation of CD80 and HCK was observed upon expression of constitutively active IKK- $\beta$  (CA-IKK2) (Supplemental Figure 2A). Using cell surface staining for CD80 and immunoblot analysis for HCK, we confirmed that the changes in mRNA transcription resulted in enhanced protein expression levels (Figure 3D and 3F). Together, these data demonstrate that the phosphomimetic MYD88 S257D mutant is a potent mediator of NF- $\kappa$ B pathway activation in B cells with an efficacy similar to that of the oncogenic MYD88 L265P mutant.

### **Phosphomimetic MYD88 S257D and oncogenic MYD88 L265P similarly promote proliferation of MYD88 wildtype DLBCL cells**

Since NF- $\kappa$ B signaling is crucial in mediating survival and proliferation of B cells, we next set out to explore the contribution of MYD88 S257D and L265P to cell growth and viability. In contrast to cells expressing wildtype MYD88, ABC DLBCL and WM cells bearing the L265P mutation have been shown to critically depend on MYD88 for their survival (1, 19). We corroborated these findings in the MYD88 WT cell lines OCI-LY7 and U2932 and the MYD88 L265P expressing cell line HBL1, using inducible shRNA-mediated silencing of MYD88. Efficient knockdown of MYD88 upon doxycycline treatment was confirmed by immunoblot analysis (Figure 4A). In line with previous studies (1), silencing of MYD88 did not affect cell growth in MYD88 WT cell lines OCI-LY7 and U2932 (Figure 4B), but strongly reduced cell growth in MYD88 L265P expressing cell line HBL1 (Figure 4C).

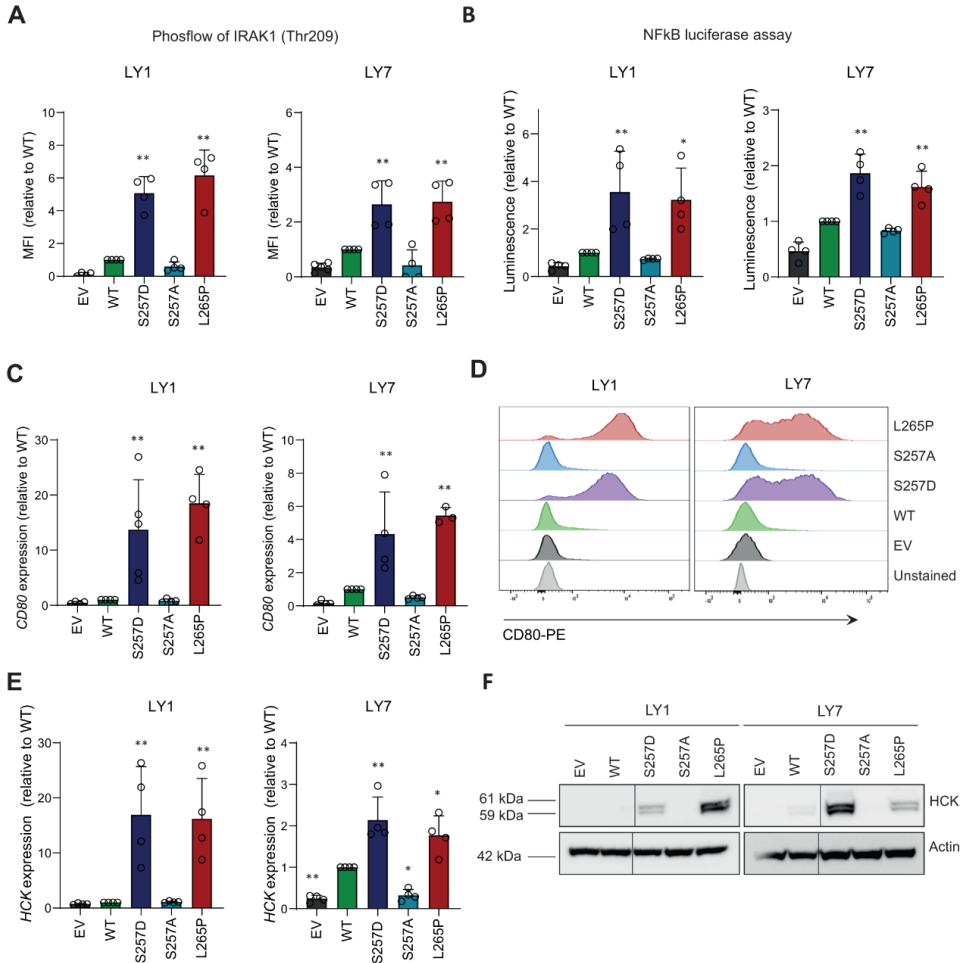


**Figure 3. Expression of MYD88 S257D and L265P promote NF-κB activation.** **A** Phosflow analysis for IRAK1(Threonine 209) in OCI-LY1 and OCI-LY7 transduced with different MYD88 mutants. Cells were transduced with an empty vector (EV) or an expression vector for MYD88 (WT, S257D, S257A or L265P) and sorted for GFP expression. Untransduced, GFP negative, cells were used as negative control. IRAK1(Thr209) phosphorylation levels are shown relative to cells expressing WT MYD88. The mean ± SD of four independent experiments is shown. \*\*P < 0.01 using 1-way ANOVA with Dunnett's multiple comparisons test. **B** NF-κB activity measured by NF-κB-dependent luciferase reporter assays in OCI-LY1 and OCI-LY7 transduced with different MYD88 mutants. Cells were stably transduced with different MYD88 mutants and subsequently transfected with plasmid DNAs encoding for NF-κB promoter-driven firefly luciferase and a Renilla luciferase as control. Cells were allowed to recover for 48 h after transfection. Firefly luciferase activity was first normalized to the activity of Renilla luciferase. Then, luciferase activity was normalized to cells expressing WT MYD88. The mean ± SD of four independent experiments performed is shown. \*P < 0.05; \*\*P < 0.01 using 1-way ANOVA with Dunnett's multiple comparisons test. **C**, **E** RT-qPCR analysis of CD80 (C) or HCK (E) expression in OCI-LY1 and OCI-LY7 transduced with different MYD88 mutants. Cells were allowed to recover for 72 h before RNA isolation. RPLP0 was used as an input control and data are normalized to the EV control expression levels. The mean ± SD of four independent experiments performed in triplicate is shown. \*\*P < 0.01 using 1-way ANOVA with Dunnett's multiple comparisons test. **D** Flow cytometric analysis showing membranous CD80 staining in OCI-LY1 and OCI-LY7 transduced with different MYD88 mutants. One representative experiment of three independent experiments is shown. **F** Immunoblot analysis for HCK in OCI-LY1 and OCI-LY7 transduced with different MYD88 mutants. β-actin was used as loading control.

Next, we assessed the effect of the different MYD88 variants on the proliferation and viability of MYD88 WT cells. To this end, we transduced OCI-LY1 and OCI-LY7 with a bicistronic vector co-expressing MYD88 and GFP. In OCI-LY7 both MYD88 S257D and MYD88 L265P expressing cells progressively outcompeted their untransduced counterparts, indicating that these cells have a competitive growth advantage (Figure 4D). By contrast, the percentage of cells transduced with an empty vector (EV) or MYD88 S257A was stable over time, while the percentage of cells ectopically expressing wildtype MYD88 showed a small, non-significant, increase. Notably, the growth advantage upon expression of MYD88 S257D and L265P was similar to that observed upon expression of CA-IKK2 (Supplemental Figure 2B). Surprisingly, in OCI-LY1 expression of MYD88 S257D and L265P, but also of CA-IKK2, did not confer a growth advantage to the cells (Supplemental Figure 2B and 2C).

4 Subsequently, we explored whether the growth advantage in OCI-LY7 could be attributed to increased cell survival or to enhanced cell proliferation. For this purpose, we performed Annexin-V-PI stainings and utilized a proliferation dye to track cell divisions. We observed approximately 10% Annexin-V-PI positive cells in EV control cells, this percentage was not significantly altered by any of the MYD88 mutants (Figure 4E). However, introduction of either MYD88 S257D or MYD88 L265P resulted in a significant increase in cell proliferation compared to expression of wildtype MYD88 (Figure 4F). These findings indicate that MYD88 S257D and L265P provide a growth advantage, not by affecting cell viability, but through increased proliferation.

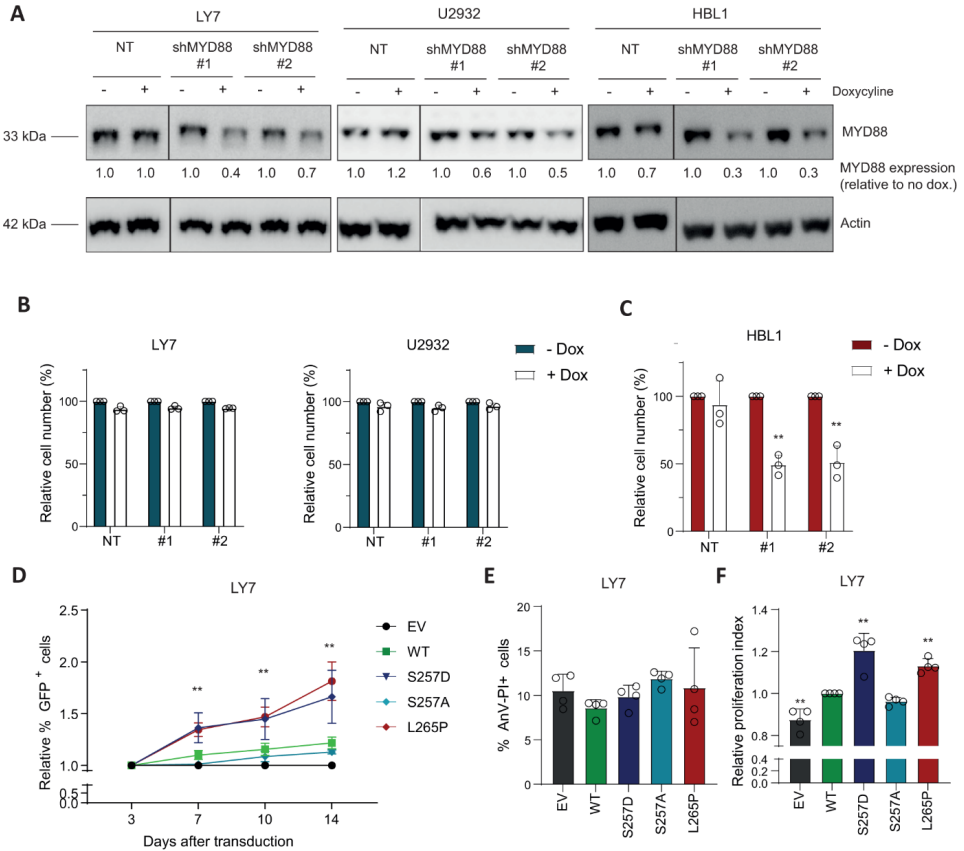


**Figure 4. MYD88 257D and L265P augment cell growth in MYD88 wildtype cells.** **A** Immunoblot analysis of MYD88 in OCI-LY7, U2932 and HBL-1 treated for 3 days with 500 ng/ml doxycycline.  $\beta$ -actin was used as loading control. **B, C** Flow cytometric analysis in OCI-LY7 and U2932 (**B**) and HBL-1 (**C**) of the number of viable cells, as determined by 7-AAD staining, after 5 days of treatment with 500 ng/ml doxycycline in cell lines transduced with inducible shRNA constructs targeting MYD88. The number of viable cells was normalized to the vehicle-treated condition. Data are presented as mean  $\pm$  SD of four independent experiments. **\*\*** $P < 0.01$  using 2-way ANOVA with Bonferroni's multiple comparisons test. **D** Flow cytometric analysis of OCI-LY7 cells transduced with an empty vector (EV) or an expression vector for MYD88 (WT, S257D, S257A or L265P) co-expressing GFP. The percentage of GFP positive cells was followed in time and plotted as the percentage of GFP+ cells, normalized to the value at day 3 following retroviral transduction. The mean  $\pm$  SD of three independent transductions is shown. **E** Flow cytometric analysis showing the percentage of cells double positive for Annexin-V and Propidium Iodide (PI) staining. OCI-LY7 cells were transduced with different MYD88 mutants or a EV control. Data are presented as mean  $\pm$  SD of four independent experiments. **F** Flow cytometric analysis showing the relative proliferative index of OCI-LY7 cells transduced with different MYD88 mutants or a EV control. Cells were stained with cell proliferation dye eFluor 660 and analyzed 3 days after staining. Values are normalized to the proliferative index of cells expressing WT MYD88. Data are presented as mean  $\pm$  SD of four independent experiments. **\*\*** $P < 0.01$  using 1-way ANOVA with Dunnett's multiple comparisons test.

### **Phosphomimetic MYD88 S257D rescues growth of DLBCL cells addicted to the MYD88 L265P oncoprotein**

Following silencing of endogenous MYD88 in L265P-expressing lymphoma cells lines, cell growth could only be sustained by mutant, but not wildtype MYD88, demonstrating that L265P is a gain-of-function mutation (1). To explore whether the phosphomimetic MYD88 S257D is also capable of rescuing cell growth, we performed a complementation experiment: We knocked-down endogenous mutant MYD88 using an shRNA targeting the MYD88 3'UTR (shRNA #2) and stably expressed either wildtype or mutant MYD88 coding domains. Because of a low retroviral transduction efficiency, the ABC DLBCL cell line HBL1 (previously used in Figure 4) could not be used in these experiments.

Efficient knockdown of MYD88 upon doxycycline treatment was confirmed by immunoblot analysis (Figure 5A). Consistent with the molecular aggregation of MYD88 previously observed in OCI-LY7, protein levels of MYD88 S257D and L265P expressed in OCI-LY10 and TMD8 were lower compared to those in wildtype MYD88 and MYD88 S257A (Figure 5B). In line with previous research (1), inducible shRNA-mediated silencing of MYD88 resulted in a significant reduction in the number of viable cells in the MYD88 L265P expressing cell lines OCI-LY10 and TMD8 (Figure 5C); introduction of MYD88 L265P, but not wildtype MYD88, annulled this effect (Figure 5D). Importantly, however, ectopic expression of phosphomimetic MYD88 S257D, but not S257A, similarly offset the effect of silencing of endogenous oncogenic MYD88 L265P (Figure 5D). In the presence of endogenous MYD88 L265P, expression of MYD88 S257A did not affect cell survival (Supplemental Figure 3). This implies that MYD88 S257A does not function as a dominant negative mutant and that MYD88 L265P can still activate the TLR-MYD88-NFKB pathway in these cells. Taken together, our findings show that phosphomimetic MYD88 S257D and oncogenic L265P are equally able to propagate cell growth in DLBCL cells addicted to oncogenic MYD88 signaling, supporting the hypothesis that the oncogenic MYD88 L265P mutation exerts its oncogenic function by mimicking the activating effect of MYD88 serine 257 phosphorylation.

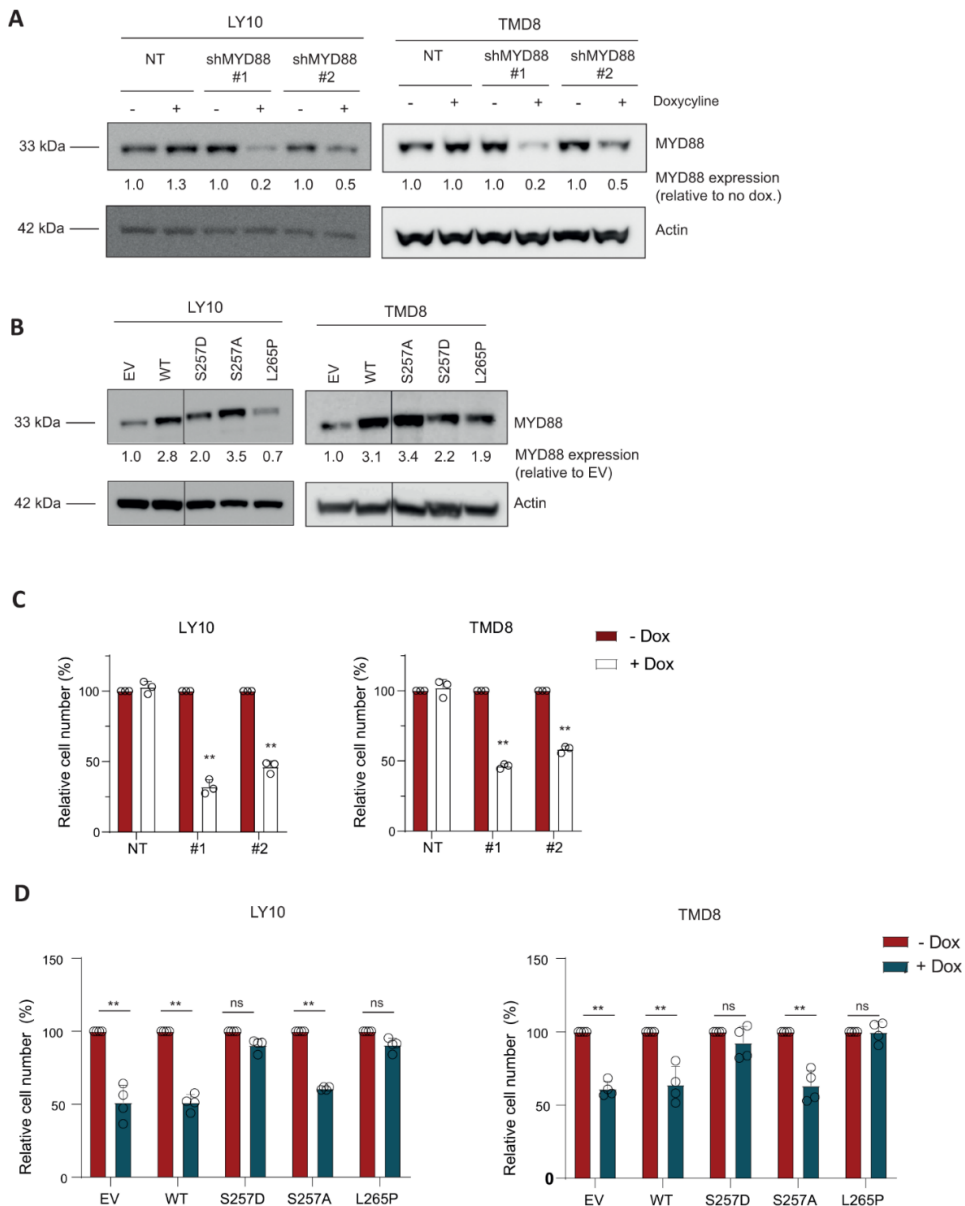


**Figure 5. MYD88 S257D rescues cell growth in MYD88 L265P addicted cell lines.** **A** Immunoblot analysis of MYD88 in OCI-LY10 and TMD8 treated for 3 days with 500 ng/ml doxycycline.  $\beta$ -actin was used as loading control. **B** Immunoblot analysis for MYD88 in OCI-LY10 and TMD8 transduced with different MYD88 mutants. Cells were transduced with an empty vector (EV) or an expression vector for MYD88 (WT, S257D, S257A or L265P) and sorted for GFP expression.  $\beta$ -actin was used as loading control. **C** Flow cytometric analysis in OCI-LY10 and TMD8 of the number of viable cells, as determined by 7-AAD staining, after 5 days of treatment with 500 ng/ml doxycycline in cell lines transduced with inducible shRNA constructs targeting MYD88. The number of viable cells was normalized to the vehicle-treated condition. Data are presented as mean  $\pm$  SD of three independent experiments. \*\* $P < 0.01$  using 2-way ANOVA with Bonferroni's multiple comparisons test. **D** Flow cytometric analysis of the number of viable cells after 5

days of treatment with 500 ng/ml doxycycline in cell lines OCI-LY10 or TMD8 transduced with an inducible shRNA construct targeting MYD88 3'UTR in combination with an empty vector (EV) or an expression vector for MYD88 (WT, S257D, S257A or L265P). The number of viable cells was normalized to the vehicle-treated condition. Data are presented as mean  $\pm$  SD of four independent experiments. \*\*\* $P < 0.01$  using 2-way ANOVA with Bonferroni's multiple comparisons test.

## DISCUSSION

4 The MYD88 TIR domain plays an essential role in the interactions with TLR/IL1-Rs as well as in MYD88 homodimerization (20). Upon dimerization, MYD88 recruits the downstream kinases IRAK1 and IRAK4 via their respective death-domains to form a large multiprotein complex called the Myddosome. Phosphorylated IRAK1 dissociates from the receptor complex to interact with the E3 ubiquitin ligase TRAF6, to finally activate the MAPK and NF- $\kappa$ B signaling pathways. In 2011, Ngo et al. first described the MYD88 L265P mutation in the hydrophobic core of the MYD88 TIR domain as oncogenic driver in DLBCL (1). Subsequent studies have identified residues of the TIR domain that are crucially involved in MYD88 homodimerization and NF- $\kappa$ B activation, in particular serine 257 (9, 10). In the current study, we show that MYD88 S257 phosphorylation is required for optimal NF- $\kappa$ B activation in DLBCL and that a phosphomimetic (S257D) mutant promotes IRAK1 phosphorylation, NF- $\kappa$ B activity, and cell growth with a similar efficacy as the oncogenic MYD88 L265P mutant and, moreover, can rescue DLBCL cells addicted to this oncogenic driver.

We demonstrate that MYD88 can be phosphorylated at S257 in DLBCL cells (Supplemental Figure 1A). Moreover, we show that substitution of this serine residue by alanine (S257A) strongly reduces TLR-induced NF- $\kappa$ B activation in DLBCL (Figure 1). These data confirm and extend previous studies showing MYD88 S257 phosphorylation in macrophages and TLR4 stable HEK293T cells and establish its importance for MYD88-dependent NF- $\kappa$ B activation in B lymphoma cells (10, 11).

Avbelj et al. previously proposed that MYD88 L265P, as well as other lymphoma-associated MYD88 mutations, are prone to spontaneously oligomerize and form Myddosome complexes (16). Using molecular dynamics simulation, these authors demonstrated that mutated residues of MYD88 L265P and other lymphoma-associated mutants are shielded and likely affect interacting residues through an allosteric effect (16). Several studies have indeed established that MYD88 L265P causes increased homodimerization of the MYD88 TIR domain leading to constitutive activity (9, 21, 22). Our current data confirm that the oncogenic MYD88 L265P mutant induces strong MYD88 aggregation, IRAK1 phosphorylation and NF- $\kappa$ B activation in DLBCL cells (Figure 2 and Figure 3). Interestingly, we moreover demonstrate that the phosphomimetic MYD88 S257D promotes aggregation, phosphorylation, and NF- $\kappa$ B activation in DLBCL

with a similar efficacy, hence mimicking the functional effects of the oncogenic mutant (Figure 2 and Figure 3). In line with these findings, studies in a cell-free system and in HEK293T cells showed that the phosphomimetic S257D mutant had a higher propensity to oligomerize as compared to wildtype MYD88 (23) and induces strong induction of NF- $\kappa$ B reporter activity (9, 24). Inversely, HEK293T cells expressing a S257A mutant, which impedes phosphorylation, displayed impaired MYD88 homodimerization, interaction with IRAKs and activation of NF- $\kappa$ B signaling (10).

Importantly, we found that the phosphomimetic MYD88 S257D and oncogenic L265P mutant were equally capable of promoting lymphoma cell growth (Figure 4). MYD88 S257D did not only promote cell growth of MYD88 wildtype cells, but, remarkably, was also able to sustain cell growth of MYD88 L265P-addicted lymphoma cells after silencing of endogenous (mutant) MYD88 (Figure 5). Based on molecular dynamics simulation studies, Vyncke et al. suggested that MYD88 S257D and L265P preferentially adopt the same conformation of the CD loop, which promotes MYD88 TIR-TIR domain interactions (9). Indeed, our observations strongly support the hypothesis that MYD88 L265P exerts its oncogenic functions by mimicking the functional and conformational effects of MYD88 serine 257 phosphorylation.

Interestingly, Xie et al. reported that the S257 residue of MYD88 can be dephosphorylated by protein phosphatase 2A catalytic subunit  $\alpha$  (PP2Ac) (11): Constitutively activated PP2Ac dephosphorylated MYD88, resulting in reduced TLR-MYD88 interactions and, consequently, suppressed MYD88-NF $\kappa$ B-dependent gene transcription (11). In line with these findings, in LPS-stimulated myeloid cells, knockout of PP2Ac resulted in increased NF- $\kappa$ B activity and enhanced secretion of pro-inflammatory cytokines (24). To date, the kinase(s) responsible for MYD88 S257 phosphorylation remain unknown. Since MYD88 L265P was shown to associate with TLR9 and the BCR in the so-called 'My-T-BCR' complex, it is tempting to speculate that MYD88 S257 phosphorylation might also play an essential part in the cooperation of TLR and BCR signaling (25). Consistent with this notion, neural network-based kinase prediction (NetPhos 3.1) designates p38MAPK as putative candidate for MYD88 S257 phosphorylation (26). Additional studies are required to unravel the signaling cascade and kinases involved in MYD88 S257 phosphorylation. Better understanding of MYD88 TIR domain assembly has resulted in the development of peptidomimetic compounds that inhibit Myddosome formation (27, 28). These compounds can provide an interesting therapeutic option for B-cell malignancies as well as for inflammatory diseases (29-32). Our findings suggest that these compounds will not only be effective in MYD88 L265P-expressing lymphomas, but also in lymphomas in which MYD88 activation is regulated by other means, such as phosphorylation.

In conclusion, our findings support a model in which the oncogenic MYD88 L265P mutant drives lymphomagenesis by genocopying the conformational effects of physiological MYD88 S257 phosphorylation on TIR domain homodimerization, resulting in constitutive IRAK1 phosphorylation, NF- $\kappa$ B signaling and enhanced cell growth. Further studies are needed to identify the actors involved in the regulation of MYD88 TIR domain phosphorylation.

#### **ACKNOWLEDGEMENTS**

This study was supported by grants from Lymph&Co to MJK and STP and to MS.

#### **AUTHORSHIP CONTRIBUTIONS**

M.M. designed the research, performed experiments, analyzed the data and wrote the paper; H.C.L., C.Z., A.J.H. performed experiments and analyzed the data. M.B., M.K., S.T.P. and M.S. supervised the study, designed the research and analyzed the data. M.S. and S.T.P. wrote the paper.

The authors declare no conflict of interest.

#### **DATA AVAILABILITY STATEMENT**

The datasets generated during and/or analysed during the current study are available from the corresponding author on reasonable request.

## REFERENCES

1. Ngo VN, Young RM, Schmitz R, Jhavar S, Xiao W, Lim KH, et al. Oncogenically active MYD88 mutations in human lymphoma. *Nature*. 2011;470(7332):115-9.
2. Kraan W, Horlings HM, van Keimpema M, Schilder-Tol EJ, Oud ME, Scheepstra C, et al. High prevalence of oncogenic MYD88 and CD79B mutations in diffuse large B-cell lymphomas presenting at immune-privileged sites. *Blood Cancer J*. 2013;3:e139.
3. Kraan W, van Keimpema M, Horlings HM, Schilder-Tol EJ, Oud ME, Noorduyt LA, et al. High prevalence of oncogenic MYD88 and CD79B mutations in primary testicular diffuse large B-cell lymphoma. *Leukemia*. 2014;28(3):719-20.
4. Treon SP, Xu L, Yang G, Zhou Y, Liu X, Cao Y, et al. MYD88 L265P somatic mutation in Waldenstrom's macroglobulinemia. *N Engl J Med*. 2012;367(9):826-33.
5. Chapuy B, Roemer MG, Stewart C, Tan Y, Abo RP, Zhang L, et al. Targetable genetic features of primary testicular and primary central nervous system lymphomas. *Blood*. 2016;127(7):869-81.
6. Bonzheim I, Giese S, Deuter C, Susskind D, Zierhut M, Waizel M, et al. High frequency of MYD88 mutations in vitreoretinal B-cell lymphoma: a valuable tool to improve diagnostic yield of vitreous aspirates. *Blood*. 2015;126(1):76-9.
7. Montesinos-Rongen M, Godlewska E, Brunn A, Wiestler OD, Siebert R, Deckert M. Activating L265P mutations of the MYD88 gene are common in primary central nervous system lymphoma. *Acta Neuropathol*. 2011;122(6):791-2.
8. Wright GW, Huang DW, Phelan JD, Coulbaly ZA, Roulland S, Young RM, et al. A Probabilistic Classification Tool for Genetic Subtypes of Diffuse Large B Cell Lymphoma with Therapeutic Implications. *Cancer Cell*. 2020;37(4):551-68 e14.
9. Vyncke L, Bovijn C, Pauwels E, Van Acker T, Ruysinck E, Burg E, et al. Reconstructing the TIR Side of the Myddosome: a Paradigm for TIR-TIR Interactions. *Structure*. 2016;24(3):437-47.
10. Loiarro M, Volpe E, Ruggiero V, Gallo G, Furlan R, Maiorino C, et al. Mutational analysis identifies residues crucial for homodimerization of myeloid differentiation factor 88 (MyD88) and for its function in immune cells. *J Biol Chem*. 2013;288(42):30210-22.
11. Xie L, Liu C, Wang L, Gunawardena HP, Yu Y, Du R, et al. Protein phosphatase 2A catalytic subunit alpha plays a MyD88-dependent, central role in the gene-specific regulation of endotoxin tolerance. *Cell Rep*. 2013;3(3):678-88.
12. Koopman G, Reutelingsperger CP, Kuijten GA, Keehnen RM, Pals ST, van Oers MH. Annexin V for flow cytometric detection of phosphatidylserine expression on B cells undergoing apoptosis. *Blood*. 1994;84(5):1415-20.
13. Nath Neerukonda S, Mahadev-Bhat S, Aylward B, Johnson C, Charavaryamath C, Arsenault RJ. Kinome analyses of inflammatory responses to swine barn dust extract in human bronchial epithelial and monocyte cell lines. *Innate Immun*. 2018;24(6):366-81.
14. Sharma K, D'Souza RC, Tyanova S, Schaab C, Wisniewski JR, Cox J, et al. Ultradeep human phosphoproteome reveals a distinct regulatory nature of Tyr and Ser/Thr-based signaling. *Cell Rep*. 2014;8(5):1583-94.
15. Mertins P, Mani DR, Ruggles KV, Gillette MA, Clauser KR, Wang P, et al. Proteogenomics connects somatic mutations to signalling in breast cancer. *Nature*. 2016;534(7605):55-62.
16. Avbelj M, Wolz OO, Fekonja O, Bencina M, Repic M, Mavri J, et al. Activation of lymphoma-associated MyD88 mutations via allostery-induced TIR-domain oligomerization. *Blood*. 2014;124(26):3896-904.
17. Loiarro M, Gallo G, Fanto N, De Santis R, Carminati P, Ruggiero V, et al. Identification of critical residues of the MyD88 death domain involved in the recruitment of downstream kinases. *J Biol Chem*. 2009;284(41):28093-103.
18. Kollwe C, Mackensen AC, Neumann D, Knop J, Cao P, Li S, et al. Sequential autophosphorylation steps in the interleukin-1 receptor-associated kinase-1 regulate its availability as an adapter in interleukin-1 signaling. *J Biol Chem*. 2004;279(7):5227-36.
19. Yang G, Zhou Y, Liu X, Xu L, Cao Y, Manning RJ, et al. A mutation in MYD88 (L265P) supports the survival of lymphoplasmacytic cells by activation of Bruton tyrosine kinase in Waldenstrom macroglobulinemia. *Blood*. 2013;122(7):1222-32.
20. Loiarro M, Sette C, Gallo G, Ciacci A, Fanto N, Mastroianni D, et al. Peptide-mediated interference of TIR domain dimerization in MyD88 inhibits interleukin-1-dependent activation of NF- $\kappa$ B. *J Biol Chem*. 2005;280(16):15809-14.
21. O'Carroll A, Chauvin B, Brown JWP, Meagher A, Coyle J, Schill J, et al. Pathological mutations differentially affect the self-assembly and polymerisation of the innate immune system signalling adaptor molecule MyD88. *BMC Biol*. 2018;16(1):149.
22. Zhan C, Qi R, Wei G, Guven-Maiorov E, Nussinov R, Ma B. Conformational dynamics of cancer-associated MyD88-TIR domain mutant L252P (L265P) allosterically tilts the landscape toward homo-dimerization. *Protein Eng Des Sel*. 2016;29(9):347-54.

23. Clabbers MTB, Holmes S, Muusse TW, Vajjhala PR, Thygesen SJ, Malde AK, et al. MyD88 TIR domain higher-order assembly interactions revealed by microcrystal electron diffraction and serial femtosecond crystallography. *Nature Communications*. 2021;12(1):2578.
24. Sun L, Pham TT, Cornell TT, McDonough KL, McHugh WM, Blatt NB, et al. Myeloid-Specific Gene Deletion of Protein Phosphatase 2A Magnifies MyD88- and TRIF-Dependent Inflammation following Endotoxin Challenge. *J Immunol*. 2017;198(1):404-16.
25. Phelan JD, Young RM, Webster DE, Roulland S, Wright GW, Kasbekar M, et al. A multiprotein supercomplex controlling oncogenic signalling in lymphoma. *Nature*. 2018;560(7718):387-91.
26. Blom N, Gammeltoft S, Brunak S. Sequence and structure-based prediction of eukaryotic protein phosphorylation sites. *J Mol Biol*. 1999;294(5):1351-62.
27. Loiarro M, Capolunghi F, Fanto N, Gallo G, Campo S, Arseni B, et al. Pivotal Advance: Inhibition of MyD88 dimerization and recruitment of IRAK1 and IRAK4 by a novel peptidomimetic compound. *J Leukoc Biol*. 2007;82(4):801-10.
28. Olson MA, Lee MS, Kissner TL, Alam S, Waugh DS, Saikh KU. Discovery of small molecule inhibitors of MyD88-dependent signaling pathways using a computational screen. *Sci Rep*. 2015;5:14246.
29. Di Padova F, Quesniaux VFJ, Ryffel B. MyD88 as a therapeutic target for inflammatory lung diseases. *Expert Opin Ther Targets*. 2018;22(5):401-8.
30. Shiratori E, Itoh M, Tohda S. MYD88 Inhibitor ST2825 Suppresses the Growth of Lymphoma and Leukaemia Cells. *Anticancer Res*. 2017;37(11):6203-9.
31. Wang X, Tan Y, Huang Z, Huang N, Gao M, Zhou F, et al. Disrupting myddosome assembly in diffuse large Bcell lymphoma cells using the MYD88 dimerization inhibitor ST2825. *Oncol Rep*. 2019;42(5):1755-66.
32. Liu X, Hunter ZR, Xu L, Chen J, Chen JG, Tsakmaklis N, et al. Targeting Myddosome Assembly in Waldenstrom Macroglobulinaemia. *Br J Haematol*. 2017;177(5):808-13.

## SUPPLEMENTAL FIGURES AND SUPPLEMENTAL METHODS

### Immunofluorescence staining (IF)

Following fixation with 4% PFA, cells were permeabilized with permeabilization buffer (PBS, 1% BSA, 0.1% Saponin) for 30 minutes at RT. Slides were incubated o/n at 4°C with mouse anti-MYD88 (clone E-11, Santa Cruz, Dallas, Texas, USA). Then, slides were incubated 1 hour at RT with goat anti-mouse IgG - Alexa Fluor 594 (Thermo Fisher Scientific) followed by a counterstain with 0.5 µg/ml DAPI in PBS for 5 min at RT. Images were acquired using the automated Leica DM5000 B microscope and Leica Application Suite (LAS) software (Leica Microsystems, Wetzlar, Germany).

### Luciferase assays

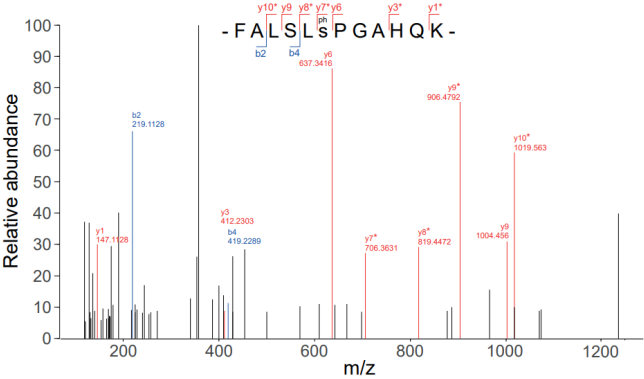
5 × 10<sup>6</sup> cells were transfected with 5 µg pNF-κB-Luc Cis-Reporter Plasmid (Agilent Technologies) and 0.1 µg pRL Renilla Luciferase Control Reporter Vector (Promega) using the Amaxa Nucleofector II in combination with program G16 and buffer T (Lonza, Basel, Switzerland). 48 hours following transfection, firefly and renilla luciferase activity were measured using the Dual-Glo<sup>®</sup> Luciferase Assay System according to manufacturer's instructions (Promega). Renilla luciferase activity served as a control for transfection efficiency.

### Mass spectrometry

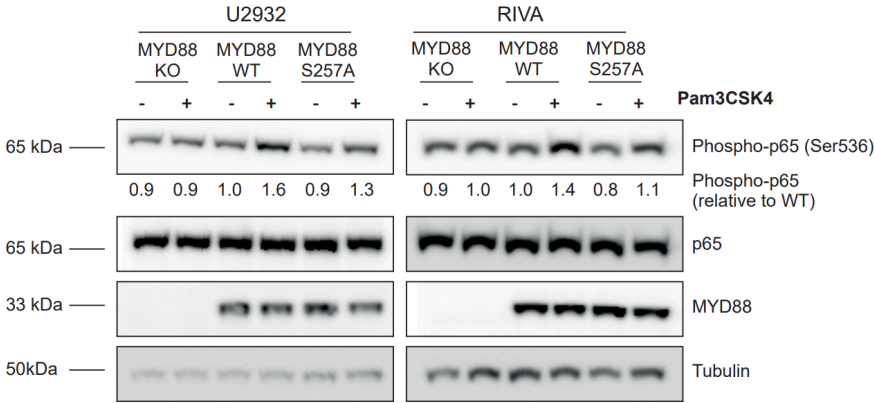
Tryptic digests were fractionated in using a High pH Reversed-Phase Peptide Fractionation kit (Pierce) according to manufacturer's instructions. Phosphopeptide enrichment was performed using Fe(III)-IMAC cartridges (Agilent) as described by Post et al. (13) on an AssayMAP BRAVO (Agilent). Peptides were separated by nanoscale C18 reverse chromatography coupled on-line to an Orbitrap Fusion Tribrid mass spectrometer (Thermo Fisher Scientific) via a nanoelectrospray ion source at 2.15 kV. Buffer A was composed of 0.1% formic acid and buffer B of 0.1% formic acid and 80% acetonitrile. Peptides were loaded for 17 min at 300 nL/min at 5% buffer B, equilibrated for 5 min at 5% buffer B (17–22 min) and eluted by increasing buffer B from 5–27.5% (22–122 min) and 27.5–40% (122–132 min), followed by a 5 min wash to 95% and a 6 min regeneration to 5%. Survey scans of peptide precursors from 300 to 1600 m/z were performed at 120,000 resolution (at 200 m/z) with a 4 × 10<sup>5</sup> ion count target. Tandem mass spectrometry was performed by isolation with the quadrupole, with isolation window 1.6, higher energy collisional dissociation (HCD) fragmentation with normalized collision energy of 30 and rapid scan mass spectrometry analysis in the orbitrap. The tandem mass spectrometry (MS2) ion count target was set to 5 × 10<sup>4</sup>, and the max injection time was 54 ms. Only those precursors with charge state 2–7 were sampled for MS2. The dynamic exclusion duration was set to 30 s with a 10 ppm tolerance

around the selected precursor and its isotopes. Monoisotopic precursor selection was turned on. The instrument was run in top N mode. All data were acquired with Xcalibur software (Thermo Fisher Scientific). RAW mass spectrometry files were processed with the MaxQuant 2.0.1.0 computational platform. Proteins and peptides were identified using the Andromeda search engine by querying the human Uniprot database (release February 2019). Standard settings with the additional options match between runs and Phospho STY was set as dynamic modification.

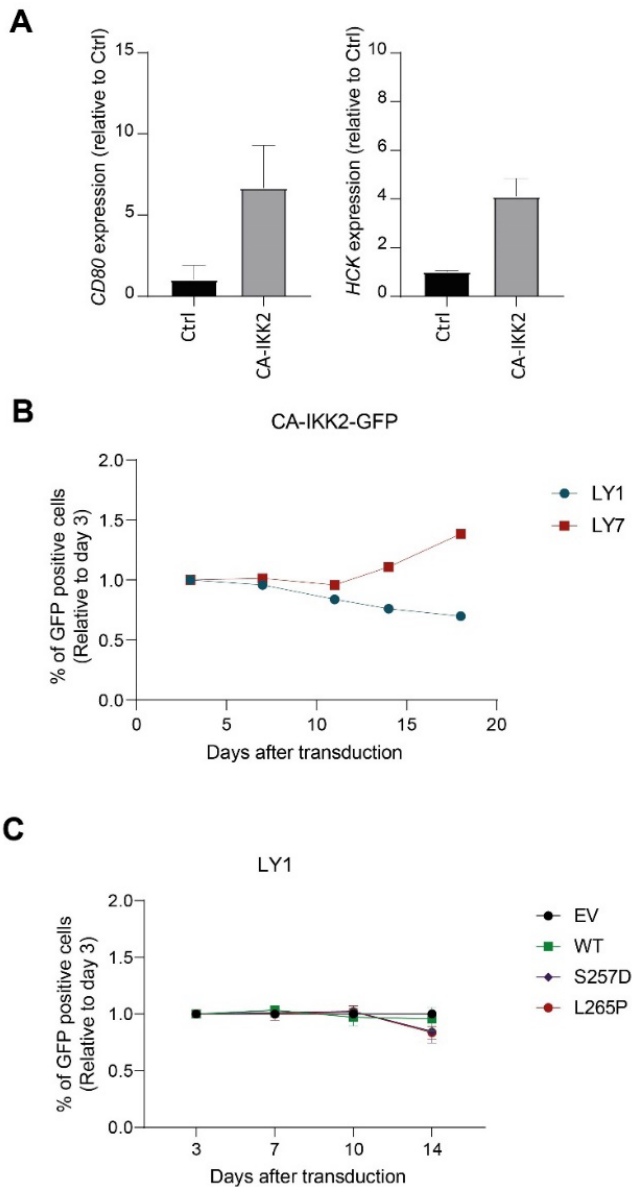
**A**



**B**

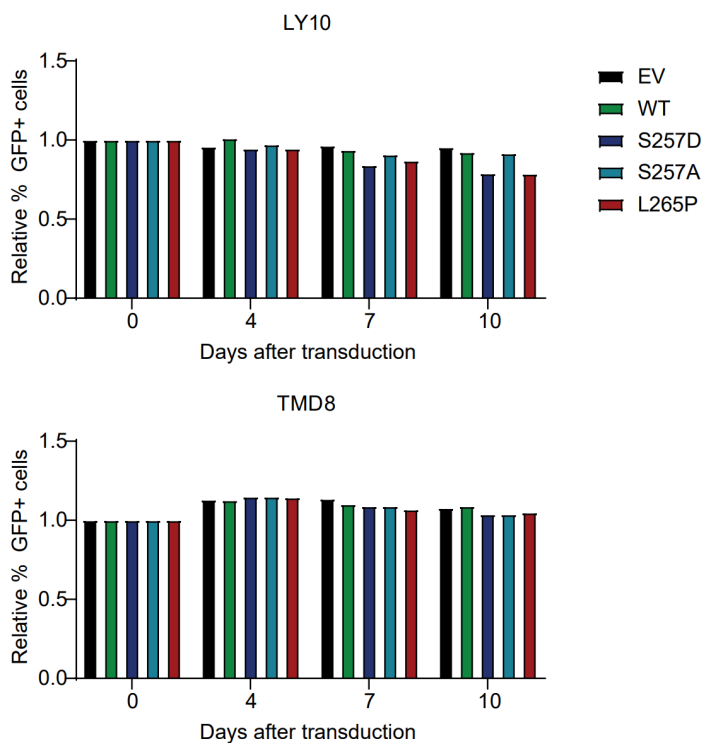


**Supplemental Figure 1.** (A) MaxQuant annotated MS/MS spectrum of the phosphorylated S257 MYD88 peptide FALSLS(phospho)PGAHQK. Each line on the x-axis represents an ion having a specific mass-to-charge ratio (m/z) and the height of the line indicates the relative abundance of the ion. b# indicate b-ion fragments with amino acid sequences in the peptide reading direction from left to right, y# ions from right to left. (B) Immunoblot analysis of phosphorylated p65 (Ser536) and MYD88 in U2932 and RIVA expressing MYD88 WT or MYD88 S257A. Cells were serum starved for 1 hour at 37°C before stimulation for 15 minutes with 1 µg/ml Pam3CSK4. Total p65 and β-tubulin were used as loading controls.



**Supplemental Figure 2.** (A) RT-qPCR analysis of CD80 and HCK expression in OCI-LY7 transduced with CA-IKK2-GFP. Cells were allowed to recover for 72 hours before RNA isolation. RPLP0 was used as an input control and data are normalized to the control expression levels. (B) Flow cytometric analysis of OCI-LY1 and OCI-LY7 cells transduced with a vector expressing CA-IKK2 and co-expressing GFP. The percentage of GFP positive cells was followed in time and plotted as the percentage of GFP+ cells, normalized to the value at day 3 following retroviral transduction. (C) Flow cytometric analysis of OCI-LY1 cells transduced with an empty vector (EV) or an expression vector for MYD88 (WT, S257D or L265P) co-expressing GFP. The percentage of GFP positive cells was followed in time and plotted as the percentage of GFP+ cells, normalized to the value at day 3 following retroviral transduction. The mean  $\pm$  S.E.M. of two independent transductions is shown.

A



**Supplemental Figure 3.** (A) Flow cytometric analysis of OCI-LY10 and TMD8 cells transduced with an empty vector (EV) or an expression vector for MYD88 (WT, S257D, S257A or L265P) co-expressing GFP. The percentage of GFP positive cells was followed in time and plotted as the percentage of GFP+ cells (relative to day 0).





# 5

## Prevalence and prognostic value of MYD88 and CD79B mutations in ocular adnexal large B-cell lymphoma: a reclassification of ocular adnexal large B-cell lymphoma

Marina Knudsen Kirkegaard <sup>1</sup>, Marthe Minderman <sup>2</sup>, Lene Dissing Sjö <sup>3</sup>, Steven T Pals <sup>2,4,5</sup>, Patrick R G Eriksen <sup>6</sup>, Steffen Heegaard <sup>7</sup>

<sup>1</sup>Department of Pathology, Eye Section, Rigshospitalet, University of Copenhagen, Copenhagen, Denmark.

<sup>2</sup>Department of Pathology, Amsterdam University Medical Centers loc. AMC, Amsterdam, The Netherlands.

<sup>3</sup>Department of Pathology, Rigshospitalet, University of Copenhagen, Copenhagen, Denmark. <sup>4</sup>Department of Pathology, Lymphoma and Myeloma Center Amsterdam-LYMMCARE, Amsterdam, The Netherlands.

<sup>5</sup>Department of Clinical Medicine, University of Copenhagen, Copenhagen, Denmark. <sup>6</sup>Department of Otorhinolaryngology, Head and Neck Surgery & Audiology, Rigshospitalet, University of Copenhagen, Copenhagen, Denmark. <sup>7</sup>Department of Pathology, Eye Section, Rigshospitalet, University of Copenhagen, Copenhagen, Denmark

## ABSTRACT

### Aims

To (1) reclassify ocular adnexal large B-cell lymphomas (OA-LBCLs) per 2016 WHO lymphoma classification and (2) determine the prevalence of MYD88 and CD79B mutations and their association with clinical parameters among OA-LBCLs.

### Methods

This study is a retrospective analysis of all OA-LBCLs diagnosed in Denmark between 1980 and 2018. Medical records and tissue samples were retrieved. Thirty-four OA-LBCLs were included. Fluorescence in situ hybridisation and Epstein-Barr-encoded RNA in situ hybridisation were used for the reclassification. Mutational status was established by allele-specific PCR and confirmed by Sanger sequencing. Primary endpoints were overall survival, disease-specific survival (DSS) and progression-free survival (PFS).

### Results

Two LBCL subtypes were identified: diffuse large B-cell lymphoma (DLBCL) (27 of 32; 84%) and high-grade B-cell lymphoma (HGBL) with MYC and BCL2 and/or BCL6 rearrangements (5 of 32; 16%). cMYC/BCL2 double-expressor DLBCLs had a poorer DSS than non-double-expressor DLBCLs (5-year DSS, 25% vs 78%) (HR 0.23; 95% CI 0.06 to 0.85;  $p=0.014$ ). MYD88 mutations were present in 10 (29%) of 34 lymphomas and carried a poorer PFS than wild-type cases (5-year PFS, 0% vs 43%) (HR 0.78; 95% CI 0.61 to 0.98;  $p=0.039$ ). CD79B mutations were present in 3 (9%) of 34 cases.

### Conclusion

OA-LBCL consists mainly of two subtypes: DLBCL and HGBL with MYC and BCL2 and/or BCL6 rearrangements. MYD88 mutations are important drivers of OA-LBCL. MYD88 mutations, as well as cMYC/BCL2 double-expressor DLBCL, appear to be associated with a poor prognosis. Implementing MYD88 mutational analysis in routine diagnostics may improve OA-LBCL prognostication.

## INTRODUCTION

Large B-cell lymphoma (LBCL) is a heterogeneous group of aggressive non-Hodgkin's lymphomas, characterised by clinical, biological and molecular diversity.<sup>1</sup> LBCL constitutes 10%–15% of lymphomas in the ocular adnexa with the most frequent subtype being diffuse large B-cell lymphoma (DLBCL).<sup>2–4</sup>

The recently updated WHO classification of lymphoid neoplasms (2016) recognises the heterogeneity of LBCL by reclassifying a subset of lymphomas with DLBCL morphology according to their biological drivers. Two new categories have been delineated: (1) Epstein-Barr virus (EBV)-positive DLBCL and (2) high-grade B-cell lymphoma (HGBL) with MYC and BCL2 and/or BCL6 rearrangements, also called double/triple-hit lymphoma.<sup>1</sup> Both entities are associated with an adverse prognosis.<sup>5–7</sup> Additionally, concurrent immunohistochemical overexpression of cMYC and BCL2, double-expressor lymphoma, has been identified as a marker for poor outcome among DLBCLs.<sup>8,9</sup>

In the search for further oncogenic drivers, recent sequencing studies have identified mutations in MYD88 and CD79B as some of the most prevalent genomic aberrations in LBCL.<sup>10–12</sup> These mutations are particularly prevalent in the so-called non-germinal centre B-cell (non-GCB)-type DLBCL according to the cell-of-origin (COO) concept.<sup>11,11</sup> MYD88 and CD79B mutations confer a selective survival advantage to non-GCB DLBCL cells by constitutively activating the nuclear factor (NF)-κB pathway signalling.<sup>11,13,14</sup> Several studies have shown that patients with LBCL with MYD88 and/or CD79B mutations are amenable to treatments targeting B-cell receptor (BCR) signalling, in particular with Bruton's tyrosine kinase inhibitors like ibrutinib, which block this pathway.<sup>13,15</sup>

The prevalence of MYD88 and CD79B mutations varies greatly among LBCLs originating at different anatomical sites. The highest prevalence is found in immune-privileged site-associated LBCLs, including vitreoretinal LBCL (MYD88, 69%–82%).<sup>11,16–19</sup> In the ocular adnexa, five out of seven cases identified in the literature harboured MYD88 mutations, indicating a high mutation prevalence.<sup>20</sup>

This has prompted us to (1) reclassify ocular adnexal LBCLs (OA-LBCLs) according to the 2016 revision of WHO classification of lymphoid neoplasms and (2) determine the prevalence of MYD88 and CD79B mutations and their relation to clinical parameters in OA-LBCL.

# MATERIALS AND METHODS

## Study design

This study is a retrospective analysis of all LBCLs of the ocular adnexal region diagnosed in Denmark between 1980 and 2018. Patients were identified using the systemised nomenclature of medicine codes to search the Danish Registry of Pathology. Formalin-fixed, paraffin-embedded tissue specimens of the identified cases were retrieved from the archives of the respective pathology departments. The specimens were reviewed and reclassified according to the 2016 revision of WHO classification of lymphoid neoplasms.

## Histopathological and molecular characterisation

The specimens were stained with H&E and analysed immunohistochemically using the following panel of antibodies: anti-CD3, CD5, CD10, CD20, CD23, CD30, CD79a, cyclinD1, PAX5, cMYC, BCL2, BCL6, MUM-1 and Ki-67. Cut-off values of  $\geq 40\%$  and  $\geq 50\%$  were used to define overexpression of MYC and BCL2, respectively.<sup>21</sup> EBV status was assessed by EBV-encoded RNA in situ hybridisation. *cMYC*, *BCL2* and *BCL6* rearrangements were analysed by fluorescence in situ hybridisation using break-apart probes. The Hans' algorithm was used for COO classification of DLBCLs. Mutational analysis of *MYD88* and *CD79B* was performed at the Amsterdam University Medical Centers, location AMC, The Netherlands. DNA was isolated using the QIAamp DNA Microkit (Qiagen) and mutational status was assessed by allele-specific PCR, using mutation-specific primers, and confirmed by Sanger sequencing, as described previously.<sup>11</sup>

## Clinical data

Clinical records were retrieved and reviewed to record the following data: age and sex of the patient, symptoms, clinical findings, laterality, extent of ocular adnexal involvement according to the American Joint Committee on Cancer (AJCC) tumour, node, metastasis (TNM) staging system<sup>22</sup> and systemic involvement according to the Ann Arbor staging system,<sup>23</sup> treatment modalities and response to therapy, survival duration, and cause of death.

Systemic involvement and laterality were determined using clinical information and diagnostic tools available at the time of diagnosis. The current complete diagnostic procedure includes positron emission tomography/CT of the entire body, CT or MRI of the ocular adnexa, and a bone-marrow biopsy.

Primary ocular adnexal lymphoma is defined as a biopsy verified lymphoma in the orbit, conjunctiva, lacrimal gland, lacrimal sac and/or eyelids, without a history of systemic lymphoma. Stage IE disease is limited to the ocular adnexal region (where E indicates

the involvement of the extranodal site); stage IIE indicates involvement of lymph node regions on the same side of the diaphragm; stage IIIE indicates involvement of lymph node regions on both sides of the diaphragm; and stage IVE indicates involvement of one or more organs or tissues outside the lymphatic system.

### Statistical analysis

Overall survival (OS), disease-specific survival (DSS), and progression-free survival (PFS) were the primary end points. The Kaplan-Meier method was applied to estimate these survival outcomes at 5 years after diagnosis. The starting point for time-to-event analysis was the date of histological diagnosis. An event for OS and DSS was defined as death from any cause and death from lymphoma, respectively. An event for PFS was defined as disease progression, relapse, or death from any cause. Observational intervals of patients without any event at the time of last follow-up were censored. Life tables and Kaplan-Meier plots were generated to visualise the survival outcomes. The different risk groups were compared using the log-rank test and individual risk factors were compared using the  $\chi^2$  test. The Cox proportional-hazards model was used to estimate HRs and 95% CIs. Adjusted HR was obtained using a multivariable Cox model. All statistical analyses were performed using the SPSS Statistics software V.26 (IBM Corporation).

## RESULTS

A total of 42 patients with OA-LBCL diagnosed in Denmark between 1980 and 2018 were identified. Eight patients were excluded due to small biopsy size, leaving 34 patients for analysis. A subset of this cohort was previously published as part of a multicentre study and a nation-based study of ocular adnexal DLBCL (OA-DLBCL).<sup>2,24</sup>

### Molecular and phenotypic characterisation

Rearrangement of *cMYC* was detected in 8 of 34 lymphomas (24%) (table 1; figure 1). *BCL2* and *BCL6* rearrangements were analysed in 32 cases and were present in 8 lymphomas (25%) each. *cMYC* rearrangements co-occurred with *BCL2* and/or *BCL6* rearrangements in 16% (5 of 32) of the lymphomas. All 34 cases were EBV-negative. Thereby, 2 subgroups of LBCL were identified in the cohort: DLBCL (84%; 27 of 32) and HGBL with *MYC* and *BCL2* and/or *BCL6* rearrangements (16%; 5 of 32).

**Table 1. Molecular and immunohistochemical analyses of 34 ocular adnexal large B-cell lymphomas**

Analysis	No. of patients* (%)
<b>NF-κβ-activating mutations</b>	
<i>MYD88</i> mutated	10 (29)
<i>CD79B</i> mutated	3 (9)
<b>Double/triple hit status</b>	
<i>cMYC</i> rearranged	8 (24)
<i>BCL2</i> rearranged	8 (25)
<i>BCL6</i> rearranged	8 (25)
<i>cMYC</i> and <i>BCL2</i> and/or <i>BCL6</i> rearranged	5 (16)
<b>Double-expressor status</b>	
<i>cMYC</i> overexpressed	16 (50)
<i>BCL2</i> overexpressed	27 (82)
<i>cMYC</i> and <i>BCL2</i> overexpressed	15 (47)

Among the five HGBLs with *MYC* and *BCL2* and/or *BCL6* rearrangements, three lymphomas had concurrent immunohistochemical overexpression of *cMYC* and *BCL2*. Among DLBCLs, 44% (12 of 27) of cases exhibited the double-expressor phenotype. DLBCLs were further subclassified according to the Hans' algorithm with 59% (16 of 27) of cases being non-GCB DLBCLs.

5

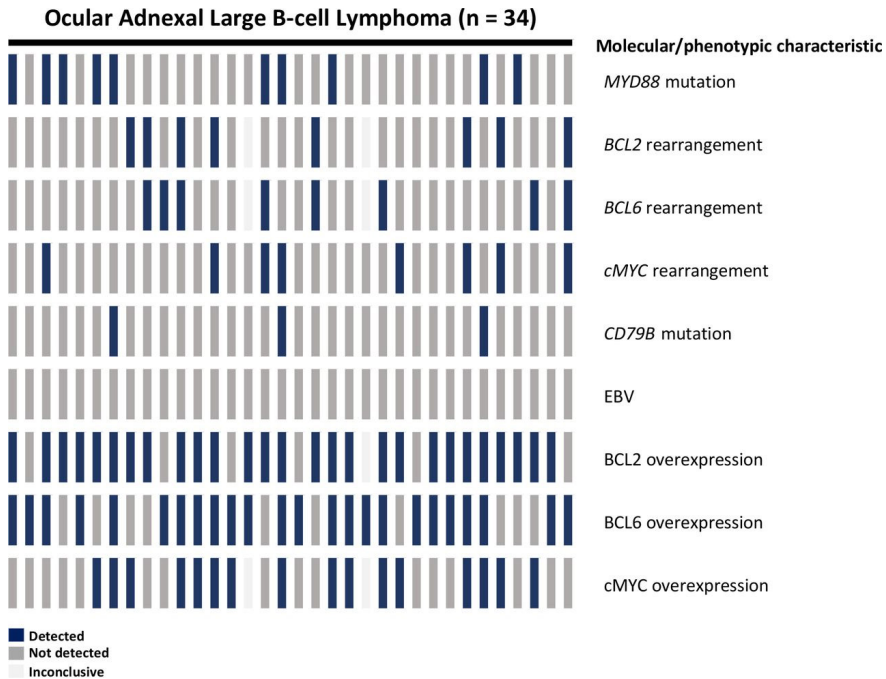


**Figure 1.** Oncoprint plot of the molecular and immunohistochemical analyses of 34 ocular adnexal large B-cell lymphomas. EBV, Epstein-Barr virus.

*MYD88* mutations were detected in 10 out of 34 lymphomas (29%). Eight (80%) of these cases harboured the hotspot *L265P* mutation; the remaining two variants were *S219C* and *S243N*. *CD79B* mutations were found in 3 of 34 lymphomas (9%). All *CD79B* mutations resided on the hotspot *Y196* and co-occurred with a *MYD88* mutation. *MYD88* mutations co-occurred with rearrangements of *cMYC* and/or *BCL2* and/or *BCL6* in 3 of 10 cases (30%), while *CD79B* mutations co-occurred with these rearrangements in 1 of 3 cases (33%).

### Patient characteristics

Across the various phenotypic and molecular backgrounds, OA-LBCL was clinically characterised by presentation after the age of 60 (60%–100%) as a unilateral (100%) orbital (80%–100%) lesion (table 2; figure 2). Most patients presented with stage IE by the Ann Arbor staging system (55%–70%) and stage T2 by the AJCC TNM staging system (63%–100%). The most common treatment modality used to manage OA-LBCL lesions was rituximab, cyclophosphamide, doxorubicin, vincristine and prednisone combination chemotherapy with or without external beam radiation therapy (33%–67%).

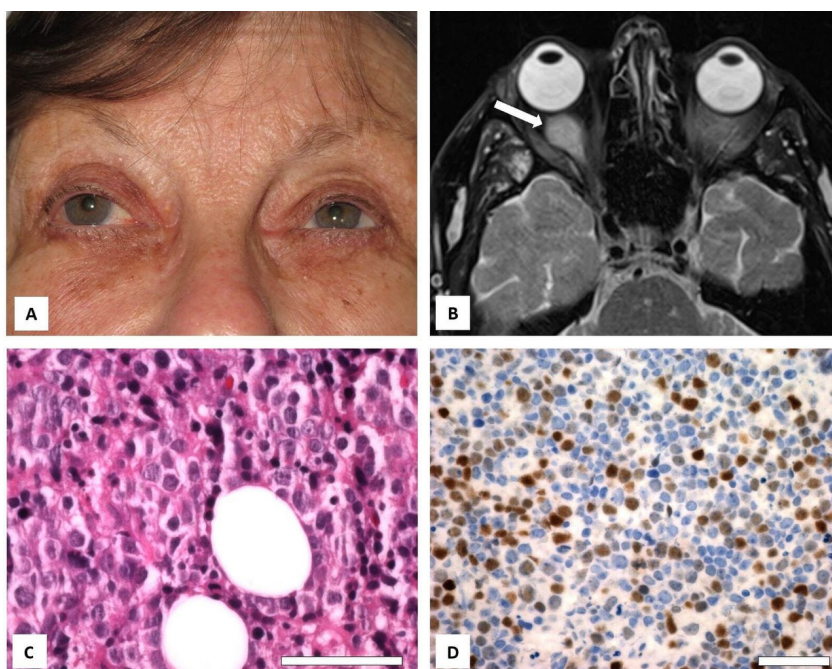


**Figure 2.** Presentation of a diffuse large B-cell lymphoma of the ocular adnexal region. (A) Clinical presentation with right-sided proptosis, restricted eye movement and upward and lateral displacement of the globe in a 79-year-old female patient. (B) Magnetic resonance imaging with contrast shows a right-sided orbital tumour mass (arrow). (C) Histological presentation with diffuse infiltration of large lymphoid tumour cells containing amphiphilic cytoplasm and oval to round vesicular nuclei with irregularly distributed chromatin (H&E; bar=50 µm). (D) MYC immunostaining with >40% of the tumour cells reacting with anti-MYC antibodies (bar=50 µm).

### Survival and clinical correlations

The median follow-up time was 16 months (range, 0–167 months). Recurrence or progression was observed in 43% (12 of 28) of patients. Survival rates at 5 years after diagnosis were: OS, 35%; DSS, 51%; and PFS, 29%. DSS was poorer among cMYC/BCL2 double-expressor DLBCLs (5-year DSS, 25%) than DLBCLs without a double-expressor phenotype (5-year DSS, 78%) (HR 0.23; 95% CI 0.06 to 0.85;  $p=0.014$ ; figure 3A). This prognostic impact was retained on adjustment for treatment modality (HR 0.24; 95% CI 0.06 to 0.95;  $p=0.046$ ). *MYD88* mutations were more frequent in non-GCB DLBCLs, occurring in 50% (8 of 16) of cases as opposed to 9% (1 of 11) of GCB DLBCLs ( $p=0.036$ ). PFS for lymphomas harbouring *MYD88* mutations was poorer (5-year PFS, 0%) compared with wild-type cases (5-year PFS, 43%) (HR 0.78; 95% CI 0.61 to 0.98;  $p=0.039$ ; figure 3B).

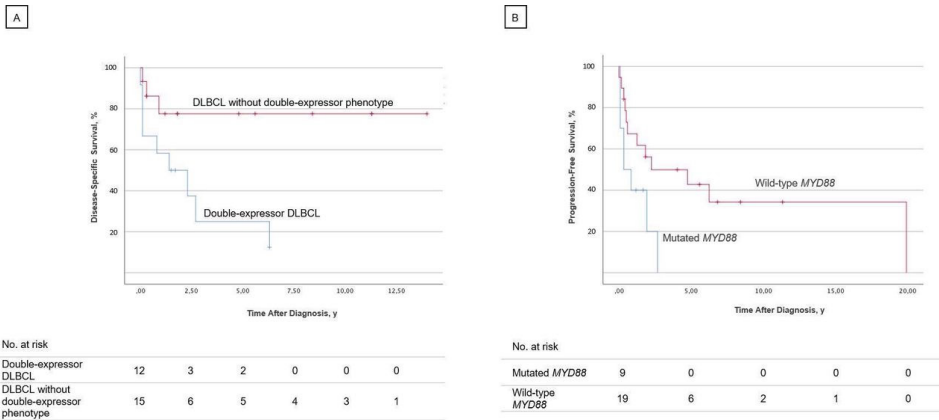


**Figure 3.** Survival among patients with ocular adnexal large B-cell lymphoma. (A) Disease-specific survival was poorer for diffuse large B-cell lymphomas exhibiting cMYC/BCL2 double-expressor phenotype (HR 0.23; 95% CI 0.06 to 0.85;  $p=0.014$ ). (B) Progression-free survival was poorer for large B-cell lymphomas harbouring *MYD88* mutations (HR 0.78; 95% CI 0.61 to 0.98;  $p=0.039$ ). DLBCL indicates diffuse large B-cell lymphoma. Hash marks indicate the occurrence of a censoring event.

**Table 2. Clinical characteristics of 34 ocular adnexal large B-cell lymphoma patients by phenotypic and molecular backgrounds**

Characteristic	LBCL group*, no. of patients (%)						
	Total cohort (n=34)	DLBCL, non-double-expressor (n=15)	Double-expressor DLBCL (n=12)	Double-expressor or BCL6 rearrangements (double/triple-hit; n=5)	Double-hit wild-type LBCL (n=27)	MYD88-mutated LBCL (n=10)	Wild-type MYD88 LBCL (n=24)
<b>Sex</b>							
Male	17 (50)	5 (33)	8 (67)	2 (40)	13 (48)	6 (60)	11 (46)
Female	17 (50)	10 (67)	4 (33)	3 (60)	14 (52)	4 (40)	13 (54)
<b>Age</b>							
≤60	4 (12)	2 (13)	0	2 (40)	2 (7)	1 (10)	3 (13)
>60	30 (88)	13 (87)	12 (100)	3 (60)	25 (93)	9 (90)	21 (88)
<b>Disease group</b>							
Primary	16 (48)	8 (53)	5 (45)	3 (60)	13 (50)	4 (40)	12 (52)
Disseminated	7 (21)	3 (20)	3 (27)	1 (20)	6 (23)	1 (10)	6 (26)
Relapsed	10 (30)	4 (27)	3 (27)	1 (20)	7 (27)	5 (50)	5 (22)
<b>Location in the OAR†</b>							
Orbit	28 (82)	12 (80)	10 (83)	5 (100)	22 (81)	8 (80)	20 (83)
Conjunctiva	3 (9)	1 (7)	2 (17)	0	3 (11)	1 (10)	2 (8)
Lacrimal gland	4 (12)	0	1 (8)	1 (20)	1 (4)	0	4 (17)
Lacrimal sac	2 (6)	2 (13)	0	0	2 (7)	1 (10)	1 (4)
Eyelid	2 (6)	1 (7)	1 (8)	0	2 (7)	1 (10)	1 (4)
<b>Laterality</b>							
Unilateral	34 (100)	15 (100)	12 (100)	5 (100)	27 (100)	10 (100)	24 (100)
Bilateral	0	0	0	0	0	0	0
<b>Ann Arbour stage</b>							
IE	18 (60)	9 (64)	7 (70)	3 (60)	16 (67)	7 (70)	11 (55)
II E	5 (17)	2 (14)	1 (10)	1 (20)	3 (13)	1 (10)	4 (20)
III E	1 (3)	1 (7)	0	0	1 (4)	1 (10)	0
IV E	6 (20)	2 (14)	2 (20)	1 (20)	4 (17)	1 (10)	5 (25)

Table 2. Continued.

Characteristic	LBCL group*, no. of patients (%)						
	Total cohort (n=34)	DLBCL, non-double-expressor (n=15)	Double-expressor DLBCL (n=12)	Double-expressor or BCL6 rearrangements (double/triple-hit; n=5)	Double-hit wild-type LBCL (n=27)	MYD88-mutated LBCL (n=10)	Wild-type MYD88 LBCL (n=24)
<b>AJCC TNM stage†</b>							
T1	0	0	0	0	0	0	0
T2	13 (81)	5 (63)	5 (100)	3 (100)	10 (77)	4 (100)	9 (75)
T3	0	0	0	0	0	0	0
T4	3 (19)	3 (38)	0	0	3 (23)	0	3 (25)
<b>Initial treatment</b>							
EBRT	8 (26)	3 (20)	5 (56)	0	8 (33)	3 (30)	5 (24)
R-CHOP±EBRT	15 (48)	10 (67)	3 (33)	2 (40)	13 (54)	5 (50)	10 (48)
CHOP±EBRT	4 (13)	1 (7)	0	2 (40)	1 (4)	0	4 (19)
Other chemotherapy±EBRT	4 (13)	1 (7)	1 (11)	1 (20)	2 (8)	2 (20)	2 (10)
<b>Recurrence or progression</b>							
No	16 (57)	9 (64)	3 (43)	4 (80)	12 (57)	5 (56)	11 (58)
Yes	12 (43)	5 (36)	4 (57)	1 (20)	9 (43)	4 (44)	8 (42)
<b>Disease status at last follow-up</b>							
Complete remission	9 (27)	6 (43)	1 (8)	2 (40)	7 (27)	2 (20)	7 (30)
Alive with disease	1 (3)	1 (7)	0	0	1 (4)	1 (10)	0
Dead from lymphoma	15 (45)	3 (21)	9 (75)	1 (20)	12 (46)	3 (30)	12 (52)
Dead from other cause	8 (24)	4 (29)	2 (17)	2 (40)	6 (23)	4 (40)	4 (17)

\*Data are not specified for all patients.

†A total of more than 100% because patients may have one or more lymphoma locations.

‡Stages primary lymphomas only.

AJCC, American Joint Committee on Cancer; EBRT, external beam radiation therapy; HGBL, high-grade B-cell lymphoma; LBCL, large B-cell lymphoma; OAR, ocular adnexal region; (R)-CHOP, (rituximab), cyclophosphamide, hydroxydaunorubicin, vincristine, prednisone.

**DATA AVAILABILITY STATEMENT**

Data are available upon reasonable request. Data are available on request from the authors.

**CONTRIBUTORS**

Study concept and design: MKK, LDS, STP, SH. Acquisition, analysis, or interpretation of data: MKK, MM, PRGE. Drafting of the manuscript: MKK. Critical revision of the manuscript for important intellectual content: MM, LDS, STP, PRGE, SH. Statistical analysis: MKK. Obtained funding: MKK, MM, STP. Study supervision: LDS, STP, SH. Guarantor: SH.

**FUNDING**

This work was supported by grants from the Synoptik Foundation, the Lymph&Co Foundation, Arvid Nielsson's Foundation, the Danish Eye Research Foundation, the Medical Sciences Part of the Faculty of Health and Medical Sciences' Foundation for Scientifically Employed Candidates and Students at the University of Copenhagen Foundation (Grant Number 2019-0090), Ms. Amalie Jørgensen's Memorial Grant, and Else and Mogens Weddell-Weddellsborg's Foundation (Grant Number 11-20-2).

**COMPETING INTERESTS**

None declared.

## REFERENCES

1. Swerdlow SH, Campo E, Harris NL. WHO classification of tumours of haematopoietic and lymphoid tissues. 4th ed. Lyon: IARC Press, 2017.
2. Munch-Petersen HD, Rasmussen PK, Coupland SE, et al. Ocular adnexal diffuse large B-cell lymphoma: a multicenter international study. *JAMA Ophthalmol* 2015;133:165–73.doi:10.1001/jamaophthalmol.2014.4644
3. Kirkegaard MM, Rasmussen PK, Coupland SE, et al. Conjunctival Lymphoma--An International Multicenter Retrospective Study. *JAMA Ophthalmol* 2016;134:406–14.doi:10.1001/jamaophthalmol.2015.6122
4. Sjö LD. Ophthalmic lymphoma: epidemiology and pathogenesis. *Acta Ophthalmol* 2009;87 Thesis 1:1–20. doi:10.1111/j.1755-3768.2008.01478.x
5. Lu T-X, Liang J-H, Miao Y, et al. Epstein-Barr virus positive diffuse large B-cell lymphoma predict poor outcome, regardless of the age. *Sci Rep* 2015;5:12168.doi:10.1038/srep12168
6. Leskov I, Pallasch CP, Drake A, et al. Rapid generation of human B-cell lymphomas via combined expression of Myc and Bcl2 and their use as a preclinical model for biological therapies. *Oncogene* 2013;32:1066–72. doi:10.1038/onc.2012.117 pmid:http://www.ncbi.nlm.nih.gov/pubmed/22484426 CrossRefPubMedGoogle Scholar
7. Lindsley RC, LaCasce AS. Biology of double-hit B-cell lymphomas. *Curr Opin Hematol* 2012;19:299–304. doi:10.1097/MOH.0b013e328353bbbd
8. Rosenthal A, Younes A. High grade B-cell lymphoma with rearrangements of MYC and BCL2 and/or BCL6: double hit and triple hit lymphomas and double expressing lymphoma. *Blood Rev* 2017;31:37–42. doi:10.1016/j.blre.2016.09.004
9. Huang S, Nong L, Wang W, et al. Prognostic impact of diffuse large B-cell lymphoma with extra copies of MYC, BCL2 and/or BCL6: comparison with double/triple hit lymphoma and double expressor lymphoma. *Diagn Pathol* 2019;14:81.doi:10.1186/s13000-019-0856-7
10. Ngo VN, Young RM, Schmitz R, et al. Oncogenically active MYD88 mutations in human lymphoma. *Nature* 2011;470:115–9.doi:10.1038/nature09671
11. Kraan W, Horlings HM, van Keimpema M, et al. High prevalence of oncogenic MYD88 and CD79B mutations in diffuse large B-cell lymphomas presenting at immune-privileged sites. *Blood Cancer J* 2013;3:e139. doi:10.1038/bcj.2013.28
12. Dubois S, Vially PJ, Bohers E, et al. Biological and clinical relevance of associated genomic alterations in MYD88 L265P and non-L265P-Mutated diffuse large B-cell lymphoma: analysis of 361 cases. *Clin Cancer Res* 2017;23:2232–44.doi:10.1158/1078-0432.CCR-16-1922
13. de Groen RAL, Schrader AMR, Kersten MJ, et al. MYD88 in the driver's seat of B-cell lymphomagenesis: from molecular mechanisms to clinical implications. *Haematologica* 2019;104:2337–48.doi:10.3324/haematol.2019.227272
14. Davis RE, Ngo VN, Lenz G, et al. Chronic active B-cell-receptor signalling in diffuse large B-cell lymphoma. *Nature* 2010;463:88–92.doi:10.1038/nature08638
15. Wilson WH, Young RM, Schmitz R, et al. Targeting B cell receptor signaling with ibrutinib in diffuse large B cell lymphoma. *Nat Med* 2015;21:922–6.doi:10.1038/nm.3884
16. Kraan W, van Keimpema M, Horlings HM, et al. High prevalence of oncogenic MYD88 and CD79B mutations in primary testicular diffuse large B-cell lymphoma. *Leukemia* 2014;28:719–20.doi:10.1038/leu.2013.348
17. Chapuy B, Roemer MGM, Stewart C, et al. Targetable genetic features of primary testicular and primary central nervous system lymphomas. *Blood* 2016;127:869–81.doi:10.1182/blood-2015-10-673236
18. Bonzheim I, Giese S, Deuter C, et al. High frequency of MYD88 mutations in vitreoretinal B-cell lymphoma: a valuable tool to improve diagnostic yield of vitreous aspirates. *Blood* 2015;126:76–9.doi:10.1182/blood-2015-01-620518
19. Raja H, Salomão DR, Viswanatha DS, et al. Prevalence of Myd88 L265p mutation in histologically proven, diffuse large B-cell vitreoretinal lymphoma. *Retina* 2016;36:624–8.doi:10.1097/IAE.0000000000000996
20. Cani AK, Soliman M, Hovelson DH, et al. Comprehensive genomic profiling of orbital and ocular adnexal lymphomas identifies frequent alterations in MyD88 and chromatin modifiers: new routes to targeted therapies. *Mod Pathol* 2016;29:685–97.doi:10.1038/modpathol.2016.79
21. Swerdlow SH, Campo E, Pileri SA, et al. The 2016 revision of the world Health organization classification of lymphoid neoplasms. *Blood* 2016;127:2375–90.doi:10.1182/blood-2016-01-643569
22. Amin MB, Edge S, Greene F. AJCC cancer staging manual. 8th edn. New York: Springer, 2017.Google Scholar
23. Carbone PP, Kaplan HS, Musshoff K, et al. Report of the Committee on Hodgkin's disease staging classification. *Cancer Res* 1971;31:1860–1.
24. Rasmussen PK, Ralfkiaer E, Prause JU, et al. Diffuse large B-cell lymphoma of the ocular adnexal region: a nation-based study. *Acta Ophthalmol* 2013;91:163–9.doi:10.1111/j.1755-3768.2011.02337.x
25. Johnson NA, Slack GW, Savage KJ, et al. Concurrent expression of MYC and BCL2 in diffuse large B-cell

- lymphoma treated with rituximab plus cyclophosphamide, doxorubicin, vincristine, and prednisone. *J Clin Oncol* 2012;30:3452–9.doi:10.1200/JCO.2011.41.0985
26. Lucioni M , Pescia C , Bonometti A , et al . Double expressor and double/triple hit status among primary cutaneous diffuse large B-cell lymphoma: a comparison between leg type and not otherwise specified subtypes. *Hum Pathol* 2021;111:1–9.doi:10.1016/j.humpath.2021.01.006
  27. Menguy S , Frison E , Prochazkova-Carlotti M , et al . Double-hit or dual expression of MYC and BCL2 in primary cutaneous large B-cell lymphomas. *Mod Pathol* 2018;31:1332–42.doi:10.1038/s41379-018-0041-7
  28. Schrader AMR, Jansen PM, Vermeer MH, et al . High incidence and clinical significance of Myc rearrangements in primary cutaneous diffuse large B-cell lymphoma, leg type. *Am J Surg Pathol* 2018;42:1488–94. doi:10.1097/PAS.0000000000001132
  29. Perry AM , Alvarado-Bernal Y , Laurini JA , et al . MYC and BCL2 protein expression predicts survival in patients with diffuse large B-cell lymphoma treated with rituximab. *Br J Haematol* 2014;165:382–91. doi:10.1111/bjh.12763
  30. Yan L-X , Liu Y-H , Luo D-L , et al . MYC expression in concert with BCL2 and BCL6 expression predicts outcome in Chinese patients with diffuse large B-cell lymphoma, not otherwise specified. *PLoS One* 2014;9:e104068.doi:10.1371/journal.pone.0104068
  31. Akyurek N , Uner A , Benekli M , et al . Prognostic significance of MYC, BCL2, and BCL6 rearrangements in patients with diffuse large B-cell lymphoma treated with cyclophosphamide, doxorubicin, vincristine, and prednisone plus rituximab. *Cancer* 2012;118:4173–83.doi:10.1002/cncr.27396
  32. Schmidt-Hansen M , Berendse S , Marafioti T , et al . Does cell-of-origin or MYC, BCL2, BCL2 or BCL6 translocation status provide prognostic information beyond the International prognostic index score in patients with diffuse large B-cell lymphoma treated with rituximab and chemotherapy? A systematic review. *Leuk Lymphoma* 2017;58:2403–18.doi:10.1080/10428194.2017.1287364
  33. Schrader AMR , Jansen PM , Willemze R , et al . High prevalence of MYD88 and CD79B mutations in intravascular large B-cell lymphoma. *Blood* 2018;131:2086–9.doi:10.1182/blood-2017-12-822817
  34. Chapuy B , Stewart C , Dunford AJ , et al . Molecular subtypes of diffuse large B cell lymphoma are associated with distinct pathogenic mechanisms and outcomes. *Nat Med* 2018;24:679–90.doi:10.1038/s41591-018-0016-8
  - Zhou XA , Louissaint A , Wenzel A , et al . Genomic analyses identify recurrent alterations in immune evasion genes in diffuse large B-cell lymphoma, leg type. *J Invest Dermatol* 2018;138:2365–76.doi:10.1016/j.jid.2018.04.038



# 6

## Sinonasal diffuse large B-cell lymphoma: molecular profiling identifies subtypes with distinctive prognosis and targetable genetic features

Patrick RG Eriksen<sup>1\*</sup>, Fleur de Groot<sup>2</sup>, Erik Clasen-Linde<sup>3</sup>, Peter de Nully Brown<sup>4</sup>,  
Ruben de Groen<sup>2</sup>, Linea C. Melchior<sup>3</sup>, Andrea D Maier<sup>5</sup>, Marthe Minderman<sup>6</sup>,  
Joost S. P. Vermaat<sup>2,5</sup>, Christian von Buchwald<sup>1,5</sup>, Steven T. Pals<sup>6,5</sup>, Steffen Heegaard<sup>2,7,5</sup>

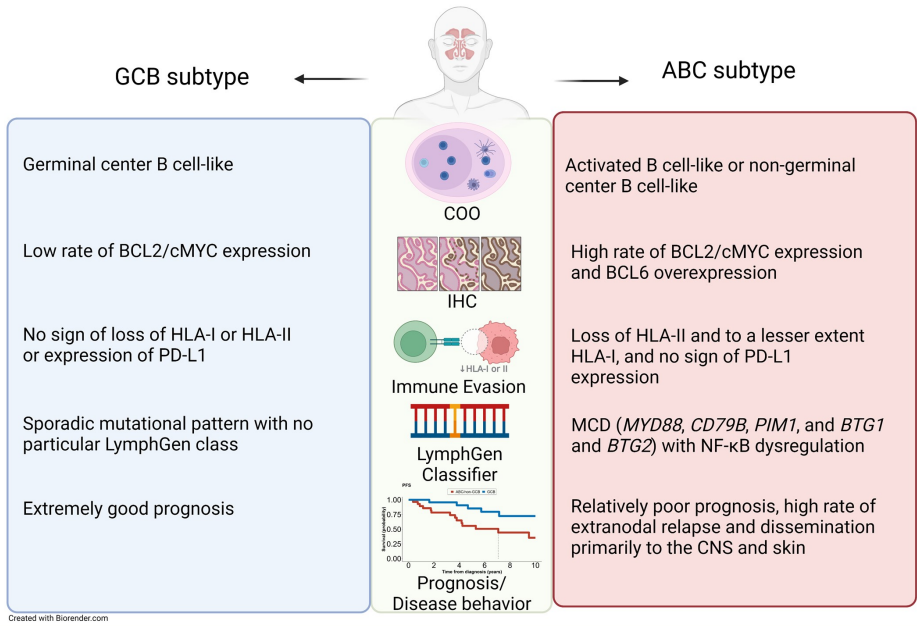
<sup>1</sup>Department of Otorhinolaryngology, Head and Neck Surgery and Audiology, Rigshospitalet, University of Copenhagen, Denmark; <sup>2</sup>Department of Hematology, Leiden University Medical Center, Leiden, The Netherlands; <sup>3</sup>Department of Pathology, Rigshospitalet, University of Copenhagen, Copenhagen, Denmark; <sup>4</sup>Department of Hematology, Rigshospitalet, University of Copenhagen, Copenhagen, Denmark; <sup>5</sup>Department of Neurosurgery, Rigshospitalet, University of Copenhagen, Copenhagen, Denmark; <sup>6</sup>Department of Pathology and Cancer Center Amsterdam (CCA), Amsterdam University Medical Centers (AUMC), Amsterdam, The Netherlands; <sup>7</sup>Department of Ophthalmology, Rigshospitalet, University of Copenhagen, Copenhagen, Denmark. <sup>5</sup>These authors share last-authorship

## ABSTRACT

Primary sinonasal diffuse large B-cell lymphoma (PSDLBCL) is a rare lymphoma with a variable prognosis and a unique relapse/dissemination pattern involving the CNS and skin. The underlying molecular mechanisms leading to this heterogeneity and progression pattern remain uncharted, hampering patient-tailored treatment. To investigate associated mechanisms, we analyzed clinical data and employed immunohistochemistry, gene-expression profiling, cytogenetics, and next-generation sequencing in a cohort of 117 PSDLBCL patients from the Danish National Pathology Registry. The distribution in cell-of-origin (COO) was 68 (58%) activated B-cell (ABC), 44 (38%) germinal center B-cell (GCB), and 5 (4%) unclassifiable. Cell-of-origin was significantly associated with progression-free-survival (PFS) and lymphoma-specific mortality (LSM) in both the overall cohort (five-year PFS, ABC 43% vs. GCB 73%; LSM, ABC 45% vs. GCB 14%) and in the subgroup of patients receiving immunochemotherapy (five-year PFS: ABC 55% vs. GCB 85%; LSM: ABC 28% vs. GCB 0%). ABC-lymphomas were mainly MCD class, showing a high prevalence of *MYD88* (74%) and *CD79B* (35%) mutations compared to GCB-lymphomas (*MYD88* 23%, *CD79B* 10%) ( $P < 0.01$ ). The ABC subtype frequently displayed cMYC/BCL2 double expression (76% vs. 18% GCB,  $P < 0.001$ ) and loss of HLA-II (48% vs. 10% GCB,  $P < 0.001$ ). PD-L1 expression and copy-number alterations were rare. Epstein-Barr virus was absent in all lymphomas. Our data suggest molecular profiling as a potent tool for detecting prognostic subgroups in PSDLBCL, exposing links to known sites of relapse/dissemination. The ABC group's MCD genetic-features, shared with lymphomas at other non-professional lymphoid sites, make them potential candidates for targeted B-cell receptor- and toll-like receptor-signaling therapy.

# VISUAL ABSTRACT

## Sinonasal diffuse large B-cell lymphoma: molecular profiling identifies subtypes with distinctive prognosis and targetable genetic features



**Widely different disease behaviors of primary sinonasal diffuse large B-cell lymphoma (PSDLBCL) based on molecular subtype**

## INTRODUCTION

Diffuse large B-cell lymphoma (DLBCL) is a common non-Hodgkin lymphoma known for its distinct phenotypic, genetic, and clinical heterogeneity; as a result, the World Health Organization (WHO) classification recognizes multiple DLBCL subgroups based on molecular and clinical characteristics.(1–3) The introduction of gene expression profiling has allowed the molecular subdivision of DLBCL by cell-of-origin (COO) into germinal center B cell-like (GCB) and activated B cell-like (ABC).(4,5) Although COO classification has proven useful in partly understanding the variability in clinical behavior and outcome of DLBCL, this phenotypic classifier incompletely accounts for the heterogeneous treatment response and disease outcome following treatment with rituximab plus cyclophosphamide, doxorubicin, vincristine, prednisone (R-CHOP), and targeted therapies. Recent multi-platform genomic studies have revealed the existence of genetic subtypes of DLBCL that are characterized by genomic aberrations in class-specific hallmark genes.(6,7) These aberrations lead to the deregulation of distinctive biological pathways and are associated with COO, clinical behavior, and susceptibility to targeted therapy.(6–8) In the MCD/C5 classes, mutations in the toll-like receptor (TLR) adapter MYD88 and B-cell receptor (BCR)-associated protein CD79 drive constitutive NF- $\kappa$ B pathway activation, promoting tumor cell proliferation and survival. Interestingly, this genetic profile is strongly associated with DLBCL arising at extranodal sites, including primary DLBCL of the central nervous system (CNS), skin (leg-type), breast, testes, and vitreoretinal compartment.(9–15). All of these lymphomas bear a high risk of dissemination to other extranodal sites, particularly the CNS.(12,13,16–18)

6

Primary sinonasal diffuse large B-cell lymphoma (PSDLBCL) is a rare extranodal lymphoma localized in the sinonasal mucosa, comprising 0.4% of all non-Hodgkin lymphomas (NHLs).(19) The ectodermally-derived sinonasal mucosa is lined with respiratory epithelium and does not contain organized secondary lymphoid tissue, unlike the rest of the endodermally-derived upper respiratory tract.(20) It is associated with site-specific diseases, such as chronic rhinosinusitis and intestinal-type sinonasal adenocarcinoma (21,22) but also with hematological neoplasms, specifically extranodal NK/T-cell lymphoma (nasal-type), solitary extraosseous plasmacytoma, and sinonasal B-cell lymphoma.(23,24) In a previous comprehensive nationwide study of sinonasal B-cell lymphoma, we found that about 85% of all included B-cell lymphomas with a primary presentation in the nasal cavity or paranasal sinuses were DLBCLs. Although most of these patients responded favorably to treatment with (immuno)chemotherapy, relapse/dissemination occurred in about a quarter. These cases preferentially affected the CNS and skin and were associated with high disease-related mortality; furthermore, an inverse relationship was observed, where primary lymphomas originating from the CNS and skin relapsed to the sinonasal mucosa.(19) In our current study, we interrogated

the molecular mechanisms underlying the heterogeneous clinical course of PSDLBCL by exploring COO, oncoprotein overexpression, Epstein-Barr virus (EBV) status, immune evasion mechanisms, and the DLBCL genetic subtype.

## MATERIALS AND METHODS

### Patient selection and clinical data

All cases of PSDLBCL were from our established nationwide cohort (1980 – 2018).<sup>(19)</sup> We defined PSDLBCL as a single lesion in the nasal cavity or paranasal sinuses with or without regional lymph node involvement at the time of diagnosis and no prior lymphoma.

Clinical records were retrieved, and the following data were extracted: age, sex, symptoms, clinical findings, laterality, lymph node involvement, treatment modalities and response to therapy, relapse/dissemination pattern, survival, and cause of death. If data on the cause of death were unavailable from autopsy reports or medical records, the Danish Register of Causes of Death (DAR) would substitute for missing data. Clinical data and diagnostic resources at the time of diagnosis determined systemic involvement and laterality at the time of diagnosis.

### Lymphoma classification

All cases were classified according to the 2017 WHO classification (11); specifications of monoclonal antibodies (mAbs) used for immunohistochemistry can be found in Supplement “Methods”. Other mAbs used were anti-HLA-DR (TAL 1B5, DAKO), anti-HLA-ABC (W6/32, DAKO), and anti-PD-L1/CD274 (22C3, DAKO); results were independently assessed by two hematopathologists (ECL and SP). Epstein-Barr virus status was established by EBV-encoded RNA in situ hybridization (EBER ISH). *BCL2*, *-6*, and *MYC* rearrangements were analyzed by fluorescence in situ hybridization (FISH) using break-apart probes; see Supplement “Methods”. Probes covering CD274 and *PDCD1LG2* (PD-L1 and PD-L2) and *CEN 9* (centromere of chromosome nine) were used to assess *PD-L1* copy number alterations (CNAs); copy number gain was defined as target-to-control probe ratios of  $\geq 2:1$ , while  $>5:1$  was classified as amplification. The immunohistochemical COO classification was performed using the algorithm by Hans *et al.*<sup>(25)</sup> For ease of reading, non-GCB (Hans’ algorithm) and ABC (Lymph2Cx) will be termed “ABC” in the Results and Discussion sections. For COO subtype classification in the survival analyses, we employed a “composite” of both approaches, with NanoString overriding immunohistochemistry in case of a discrepant subtype assignment.

## Gene expression profiling (GEP)

Micro-dissection of the paraffin-embedded tumor was performed using hematoxylin-eosin and CD20 stained slides, marking the tumor area; see Supplement “Methods” for further details on mRNA extraction, concentration measurements, and quality control. We determined COO by mRNA expression profiling using the NanoString Lymph2Cx Panel, which includes 15 target genes and five housekeeping genes; see Supplement “Methods” for analysis methods and subtype determination using the validated lymphoma subtyping (LST) signature.(26)

## Targeted next-generation sequencing

BLYMFv2 is a custom-made, validated Ion-Torrent-based AmpliSeq panel (Thermo Fisher Scientific) consisting of 3,359 amplicons covering 128 B-cell lymphoma-relevant genes. It is an updated version of the already published LYMFv1 and BLYMF200 panels (27,28); see Supplement “Methods” for detailed information. The unaligned sequence reads were aligned to the human reference genome (GRCh37/hg19) using TMAP 5.07 software (default parameters). Variants were called using TMAP 5.07 software with a minimum of 100 reads and a 10% variant allele frequency threshold. Identified variants were annotated into five pathogenicity classes using Geneticist Assistant NGS Interpretive Workbench. Pathogenicity classes 4 and 5 were interpreted as pathogenic. Class 3 variants were assessed using risk classifiers and called pathogenic if the CADD-PHRED score was higher than 25 and/or if two or more of the Sift, PolyPhen, LRT, and MutationTaster scores indicated pathogenicity. See Supplement “Methods”, Supplementary Figure 1 for number of variants allocated to each pathogenicity class. Manual calling of mutations in specific hotspots *MYD88*(L265P) and *CD79B*(Y196\*) was performed, even in samples affected by deamination. By adding cytogenetic information to the sequencing data, we subclassified the samples using the publicly available algorithm provided by the NIH (<https://lmpp.nih.gov/lymphgen/lymphgendataportal.php>); only samples with >90% probability of a class would be allocated, alternatively being subclassified as “other.” As an alternative to LymphGen, we employed the newly published simplified LymphPlex algorithm containing 38 genes based on partition around medoid (PAM) clustering (29) and the “two-step” approach by Pedrosa et al., which is based on the LymphGen classifier. In the first step of the “two-step” approach, classification is determined by the presence of highly specific mutations characteristic of each class. In case of a tie in the first step, the second step of the classification relies on mutations from a wider range of subclass-associated mutations (30); the algorithms are available at <https://kylinmu.shinyapps.io/LymphPlexR/> and <https://github.com/Lymphoma-IDIPHISA/Two-step-classifier>. The NGS data reported in this paper have been deposited in the Sequence Read Archive (accession number PRJNA1004445).

## Statistics

Overall survival (OS), progression-free survival (PFS), and lymphoma-specific mortality (LSM) were estimated using the Kaplan-Meier and Aalen-Johansen estimators. Overall survival was defined as time to death from any cause, while PFS was time to either relapse, progression, or death from any cause. Death from causes other than lymphoma was considered a competing risk. We used the log-rank test and Gray's test to determine significant differences between curves. Categorical variables were tested for significance using Fisher's exact test. All statistical analyses were performed using R ("survival", "ComplexHeatmap", and "cmprsk" packages, version 4.0.5, R core team). The significance level was set at 5%.

## RESULTS

### Patient characteristics

Our current study cohort comprised 117 patients with PSDLBCL.(19) The majority of lesions originated from the nasal cavity (n=43, 37%) and maxillary sinus (n=37, 32%), while only a few involved other sinuses: ethmoid (n=9, 8%), sphenoid (n=3, 3%), frontal sinuses (n=3, 3%), or unknown sinus (n=7, 6%). Fifteen patients (11%) had multiple sinonasal lesions, and 15 (11%) showed involvement of regional cervical lymph nodes at the time of diagnosis; when stratifying the cohort by Ann Arbor stage, no differences in clinical characteristics were detected, see Supplement "Cohort", Supplementary Table 1. For staging purposes, all patients apart from one had computed tomography or magnetic resonance imaging of the head and neck.

### Impact of cell-of-origin (COO) in PSDLBCL - COO subtype predicts dissemination, relapse, and survival

To assess the COO subtype and its prognostic value in our PSDLBCL cohort, we used Lymph2Cx (mRNA profiling) and Hans' algorithm (immunohistochemistry-based profiling). mRNA analysis was feasible in 66% (77/117) of cases, with 56% ABC, 36% GCB, and 8% "unclassifiable". Classification by Hans' algorithm was possible in 96% (112/117) of cases; 59% were classified as ABC, and 41% as GCB. There was a high concordance (92%) between Lymph2Cx and Hans' defined COO class, with only a few discordant cases. In our analyses of the impact of COO, mRNA profiling was prioritized over immunohistochemistry in cases with a discrepant subtype assignment. The combined classifiers identified 61% (68/112) of lymphomas as ABC and 39% (44/112) as GCB (Figure 1).

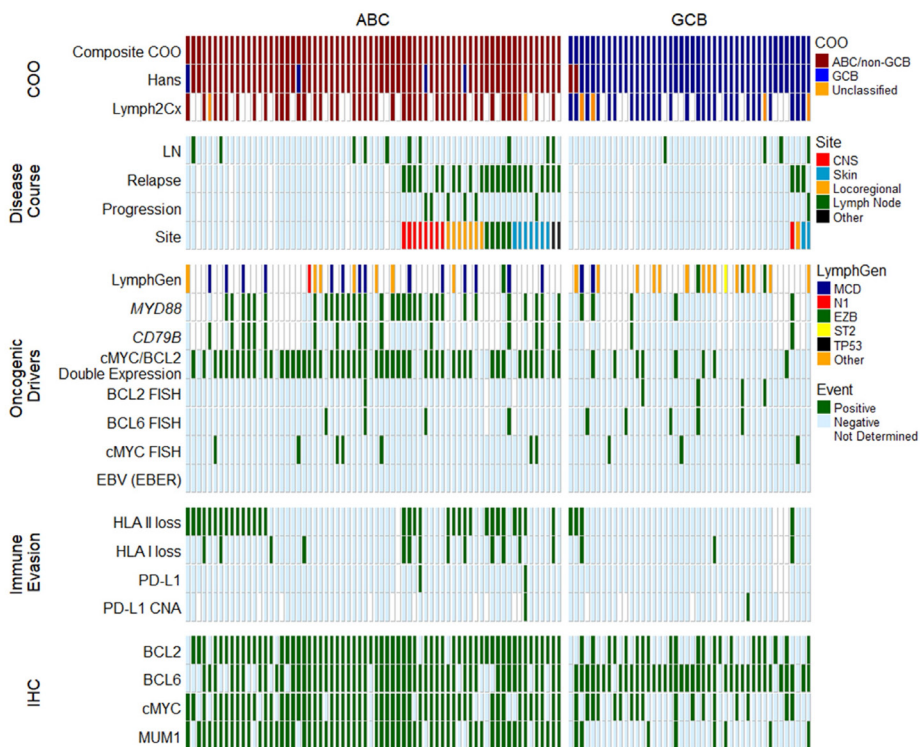


**Figure 1.** Diagram of 112 cases of PSDLBCL depicting cell-of-origin (COO), relapse/dissemination pattern, immunohistochemistry (IHC), cytogenetics, and mutations/LymphGen. Cell-of-origin (COO) was determined hierarchically, with Lymph2Cx overriding Hans' algorithm in cases of discordance. Cases with undetermined COO were excluded. ABC, activated B cell-like; GCB, germinal center B cell-like; LN, regional lymph node involvement; HLA, human leukocyte antigen; PD-L1, programmed death-ligand 1; CNS, central nervous system.

Of all cases with sufficient clinical data to evaluate disease relapse or progression, 32% (33/104) relapsed. Relapses were significantly more common in the ABC- (46%, 29/63) vs. GCB-subtype (14%, 4/29) lymphomas ( $P < 0.01$ ) (Figure 1). Survival analysis including all COO-classified patients, irrespective of the treatment regimen, revealed that the ABC subtype was a strong predictor of poor disease outcome: ABC cases showed a significantly decreased progression-free survival (PFS) and overall survival (OS), as well as increased lymphoma-specific mortality (LSM). The five-year PFS, OS, and LSM for ABC- vs. GCB-subtype lymphoma were 43% vs. 73% (log-rank test,  $P < 0.01$ ), 47% vs. 71% (log-rank test,  $P = 0.01$ ), and 45% vs. 14% (Gray's test,  $P < 0.001$ ), respectively. We found a similar impact of COO on survival in the subgroup of 52 patients treated with contemporary R-CHOP or R-CHOP-like immunochemotherapy. The five-year PFS and OS for ABC- and GCB-subtype cases were 55% vs. 85% (log-rank test,  $P = 0.02$ ) and 59%

vs. 89% (log-rank test, P=0.05), respectively, while the LSM was 28% vs. 0% (Gray's test, P<0.01) (Figure 2). To exclude the idea of treatment variation influencing the observed prognostic differences, we compared the treatment regimens between COO subtypes for the entire cohort (Table 1) and within the ABC subgroup for cases with or without relapse or progression (Supplement "Cohort", Supplementary Table 2). No significant differences were identified. Further insight into specific chemotherapy regimens and year of diagnosis by COO can be found in Supplement "Cohort", Supplementary Tables 3 and 4.

**Molecular characterization of PSDLBCL: low frequency of BCL2-, BCL6-, and cMYC-translocations and absence of EBV, but high prevalence of BCL2/cMYC double expression and BCL6 overexpression in the ABC-subtype**

To explore the molecular basis of PSDLBCL and its position in the complex DLBCL landscape, we investigated several oncogenic drivers with an established role in the pathogenesis of specific DLBCL subtypes (Figure 1).

**Table 1. Clinical characteristics, treatment, and disease outcome of patients with PSDLBCL stratified by COO.**

	ABC/non-GCB (N=68)	GCB (N=44)	P-value	Total (N=112)
<b>Age</b>				
Mean (SD)	73.7 (11.1)	70.8 (12.4)	0.199	72.6 (11.7)
Median [min, max]	76.0 [45.0, 100]	71.5 [36.0, 91.0]		75.0 [36.0, 100]
<b>Sex</b>				
Female	27 (39.7%)	19 (43.2%)	0.844	46 (41.1%)
Male	41 (60.3%)	25 (56.8%)		66 (58.9%)
<b>Regional Lymph Node involvement</b>				
Yes	10 (14.7%)	4 (9.1%)	0.56	14 (12.5%)
No	58 (85.3%)	40 (90.9%)		98 (87.5%)
<b>Performance Status</b>				
≥ 1	61 (89.7%)	41 (93.2%)	0.737	102 (91.1%)
>1	7 (10.3%)	3 (6.8%)		10 (8.9%)
<b>Chemotherapy</b>				
Yes	54 (79.4%)	36 (81.8%)	1	90 (80.4%)
No	10 (14.7%)	6 (13.6%)		16 (14.3%)
<b>Rituximab</b>				
Yes	29 (42.6%)	24 (54.5%)	0.248	53 (47.3%)
No	39 (57.4%)	20 (45.5%)		59 (52.7%)
<b>CNS Prophylaxis</b>				
Yes	20 (29.4%)	18 (40.9%)	0.226	38 (33.9%)
No	48 (70.6%)	26 (59.1%)		74 (66.1%)

**Table 1. Continued.**

	ABC/non-GCB (N=68)	GCB (N=44)	P-value	Total (N=112)
<b>Consolidative Radiotherapy</b>				
Yes	42 (61.8%)	26 (59.1%)	0.844	68 (60.7%)
No	26 (38.2%)	18 (40.9%)		44 (39.3%)
<b>Status</b>				
Alive without disease	19 (27.9%)	24 (54.5%)	<0.001	43 (38.4%)
Dead of disease	36 (52.9%)	7 (15.9%)		43 (38.4%)
Dead from other cause	13 (19.1%)	13 (29.5%)		26 (23.2%)

Demographical and clinical characteristics of patients with primary sinonasal diffuse large B-cell lymphoma (PSDLBCL) and sufficient material for cell-of-origin classification. ABC, activated B cell-like; GCB, germinal center B cell-like; PS, performance status. Chemotherapy consisted of CHOP (cyclophosphamide, hydroxydaunorubicin, vincristine, prednisone) or CHOP-like regimens. CNS-prophylaxis mainly consisted of high-dose methotrexate either given intrathecally or systemically.

First, we assessed the presence of translocations of the oncogenes *BCL2*, *BCL6*, and *cMYC*, important in the subclassification of DLBCL into genetic subtypes (6) and, in the case of *BCL2*, potentially indicating transformed follicular lymphoma.(31) Using FISH, we detected these translocations in only a minor percentage of the PSDLBCLs: *BCL2*, 4% (4/110); *BCL6*, 8% (9/110); and *cMYC*, 9% (10/112). Their presence was not significantly correlated to the COO (Figure 1).

Double expression of the oncoproteins BCL2 and cMYC, termed “double expression”, is associated with an unfavorable prognosis and secondary involvement of the CNS. (32) Interestingly, double expression and concurrent BCL6 overexpression is frequently observed in extranodal lymphomas, including primary CNS DLBCL (~80%) and primary cutaneous DLBCL (leg-type) (~70%).(11–13,19,33–35) Our analysis revealed a high incidence of double expression in the ABC-subtype: 77% (52/68) vs. 18% (8/44) in the GCB subtype (P<0.001) and high rates of BCL6 overexpression in both subtypes, ABC-77% vs. GCB subtype 88% (Figure 1).

The association of EBV with sinonasal DLBCL has never previously been investigated. To address this, we conducted EBER ISH analyses. Our findings revealed no evidence of EBV involvement.

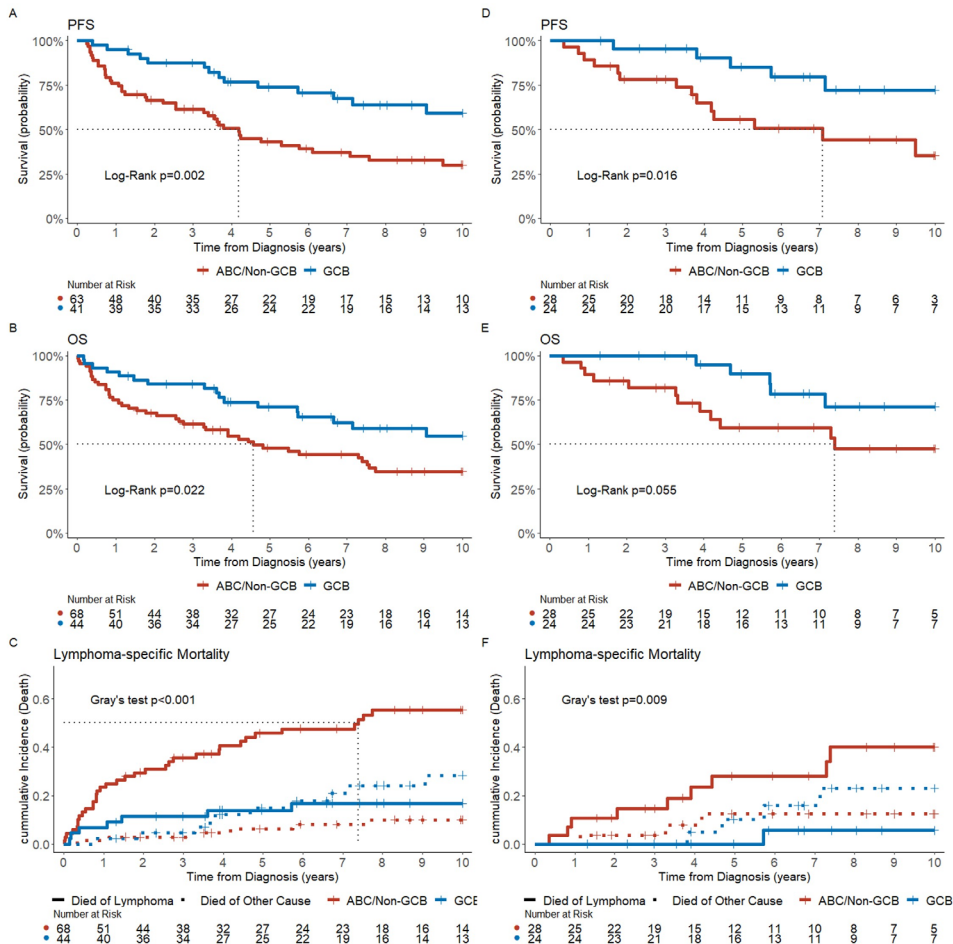


**Figure 2.** Survival curves for patients with PSDLBCL stratified by cell-of-origin (COO); the left side represents the entire cohort (A–C) [OS n=112, PFS n=104], while the right side represents the subgroup treated with R-CHOP or R-CHOP-like regimens (D–F) [n=52]. The dotted vertical line represents median survival. ABC, activated B cell-like; GCB, germinal cell B cell-like.

### Next-generation sequencing reveals marked differences in the mutational landscape of PSDLBCLs, with the ABC subtype exhibiting a high prevalence of MCD genetic features

Mutations impacting the *MYD88* and *CD79B* genes are important drivers of lymphomas presenting at immune-privileged sites, such as the CNS and testes, as well as at other extranodal sites, like the skin (leg-type) and intravascular space.(11,12,36) These mutations activate the NF-κB pathway, promoting cell proliferation and survival.(6) Employing NGS, we manually called the canonical hotspot mutations *MYD88* (L265P) and *CD79B* (Y196\*). Among the 74 samples analyzed (43 ABC, 31 GCB), *MYD88* (L265P),

mutations were more prevalent in ABC-subtype lymphomas (74%) compared to GCB (24%) ( $P < 0.001$ ). Similarly, *CD79B* (Y196\*) hotspot mutations were significantly associated with the ABC subtype (37% ABC- vs. 6% in the GCB subtype ( $P = 0.03$ )). All cases, apart from one with a *CD79B* (Y196\*) mutation, had a concurrent *MYD88* (L265P) mutation. Notably, 78% (7/9) of patients with secondary CNS involvement harbored an *MYD88* (L265P) mutation (Figure 1).

To further uncover the mutational landscape of PSDLBCL, we employed a 128 lymphoma-related gene panel with stringent quality criteria (Supplement “Cohort”). We successfully sequenced 43 cases, 23 ABC- and 20 GCB-subtype lymphomas. The most prevalent mutations in the ABC subtype were *MYD88* (70%), *PIM1* (61%), and *CD79B* (39%). Other mutations of interest involved the tumor suppressor genes *BTG2* and *BTG1*, with 35% and 30% of the ABC subtype harboring a mutation. Interestingly, *BTG2* mutations were primarily present in cases that relapsed or progressed: 6/8 cases of relapse or progression harbored a *BTG2* mutation (Figure 3). To contextualize the genetic composition of PSDLBCL, we explored the mutational rate of some of the most prevalent mutations and compared these to four major DLBCL cohorts.(7,8,31,37) This showed that the occurrence of mutations in the *MYD88*, *BTG1*, and *TBL1XR1* genes was significantly higher compared to rates in ABC DLBCL in general; see Figure 3 and Supplement (Cohort), Supplementary Figure 1.

To further classify PSDLBCL, we utilized the probabilistic LymphGen classifier, which groups lymphomas into genetic superfamilies based on their mutational and cytogenetic profiles. In the ABC subtype, 14 out of 23 cases (60%) were classified as MCD. Among the analyzed GCB-subtype PSDLBCLs ( $n = 20$ ), 15 were classified as “other”, while a few were categorized as EZB, ST2, or MCD. MCD class samples in the GCB subgroup were “unclassifiable” by the Lymph2Cx classifier, implying more uncertainty about their definitive COO. The classification of lymphomas by the LymphPlex algorithm was consistent with the LymphGen model. However, there were minor discrepancies, as two further ABC-subtype samples, otherwise classified as “other” by the LymphGen model, were allocated to the MCD group. The simpler “two-step” approach classified 70% (16/23) of ABC-PSDLBCL as MCD, 13% (3/23) as N1, and 4% (1/23) as EZB. The “two-step” algorithm had difficulty classifying the mutational profile of GCB-subtype PSDLBCL, similarly to the other more complex classifiers we applied. However, it classified slightly more cases as ST2 class. Furthermore, this approach classified two additional cases of GCB-subtype PSDLBCL as MCD, solely based on the presence of *PIM1* mutations without *MYD88* or *CD79B* aberrations present (Figure 3). To provide a frame of reference, we examined the rate of MCD, categorized by the LymphGen classifier, in 173 nodal ABC DLBCLs in the publicly available data from the Phoenix Phase III clinical trial by Wilson et al..(38) This revealed that 29 out of 173 cases (16%) of nodal ABC DLBCL were classified

as MCD, in contrast to the 14 out of 23 cases (60%) seen in ABC-subtype PSDLBCL ( $P < 0.001$ ).

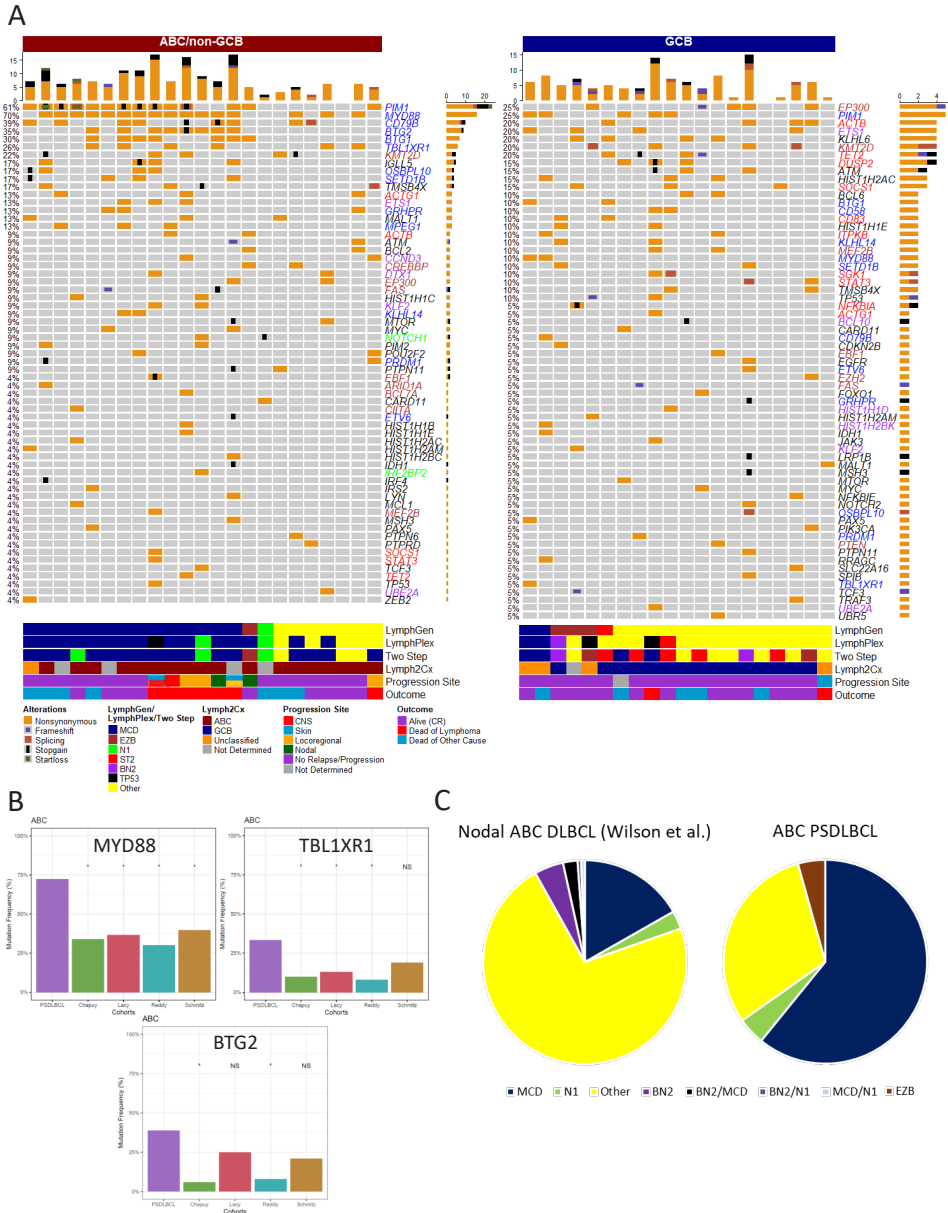


**Figure 3.** A) An oncoPrint plot of PSDLBCL eligible for sequencing ( $n=43$ , 23 ABC and 20 GCB). Each row represents a specific gene and alteration, and each column represents a case. The color of the gene name corresponds to the LymphGen class with which the gene is most associated. The category “TP53” is only applicable to the LymphPlex classification. Only truncation mutations to the PEST domain of the

NOTCH1 gene are considered to raise the probability of a sample belonging to the N1 class when using the LymphGen classifier. The top bar chart illustrates the number of mutation types per patient, while the bar chart on the right shows the number of alterations per gene. Cell-of-origin (COO) is a hierarchical composite with Lymph2Cx overriding Hans' algorithm. The outcome, progression site, and LymphGen, LymphPlex and two-step classifications are annotated at the bottom. B) A comparison of mutations with a significantly higher rate in Lymph2Cx-varified ABC-subtype PSDLCL as compared to ABC DLBCL from four extensive international cohorts.(7,8,31,37) C) Pie charts showing the distribution of LymphGen class in ABC-subtype PSDLBCL (n=23) relative to purely nodal ABC DLBCL (n=173).(38) ABC, activated B cell-like; GCB, germinal center B cell-like; \*, P<0.05.

### **Immune evasion in PSDLBCL: Frequent loss of HLA in the ABC subtype, while loss of PD-L1 expression is rare**

Immune evasion is a major hurdle for effective anticancer therapy. Tumor cells employ several strategies to evade T- and NK-cell recognition, including major histocompatibility complex (MHC) downregulation and activation of immune checkpoints (39), in particular, programmed cell death 1 (PD-1) and its ligands PD-L1 and PD-L2.(12,40,41) Both strategies are used by hematological malignancies, including B-cell lymphomas. (12,40,41) Assessment of HLA expression revealed that HLA-I loss was present in only a minority of the PSDLBCLs, and while there was a higher prevalence in ABC- than in GCB subtype lymphomas, this difference was not statistically significant: 19% (13/67) of ABC- vs. 7% (3/41) of GCB subtype (P=0.10). Noticeably, when comparing cases with and without relapse or progression among ABC-subtype lymphomas, those with relapse or progression had a 31% HLA-I loss rate (9/29), while those without had 9% (4/33) (P=0.05). Moreover, HLA-II loss was highly prevalent in ABC-subtype PSDLBCL, 48% (32/67), but much less common in GCB-subtype tumors, 9% (4/41) P<0.001 (Figure 1). In addition, we also explored the possible role of the PD-1/PD-L1 checkpoint by analyzing PD-L1 protein expression and *PD-L1/2* CNAs. Both PD-L1 expression and CNAs were rare, only evident in 2% of the PSDLBCLs (Figure 1).

## **DISCUSSION**

Our large nationwide PSDLBCL cohort allowed us to comprehensively investigate the molecular mechanisms underlying the highly variable clinical outcome of the disease.(19) We demonstrated that PSDLBCL can be stratified into two COO-defined subtypes with distinctive biological and clinical behavior: *GCB subtype* with an excellent prognosis and *ABC subtype* prone to relapse or progression, resulting in substantial disease-specific mortality despite treatment with immunochemotherapy. Most of the ABC-subtype PSDLBCL displayed MCD-class molecular features, specifically a high prevalence of *MYD88* and *CD79B* mutations, frequent *cMYC/BCL2* double expression, *BCL6* overexpression, as well as loss of HLA-I and -II. Interestingly, these molecular features are shared with lymphomas at other non-professional lymphoid sites, including

CNS, testes, and skin (leg-type), all of which are typical sites of relapse or dissemination for PSDLBCL. In addition, these locations are often the primary sites for lymphomas that relapse to the sinonasal mucosa.(18)

COO subclass strongly correlates to specific extranodal locations.(12,27,36) Our study is the first to demonstrate the prognostic value of COO subclassification for PSDLBCL. Consistent with our results, a previous study also found sinonasal tract DLBCL to comprise ABC- as well as GCB-subtype tumors, with ABC as the predominant COO; however, this study did not report survival data.(42) Our data showed that the ABC subtype represents a distinct disease entity different from GCB-subtype PSDLBCL, invariably exhibiting a much higher mortality rate both in the overall cohort as well as the subset of patients receiving immunochemotherapy. Moreover, the ABC subtype encompassed nearly all cases of relapse or progression (Figure 1). Our findings align with the substantial evidence showing that the prognosis of ABC-subtype DLBCL treated with standard immunochemotherapy is unfavorable compared to that of GCB-subtype tumors.(4,5,43–46). Furthermore, relapse or dissemination was mainly to sites strongly associated with the ABC gene expression profile, e.g., CNS and skin (leg-type). (12,47) Additionally, our study showcased the remarkable interchangeability between Hans' algorithm and Lymph2Xc for the accurate COO classification of these extranodal lymphomas.

Our mutational analysis revealed that most ABC-subtype lymphomas display MCD-class genetic features: 74% contained *MYD88* and 34% *CD79B* mutations (Figure 1); similar percentages were obtained in the subset of comprehensively sequenced patients: 70% contained *MYD88* and 39% *CD79B* mutations (Figure 3). These gain-of-function mutations enhance TLR and BCR pathway activity leading to a multiprotein supercomplex formed by *MYD88*, *TLR9*, and the BCR. The My-T-BCR supercomplex and mTOR come together in endolysosomes, where they actively promote both pro-survival NF- $\kappa$ B and mTOR signaling.(48) In addition, ABC-lymphomas showed enrichment for mutations in *PIM1* and two cell-cycle regulatory genes, *BTG1* (30%) and *BTG2* (35%).(45) *BTG2* mutation is strongly linked to the MCD class and has previously been reported to carry a poor prognosis in primary testicular lymphoma.(6,49) In line with this, we also found a high percentage of relapse or progression cases harboring this mutation. Furthermore, by placing PSDLBCL within the broader framework of DLBCL, we demonstrated that ABC PSDLBCL exhibits a distinct mutational profile compared to the ABC subtype of DLBCL as a whole. Additionally, an analysis of nodal ABC DLBCLs emphasized that ABC-subtype PSDLBCL is a distinct entity with its own mutational profile.

Particularly noteworthy is the elevated rate of *TBL1XR1* aberrations in PSDLBCL, supporting the hypothesis of an aberrant memory B-cell as a probable cell of origin for

the MCD subclass DLBCLs, as proposed by Venturutti and Melnick.(50)

Subclassification by the LymphPlex algorithm and the two-step approach replicated the high prevalence of MCD class tumors identified by the LymphGen algorithm. In fact, these alternative approaches labeled a few additional cases as MCD (Figure 3), reflecting the significance of these mutations in the alternative models. Due to the stochastic distribution of mutations in GCB-subtype PSDLBCLs, subclassification was challenging (Figure 3).

The MCD subtype provides an intriguing genetic link between PSDLBCL and other primary extranodal lymphomas, including CNS, skin (leg-type), testes, and breast, especially in conjunction with our previous findings on the site-specific relapse or progression of sinonasal DLBCL and sites relapsing to the sinonasal membrane.(19) In addition to the genetic subtype, the ABC subtype exhibited several molecular characteristics shared with the most associated sites of relapse and dissemination, including high levels of BCL2/cMYC double expression and BCL6 overexpression. Our findings suggest a superordinate family of lymphomas with shared phenotypic and genotypic attributes and a predilection for specific anatomical locations. To further substantiate this, we compared the rate of MCD to pure nodal ABC lesion found in publicly available data, showing a clear distinction to nodal disease. Our findings hold significant value for future patients with PSDLBCL as substantial strides have been made in the targeted treatment of DLBCL based on genetic subtypes. Recent studies have reported a high response rate in young patients (age < 60) with MCD DLBCLs treated with the Bruton's tyrosine kinase (BTK) inhibitor ibrutinib.(38)

6

Upon tumor expansion, cells become targets of immune surveillance by T-cells, necessitating the activation of immune evasion strategies to survive. Consistent with this scenario, the majority of primary CNS and testicular lymphomas display loss of HLA-I expression, impairing antigen presentation to cytotoxic T-cells but also subjecting themselves to surveillance of "missing self" by NK-cells.(51) However, NK-cells are somewhat restricted from entering these locations under normal physiological conditions, making tumors less exposed to NK-cell surveillance.(52) HLA-I loss was relatively uncommon in ABC-subtype PSDLBCL (19%) and even more so in GCB tumors (7%). This comparatively low frequency of HLA-I loss may result from selective pressure by NK-cells, which seem to play an important role in nasal immunity.(53) Nevertheless, our data suggest that immune surveillance by cytotoxic T-cells plays a significant role in the control of PSDLBCL, as ABC-subtype cases with HLA-I loss showed a significantly increased risk of relapse or progression.

HLA-II was lost in nearly half (48%) of the ABC subtype, whereas it was less frequent (9%) in GCB-subtype tumors. Several studies have found approximately half of all primary CNS

and testicular lymphomas to have a loss of HLA-II(12,54), yet again indicating a similarity between ABC-subtype PSDLBCL and lymphomas originating from these locations. Compared to HLA-I loss, the consequences of HLA-II loss for immune recognition are less clear-cut. However, since B-cells are professional antigen-presenting cells, impaired antigen presentation to helper- and regulatory-T cells most likely plays a central role in T-cell infiltration of tumors and may explain some of the variance in prognosis between COOs.(55,56)

In addition to HLA loss, we addressed the possible activation of the PD-1/PD-L1 immune checkpoint, which suppresses T-cell activity in the tumor microenvironment of various hematological malignancies such as Hodgkin's lymphoma and primary mediastinal B-cell lymphoma.(41) Although an initial study reported a high prevalence of PD-L1 expression and *PDL1/2* CNAs in primary CNS and testicular lymphoma (57), subsequent studies did not confirm this result; conversely finding PD-L1 expression and CNAs to be uncommon.(12,58–60) Furthermore, a phase-II clinical trial from 2021 investigating patients with relapsed or refractory primary CNS lymphoma treated with nivolumab yielded disappointing results (data not published; clinicaltrials.gov: NCT02857426). In our PSDLBCL cohort, PD-L1 expression and *PDL1/2* CNAs were rare (2%), implying that activation of this checkpoint is unlikely. These findings corroborate with literature data on the PD-1/PD-L1 checkpoint activation in MCD lymphomas at other anatomical sites and show that immune evasion in MCD lymphomas, including ABC-subtype PSDLBCL, involves HLA loss rather than activation of the PD-1/PD-L1 checkpoint.

Diffuse large B-cell lymphomas related to chronic inflammation are often EBV-associated and chronic inflammation of the sinonasal membrane is very common in the general public.(3,22) Moreover, EBV is a hallmark of extranodal NK/T cell lymphoma (nasal-type), prototypically localized in the sinonasal mucosa.(3,23) This made it relevant to test the association of EBV in PSDLBCL. In situ hybridization to EBER assessment revealed no evidence of EBV involvement in PSDLBCL, excluding EBV as a driver in PSDLBCL.

In conclusion, molecular profiling of this large nationwide cohort of PSDLBCLs allowed us to identify two separate COO-defined subtypes with distinctive tumor biology and prognosis among these rare extranodal lymphomas. Interestingly, the predominance of the MCD class in the ABC group designates these PSDLBCLs as members of an expanded family of lymphomas, characterized by presenting at “non-professional” lymphoid sites, and sharing genetic characteristics, immune-evasion strategies, oncoprotein expression, lack of translocations, and clinical features, including a typical progression pattern. The fact that PSDLBCLs have MCD features has potentially important clinical implications as it labels these lymphomas as candidates for therapies targeting BCR- and TLR-signaling.

## **AUTHORSHIP**

Contributions: *PRGE*: established cohort and extracted data, COO analyses, statistical calculations, diagrams and figures, and wrote the paper. *FdG*: performed NGS and analyzed data. *EC-L*: validated diagnoses and analyzed markers of immune evasion. *PdNB*: designed the research and provided data. *RdG*: NGS and genetic subclassification. *LCM*: analyses. *ADM*: analyses. *MM*: performed experiments. *JV*: supervision of analyses and wrote manuscript. *CvB*: designed the study, supervised. *STP*: designed the research and analysis, supervised, data analysis, interpretation of analyses, and wrote manuscript. *SH*: designed the study, supervised.

## **FUNDING**

The study was supported by the following non-profit foundations: Candys Foundation (Grant nr. 2019-333), the Fabrikant Einar Willumsens Mindelegat, the Tømrrermester Jørgen Holm og Hustru Elisa F-Hanses Mindelegat, the Arvid Nielsens Fond, and Lymph&Co.

## **DISCLOSURES**

The authors declare that the research was conducted without any commercial or financial relationships that could be construed as a potential conflict of interest.

## **ETHICS**

The study was authorized by the Scientific Ethics Committee of the Capital Region of Denmark (file no. H-16023080) and the Danish Data Protection Agency (file no. P-2020-588).

## REFERENCES

1. Ollila TA, Olszewski AJ. Extranodal diffuse large B cell lymphoma: molecular features, prognosis, and risk of central nervous system recurrence. *Curr Treat Options Oncol.* 2018;19:1–20.
2. Ollila T, Kurt H, Waroich J, Vattevich J, Sturtevant A, Patel N, m.fl. Genomic subtypes may predict the risk of central nervous system recurrence in diffuse large B-cell lymphoma. *Blood.* 2. september 2020;137.
3. Swerdlow S, Campo E, Jaffe E. WHO Classification of Tumours of Haematopoietic and Lymphoid Tissues. 4th udg. Bd. 2. Lyon: WHO; 2017.
4. Alizadeh AA, Eisen MB, Davis RE, Ma C, Lossos IS, Rosenwald A, m.fl. Distinct types of diffuse large B-cell lymphoma identified by gene expression profiling. *Nature.* 1. februar 2000;403(6769):503–11.
5. Rosenwald A, Wright G, Chan WC, Connors JM, Campo E, Fisher RI, m.fl. The Use of Molecular Profiling to Predict Survival after Chemotherapy for Diffuse Large-B-Cell Lymphoma. *N Engl J Med.* 20. juni 2002;346(25):1937–47.
6. Wright G, Huang DW (David), Phelan J, Coulibaly Z, Roulland S, Young R, m.fl. A Probabilistic Classification Tool for Genetic Subtypes of Diffuse Large B Cell Lymphoma with Therapeutic Implications. *Cancer Cell.* 1. april 2020;37:551–568.e14.
7. Chapuy B, Stewart C, Dunford AJ, Kim J, Kamburov A, Redd RA, m.fl. Molecular subtypes of diffuse large B cell lymphoma are associated with distinct pathogenic mechanisms and outcomes. *Nat Med.* 1. maj 2018;24(5):679–90.
8. Schmitz R, Wright GW, Huang DW, Johnson CA, Phelan JD, Wang JQ, m.fl. Genetics and Pathogenesis of Diffuse Large B-Cell Lymphoma. *N Engl J Med.* 12. april 2018;378(15):1396–407.
9. Cao X xin, Li J, Cai H, Zhang W, Duan M hui, Zhou D bin. Patients with primary breast and primary female genital tract diffuse large B cell lymphoma have a high frequency of MYD88 and CD79B mutations. *Ann Hematol.* 1. november 2017;96(11):1867–71.
10. Ducharme O, Beylot-Barry M, Pham-Ledard A, Bohers E, Viailly PJ, Bandres T, m.fl. Mutations of the B-Cell Receptor Pathway Confer Chemoresistance in Primary Cutaneous Diffuse Large B-Cell Lymphoma Leg Type. *J Invest Dermatol.* 1. november 2019;139(11):2334–2342.e8.
11. Mareschal S, Pham-Ledard A, Viailly PJ, Dubois S, Bertrand P, Maingonnat C, m.fl. Identification of Somatic Mutations in Primary Cutaneous Diffuse Large B-Cell Lymphoma, Leg Type by Massive Parallel Sequencing. *J Invest Dermatol.* 1. september 2017;137(9):1984–94.
12. Minderman M, Amir A, Kraan W, Schilder-Tol EJM, Oud MECM, Scheepstra CG, m.fl. Immune evasion in primary testicular and central nervous system lymphomas: HLA loss rather than 9p24.1/PD-L1/PD-L2 alterations. *Blood.* 30. september 2021;138(13):1194–7.
13. Kraan W, Horlings HM, van Keimpema M, Schilder-Tol EJM, Oud MECM, Scheepstra C, m.fl. High prevalence of oncogenic MYD88 and CD79B mutations in diffuse large B-cell lymphomas presenting at immune-privileged sites. *Blood Cancer J.* 1. september 2013;3(9):e139–e139.
14. Yonese I, Takase H, Yoshimori M, Onozawa E, Tsuzura A, Miki T, m.fl. CD79B mutations in primary vitreoretinal lymphoma: Diagnostic and prognostic potential. *Eur J Haematol.* 1. februar 2019;102(2):191–6.
15. Kraan W, van Keimpema M, Horlings HM, Schilder-Tol EJM, Oud MECM, Noorduyin LA, m.fl. High prevalence of oncogenic MYD88 and CD79B mutations in primary testicular diffuse large B-cell lymphoma. *Leukemia.* 1. marts 2014;28(3):719–20.
16. Kridel R, Telio D, Villa D, Sehn L, Gerrie A, Shenkier T, m.fl. Diffuse large B-cell lymphoma with testicular involvement: Outcome and risk of CNS relapse in the rituximab era. *Br J Haematol.* 1. oktober 2016;176.
17. Hosein PJ, Maragulia JC, Salzberg MP, Press OW, Habermann TM, Vose JM, m.fl. A multicentre study of primary breast diffuse large B-cell lymphoma in the rituximab era. *Br J Haematol.* 1. maj 2014;165(3):358–63.
18. Yhim HY, Kang HJ, Choi YH, Kim SJ, Kim WS, Chae YS, m.fl. Clinical outcomes and prognostic factors in patients with breast diffuse large B cell lymphoma; Consortium for Improving Survival of Lymphoma (CISL) study. *BMC Cancer.* 22. juni 2010;10(1):321.
19. Eriksen PRG, Clasen-Linde E, Nully Brown P de, Haunstrup L, Christoffersen M, Asdahl P, m.fl. Sinonasal B-cell lymphomas: A nationwide cohort study, with an emphasis on the prognosis and the recurrence pattern of primary diffuse large B-cell lymphoma. *Hematol Oncol.* 1. april 2022;40(2):160–71.
20. Ali M. Histology of the human nasopharyngeal mucosa. *J Anat.* 1965;99(Pt 3):657.
21. Sjöstedt S, Schmidt AY, Vieira FG, Willemoie GL, Agander TK, Olsen C, m.fl. Major driver mutations are shared between sinonasal intestinal-type adenocarcinoma and the morphologically identical colorectal adenocarcinoma. *J Cancer Res Clin Oncol.* 2021;147:1019–27.
22. Fokkens W, Lund V, Hopkins C, Hellings PW, Kern R, Reitsma S, m.fl. European Position Paper on Rhinosinusitis and Nasal Polyps 2020. *Rhinol J.* 1. februar 2020;58:1–464.
23. Eriksen PRG, Clasen-Linde E, Brown P de N, Haunstrup L, Christoffersen M, Asdahl P, m.fl. NK- and T-cell lymphoma of the nasal cavity and paranasal sinuses in Denmark 1980–2017: a nationwide cohort study. *Leuk Lymphoma.* 14. juni 2022;1–10.

24. Alexiou C, Kau RJ, Dietzfelbinger H, Kremer M, Spieß JC, Schratzenstaller B, m.fl. Extramedullary plasmacytoma. *Cancer*. 1. juni 1999;85(11):2305–14.
25. Hans CP, Weisenburger DD, Greiner TC, Gascoyne RD, Delabie J, Ott G, m.fl. Confirmation of the molecular classification of diffuse large B-cell lymphoma by immunohistochemistry using a tissue microarray. *Blood*. 1. januar 2004;103(1):275–82.
26. Scott DW, Wright GW, Williams PM, Lih CJ, Walsh W, Jaffe ES, m.fl. Determining cell-of-origin subtypes of diffuse large B-cell lymphoma using gene expression in formalin-fixed paraffin-embedded tissue. *Blood*. 20. februar 2014;123(8):1214–7.
27. Groen R, Eijk R, Böhringer S, van Wezel T, Raghoo R, Ruano D, m.fl. Frequent mutated B2M , EZH2 , IRF8 , and TNFRSF14 in primary bone diffuse large B-cell lymphoma reflect a GCB phenotype. *Blood Adv*. 3. september 2021;5.
28. Groot F, Haan L, Groen R, Heijmen L, van Wezel T, Eijk R, m.fl. Synchronous diffuse large B-cell lymphoma and mantle cell lymphoma: support for low-threshold biopsies and genetic testing. *Leuk Lymphoma*. 21. december 2021;1–5.
29. Shen R, Fu D, Dong L, Zhang MC, Shi Q, Shi ZY, m.fl. Simplified algorithm for genetic subtyping in diffuse large B-cell lymphoma. *Signal Transduct Target Ther*. 10. april 2023;8(1):145.
30. Pedrosa L, Fernández-Miranda I, Pérez-Callejo D, Quero C, Rodríguez M, Martín-Acosta P, m.fl. Proposal and validation of a method to classify genetic subtypes of diffuse large B cell lymphoma. *Sci Rep*. 2021;11(1):1–14.
31. Lacy SE, Barrans SL, Beer PA, Painter D, Smith AG, Roman E, m.fl. Targeted sequencing in DLBCL, molecular subtypes, and outcomes: a Haematological Malignancy Research Network report. *Blood*. 14. maj 2020;135(20):1759–71.
32. Savage KJ, Slack GW, Mottok A, Sehn LH, Villa D, Kansara R, m.fl. Impact of dual expression of MYC and BCL2 by immunohistochemistry on the risk of CNS relapse in DLBCL. *Blood J Am Soc Hematol*. 2016;127(18):2182–8.
33. Lucioni M, Pescia C, Bonometti A, Fraticelli S, Moltrasio C, Ramponi A, m.fl. Double expressor and double/triple hit status among primary cutaneous diffuse large B-cell lymphoma: a comparison between leg type and not otherwise specified subtypes. *Hum Pathol*. 1. maj 2021;111:1–9.
34. Chen Y, Chen H, Chen L, Zheng X, Yang X, Zheng Z, m.fl. Immunohistochemical overexpression of BCL-2 protein predicts an inferior survival in patients with primary central nervous system diffuse large B-cell lymphoma. *Medicine (Baltimore)*. 1. november 2019;98:e17827.
35. Brunn A, Nagel I, Montesinos-Rongen M, Klapper W, Vater I, Paulus W, m.fl. Frequent triple-hit expression of MYC, BCL2, and BCL6 in primary lymphoma of the central nervous system and absence of a favorable MYC<sup>low</sup>BCL2<sup>low</sup> subgroup may underlie the inferior prognosis as compared to systemic diffuse large B cell lymphomas. *Acta Neuropathol (Berl)*. 1. oktober 2013;126(4):603–5.
36. Schrader A, Jansen P, Vermeer M, Kleiverda J, Vermaat J, Willemze R. High Incidence and Clinical Significance of MYC Rearrangements in Primary Cutaneous Diffuse Large B-Cell Lymphoma, Leg Type. *Am J Surg Pathol*. 1. august 2018;42:1.
37. Reddy A, Zhang J, Davis NS, Moffitt AB, Love CL, Waldrop A, m.fl. Genetic and functional drivers of diffuse large B cell lymphoma. *Cell*. 2017;171(2):481–94.
38. Wilson WH, Wright GW, Hodgkinson B, Balasubramanian S, Fan Y, Vermeulen J, m.fl. Effect of ibrutinib with R-CHOP chemotherapy in genetic subtypes of DLBCL. *Cancer Cell*. 2021;39(12):1643–53.
39. Marie de Charette, Roch Houot. Hide or defend, the two strategies of lymphoma immune evasion: potential implications for immunotherapy. *Haematologica*. 1. august 2018;103(8):1256–68.
40. Steidl C, Gascoyne RD. The molecular pathogenesis of primary mediastinal large B-cell lymphoma. *Blood*. 8. september 2011;118(10):2659–69.
41. Green MR, Monti S, Rodig SJ, Juszczynski P, Currie T, O'Donnell E, m.fl. Integrative analysis reveals selective 9p24. 1 amplification, increased PD-1 ligand expression, and further induction via JAK2 in nodular sclerosing Hodgkin lymphoma and primary mediastinal large B-cell lymphoma. *Blood J Am Soc Hematol*. 2010;116(17):3268–77.
42. Vähämurto P, Mannisto S, Pollari M, Karjalainen-Lindsberg ML, Mäkitie AA, Leppä S. Clinical features and outcome of the patients with sinonasal tract diffuse large B-cell lymphoma in the pre-rituximab and rituximab eras. *Eur J Haematol*. 1. juni 2019;102(6):457–64.
43. Gutiérrez-García G, Cardesa-Salzmann T, Climent F, González-Barca E, Mercadal S, Mate JL, m.fl. Gene-expression profiling and not immunophenotypic algorithms predicts prognosis in patients with diffuse large B-cell lymphoma treated with immunochemotherapy. *Blood J Am Soc Hematol*. 2011;117(18):4836–43.
44. Scott DW, Mottok A, Ennishi D, Wright GW, Farinha P, Ben-Neriah S, m.fl. Prognostic Significance of Diffuse Large B-Cell Lymphoma Cell of Origin Determined by Digital Gene Expression in Formalin-Fixed Paraffin-Embedded Tissue Biopsies. *J Clin Oncol*. 10. september 2015;33(26):2848–56.
45. Lenz G, Wright G, Dave SS, Xiao W, Powell J, Zhao H, m.fl. Stromal Gene Signatures in Large-B-Cell Lymphomas. *N Engl J Med*. 27. november 2008;359(22):2313–23.
46. Xu-Monette ZY, Zhang H, Zhu F, Tzankov A, Bhagat G, Visco C, m.fl. A refined cell-of-origin classifier

- with targeted NGS and artificial intelligence shows robust predictive value in DLBCL. *Blood Adv.* 28. juli 2020;4(14):3391–404.
47. Schrader AMR, de Groen RAL, Willemze R, Jansen PM, Quint KD, Cleven AHG, m.fl. Genetic Stability of Driver Alterations in Primary Cutaneous Diffuse Large B-Cell Lymphoma, Leg Type and Their Relapses: A Rationale for the Use of Molecular-Based Methods for More Effective Disease Monitoring. *Cancers.* 2022;14(20).
  48. Phelan JD, Young RM, Webster DE, Roulland S, Wright GW, Kasbekar M, m.fl. A multiprotein supercomplex controlling oncogenic signalling in lymphoma. *Nature.* 1. august 2018;560(7718):387–91.
  49. Guo D, Hong L, Ji H, Jiang Y, Lu L, Wang X, m.fl. The mutation of BTG2 gene predicts a poor outcome in primary testicular diffuse large B-cell lymphoma. *J Inflamm Res.* 2022;1757–69.
  50. Venturutti L, Melnick AM. The dangers of déjà vu: memory B cells as the cells of origin of ABC-DLBCLs. *Blood.* 12. november 2020;136(20):2263–74.
  51. Orr M, Lanier L. Natural Killer Cell Education and Tolerance. *Cell.* 17. september 2010;142:847–56.
  52. Shi FD, Ransohoff RM. Nature killer cells in the central nervous system. I: Natural Killer Cells. Elsevier; 2010. s. 373–83.
  53. Horvath KM, Herbst M, Zhou H, Zhang H, Noah TL, Jaspers I. Nasal lavage natural killer cell function is suppressed in smokers after live attenuated influenza virus. *Respir Res.* 1. december 2011;12(1):102.
  54. Riemersma SA, Jordanova ES, Schop RFJ, Filippo K, Looijenga LHJ, Schuurung E, m.fl. Extensive genetic alterations of the HLA region, including homozygous deletions of HLA class II genes in B-cell lymphomas arising in immune-privileged sites. *Blood.* 15. november 2000;96(10):3569–77.
  55. Rimsza LM, Roberts RA, Miller TP, Unger JM, LeBlanc M, Braziel RM, m.fl. Loss of MHC class II gene and protein expression in diffuse large B-cell lymphoma is related to decreased tumor immunosurveillance and poor patient survival regardless of other prognostic factors: a follow-up study from the Leukemia and Lymphoma Molecular Profiling Project. *Blood.* 1. juni 2004;103(11):4251–8.
  56. Ennishi D, Takata K, Béguelin W, Duns G, Mottok A, Farinha P, m.fl. Molecular and Genetic Characterization of MHC Deficiency Identifies EZH2 as Therapeutic Target for Enhancing Immune Recognition. *Cancer Discov.* 1. april 2019;9(4):546–63.
  57. Chapuy B, Roemer MGM, Stewart C, Tan Y, Abo RP, Zhang L, m.fl. Targetable genetic features of primary testicular and primary central nervous system lymphomas. *Blood.* 18. februar 2016;127(7):869–81.
  58. Berghoff AS, Ricken G, Widhalm G, Rajky O, Hainfellner JA, Birner P, m.fl. PD1 (CD279) and PD-L1 (CD274, B7H1) expression in primary central nervous system lymphomas (PCNSL). *Clin Neuropathol.* 2014;33(1):42–9.
  59. Furuse M, Kuwabara H, Ikeda N, Hattori Y, Ichikawa T, Kagawa N, m.fl. PD-L1 and PD-L2 expression in the tumor microenvironment including peritumoral tissue in primary central nervous system lymphoma. *Bmc Cancer.* 2020;20(1):1–12.
  60. Hayano A, Komohara Y, Takashima Y, Takeya H, Homma J, Fukai J, m.fl. Programmed cell death ligand 1 expression in primary central nervous system lymphomas: a clinicopathological study. *Anticancer Res.* 2017;37(10):5655–66.

# SUPPLEMENT “COHORT”

## Cohort information

The original study cohort, comprising 116 patients, has previously been described. (1) The current analyses involved 117 patients since one patient with probable post-transplant lymphoproliferative disease (EBV-positive) was excluded, and two patients, upon written consent, were included after the initial cohort's last follow-up.

**Supplementary Table 1. Patient characteristics by Ann Arbor stage at diagnosis**

	Stage IIE (N=14)	Stage I (N=98)	Total (N=112)	P-value
<b>Age</b>				
Mean (SD)	74.1 (10.1)	72.3 (11.9)	72.6 (11.7)	0.607
Median [Min, Max]	76.5 [58.0, 89.0]	74.5 [36.0, 100]	75.0 [36.0, 100]	
<b>Sex</b>				
Female	3 (21.4%)	43 (43.9%)	46 (41.1%)	0.149
Male	11 (78.6%)	55 (56.1%)	66 (58.9%)	
<b>Performance Status</b>				
≤ 1	10 (71.4%)	92 (93.9%)	102 (91.1%)	0.0212
>1	4 (28.6%)	6 (6.1%)	10 (8.9%)	
<b>Composite COO</b>				
ABC/non-GCB	10 (71.4%)	58 (59.2%)	68 (60.7%)	0.56
GCB	4 (28.6%)	40 (40.8%)	44 (39.3%)	
<b>CD79B (Y196*) Mutation</b>				
Mutated	2 (14.3%)	16 (16.3%)	18 (16.1%)	1
Wildtype	7 (50.0%)	49 (50.0%)	56 (50.0%)	
<b>MYD88 (L265P) Mutation</b>				
Mutated	5 (35.7%)	32 (32.7%)	37 (33.0%)	1
Wildtype	4 (28.6%)	33 (33.7%)	37 (33.0%)	
<b>Double Expressor</b>				
Yes	7 (50.0%)	53 (54.1%)	60 (53.6%)	0.783
No	7 (50.0%)	45 (45.9%)	52 (46.4%)	
<b>HLA I loss</b>				
Yes	4 (28.6%)	12 (12.2%)	16 (14.3%)	0.1
No	9 (64.3%)	83 (84.7%)	92 (82.1%)	
<b>HLA II loss</b>				
Yes	5 (35.7%)	31 (31.6%)	36 (32.1%)	0.757
No	8 (57.1%)	64 (65.3%)	72 (64.3%)	

Composite COO subclassifies samples to ABC or GCB, where LymphC2X results outweigh COO subgrouping by Hans' algorithm. Double expressor is a sample both positive for cMYC and BCL2 on immunohistochemistry. HLA, Human leucocyte antigen.

**Supplementary Table 2. Treatment stratified by relapse/dissemination for ABC-subtype primary sinonasal diffuse large B-cell lymphoma**

	Complete Response (N=34)	Relapse/Dissemination (N=29)	P-value	Total (N=63)
<b>Age</b>				
Mean (SD)	73.7 (11.5)	71.8 (9.52)	0.473	72.8 (10.6)
Median [Min, Max]	77.5 [45.0, 89.0]	74.0 [51.0, 90.0]		76.0 [45.0, 90.0]
<b>Sex</b>				
Female	17 (50.0%)	8 (27.6%)	0.0787	25 (39.7%)
Male	17 (50.0%)	21 (72.4%)		38 (60.3%)
<b>Regional Lymph Node involvement</b>				
Yes	4 (11.8%)	5 (17.2%)	0.721	9 (14.3%)
No	30 (88.2%)	24 (82.8%)		54 (85.7%)
<b>PS</b>				
≤ 1	32 (94.1%)	27 (93.1%)	1	59 (93.7%)
>1	2 (5.9%)	2 (6.9%)		4 (6.3%)
<b>Chemotherapy</b>				
Yes	28 (82.4%)	25 (86.2%)	0.741	53 (84.1%)
No	6 (17.6%)	4 (13.8%)		10 (15.9%)
<b>Rituximab</b>				
Yes	18 (52.9%)	11 (37.9%)	0.312	29 (46.0%)
No	16 (47.1%)	18 (62.1%)		34 (54.0%)
<b>CNS Prophylaxis</b>				
Yes	13 (38.2%)	7 (24.1%)	0.284	20 (31.7%)
No	21 (61.8%)	22 (75.9%)		43 (68.3%)
<b>Consolidative Radiotherapy</b>				
Yes	20 (58.8%)	22 (75.9%)	0.187	42 (66.7%)
No	14 (41.2%)	7 (24.1%)		21 (33.3%)

Table includes 63 patients with activated B cell-like (ABC) PSDLBCL; the entire subclassified consists of 68 patients, but five were not included for analysis as they did not have information on progression. PS, performance status; CNS, central nervous system

Supplementary Table 3. Specific chemotherapy regimens and year of diagnosis by COO

	ABC/non-GCB (N=68)	GCB (N=44)	Total (N=112)	P-value
<b>Chemotherapy</b>				
Yes	54 (79.4%)	36 (81.8%)	90 (80.4%)	1
No	10 (14.7%)	6 (13.6%)	16 (14.3%)	
<b>Chemotherapy Regimen</b>				
CEOP	2 (2.9%)	1 (2.3%)	3 (2.7%)	0.648
CHOEP	2 (2.9%)	1 (2.3%)	3 (2.7%)	
CHOP	42 (61.8%)	32 (72.7%)	74 (66.1%)	
CNOP	4 (5.9%)	2 (4.5%)	6 (5.4%)	
COP	4 (5.9%)	0 (0%)	4 (3.6%)	
CVP	1 (1.5%)	0 (0%)	1 (0.9%)	
Other	1 (1.5%)	2 (4.5%)	3 (2.7%)	
<b>Year of Diagnosis</b>				
1989 — 1989	5 (7.4%)	2 (4.5%)	7 (6.3%)	0.214
1990 — 1999	18 (26.5%)	6 (13.6%)	24 (21.4%)	
2000 — 2009	25 (36.8%)	20 (45.5%)	45 (40.2%)	
2010 — 2019	20 (29.4%)	14 (31.8%)	34 (30.4%)	
2020 —	0 (0%)	2 (4.5%)	2 (1.8%)	

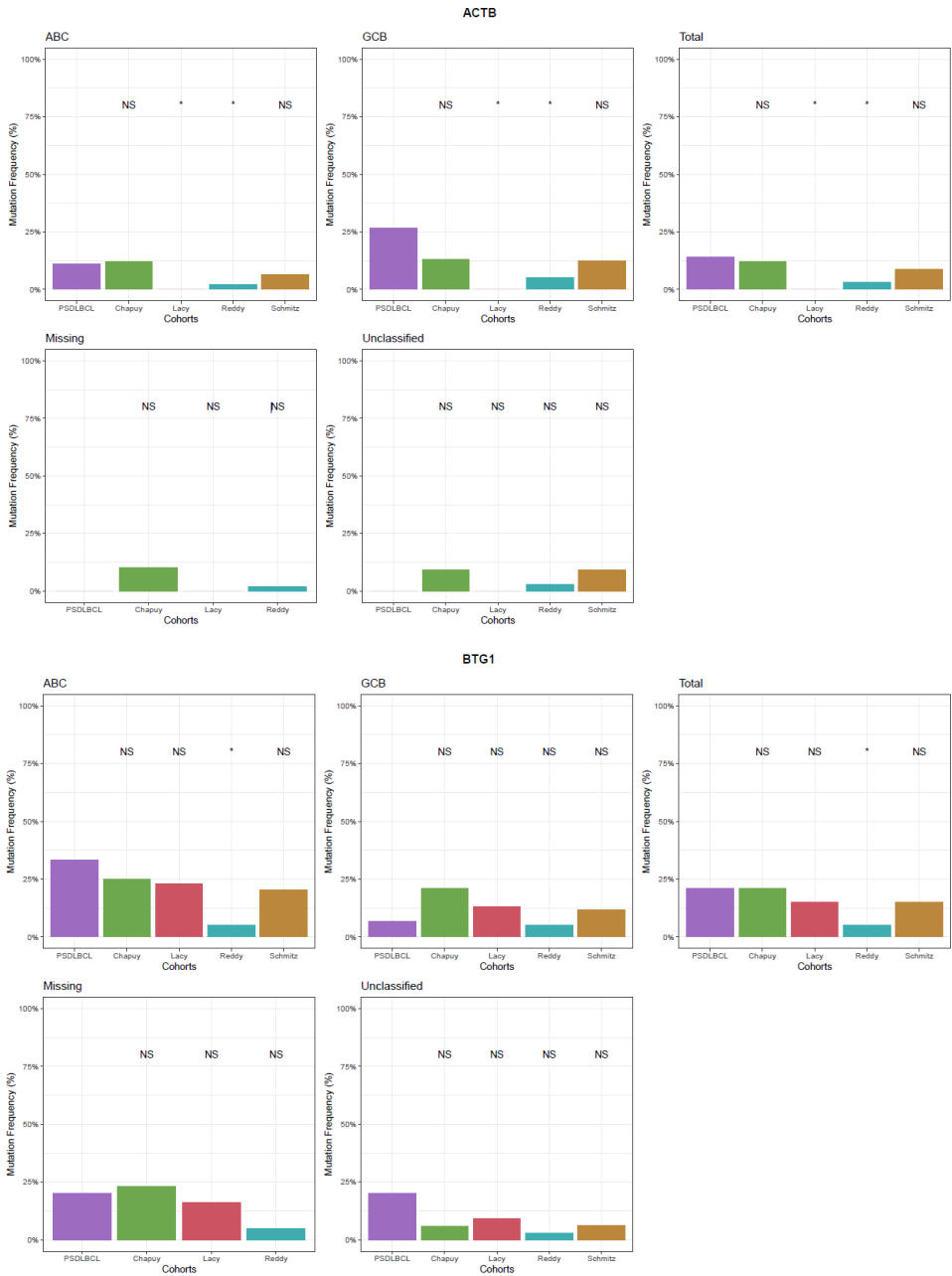
None of the patients received surgery as a treatment modality. CHOP: cyclophosphamide, hydroxydaunomycin (doxorubicin), Oncovin® (vincristine), and prednisolone. CHOEP: CHOP + etoposide. CVP/COP: cyclophosphamide, Oncovin®/vincristine, and prednisolone. CNOP: CVP/COP + mitoxantrone (Novantrone). ABMT: autologous bone marrow transplant. Other regimens included MIME (methyl-gag, ifosfamide, methotrexate, and etoposide), DHAP (dexamethasone, high-dose Ara-C, and cisplatin [Platinol®]); ICE (ifosfamide, carboplatin, and etoposide); and VIM (ifosfamide, mitoxantrone, and etoposide).

Supplementary Table 4. Cox proportional hazard model for the overall survival of the entire cohort.

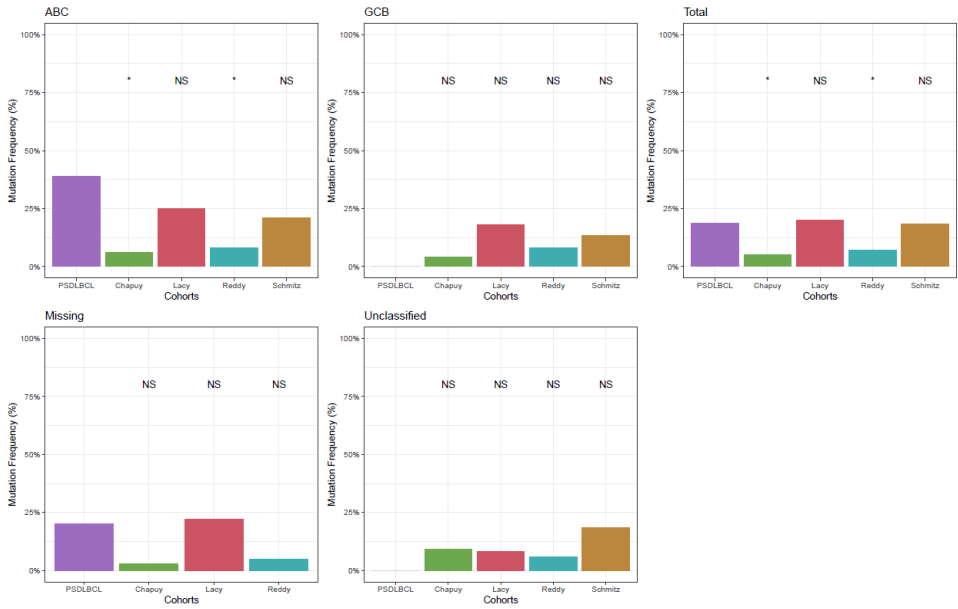
Overall survival		HR (univariate)	HR (multivariate)	PH
<b>COO</b>				
	GCB	0.52 (0.30-0.92, P=0.024)	0.55 (0.31-0.98, P=0.043)	.32
<b>Sex</b>				
	Female	0.76 (0.45-1.29, P=0.308)	0.53 (0.31-0.94, P=0.029)	.86
<b>Age (year)</b>				
	+1	1.08 (1.05-1.11, P<0.001)	1.08 (1.04-1.11, P<0.001)	.27
<b>Year of Diagnosis</b>				
	>1999	0.68 (0.40-1.16, P=0.155)	1.19 (0.61-2.33, P=0.603)	.94
<b>Rituximab</b>				
	Received	0.40 (0.23-0.70, P=0.001)	0.42 (0.21-0.84, P=0.014)	.06

COO, Cell-of-Origin; HR, Hazard Ratio; ABC, Activated B-cell like; GCB, Germinal B-cell like; PH, the p-value for proportional hazards using Schoenfeld residuals. Global p-value 0.21The regression shows the year of diagnosis does not affect the overall survival when adjusted for cell-of-origin, sex, age at diagnosis, and rituximab treatment. See the distribution of year of diagnosis by COO in Supplementary Table 2.

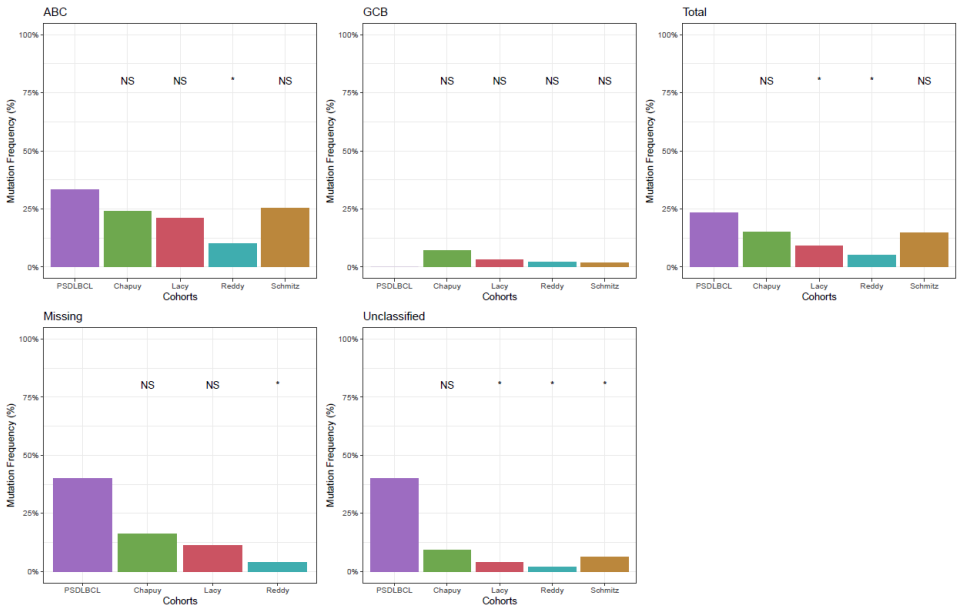
Supplementary Figure 1. Gene mutation rate by cell-of-origin (NanoString) compared to extensive international cohorts.



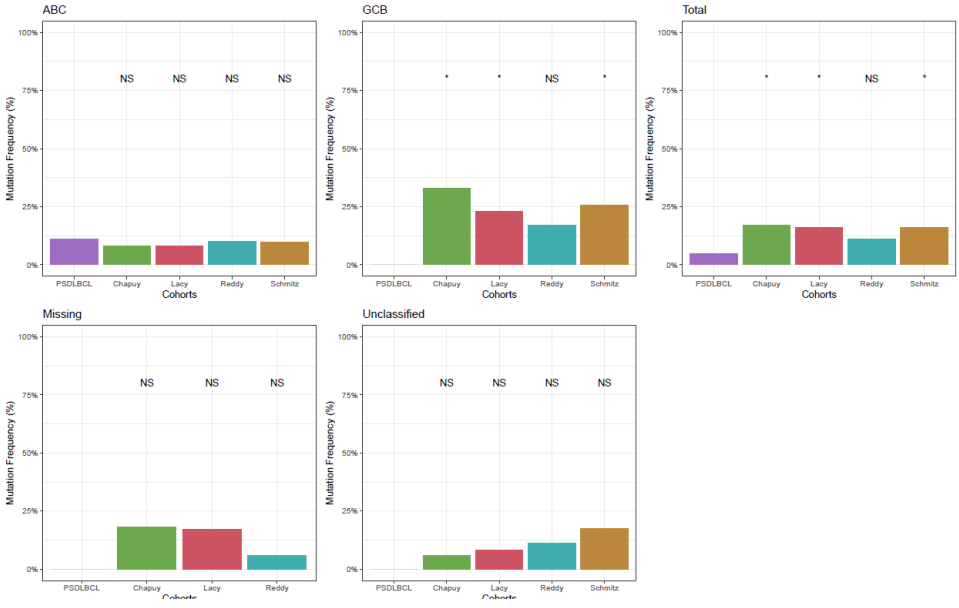
**BTG2**



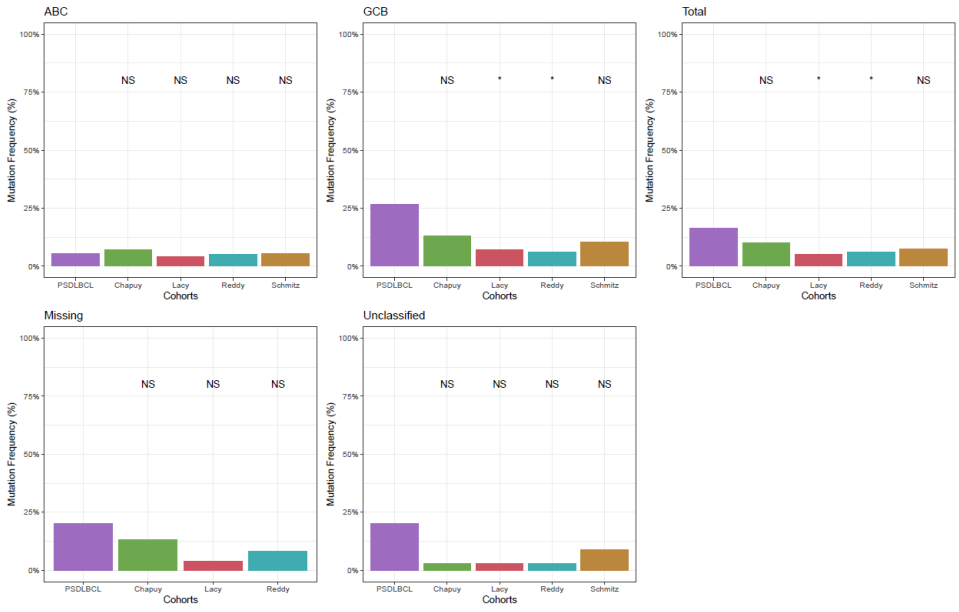
**CD79B**



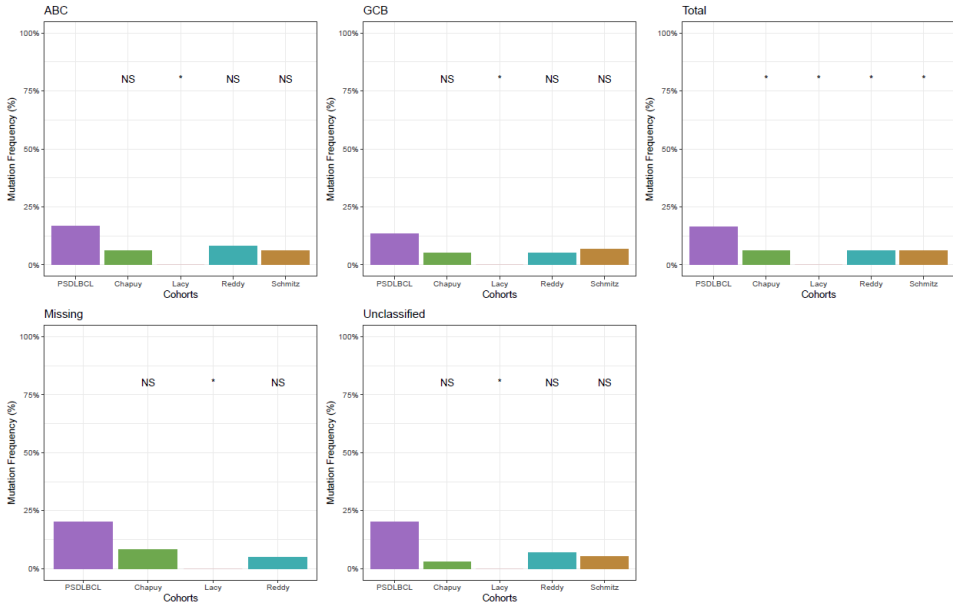
CREBBP



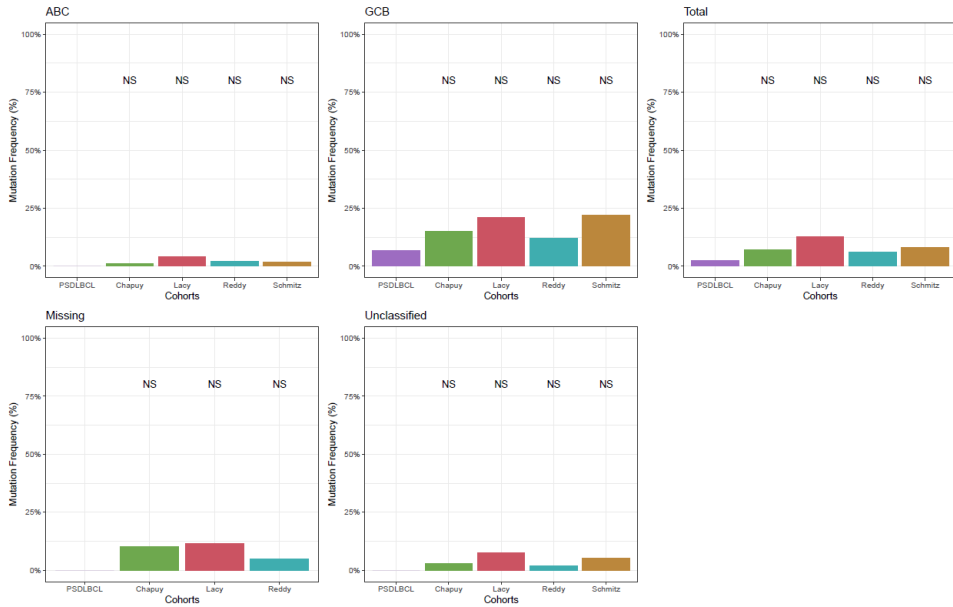
EP300



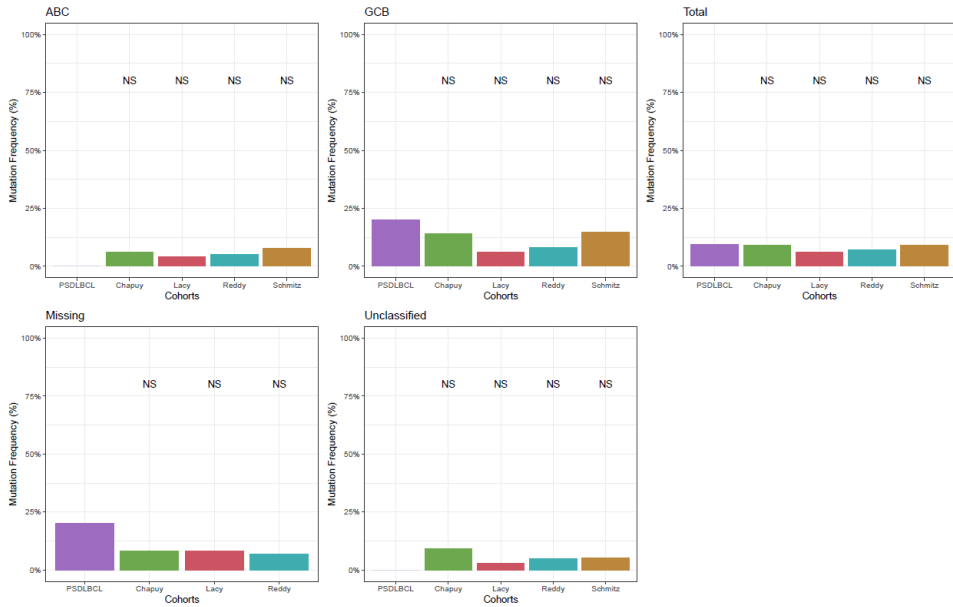
ETS1



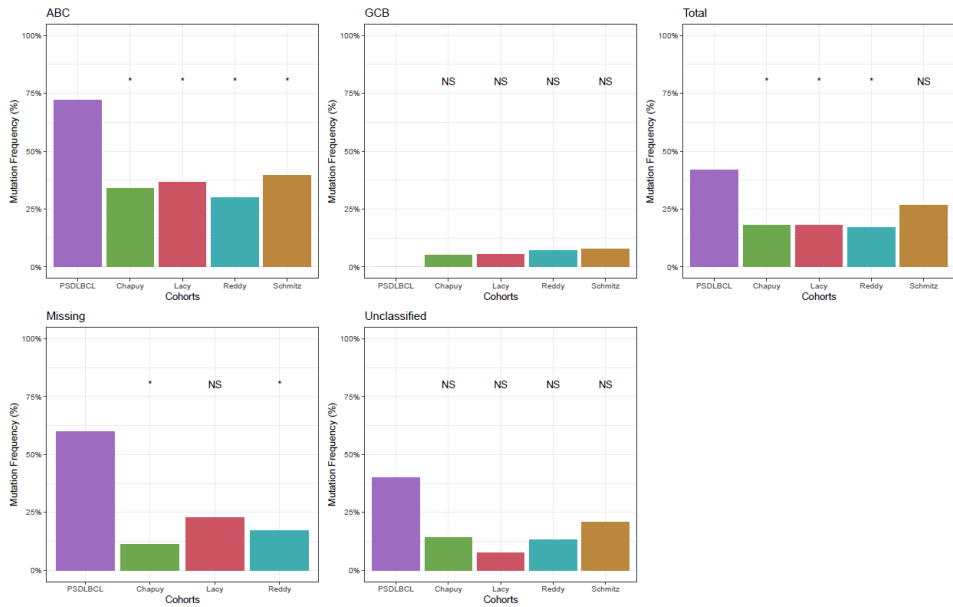
EZH2



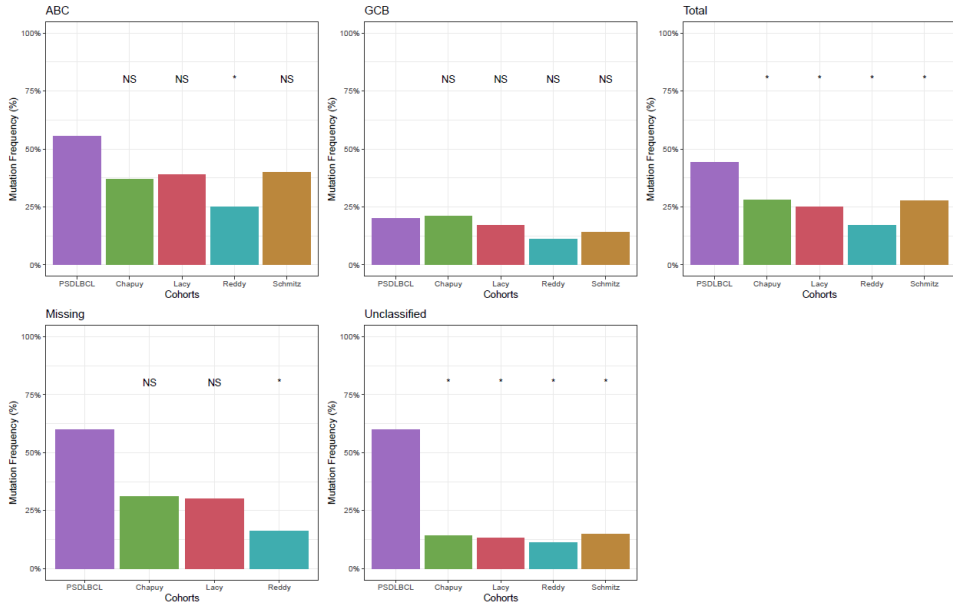
KLHL6



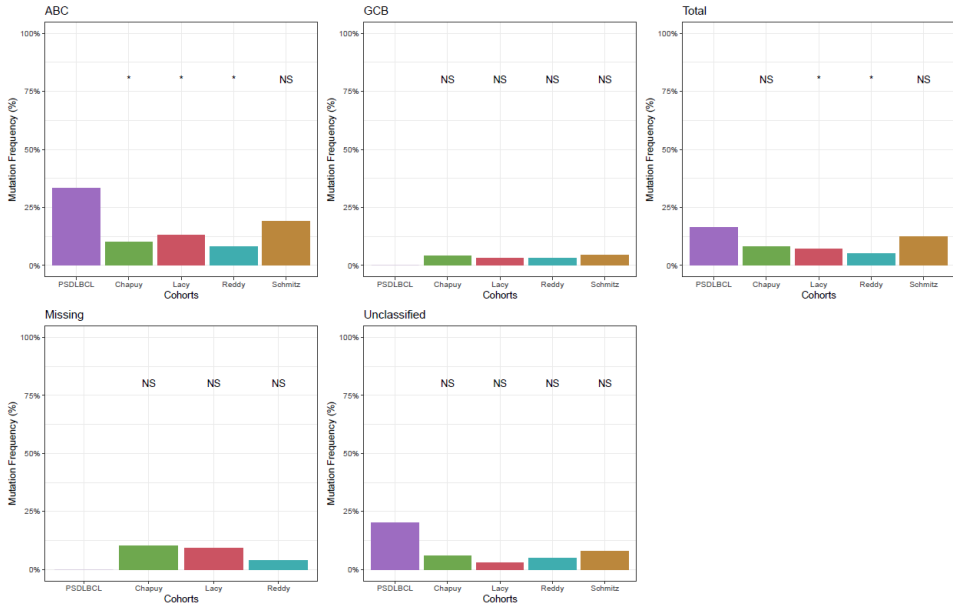
MYD88

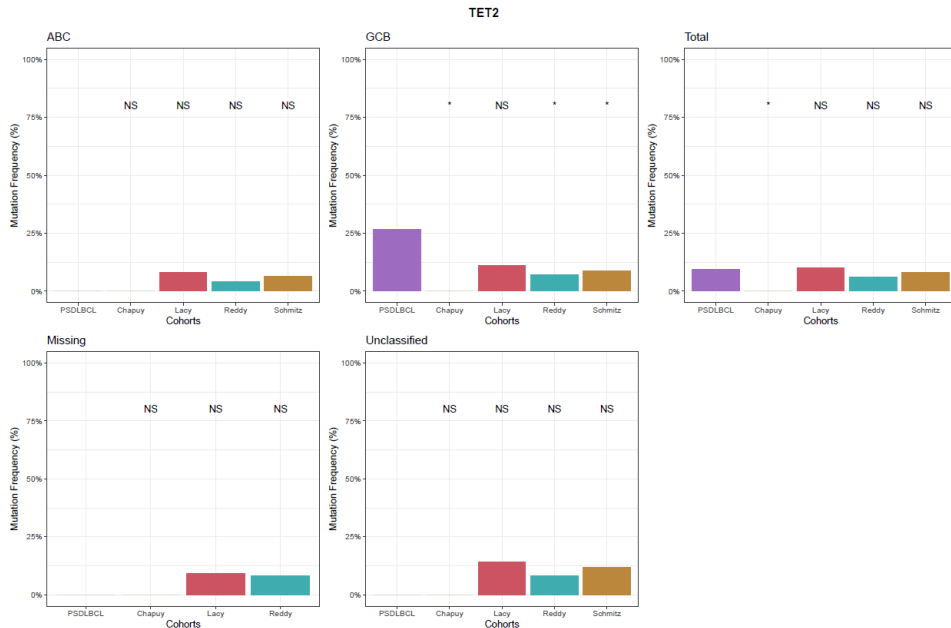


PIM1



TBL1XR1





**Supplementary Figure 1.** ABC, Activated B-cell-like; GCB, Germinal Center B-cell-like; NS, non-significant; \* P<0.05.

## SUPPLEMENT “METHODS”

### Stains used to validate primary sinonasal diffuse large B-cell lymphoma

The following panel of antibodies was used for validation: anti-CD3 (poly, DAKO), CD5 (4C7, Agilent), CD10 (SP67, DAKO), CD20 (L26, DAKO), CD23 (DAK-CD23, DAKO), CD30 (Ber-H2, Agilent), CD79a (JCB117, Agilent), cyclinD1 (EP12, DAKO), PAX5 (DAK-PAX2, DAKO), cMYC (EP121, DAKO), BCL2 (124, Agilent), BCL6 (PG-B6p, DAKO), and MUM-1 (MUM1p, DAKO).

### Fluorescent In Situ Hybridization (FISH)

We performed rearrangement analysis following the manufacturer’s protocol using the HYBrite platform (Abbott Molecular). After hybridization, nuclei were counterstained with DAPI II (ZytoVision). One hundred nuclei were counted for each sample, with a positive threshold of 10%. We only included nuclei if the entire nuclear membrane was visible in the counting process. For PD-L1 analysis the ZytoLight® SPEC CD274,PCDC1LG2/CEN 9 Dual Color Probe was employed. Forty CD20-varified cells were counted, and the ratio of PD-L1(CD274)/PD-L2(PCDC1LG2) signals and CEN9 was calculated as a mean.

### RNA extraction

Micro-dissection of the paraffin-embedded tumor was performed using hematoxylin-eosin and CD20 stained slides, 10 µm thick slides were cut from formalin-fixed paraffin-embedded (FFPE) tumor blocks, and RNA was extracted. The extraction was performed using the High Pure FFPE RNA Isolation kit (Roche, Austria) according to the manufacturer's instructions. We evaluated the length of RNA transcripts (DV200, % of fragments >200 nucleotides long), RIN (RNA integrity number), and concentration using the Bioanalyzer 2100 System (Agilent Technologies, Santa Clara, USA). A second concentration measurement was performed with Invitrogen Qubit Fluorometer (ThermoFisher Scientific, Massachusetts, USA), and the final RNA input was calculated as a mean of the two measurements. Purity was measured with the Nanodrop Spectrophotometer (ThermoFisher Scientific).

### DNA extraction

DNA was isolated from FFPE material using an in-house raw extraction method (Proteinase K and Tris EDTA) and quantified using the Qubit 2.0 Fluorometer High Sensitivity kit (Thermo Fisher Scientific, Waltham, MA, USA).

### Cell-of-origin (NanoString)

RNA transcripts were subtyped using the NanoString Lymph2Cx Panel including 15 target genes and 5 housekeeping genes. Low DV200 was compensated by increasing total RNA input (calculated as  $100 \text{ ng} \times (100 / \text{DV200})$ ); the total RNA input ranges from 150-350 ng following the NanoString Inc. manual MAN-10050-05. RNA was hybridized with reporter probes and capture probes from the nCounter CodeSet gene expression assay for 18 hours at 65°C (NanoString Inc. MAN 10056-05). Excess capture and reporter probes were removed using the NanoString Prep Station, and target-probe complexes were immobilized on cartridges for imaging on the nCounter Digital Analyzer.

The software package nSolver 4.0 was used to assess the technical success of the analysis. The dataset was analyzed using the research use only (RUO) version of the NanoString Lymphoma Subtyping Test (LST), which is based on the Lymph2Cx assay, to determine the COO molecular subtype of each sample (<https://llmpp.nih.gov/LYMPHCX/>).<sup>(1)</sup> If there were insufficient tissue for GEP, the probabilistic model could not classify the sample into any subtype with more than 90% certainty ("unclassified"), or the sample did not pass quality control, the Hans' algorithm would surrogate for gene expression profiling.

Technical success of the experiment was assessed by an overall quality control (QC) check and by the hybridization effectiveness. Zero flags were present in the QC and none were rerun.

Variability on a run-to-run basis was normalized by eight negative and six positive probes included in the CodeSet. Sample-sample variability was normalized using five housekeeping genes included in the CodeSet.

### **Next-generation sequencing**

All libraries were manually prepared following manufacturer procedures. For PCR, 4  $\mu\text{L}$  of 4 ng/ $\mu\text{L}$  sample DNA was mixed with 2  $\mu\text{L}$  of 5x Ion AmpliSeq HiFi Mix (Ion AmpliSeq™ Library Kit 2.0; ThermoFisher Scientific 4480441) and 5  $\mu\text{L}$  of 2x BLYMFv2 Ion AmpliSeq primer pool (ThermoFisher Scientific; WG\_IAD150606\_v2). Amplification was performed with a Bio-Rad C1000 Thermal Cycler with the following steps: 99 °C for 2 minutes, 18 cycles of 99 °C for 15 seconds, and 60 °C for 16 minutes.

After the PCR procedure, both pools were combined and primers were digested by adding 1  $\mu\text{L}$  of FuPa reagent (Ion AmpliSeq™ Library Kit 2.0) diluted with 1  $\mu\text{L}$  of water and heated in the Thermal Cycler at 50 °C for 10 minutes, 55 °C for 10 minutes, and 60 °C for 20 minutes. After the primer-digestion, samples were barcoded by adding 2  $\mu\text{L}$  of the barcode primers (Ion AmpliSeq™ Library Kit 2.0), 4  $\mu\text{L}$  of switch solution (Ion AmpliSeq™ Library Kit 2.0) and 2  $\mu\text{L}$  of DNA ligase (Ion AmpliSeq™ Library Kit 2.0) and heated at 22 °C for 60 minutes and 72 °C for 10 minutes.

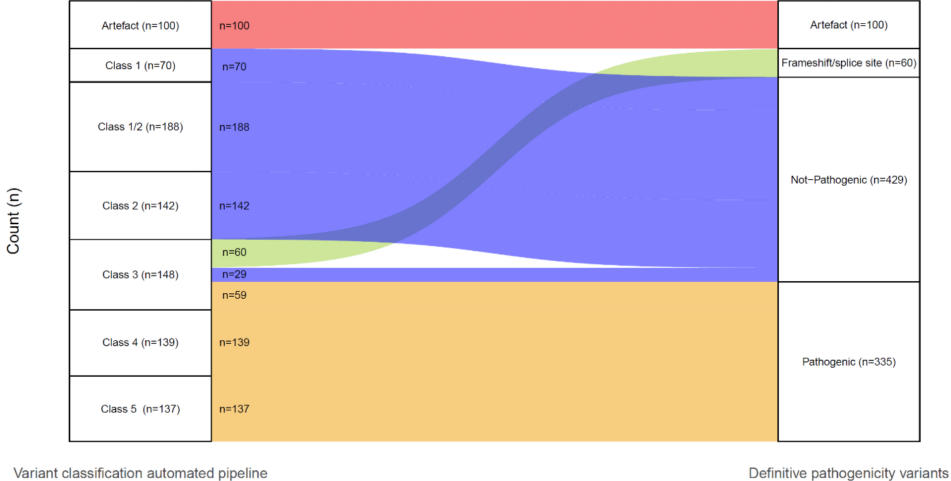
After barcoding, samples were manually purified with low TE solution and AMPure XP beads (Beckman Coulter; A63882), according to the library purification protocol (manufacturer procedures). Purification was followed by qPCR using 5  $\mu\text{L}$  of Ion Library TaqMan qPCR Master Mix (2x) and 0.5  $\mu\text{L}$  of Ion Library TaqMan Quantitation Assay (20x; Ion Library TaqMan™ Quantitation Kit; ThermoFisher Scientific; 4468802) with 4.5  $\mu\text{L}$  of 100-times diluted purified sample library. Together with a calibration curve consisting of 10-, 100-, and 1000-times diluted *E. coli* (68 pM), qPCR was performed on a Bio-Rad S1000 thermal Cycler with the following settings: 50 °C for 2 minutes, 95 °C for 20 seconds, followed by 32 cycles of 95 °C for 3 seconds and 60 °C for 20 seconds. Based on qPCR data, samples were normalized and pooled and subsequently another qPCR was performed with similar conditions. A final concentration of 60 pM pooled libraries was used for sequencing preparation with the Ion Chef™ instrument (ThermoFisher Scientific; 4484177) with the Ion 540™ Chip Kit (ThermoFisher Scientific; A27765). Sequencing was performed with the Ion S5™ Sequencing platform (ThermoFisher Scientific; A27212), according to the manufacturer's protocol (ThermoFisher Scientific).

Genes included in the 128 gene next-generation sequencing panel						
ACTB	CD58	EZH2	IRF4	MYD88	RRAGC	TP53
ACTG1	CD70	FAS	IRF8	NFKBIA	S1PR2	TRAF2
ARID1A	CD79A	FBXW7	IRS2	NFKBIE	SETD1B	TRAF3
ARID1B	CD79B	FOXO1	ITPKB	NFKBIZ	SF3B1	UBE2A
ATM	CD83	GNA13	JAK3	NOTCH1	SGK1	UBR5
B2M	CDKN2A	GNAI2	KLF2	NOTCH2	SLC22A16	XBP1
BCL10	CDKN2B	GRHRP	KLHL14	NSD2 (WHSC1)	SLCO1A2	ZEB2
BCL2	CIITA	HIST1H1B	KLHL6	NTRK1	SOCS1	ZFAT
BCL6	CREBBP	HIST1H1C	KMT2D	OSBPL10	SPIB	
BCL7A	CTNNB1	HIST1H1D	KRAS	PAX5	STAT3	
BCOR	CXCR4	HIST1H1E	LRP1B	PIK3CA	STAT6	
BIRC3	CXCR5	HIST1H2AC	LYN	PIM1	TBL1XR1	
BRAF	DTX1	HIST1H2AM	MALT1	PIM2	TCF3	
BTG1	DUSP2	HIST1H2BC	MAP2K1	PLCG2	TCL1A	
BTG2	EBF1	HIST1H2BK	MCL1	POU2F2	TET2	
BTK	EEF1A1	ID3	MEF2B	PRDM1	TMEM30A	
CARD11	EGFR	IDH1	MPEG1	PTEN	TMSB4X	
CCND1	EP300	IGLL5	MSH3	PTPN11	TNFAIP3	
CCND3	ETS1	IKBKB	MTOR	PTPN6	TNFRSF14	
CD37	ETV6	IRF2BP2	MYC	PTPRD	TOX	

After sequencing with the BLYMFv2 panel, the sequencing data was aligned to the human reference genome (GRCh37/hg19) with the TMAP 5.0.7 software (default parameters, <https://github.com/iontorrent/TS>). Variants were called by the Torrent Variant Caller (Thermo Fisher Scientific) and added to the Geneticist Assistant NGS Interpretive Workbench (SoftGenetics) for functional annotation by a clinical molecular biologist. Variants with a population frequency of above 1% in the 1000 Genomes Project or variants in three DNA mixtures of “healthy” individuals (n=288; sequenced during validation) were assigned as a single nucleotide polymorphism (SNP). These SNPs, together with sequencing-artifacts induced by homopolymeric regions and variants with a high strand bias (>90%), were excluded from further analysis. All remaining variants with a variant allele frequency (VAF) of  $\geq 10\%$  and read depth of  $\geq 100$  reads, were categorized based upon their pathogenicity: class 1 - benign, class 2 - likely benign, class 3 - unknown significance, class 4 - likely pathogenic, and class 5 - pathogenic. Classification was performed with data from dbSNP(2), ClinVar(3), COSMIC(4), and available literature. If variant were unknown in the pipeline were checked in the gnomAD database. See Supplementary Figure 1 for the number of variants allocated to each class.

All variants with unknown pathogenicity were separated into their potential pathogenicity, based on the following prediction-score protocol: variants with a high CADD-phred score ( $\geq 25$ ) were classified as “pathogenic”, and variants with an average CADD-phred score (10-25) were only classified as “likely-pathogenic” if two or more prediction scores identified the variant as deleterious (SIFT, Polyphen2\_HDIV, LRT, and MutationTaster). Remaining variants were either designated as “not pathogenic” or variants of unknown significance. Frameshift and splice-site mutations with unknown significance were subsequently analyzed using additional information from the franklin.genoox.com website. The variants of unknown significance were not included in the oncoplot.” This method has been used before for primary DLBCL of the bone.(5)

**Supplementary Figure 1 – Alluvial plot of variant classes in the automated pipeline vs. the definitive variant allocation**



**Supplementary Figure 1.** The automated pipeline called 924 potential variants. All these variants were manually checked in Integrative Genomics Viewer. One hundred variants were, after visual inspection, called as artifacts. Sixty were splice site and frameshift variants with unknown or uncertain pathogenicity when employing the online classification tools. These were not reported. In total, 429 variants were called and were deemed non-pathogenic according to the annotation pipeline. Consequently, this left us with 335 variants that were functionally annotated as pathogenic.

## SUPPLEMENTAL REFERENCES

1. Scott DW, Wright GW, Williams PM, Lih CJ, Walsh W, Jaffe ES, et al. Determining cell-of-origin subtypes of diffuse large B-cell lymphoma using gene expression in formalin-fixed paraffin-embedded tissue. *Blood*. 2014 Feb 20;123(8):1214–7.
2. Sherry ST, Ward M, Sirotkin K. dbSNP—database for single nucleotide polymorphisms and other classes of minor genetic variation. *Genome Res*. 1999;9(8):677–9.
3. Landrum MJ, Lee JM, Benson M, Brown GR, Chao C, Chitipiralla S, et al. ClinVar: improving access to variant interpretations and supporting evidence. *Nucleic Acids Res*. 2018;46(D1):D1062–7.
4. Tate JG, Bamford S, Jubb HC, Sondka Z, Beare DM, Bindal N, et al. COSMIC: the catalogue of somatic mutations in cancer. *Nucleic Acids Res*. 2019;47(D1):D941–7.
5. Groen R, Eijk R, Böhringer S, van Wezel T, Raghoo R, Ruano D, et al. Frequent mutated B2M , EZH2 , IRF8 , and TNFRSF14 in primary bone diffuse large B-cell lymphoma reflect a GCB phenotype. *Blood Adv*. 2021 Sep 3;5.





# 7

## Immune evasion in primary testicular and central nervous system lymphomas: HLA I and II loss rather than 9p24.1/*PD-L1*/*PD-L2* alterations

Marthe Minderman<sup>1,3</sup>, Avital Amir<sup>1,3</sup>, Willem Kraan<sup>1,3</sup>, Esther J. M. Schilder-Tol<sup>1,3</sup>,  
Monique E. C. M. Oud<sup>1,3</sup>, Cornelis G. Scheepstra<sup>4</sup>, Arnold L. Noorduy<sup>5</sup>, Philip M. Klui<sup>6</sup>,  
Marie José Kersten<sup>2,3</sup>, Marcel Spaargaren<sup>1,3\*</sup>, and Steven T. Pals<sup>1,3,\*</sup>

<sup>1</sup>Department of Pathology and <sup>2</sup>Hematology, Cancer Center Amsterdam (CCA), Amsterdam University Medical Centers loc. AMC, University of Amsterdam, 1105 AZ Amsterdam, The Netherlands; <sup>3</sup>Lymphoma and Myeloma Center Amsterdam – LYMMCARE, The Netherlands; <sup>4</sup>Department of Pathology and Hematology, Onze Lieve Vrouwe Gasthuis, Amsterdam, The Netherlands; <sup>5</sup>Pathology Laboratory, Dordrecht, The Netherlands. <sup>6</sup>Department of Pathology, University Medical Center, Groningen, The Netherlands. \* these authors share last authorship

## TO THE EDITOR

Cancer immune evasion is a major hurdle for effective anticancer therapy. Key strategies of tumor cells to avoid T-cell recognition include downregulation of major histocompatibility complex (MHC) molecules and activation of immune checkpoints<sup>1,2</sup>. Particularly the immune checkpoint protein programmed cell death 1 (PD-1) and its ligands PD-L1 and PD-L2 play a key role in repressing T-cell activity in the tumor microenvironment, not only in solid cancers but also in hematological malignancies. Specifically in advanced classical Hodgkin's lymphoma (cHL), blockade of the PD-1/PD-L1/L2 axis yields outstanding clinical responses<sup>3</sup>. Most cHLs are infiltrated by PD-1 positive T cells and the tumor cells show strong expression of PD-L1/PD-L2 due to copy-number alterations (CNA) at chromosome 9p24.1, containing the loci for *PD-L1/PD-L2* and *JAK2*<sup>4</sup>, or alternatively, driven by Epstein-Barr virus (EBV) infection<sup>5</sup>.

Primary testicular lymphomas (PTLs) and primary central nervous system lymphomas (PCNSLs) are uncommon and aggressive large-B cell lymphomas with a poor response to therapies and prognosis and shared molecular characteristics. PTLs and PCNSLs, which arise at sites considered to be immune-privileged<sup>6</sup>, display a remarkably high prevalence of activating somatic *MYD88* mutations, often with a concurrent activating mutation in the immunoreceptor tyrosine-based activation motif (ITAM) of *CD79B*<sup>7,8</sup>. Regarding immune evasion, both PTLs and PCNSLs were previously shown to exhibit frequent loss of HLA class I and II expression and/or loss of HLA-loci<sup>9,10</sup>. More recently, Chapuy *et al.* reported frequent 9p24.1/*PD-L1/2* CNAs and translocations with concomitant protein overexpression in PTLs and PCNSLs<sup>11</sup>. A subsequent study by the same authors in a small series (n=5) of PTL and PCNSL patients suggested clinical activity of PD-1 blockade with nivolumab<sup>12</sup>. Based on these reports, several clinical trials exploring the efficacy of PD-1/PD-L1 blockade have been initiated (<https://clinicaltrials.gov/>; i.a. NCT02779101, NCT03255018, NCT04401774, NCT02857426). In the current study, we revisited the immune evasion mechanisms operating in PTLs and PCNSLs. We were able to confirm a high frequency of HLA class I and II expression loss. However, with the exception of EBV-positive PCNSLs, which were PD-L1 positive, PTLs and PCNSLs seldomly expressed PD-L1 and, accordingly, 9p24.1/*PD-L1/2* CNAs were rarely found.

We assessed HLA class I and II expression, PD-L1 expression and 9p24.1/*PD-L1/2* CNAs in a panel of lymphomas diagnosed as PTLs (n=25) or PCNSLs (n=22) according to the World Health Organization (WHO) classification<sup>13</sup>, employing immunohistochemistry (IHC) and fluorescent in-situ hybridization (FISH), respectively (Table 1). For comparison, a set of diffuse large B-cell lymphomas (DLBCLs, n=22), enriched for cases with a non-germinal center B-cell (GCB) phenotype to better match the PTLs and PCNSLs, were studied. All lymphomas were classified as either GCB- or non-GCB like, using the immunohistochemical algorithm

of Hans *et al.*<sup>14</sup>. In addition, the presence of somatic mutations in *MYD88* and *CD79B*, of translocations of *cMYC*, *BCL2* and *BCL6*, as well as EBV status, were assessed as described previously<sup>7,8</sup>. Consistent with previous reports<sup>7,8,11</sup>, *MYD88* mutations were detected at high frequency in PTL (76%) and PCNSL (64%), and co-existent mutations in *CD79B* were often found. Presence of these *MYD88* and *CD79* mutations was almost mutually exclusive with translocations of *cMYC*, *BCL2* and *BCL6* or with EBV expression (Figure 1A). A propos immune evasion, we observed a high prevalence of loss of HLA class I expression in both PTL (68%) and PCNSL (64%). Similarly, HLA class II loss was also common in both PTL (84%) and PCNSL (59%). These findings are in line with previous studies by Riemersma *et al.*<sup>10</sup> and Booman *et al.*<sup>15</sup>, which also reported frequent HLA class I and II loss in PTLs and PCNSLs. In marked contrast to the study by Chapuy *et al.*, however, we hardly detected expression of PD-L1 or 9p24.1/*PD-L1/2* CNAs in our cohort of PTLs and PCNSLs. A notable exception were EBV-positive tumors, which showed strong PD-L1 expression (Figure 1A). In the entire group of EBV-negative PCNSLs and PTLs (n=42), only three cases with PD-L1 expression and one case with a 9p24.1/*PD-L1/2* copy number gain were found. The frequency of PD-L1 expression and 9p24.1/*PD-L1/2* CNA did not significantly differ from that in the DLBCLs. In approximately half of the cases, we did observe variable, mostly weak, PD-L1 expression by macrophages in the tumor-microenvironment. Representative PD-L1/PAX5 IHC images are shown in Supplemental Figure 1.

In view of the vast discrepancy between our finding and those of Chapuy<sup>11</sup>, we sought to further reinforce our data. First, to validate the techniques employed to detect PD-L1 expression and 9p24.1/*PD-L1/2* CNAs, a series of primary mediastinal B-cell lymphomas (PMBCLs, n=25) were studied. Like cHLs, these lymphomas frequently show genetic aberrations of chromosome 9p24.1 with consequent PD-L1 overexpression<sup>4</sup>. Indeed, we detected strong PD-L1 expression in a large proportion (68%) of the PMBCLs (Supplemental table 1), while 9p24.1/*PD-L1/2* CNAs were observed in over half of the cases (Figure 1B). Notably, in contrast to PTLs and PCNSLs, loss of HLA class I and II expression was uncommon in these PMBCLs (Supplemental table 1). Secondly, we studied *PD-L1* mRNA expression data extracted from publicly available databases. These mRNA data reveal enhanced expression of *PD-L1* in PMBCLs, but not in PTLs and PCNSLs, a finding consistent with the lack of PD-L1 expression in our current data set (Figure 1C). Notably, in line with our results, in a study of PCNSLs recently reported by Sehti *et al.*<sup>16</sup>, PD-L1 expression and/or 9p24.1/*PD-L1/2* CNAs were also barely found, except in EBV-positive tumors, which were PD-L1 positive. A possible explanation for the discordantly high prevalence of 9p24.1/*PD-L1/2* CN gains reported by Chapuy *et al.* is an incorrectly low threshold-setting in the qPCR assays used to detect CNAs in the large 'extension cohort' of their study. This could also explain the strikingly lower percentage of CNAs in the initial 'discovery cohort', which were identified by employing high density single nucleotide polymorphism arrays (HD-SNP).

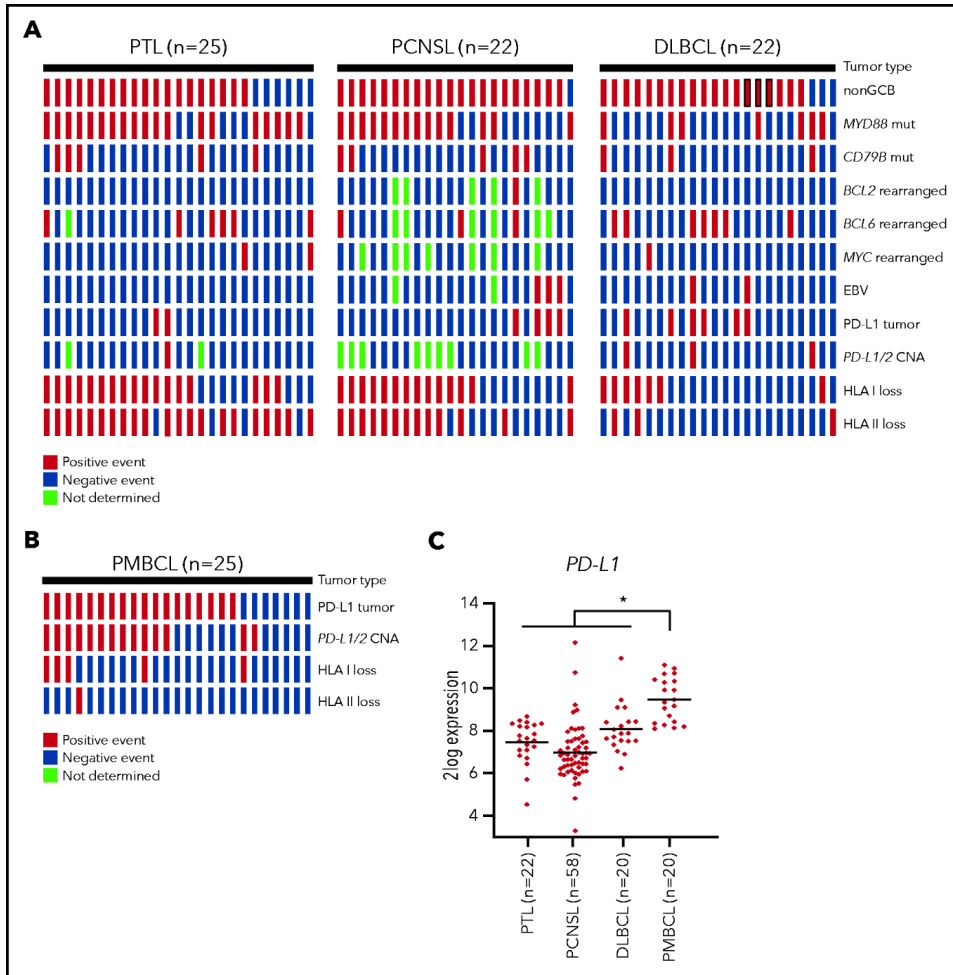


**Figure 1. Oncoprint plot.** Shown is the molecular analysis of the PTLs, PCNSLs, and DLBCLs (A) and PMBCLs (B). All tissue samples were obtained during standard diagnostic procedures. Immunohistochemistry was performed on formalin-fixed, paraffin-embedded tissue using anti-HLA class I (clone HC10, Nordic-MUBio), anti-HLA-DP,DQ,DR (clone CR3/43, DAKO), anti-PD-L1 (clone 22C3, DAKO), anti-PAX5 (clone SP43, Cell Marque), anti-CD10 (clone 56C6, ThermoFisher), anti-MUM1 (clone MUM1p, DAKO), anti-BCL2 (clone 124, Dako), and anti-BCL6 (clone PG-B6p, Dako) on a Labvision Autostainer 480S (ThermoFisher). Samples were scored positive for PD-L1 when membranous staining was observed in at least 5% of the malignant cells. Expression of EBV was determined by EBV-encoded RNA in-situ hybridization (EBER) probes (Biogenex). FISH for detection of BCL2, BCL6, and cMYC breaks was performed using probes and a FISH accessory kit (Dako). FISH for detection of PD-L1/2 CNAs was performed with the Zytolight CD274/PDCD1LG2/CEN 9 Dual Color Probe (ZytoVision). FISH slides were evaluated in the context of serial sections stained for PD-L1 and B-cell markers (CD20 and PAX5) to localize tumor infiltrates. Samples were scored as having 9p24.1 disomy, polysomy, copy gain, or amplification. The presence of 3 or 4 green signals was classified as gain and the presence of 5 or more green signals was classified as amplification. Testing for somatic MYD88 and CD79B mutations was performed with allele-specific polymerase chain reaction, as described previously.<sup>7</sup> Sanger sequencing was used to verify the presence of a mutation. (C) PD-L1 mRNA expression analysis of publicly available microarray data sets derived from the National Center for Biotechnology Information (NCBI) Gene Expression Omnibus (accession numbers GSE10524, GSE61578, GSE34771 and GSE87371). All microarray data sets were generated with Affymetrix Human

Genome U133 Plus 2.0 Array, and data analysis was performed with the R2: Genomics Analysis and Visualization Platform (<http://r2.amc.nl>). The horizontal line represents the median expression within each group. Differences among subtypes were tested by Kruskal-Wallis test with the post hoc Dunn's test. \*P < .05.

In conclusion, our study indicates that different large B-cell lymphoma subtypes employ distinct immune evasion strategies: while PTLs and PCNSLs seem to hardly use the PD1/PD-L1/2 checkpoint, but instead employ loss of MHC expression as major mechanism of immune evasion, in PMBCLs PD-L1 overexpression often caused by 9p24.1/PD-L1/2 CNAs, appears to play a major role. This suggests that PBMCL patients, but not PTL and PCNSL patients, are likely to benefit from treatment with PD-1/PD-L1 immune checkpoint inhibitors. Indeed, although a preliminary clinical study suggested activity of nivolumab treatment<sup>12</sup>, the results of the phase 2 trial with nivolumab in recurrent and refractory PCNSL and PTL patients (NCT02857426), which was initiated based on these initial findings, are highly disappointing: the objective response rate (ORR) was only 6.4% in 47 analyzed patients. Similarly, nivolumab monotherapy resulted in an ORR of only 3-10% in patients with relapsed/refractory DLBCL<sup>17</sup>. In contrast, interim analysis of the phase 2 KEYNOTE-170 study (NCT02576990) showed an ORR of 45% in relapsed/refractory PBMCL patients<sup>18</sup>. Considering the ongoing clinical trials involving immune checkpoint inhibitors in PCNSL/PTL patients (NCT04421560, NCT03770416, NCT04609046), we believe that a critical reappraisal of the prevalence of PD-L1 expression and 9p24.1 alterations in these lymphomas is of crucial importance.

## **ACKNOWLEDGMENTS**

The authors thank M.F.M. de Rooij for his helpful contributions to the data presentation. This study is supported by a grant from Lymph&Co to M.J. Kersten and S.T. Pals.

## **AUTHORSHIP**

### ***Contributions***

M.M. performed experiments, analyzed the data and wrote the paper, A.A. designed the research, supervised the study and analyzed the data., W.K. performed experiments and analyzed the data, E.S. and M.O. performed experiments, C.S. A.N. and P.K. provided patient material, M.J.K., M.S. and S.T.P. designed the research, supervised the study, analyzed the data, and wrote the paper.

### ***Conflict-of-interest disclosure***

The authors declare no competing financial interests.

**Table 1. Clinical and molecular characteristics of PTLs, PCNSLs and DLBCLs**

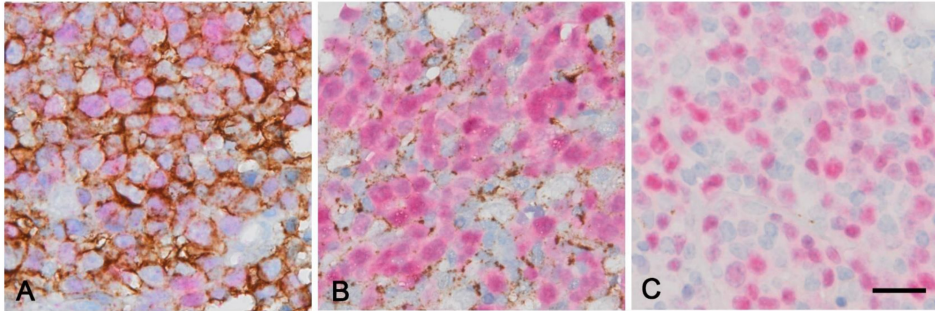
		<b>PTL (n=25)</b>	<b>PCNSL (n=22)</b>	<b>DLBCL (n=22)</b>
<b>Age</b>	<b>Median (range)</b>	74 (58 – 89)	69 (49 – 83)	63 (4 – 89)
<b>Gender</b>	<b>Male</b>	100% (25/25)	67% (14/21)	64% (14/22)
	<b>Female</b>	0% (0/25)	33% (7/21)	36% (8/22)
<b>EBV status</b>	<b>Positive</b>	0% (0/25)	15% (3/20)	9% (2/22)
<b>MYC</b>	<b>Rearranged</b>	8% (2/25)	0% (0/15)	5% (1/22)
<b>BCL2</b>	<b>Rearranged</b>	0% (0/25)	6% (1/17)	0% (0/22)
<b>BCL6</b>	<b>Rearranged</b>	25% (6/24)	19% (3/16)	32% (7/22)
<b>MYD88</b>	<b>Mutated</b>	76% (19/25)	64% (14/22)	32% (7/22) **
<b>CD79B</b>	<b>Mutated</b>	20% (5/25)	23% (5/22)	14% (3/22)
<b>COO</b>	<b>Non-GCB</b>	76% (19/25)	95% (21/22)	86% (19/22)
	<b>GCB</b>	24% (6/25)	5% (1/22)	14% (3/22)
<b>PD-L1 tumor</b>	<b>Negative</b>	92% (23/25)	82% (18/22)	73% (16/22)
	<b>Weak</b>	0% (0/25)	4% (1/22)	9% (2/22)
	<b>Positive</b>	8% (2/25)	14% (3/22)	18% (4/22)
<b>PD-L1/2 CNA</b>	<b>Gain</b>	4% (1/23)	0% (0/13)	14% (3/22)
	<b>Polysomy</b>	0% (0/23)	0% (0/13)	0% (0/22)
<b>HLA class I</b>	<b>Loss</b>	68% (17/25)	64% (14/22)	32% (7/22) *
<b>HLA class II</b>	<b>Loss</b>	84% (21/25)	59% (13/22)	14% (3/22) **

Abbreviations: PTL, primary testicular lymphoma; PCNSL, primary central nervous system lymphoma; DLBCL, diffuse large B cell lymphoma; EBV, Epstein-Barr virus; COO, cell of origin; GCB, germinal center B-cell like; CNA, copy number alteration. The correlation between the clinical and molecular characteristics among the different tumor types was examined using the chi-square ( $\chi^2$ ) test. P-values were two-sided and  $p < 0.05$  was considered statistically significant. \* $P < 0.05$ ; \*\* $P < 0.01$

## REFERENCES

1. Pardoll DM. The blockade of immune checkpoints in cancer immunotherapy. *Nat Rev Cancer*. 2012;12(4):252-64.
2. Mahoney KM, Rennert PD, Freeman GJ. Combination cancer immunotherapy and new immunomodulatory targets. *Nat Rev Drug Discov*. 2015;14(8):561-84.
3. Ansell SM, Lesokhin AM, Borrello I, Halwani A, Scott EC, Gutierrez M, et al. PD-1 blockade with nivolumab in relapsed or refractory Hodgkin's lymphoma. *N Engl J Med*. 2015;372(4):311-9.
4. Green MR, Monti S, Rodig SJ, Juszczynski P, Currie T, O'Donnell E, et al. Integrative analysis reveals selective 9p24.1 amplification, increased PD-1 ligand expression, and further induction via JAK2 in nodular sclerosing Hodgkin lymphoma and primary mediastinal large B-cell lymphoma. *Blood*. 2010;116(17):3268-77.
5. Chen BJ, Chapuy B, Ouyang J, Sun HH, Roemer MG, Xu ML, et al. PD-L1 expression is characteristic of a subset of aggressive B-cell lymphomas and virus-associated malignancies. *Clin Cancer Res*. 2013;19(13):3462-73.
6. Shechter R, London A, Schwartz M. Orchestrated leukocyte recruitment to immune-privileged sites: absolute barriers versus educational gates. *Nat Rev Immunol*. 2013;13(3):206-18.
7. Kraan W, Horlings HM, van Keimpema M, Schilder-Tol EJ, Oud ME, Scheepstra C, et al. High prevalence of oncogenic MYD88 and CD79B mutations in diffuse large B-cell lymphomas presenting at immune-privileged sites. *Blood Cancer J*. 2013;3:e139.
8. Kraan W, van Keimpema M, Horlings HM, Schilder-Tol EJ, Oud ME, Noorduy LA, et al. High prevalence of oncogenic MYD88 and CD79B mutations in primary testicular diffuse large B-cell lymphoma. *Leukemia*. 2014;28(3):719-20.
9. Booman M, Suzhai K, Rosenwald A, Hartmann E, Kluin-Nelemans H, de Jong D, et al. Genomic alterations and gene expression in primary diffuse large B-cell lymphomas of immune-privileged sites: the importance of apoptosis and immunomodulatory pathways. *J Pathol*. 2008;216(2):209-17.
10. Riemersma SA, Jordanova ES, Schop RF, Philippo K, Looijenga LH, Schuurring E, et al. Extensive genetic alterations of the HLA region, including homozygous deletions of HLA class II genes in B-cell lymphomas arising in immune-privileged sites. *Blood*. 2000;96(10):3569-77.
11. Chapuy B, Roemer MG, Stewart C, Tan Y, Abo RP, Zhang L, et al. Targetable genetic features of primary testicular and primary central nervous system lymphomas. *Blood*. 2016;127(7):869-81.
12. Nayak L, Iwamoto FM, LaCasce A, Mukundan S, Roemer MGM, Chapuy B, et al. PD-1 blockade with nivolumab in relapsed/refractory primary central nervous system and testicular lymphoma. *Blood*. 2017;129(23):3071-3.
13. Swerdlow SH, Campo E, Harris N.L., Jaffe E.S., Pileri S.A., Stein H., Thiele J., Vardiman J.W. WHO Classification of Tumours of Haematopoietic and Lymphoid Tissues. 4th rev. ed, 2017.
14. Hans CP, Weisenburger DD, Greiner TC, Gascoyne RD, Delabie J, Ott G, et al. Confirmation of the molecular classification of diffuse large B-cell lymphoma by immunohistochemistry using a tissue microarray. *Blood*. 2004;103(1):275-82.
15. Booman M, Douwes J, Glas AM, Riemersma SA, Jordanova ES, Kok K, et al. Mechanisms and effects of loss of human leukocyte antigen class II expression in immune-privileged site-associated B-cell lymphoma. *Clin Cancer Res*. 2006;12(9):2698-705.
16. Sethi TK, Kovach AE, Grover NS, Huang LC, Lee LA, Rubinstein SM, et al. Clinicopathologic correlates of MYD88 L265P mutation and programmed cell death (PD-1) pathway in primary central nervous system lymphoma. *Leuk Lymphoma*. 2019;60(12):2880-9.
17. Ansell SM, Minnema MC, Johnson P, Timmerman JM, Armand P, Shipp MA, et al. Nivolumab for Relapsed/Refractory Diffuse Large B-Cell Lymphoma in Patients Ineligible for or Having Failed Autologous Transplantation: A Single-Arm, Phase II Study. *J Clin Oncol*. 2019;37(6):481-9.
18. Armand P, Rodig S, Melnichenko V, Thieblemont C, Bouabdallah K, Tumyan G, et al. Pembrolizumab in Relapsed or Refractory Primary Mediastinal Large B-Cell Lymphoma. *J Clin Oncol*. 2019;37(34):3291-9.

## SUPPLEMENTAL DATA



**Supplemental Figure 1. PD-L1 expression in PTL and PCNSL.** Representative examples of lymphomas with: A) PD-L1 expression by tumor cells; malignant cells showing double staining for PAX5 (red) and PD-L1 (brown). B) PD-L1 expression by macrophages; macrophages expressing PD-L1, nuclei are PAX5 negative; C) no PD-L1 expression by tumor cells (PAX5 positive) or by the tumor microenvironment. Scale bar = 30  $\mu$ m.

**Supplemental Table 1. Clinical and molecular characteristics of PMBCLs**

		PMBCL (n=25)
Age	Median (range)	39 (18 - 71)
Gender	Male	60% (15/25)
	Female	40% (10/25)
PD-L1 tumor	Negative	28% (7/25)
	Weak	4% (1/25)
	Positive	68% (17/25)
PD-L1/2 CNA	Gain	40% (10/25)
	Polysomy	16% (4/25)
HLA class I	Loss	20% (5/25)
HLA class II	Loss	4% (1/25)

Abbreviations: PMBCL, primary mediastinal B cell lymphoma; CNA, copy number alteration.





# 8

## General discussion

## GENERAL DISCUSSION

Diffuse large B cell lymphomas (DLBCLs) belonging to the MCD subtype (named after the co-occurrence of *MYD88* and *CD79B* gene mutations) have distinct clinical, genetic and molecular features. Notably, MCD DLBCLs display frequent involvement of extranodal sites and their mutational spectrum is largely similar to the mutational spectrum observed in DLBCL arising at extranodal, immune-privileged (IP) sites. This indicates that the pathogenesis of MCD DLBCL is strongly related to the pathogenesis of primary extranodal lymphomas. First, we will evaluate the molecular features of IP-associated (MCD) DLBCL and specifically zoom into the immune evasion mechanism employed by these lymphomas. Second, we will discuss the functional consequences of (co-occurring) *MYD88* and *CD79B* mutations. Lastly, we provide the rationale for targeting these pathways to improve treatment options for this aggressive class of lymphomas.

### Molecular genetic features of IP-associated (MCD) DLBCL

MCD DLBCLs predominantly belong to the activated B cell-like (ABC) type of DLBCL and display significantly inferior survival when compared to other genetic subtypes (1). In line with the ABC subtype, chromosomal rearrangements involving the *MYC* and *BCL2* loci are rare, whereas rearrangements of the *BCL6* locus occur in approximately 25% of cases (2-4). MCD DLBCL is characterized by frequent, often biallelic, deletions or mutations of the cell-cycle inhibitory gene *CDKN2A* (1, 5, 6). Other tumor suppressor genes frequently deleted in MCD DLBCL include the transcriptional regulators *ETV6*, *BTG1* and *BTG2* (1, 6). Other frequent genetic alterations include amplifications of the *BCL2* locus and mutations in *PIM1*, a proto-oncogene that encodes a serine/threonine kinase (1). PIM mutations were shown to increase cellular migratory potential suggesting they might play a role in extranodal localization and tumor dissemination (7). Importantly, highly frequent mutations in the TLR adaptor protein *MYD88* and BCR-associated protein *CD79B* drive constitutive activation of the NF- $\kappa$ B pathway. Interestingly, primary testicular lymphomas (PTLs) and primary central nervous system lymphomas (PCNSLs) show a similar spectrum of mutations as MCD DLBCL (4, 5, 8). The same holds true for primary vitreoretinal lymphoma (PVRLs), which is the most common type of primary intraocular lymphoma and considered to be a subtype of PCNSL (9). Our recent studies in ocular adnexal large B-cell lymphoma and primary sinonasal DLBCL demonstrate that these types of lymphoma are also characterized by a high frequency of (co-occurring) *MYD88* and *CD79B* mutations, especially in cases classified as ABC-like DLBCL according to the cell-of-origin classification (10, 11). Interestingly, the central nervous system, testis and vitreoretinal compartment are all considered immune-privileged areas. Surprisingly, MCD DLBCL and primary extranodal lymphomas frequently harbor various genetic aberrations which favor immune escape mechanisms.

## Immune evasion mechanisms

Immune privilege is a longstanding concept originally referring to the observation that tissue grafts placed within certain anatomical sites can persist for prolonged periods of time without being rejected (12). The graft-associated antigens were believed to be concealed from the immune system by physical barriers, such as the blood-brain-barrier (BBB). This concept has been largely revised, since we now know that immune effector cells do have access to immune-privileged areas. This implies, that immune privilege does not refer to an absolute absence of immunological components, but is an tightly regulated, active process required to maintain immune tolerance (13, 14).

Classical Hodgkin lymphoma (cHL) and primary mediastinal large B-cell lymphoma (PMBCL) frequently harbor amplifications of the *PD-L1/2* locus on chromosome 9p24.1 resulting in high programmed cell death ligand 1 (PD-L1) membrane expression (15). Also Epstein-Barr virus (EBV)-associated PCNSL show strong expression of PD-L1 and PD-L2 (16). Binding of PD-L1 to PD-1 promotes SHP-1/2 mediated suppression of TCR and CD28 proximal signaling molecules, thereby inhibiting T cell effector functions resulting in an anergic and exhausted T cell phenotype (17). The strong expression of PD-L1 in cHL and PMBCL might explain the exquisite sensitivity of these lymphomas to immune checkpoint blockade therapy (18, 19). Initial studies suggested that also PTLs and PCNSLs frequently use *9p24.1/PD-L1/PD-L2* amplifications as primary mechanism to evade immune surveillance (5). However, our studies showed that PTLs and PCNSLs rarely upregulate expression of PD-1 and its ligands (PD-L1, PD-L2), but instead use the loss of MHC class I and II expression as a major mechanism of immune evasion (3). In line with this, our results also demonstrate loss of MHC class II as the primary mechanism of immune evasion in primary sinonasal DLBCL (11). Loss of MHC class I was observed, but less frequently compared to other nodal and extranodal DLBCL cases. The relatively low frequency of MHC class I loss may result from selective pressure by natural killer (NK) cells. NK cell surveillance seems to play an important role in nasal immunity, but NK cell entry into the CNS and testis is somewhat restricted under normal physiological conditions (20, 21). In line with our findings in PCNSL and PTL, PD-L1 expression and *PD-L1* CNAs were hardly observed in primary sinonasal DLBCL. Interestingly, Weissinger *et al.* detected *PD-L1/2* gains/amplifications in a subset of extranodal DLBCL, but found no significant correlation with PD-L1 expression established using immunohistochemistry (22).

Loss of MHC class I molecules hampers immune recognition by CD8<sup>+</sup> cytotoxic T cells and is frequently caused by deletions and/or mutational inactivation of the *B2M* gene, which is essential for successful assembly of the MHC class I-complex on the cell surface (23, 24). In addition, *HLA-A*, *HLA-B* and *HLA-C* gene deletions or mutations represent an alternative mechanism to explain the loss of MHC class I expression in B2M expressing lymphomas (25). Interestingly, in both PCNSL and PTL, low HLA class I expression was associated

with reduced immune cell infiltration and poor patient outcome (26, 27). In addition to MHC class I, B cells normally express MHC class II molecules on their surface to allow interaction with CD4<sup>+</sup> T helper cells. Homozygous and heterozygous deletions of the MHC class II locus are the primary mechanism of MHC class II deficiency in PCNSL and PTL (28, 29). This is in contrast to nodal DLBCL and PMBCL where MHC class II downregulation mainly occurs at the transcriptional level through inactivating mutations in *CREBBP* and *CIITA* (30). The consequences of MHC class II loss are less established compared to loss of MHC class I. However, studies have shown that loss of MHC class II was correlated to reduced infiltration of CD8<sup>+</sup> cytotoxic T cells, suggesting that impaired antigen presentation to helper T cells is essential for optimal immune recognition (31).

In addition to loss of MHC class I/II expression, other studies have shown that IP-associated lymphomas display reduced antigen presentation due to truncating mutations of *TAP1* and diminished NK cell activation due to deletion of *CD58* (24, 25). *TAP1* is a transporter protein required for presentation of intracellular peptides in the context of MHC class I (32). *CD58* acts as a ligand for the CD2 receptor on T and NK cells and contributes to the adhesion and activation of these cells. Since loss of MHC class I normally triggers recognition and lysis by NK cells, this can explain why DLBCLs often concomitantly lose the expression of *CD58* and MHC class I to escape from both NK and T cell recognition (24).

In addition to PCNSL and PTL, immune evasion mechanisms are also frequently detected in primary cutaneous diffuse large B-cell lymphoma, leg type (PCLBCL-LT) and intravascular large B cell lymphoma (IVLBCL), other primary extranodal lymphomas characterized by a high prevalence of *MYD88* and *CD79B* mutations (33-37). PCLBCL-LT frequently display deletions of chromosome 6p21 (encoding *HLA I* and *HLA II* genes) as well as mutations in *B2M*, *CIITA* and *CD58* (34, 35). Likewise, IVLBCL show frequent deletions/mutations of *HLA* class I genes and to a lesser extent also of *HLA* class II, *CIITA* and *CD58* (37). Interestingly, for both PCLBCL-LT and IVLBCL a high incidence of alterations in *PD-L1* and *PD-L2* genes has been reported (35, 37). However, in PCLBCL-LT, *9p24.1* copy number alterations only partially correlated to PD-L1 or PD-L2 overexpression by tumor cells (35). Moreover, a study in a larger series of PCLBCL-LT patients, showed that *9p24.1* rearrangements and concomitant PD-L1/2 expression are rare (38). In line with our studies in PCNSL and PTL, both studies evaluating PD-L1/2 expression in PCLBCL-LT, showed strong PD-L1 expression in tumor-associated macrophages (TAMs) (3, 35, 38). The complete role of PD-L1 expressing TAMs on disease outcome and the efficacy of conventional therapies and checkpoint inhibitors remains to be established by future studies.

Taken together, these results suggest that IP-associated lymphomas are highly immunogenic and, therefore, can only survive in immunologically silent areas. However, when the tumor continues to grow, nature barriers such as the BBB are insufficient

to completely avoid immune eradication and other immune evasion strategies are required. Several studies have indicated that IP-associated lymphomas are characterized by aberrant activation-induced cytidine deaminase (AID) activity and consequently, increased somatic hypermutation (SHM) and tumor mutational burden (TMB), which might increase the amount of presented immunogenic neo-antigens (39-46). In DLBCL, a higher mutational load and higher number of (predicted) neo-antigens was associated with loss of MHC class I expression, suggesting these lymphomas indeed are under selective pressure to escape immune surveillance (25).

### **MYD88 mutations in B cell malignancies**

The high prevalence of *MYD88* mutations in DLBCL arising in immune-privileged, non-professional lymphoid tissues suggests that *MYD88* mutations specifically contribute to the pathogenesis of IP-associated DLBCL. Since these lymphomas arise in relatively immunologically silent areas with very limited stimulation by IL-1/IL-18 and TLR ligands, it is tempting to speculate that *MYD88* mutations might provide a selective growth advantage to these lymphomas. In line with this hypothesis, the prevalence of *MYD88* mutations in extranodal lymphoma of the gastrointestinal tract, where TLR ligands are omnipresent, is relatively low (4, 47). Primary lymphoma of the bone is another type of extranodal lymphoma where *MYD88* mutations are rare (48). However, primary bone DLBCL is often characterized by a GCB phenotype and a GCB-associated mutational profile, suggesting it represents a distinct extranodal DLBCL entity (49).

In 2011, Ngo and colleagues first described that mutations in TLR-adaptor protein *MYD88* contribute to constitutive activation of NF- $\kappa$ B in a large number of DLBCL patients (50). Intriguingly, the authors demonstrated that up to 29% of ABC DLBCL patients harbor a single nucleotide substitution resulting in a leucine to proline change at position 265 (L265P) in the Toll/IL-1R (TIR) domain of *MYD88*. The same mutation was detected in 7-9% of mucosa-associated lymphoid tissue (MALT) lymphomas, but hardly detected in GCB DLBCL, PMBCL and BL (50, 51). As of now, the *MYD88* L265P mutation has been described in 0-4% of CLL cases, 0% of MCL cases, 0-2% of BL cases, 0-4% of FL cases, 0-10% of GCB DLBCL cases, 8-32% of ABC DLBCL cases, 79-100% of Waldenström macroglobulinemia (WM) cases, 10-87% of IgM monoclonal gammopathy of undetermined significance cases (IgM-MGUS) cases and 0% of multiple myeloma (MM) cases (Supplementary table 1). Next to the L265P mutation a number of other somatic mutations in the *MYD88* TIR domain have been identified, but these variants are more rare. Of these non-L265P mutations the S243N and S219C variant are most frequent, being present in 2-14% and 3-8% of DLBCL cases respectively. Interestingly, whereas L265P mutations hardly occur in GC type DLBCL patients, 25-46% of the S243N and of the 40-75% S219C mutated DLBCLs belong to the GCB type (50, 52).

Following knockdown of endogenous *MYD88* in L265P mutated ABC DLBCL and WM

cell lines, only exogenous expression of mutated *MYD88*, but not wildtype *MYD88*, could rescue cell survival, underlining that the L265P variant is a gain of function mutation (50). Avbelj *et al.* proposed that lymphoma-associated *MYD88* mutations potentiate NF- $\kappa$ B signaling by augmenting MYD88 TIR domain oligomerization and, potentially, Myddosome formation (53). However, ABC DLBCL cell lines harboring an L265P mutation are not only dependent on MYD88 itself and downstream kinases IRAK4 and IRAK1, but still require TLR expression for their survival. Recently, Phelan *et al.* demonstrated that cell lines harboring *MYD88* mutations still rely on TLR9 expression as well as on expression of its chaperones UNC93B1 and CNPY3 (54). This is in line with earlier findings by Wang *et al.*, who demonstrated that MYD88 L265P-induced B-cell proliferation is dependent on expression of UNC93B1, TLR9 and optimal endosomal acidification, a prerequisite for TLR9 function (55). Together, these data suggest that MYD88 L265P does not render a constitutively active protein, but is still dependent on upstream TLR ligand recognition for signaling.

Next to increased NF- $\kappa$ B activity, *MYD88* mutations promote ABC DLBCL survival through increased expression of interleukin 6 (IL-6) and interleukin 10 (IL-10) leading to activation of the pro-survival Janus kinase/signal transducers and activators of transcription (JAK/STAT) pathway (50). Moreover, MYD88 (wildtype and mutant) signaling promotes expression of the hematopoietic cell kinase (HCK), which drives pro-survival signaling in MYD88 mutated WM and ABC DLBCL cells as well as in MYD88 wildtype MCL cells (56, 57). In addition, HCK controls integrin-mediated adhesion to the extracellular matrix and stromal cells, suggesting that it plays an important role in homing and adhesion of malignant cells to the tumor microenvironment (50).

### **CD79A/B mutations and chronic BCR signaling**

Like mutations in *MYD88*, *CD79A/B* mutations are more prevalent in extranodal DLBCL compared to DLBCL arising in lymph nodes. In Figure 1 and Supplemental Table 2 we show the frequency of *MYD88* and *CD79A/B* mutations in lymphomas arising at different anatomical locations. Since these genetic aberrations are significantly associated with the ABC subtype of DLBCL (50, 58), we only show the prevalence of *MYD88* and *CD79A/B* mutations within the ABC subtype of each cohort. Interestingly, in both nodal and extranodal DLBCL, mutations in *MYD88* and *CD79A/B* ITAM domains co-exist far more frequently than expected by chance. In PCNSL, PTL, sinonasal DLBCL and OA-LBCLs CD79 mutations hardly occur solely, but were mostly found together with mutations in *MYD88* (4, 10, 11). In contrast to *CARD11* mutations, *CD79B* ITAM mutations do not directly lead to increased NF- $\kappa$ B activity in B cells (58). Moreover, exogenous expression of *CD79B* mutants does not result in autonomous clustering of the BCR, which is normally observed in B cells after antigen exposure (58, 59). These observations suggest that continuous antigen stimulation is required for chronic BCR signaling and that *CD79A/B*

ITAM mutations will likely amplify BCR signaling.

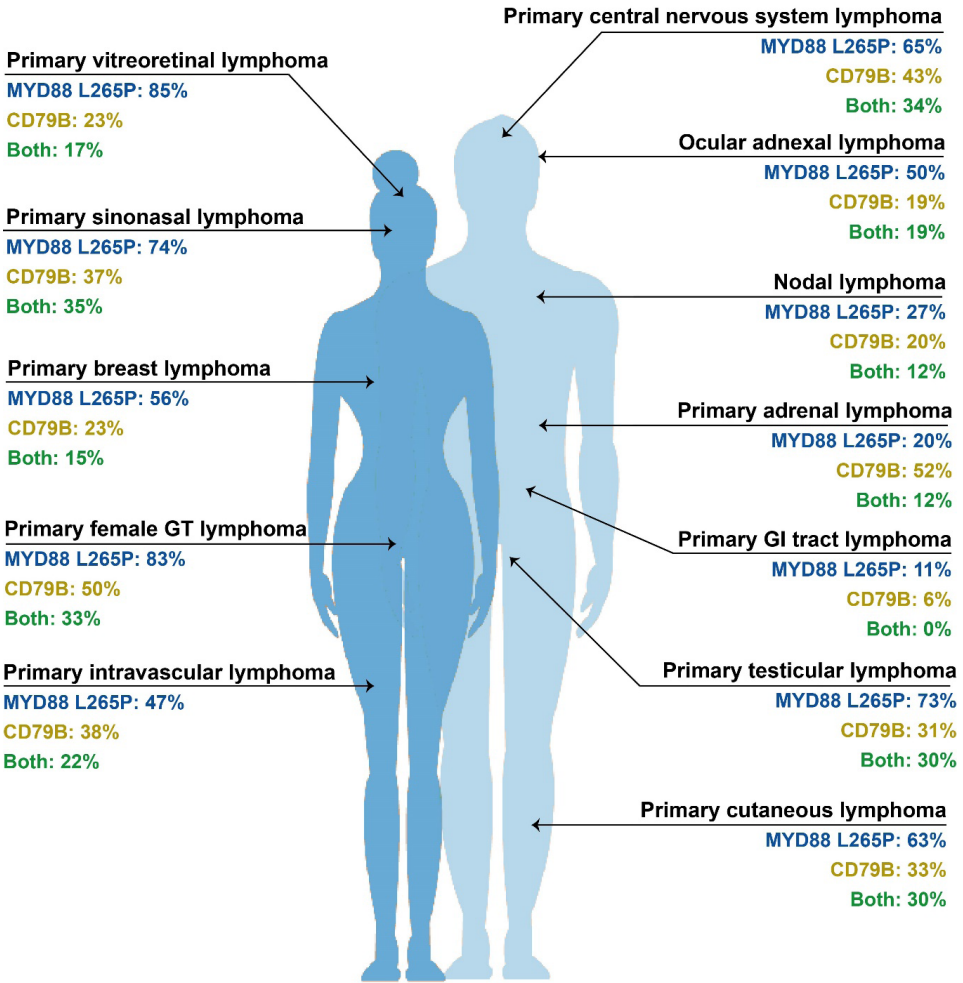


**Figure 1. Prevalence of MYD88 and CD79A/B mutations in ABC DLBCL according to localization.** The prevalence of MYD88 mutations in each of the indicated lymphoma types is visualized in blue, the prevalence of CD79A/B mutations in yellow and co-occurrence of both mutations in green. Nodal DLBCL (n=288), GI tract (n=18), adrenal (n=25), breast (n=16), cutaneous, leg type (n=30), female GT (n=6), ocular adnexa (n=16), sinonasal (n=43), CNS (n=274), testis (n=105), vitreoretinal (n=48). Abbreviations: GT, genital tract; GI, gastro-intestinal.

In murine mature B cells, mutations of tyrosine residues in the *CD79B* ITAM motifs paradoxically resulted in reduced SRC and SYK activity following BCR engagement. Interestingly, these *CD79B* mutant B cells displayed prolonged BCR signaling, higher

levels of membrane IgM expression and reduced antigen-induced BCR internalization (60). BCR internalization is predominantly mediated by adaptor protein 2 (AP2), which promotes receptor endocytosis via clathrin-coated pits. Busman-Sahay *et al.* demonstrated that mutations of the membrane-proximal ITAM tyrosine of *CD79B*, which is involved in AP2 binding, completely abrogated internalization of the BCR (61). Furthermore, the authors established that the cytoplasmic domain of CD79A is essential for AP2 binding to the CD79B ITAM motif. Several studies have indicated that LYN kinase activity is essential for BCR internalization and that *LYN*-deficient B cells are hyper responsive to BCR crosslinking (62, 63). Davis and colleagues confirmed in DLBCL cell lines that exogenous expression of *CD79B* ITAM mutants increased BCR surface expression by attenuating LYN-mediated internalization of the BCR (58).

### **Cooperation between TLR/MYD88 and BCR signaling**

Both BCR signaling as well as TLR signaling through MYD88 can strongly induce NF- $\kappa$ B activity in B cells. Interestingly, the *MYD88* L265P mutation co-occurs with *CD79* ITAM mutations much more frequent than predicted by chance, indicating that these pathways are complementary and non-redundant. Also the fact that ABCL DLBCL cell lines harboring *MYD88* and *CD79B* mutations are dependent on both MYD88 as well as BCR signaling for their survival, supports the hypothesis that these pathways are non-redundant and might act in a synergistic way.

Cooperation between BCR and TLR signaling can occur at different levels. BCR-induced NF- $\kappa$ B activation requires activation of the paracaspase MALT1, which cleaves different negative regulators of NF- $\kappa$ B such as A20 and CYLD (64, 65). Our recent findings demonstrate that low expression of *CYLD* is associated with poor prognosis of patients with ABC DLBCL and MCL and that chronic BCR signaling promotes continuous cleavage of CYLD by stimulating MALT1 protease activity (66). Moreover, our results show that ectopic overexpression of CYLD reduced phosphorylation of I $\kappa$ B $\alpha$ , repressed transcription of canonical NF- $\kappa$ B target genes and impaired growth of BCR-dependent lymphoma cell lines. Conversely, silencing of CYLD enhanced cell growth and canonical NF- $\kappa$ B activity. Additionally, our results demonstrate that following MALT1-mediated cleavage, the generated CYLD fragments are rapidly degraded by the proteasome. The C-terminal CYLD fragment, which contains the catalytic ubiquitin-specific protease (USP) domain, showed some remaining functionality, but since its rapidly degraded, we conclude that MALT1-mediated cleavage of CYLD result in its inactivation. Inactivation of CYLD (and A20) can not only affect BCR, but also TLR signaling to NF- $\kappa$ B. For example, A20 can block TLR-induced NF- $\kappa$ B activity by removing ubiquitin chains from TRAF6 (67). Likewise, CYLD negatively regulates TLR2-dependent activation of NF- $\kappa$ B by deubiquitinating TRAF6 and TRAF7 (68). In addition, CYLD was shown to directly interact with MYD88 and suppress lysine 63 (K63)-linked polyubiquitination of MYD88 following

exposure to a bacterial pathogen (69). Various stimuli, including TLR ligands, can induce expression of A20 and CYLD suggesting that these deubiquitinating enzymes are part of a negative feedback loop which regulates the termination of NF- $\kappa$ B signaling (66-68, 70). In lymphomas with chronic BCR signaling this regulatory feedback loop is seemingly disrupted by continuous MALT1-mediated cleavage of these negative regulators.

Co-localization of TLRs and the BCR seems to play a crucial role in establishing crosstalk between these pathways. In DLBCL cell lines harboring *CD79B* and *MYD88* L265P mutations, it was shown by means of proximity ligation assays (PLA) that MYD88, TLR9 and the BCR co-localize in endolysosomes, where they form a multiprotein signaling complex (the MY-T-BCR) that hyperactivates NF- $\kappa$ B (54). In MYD88 L265P harboring WM and DLBCL cell lines, it was demonstrated that MYD88 co-immunoprecipitates with BTK, with a preference for phosphorylated BTK, whereas wildtype MYD88 showed little interaction with either form of BTK (71). This interaction was abrogated by treatment with the BTK inhibitor ibrutinib. Likewise, both total and phosphorylated SYK were shown to co-immunoprecipitate with MYD88 exclusively in L265P expressing cells. Moreover, SYK was highly phosphorylated in both *MYD88*-mutated WM and DLBCL cells, which was reduced following treatment with a MYD88 peptide inhibitor (72). This is in line with a study showing that inhibition of MYD88 signaling in L265P expressing DLBCL cell lines, with an inhibitory peptide or shRNA, resulted in reduced chronic BCR signaling apparent from decreased levels of SRC, SYK and BTK phosphorylation (73). Intriguingly, the SRC family kinase HCK was recently shown to be responsible for SYK activation in MYD88 L265P expressing cell lines (74). In addition to activation of SYK, HCK triggered activation of other pro-survival pathways, including PI3K/AKT and MAPK/ERK1/2 signaling. These results suggest that HCK plays an important role in establishing crosstalk between TLR and BCR signaling. Our recent findings in MCL suggest that HCK can also facilitate TLR/BCR crosstalk in non-MYD88 mutated lymphomas where HCK is aberrantly expressed (57).

Our recent findings demonstrate that, in non-MYD88 mutated lymphomas, MYD88 activation may be mediated by serine 257 phosphorylation (75). Expression of a phosphomimetic mutant of MYD88, which mimics physiological phosphorylation at this position, promotes TIR domain homodimerization, resulting in constitutive IRAK1 phosphorylation, NF- $\kappa$ B signaling and enhanced cell growth (75-77). Interestingly, molecular dynamics simulation studies, indicate that MYD88 S257D and L265P preferentially adopt the same conformation of the CD loop of MYD88 (76). Protein phosphatase 2A catalytic subunit  $\alpha$  (PP2Ac) can dephosphorylate the S257 residue of MYD88, but the kinase(s) responsible for its phosphorylation remains unknown (78). Whether BCR signaling could be involved in driving MYD88 S257 phosphorylation remains a compelling question for future studies. The (potential) mechanisms of crosstalk between TLR and BCR signaling are schematically visualized in Figure 2.

### BCR and TLR signaling co-operate to breach B cell tolerance

There is accumulating evidence that aberrant BCR and TLR pathway activation play a crucial role in breaching peripheral immunological tolerance to self-associated antigens. B cells that are chronically exposed to self-antigens, but have escaped elimination, become anergic or undergo apoptosis. These mechanisms are largely regulated by BIM, a pro-apoptotic protein, in combination with SHIP, a phosphatase that can function as an intrinsic brake on BCR signaling (79, 80). Next to BCR signaling, the discrimination of self from non-self by TLRs is of utmost importance for B cell tolerance. Interestingly, both *MYD88* and *CD79* mutations have been associated with disruption of normal peripheral B cell tolerance checkpoints.

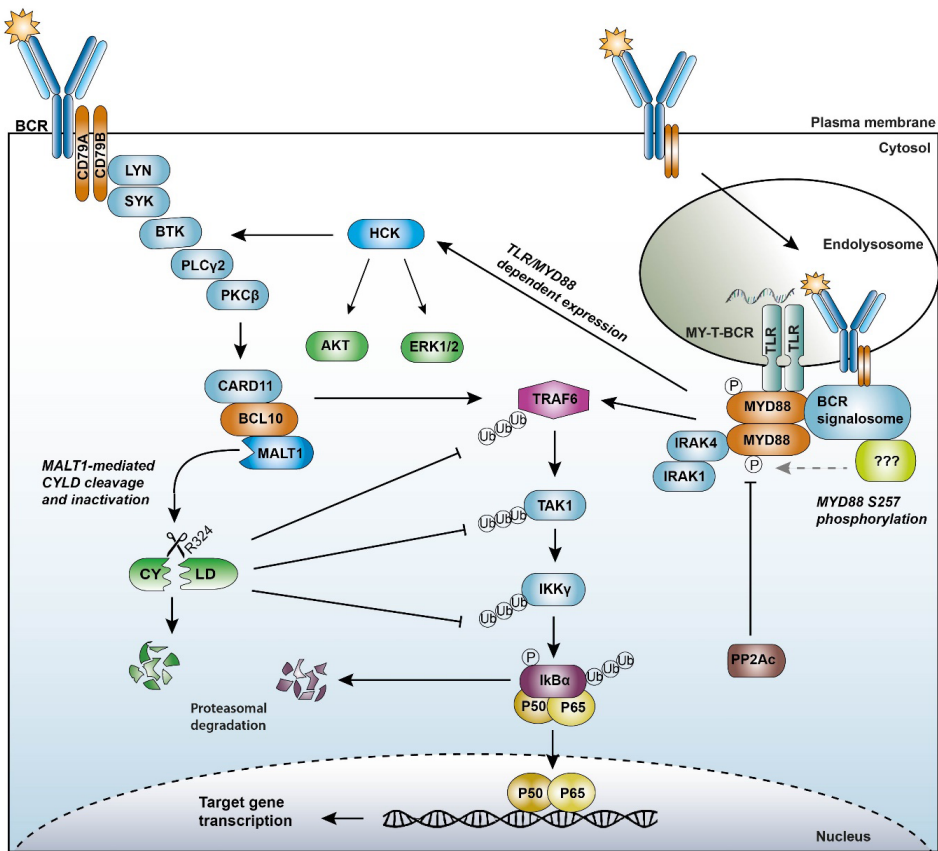


**Figure 2. Schematic representation of potential mechanisms of cross-talk between TLR and BCR signaling.** (1) First, MYD88, TLR9 and the BCR co-localize in endolysosomes, where they form a multiprotein signaling complex (the MY-T-BCR). (2) Second, the deubiquitinating enzyme CYLD hydrolyzes Lys-63-linked polyubiquitin chains of TRAF6, TAK1, and/or IKK-γ. Therefore, CYLD can suppress canonical NF-κB activation downstream of both BCR and TLR signaling. (3) Third, MYD88 activation induces expression of HCK. HCK subsequently activates SYK and BTK, which are key intermediates of BCR signaling. Moreover, HCK activation results in AKT and ERK1/2 pathway activation. (4) Fourth, in MYD88 wildtype cells, MYD88

activation can be mediated through serine 257 phosphorylation. Dephosphorylation of this site is mediated by the phosphatase PP2Ac, but the kinase responsible for phosphorylation of this site remains unknown. Intermediates of BCR signaling could be potential drivers of MYD88 phosphorylation. Abbreviations: SYK, spleen tyrosine kinase; BTK, Bruton's tyrosine kinase; PLC $\gamma$ 2, Phospholipase Cy2; PKC $\beta$ , Protein kinase C $\beta$ ; CARD11, Caspase activation and recruitment domain 11; BCL10, B-cell lymphoma 10; MALT1, Mucosa-associated lymphoid tissue lymphoma translocation protein 1; HCK, hematopoietic cell kinase; PP2Ac, protein phosphatase 2A catalytic subunit  $\alpha$ , TLR, toll-like receptor; MYD88, myeloid differentiation primary response 88; IRAK4/1, interleukin-1 receptor (IL-1R) associated kinase 4/1; TRAF6, TNF receptor associated factor 6; TAB1/2, TGF- $\beta$ -activated kinase 1 binding protein 1/2; TAK1, TGF- $\beta$ -activated kinase 1; IKK $\alpha$ / $\beta$ / $\gamma$ , I $\kappa$ B kinase  $\alpha$ / $\beta$ / $\gamma$ ; I $\kappa$ B $\alpha$ , Inhibitor kappa B- $\alpha$ ; Cylindromatosis, CYLD; Ub, ubiquitin; P, phosphate group.

Jeelall *et al.* demonstrated that lymphoma-associated *CARD11* mutations are sufficient to block self-antigen-induced cell death and promote T cell-independent B-cell proliferation and plasma cell differentiation (81). In contrast, MYD88 L265P was only able to prevent self-antigen-induced cell death when combined with overexpression of *Bcl2*, to counteract Bim-dependent apoptosis. Although MYD88 L265P was insufficient to block self-antigen-induced cell death, its expression did break the tolerance to nucleic acid-sensing TLRs (55). Nucleic acid sensing receptors TLR7 and TLR9 recognize double-stranded RNA and unmethylated CpG-rich DNA sequences, which are highly enriched in microbial nucleic acids, but occasionally also found in self-nucleic acids. Restricted expression of these TLRs on intracellular vesicles should theoretically ensure tolerance to self-nucleic acids, but this tolerance is broken when BCR tolerance mechanisms fall short. Intriguingly, unlike *CARD11* mutations, *CD79B* mutations were unable to protect against self-antigen-induced cell death (82). In addition, the authors demonstrated that whereas *CD79B* mutants markedly increased surface IgM levels, expression of surface IgM was strongly reduced upon expression of *MYD88* L265P. Reduced surface expression resulted from diminished intracellular BCR maturation, which is mechanistically similar to the block in intracellular trafficking observed in anergic B cells chronically stimulated by self-antigens (82, 83). Reduced BCR surface expression represses tonic PI3K-AKT-FOXO1 survival signaling and could potentially explain why the proliferation of MYD88 L265P expressing cells is rapidly terminated. Interestingly, expression of CD79B ITAM mutants or wildtype CD79B counteracted this inhibitory effect of MYD88 L265P on BCR surface expression and rescued B cells from self-antigen-induced deletion *in vivo* (82). These observations naturally raise the question whether B-cell receptor engagement by self-antigens is implicated in chronic BCR signaling in DLBCL cases.

### **A role for self-antigen in the pathogenesis of DLBCL**

There is growing evidence for antigenic stimulation, by either foreign or self-antigen, as a key driver of B-cell lymphoma development (84). However, the role of antigenic stimulation in the development of DLBCL remains incompletely understood. Characteristics of chronic BCR signaling in DLBCL, such as membrane clustering of the BCR, closely resemble antigen-dependent BCR stimulation in normal B cells (59). Also the

finding that *CD79B* ITAM mutations can amplify but not initiate BCR signaling, supports the hypothesis that these lymphomas are still dependent on ongoing BCR stimulation. Examining the immunoglobulin heavy chain variable (*IGHV*) gene usage and Ig mutational status can provide great insight into antigen reactivity in (malignant) B cells. Interestingly, approximately 30% of ABCL DLBCL cases show usage of the *IGHV4-34* segment compared to only 9% in GCB DLBCL cases and 4% in normal B cells (85). In healthy individuals, B cells utilizing *IGHV4-34* are predominantly present in the naive repertoire and underrepresented in the memory compartment (86). Usage of *IGHV4-34* is also enriched in other BCR-dependent lymphomas such as CLL and MCL and frequently associated with intrinsic, germline encoded autoreactivity to self-glycoproteins containing N-acetyl-lactosamine moieties (87, 88). The germline-encoded autoreactivity of *IGHV4-34* requires two motifs within the FR1 region; the AVY and QW motif. *IGHV4-43* expressing B cells of healthy individuals that do enter the memory pool, frequently show mutations within the AVY and/or QW motif, directing them away from self-reactivity. This is in sharp contrast with IgM<sup>+</sup> ABC DLBCL, which were almost exclusively wildtype for both motifs in the FR1 region (85). In addition, over 60% of *IGHV4-43* expressing ABC DLBCL harbor a somatic mutation in a CDR2 NHS motif. Mutations of this motif block N-linked glycosylation, thereby enhancing antigen binding, presumably by abolishing steric hindrance of polysaccharide chains (89).

Montesinos-Rongen *et al.* demonstrated that, in a cohort of 10 PCNSL cases, the *IGHV4-34* segment was used in 50% of cases. Moreover, all *IGHV4-34* expressing PCNSLs in this cohort expressed a wildtype QW motif in the FR1 region, suggesting a high level of autoreactivity (90). In a follow-up study, preferential usage of the *IGHV4-34* gene segment was observed in 36% of cases in a cohort of 50 PCNSL patients (91). The authors observed large differences in both amino acid composition and length of the CDR3 region, arguing against the involvement of a single antigen. In line with this, recombinantly produced antibodies from a panel of PCNSL patients recognized a large number of self-proteins one of them being galectin-3, which is highly expressed in the CNS microenvironment (92). In addition, Spies *et al.* demonstrated high reactivity of recombinantly produced BCRs from 10 PCNSL patients towards different structures of the human cerebellum (93). Likewise, Thurner *et al.* described that 8 out of 12 analyzed PCNSL patients expressed BCRs specific for hyper-N-glycosylated SAMD14 and neurabin-I, 2 which are also predominantly expressed in the CNS (94). Interestingly, Montesinos-Rongen *et al.* showed that reverting somatic mutations to the naïve BCR sequence yielded an auto- and polyreactive BCR in 10 PCNSL cases. Moreover, the authors demonstrated that in the tumor cell derived BCR reactivity towards CNS proteins was increased as a result of somatic hypermutation (95). Therefore, the BCR reactivity towards CNS-associated antigens can, at least partially, explain the unique organ tropism of PCNSL. Also PVRL patients displayed a strikingly biased Ig VH gene

repertoire, with the IGHV4-34 gene being used in 64% of cases compared to 35% in PCNSL or 30% in systemic DLBCL, implying that antigen selection plays a role in PVRL development (96). Another small study showed that the IGHV4-34 segment was used by 4 out of 8 (50%) analyzed primary intraocular lymphoma cases (97).

Also in three *MYD88* and *CD79* mutated DLBCL cell lines it was shown that their respective BCRs are able to recognize distinct self-antigens (85). One of the cell lines expresses a VH4-34<sup>+</sup> BCR, which specifically recognizes n-acetyl-lactosamine residues on glycoproteins on the cell surface. Since *CD79B* and *MYD88* L265P mutations were demonstrated to impede peripheral deletion in murine autoreactive B cells, it is tempting to speculate that these mutations also contribute to breaking the tolerance to self-antigens in these (extranodal) B cell lymphomas.

### Targeted therapy of (MCD) DLBCL

The standard treatment regimen for DLBCL consists of a combination of the anti-CD20-antibody rituximab with CHOP-therapy (cyclophosphamide, doxorubicin, vincristine and prednisone). Since 15% of patients display primary refractory disease and around 25% of patients relapse after an initial response, there is a strong need for the development of novel, targeted therapies (98). Seeing that inhibition of NF- $\kappa$ B activation using IKK $\beta$  inhibitors is associated with substantial on-target toxicity, many studies have focused on developing alternative means to target NF- $\kappa$ B signaling. The main focus has been on the development of BCR pathway inhibitors, with the BTK inhibitor ibrutinib, which is already clinically approved for use in CLL, MCL and WM, being the most promising example (99-101).

The efficacy of the selective, covalent and irreversible BTK inhibitor ibrutinib was evaluated in a phase 1/2 clinical trial involving 80 patients with relapsed or refractory DLBCL. Ibrutinib produced partial responses (PR) in 15% of cases and complete responses (CR) in 10% of cases. Interestingly, in patients with ABC DLBCL the response rate to ibrutinib was 37% compared to only 5% in GCB DLBCL patients (73). Moreover, tumors harboring *CD79B* mutations showed significantly higher response rates than *CD79B* wildtype tumors (55% versus 31%). However, the observation that a large proportion of ibrutinib responders lack *CD79B* mutations further supports the hypothesis that recognition of (self-)antigens drives BCR signaling in these cases. Intriguingly, in lymphomas harboring both *CD79B* ITAM mutations as well as a mutation in *MYD88*, the observed response to ibrutinib was 80%. On the other hand, cases harboring a mutation in *MYD88*, but expressing wildtype *CD79B*, were completely resistant to ibrutinib treatment (83). However, in a phase 1b study in PCNSL, one patient having a *MYD88* L265P mutation, but no *CD79B* mutation, did show responsiveness to ibrutinib monotherapy (102). Likewise, a case report on described an impressive response to ibrutinib monotherapy in a relapsed PCDLBL-LT patient with

mutant *MYD88* and wildtype *CD79B* (103).

The data presented above suggest that IP-associated DLBCL, characterized by a high prevalence of co-occurring *MYD88* and *CD79B* mutations, are specifically sensitive to ibrutinib treatment. Indeed, a small study showed that in 18 PCNSL patients, ibrutinib monotherapy showed clinical activity in 94% of patients (102). Accordingly, Grommes *et al.*, reported clinical responses to ibrutinib in 10 out of 13 (77%) PCNSL patients, including five complete responses (104). A follow-up study, evaluating the sequential combination of ibrutinib with high-dose methotrexate and rituximab showed clinical responses in 12 of 15 (80%) PCNSL patients (105). These preliminary results suggest that other BCR-dependent ABC-type DLBCL cases harboring mutations in *CD79B*, either alone or in combination with *MYD88* L265P, might also be largely responsive to ibrutinib. Indeed, interim analysis of the iLOC phase 2 study, which included 12 PCNSL and 6 PVRL patients, showed efficacy of ibrutinib in 15 out of 18 patients (83%) (106).

Based on these preliminary (pre-)clinical studies, the large phase III randomized Phoenix trial was initiated. This study evaluated the addition of ibrutinib to standard R-CHOP chemotherapy in newly diagnosed non-GCB DLBCL patients (107). In a post-hoc analysis of patients younger than 60 years, ibrutinib plus R-CHOP improved event-free survival (EFS). However, in patients older than 60 years, ibrutinib plus R-CHOP worsened EFS, probably since these patients experienced significantly more toxicity and received fewer cycles of R-CHOP compared to the control group. In 2021, Wilson *et al.* re-analyzed biopsies from Phoenix trial patients and divided them according to the three genetic subtypes that are prevalent in non-GCB DLBCL: MCD, BN2, and N1 (108). The authors demonstrated that in both MCD and N1 DLBCL, the addition of ibrutinib to R-CHOP chemotherapy significantly improved survival of younger patients (age  $\leq 60$  years). Ibrutinib was also beneficial in younger, genetically unassigned, non-GCB DLBCL patients, albeit to a lesser degree. In contrast, younger patients with BN2 DLBCL did not benefit from addition of ibrutinib to R-CHOP. Additionally, the GUIDANCE-01 phase II clinical trial demonstrates efficacy and safety of genetic subtype-guided immunochemotherapy in newly diagnosed DLBCL. For B2N and MCD classified DLBCL the treatment regimen in this study consisted of R-CHOP in combination with ibrutinib (109).

Despite the promising clinical activity in the studies mentioned above, ibrutinib treatment was significantly associated with pulmonary and cerebral *Aspergillus* infections, a result of BTK inhibition in innate immune cells (110). A phase I study in PCNSL indicates that co-administration of isavuconazole, a triazole antifungal agent, could prevent *Aspergillus* infections without affecting safety and efficacy (111). In addition, since ibrutinib irreversibly inhibits a number of alternative kinase targets, more selective BTK inhibitors are being developed. Acalabrutinib, a highly selective, second-generation BTK inhibitor is already

FDA-approved for patients with relapsed CLL and MCL and is currently under evaluation for DLBCL patients (ClinicalTrials.gov identifier: NCT03571308, NCT02112526)(112, 113). Zanubrutinib, a second-generation small-molecule inhibitor of BTK, resulted in an overall response rate (ORR) of 36% in ABC DLBCL patients, similar to ibrutinib (114). Interestingly, the ORR was 50% in DLBCL patients with mutations in both *CD79B* and *MYD88* genes. Moreover, tirabrutinib, another second-generation BTK inhibitor, produced an ORR of 64% in relapsed/refractory PCNSL patients (115).

In addition to BTK inhibitors, various PI3K inhibitors have been evaluated for the treatment of patients with DLBCL. Idelalisib, an oral inhibitor of the delta isoform of PI3K, was approved in 2014 for treatment of CLL, FL and small lymphocytic lymphoma (116). However, idelalisib monotherapy showed very limited activity in relapsed/refractory DLBCL (117). Additional clinical studies investigating idelalisib in combination with monoclonal antibodies or chemotherapy were prematurely discontinued due to severe toxic side effects (118, 119). Interestingly, pre-clinical studies demonstrated that simultaneous inhibition of PI3K- $\delta$  and PI3K- $\alpha$  is required to induce cytotoxicity in ABC DLBCL cells (120, 121). Based on these findings, a phase II trial using copanlisib, a pan-class I PI3K inhibitor, as monotherapy was performed in patients with relapsed/refractory DLBCL (122). In this study, copanlisib demonstrated a manageable safety profile and the ORR was 32% in ABC DLBCL versus 13% in GCB DLBCL patients. Surprisingly, the mutational status of *CD79B* or *MYD88* did not correlate with the overall response to copanlisib treatment. The combination of copanlisib with standard R-CHOP therapy is currently under evaluation in a phase II trial in previously untreated DLBCL patients (ClinicalTrials.gov identifier: NCT04263584). Additionally, targeting mTOR downstream of PI3K resulted in partial responses in ~30% of DLBCL and PCNSL patients (123, 124).

Our recent findings underline that MALT1 inhibitors could be promising therapeutic targets for MCD DLBCL depending on chronic BCR signaling (66). Moreover, inhibition of MALT1 proteolytic activity could be an interesting treatment option for patients with primary or secondary resistance to ibrutinib (125, 126). Whereas the MALT1 inhibitory peptide z-VRPR-fmk and the small molecule inhibitor MI-2 induce killing of ABC DLBCL cells *in vitro* and *in vivo*, these compounds are not suitable for clinical use due to limited potency and specificity (64, 127, 128). The phenothiazine-derivative mepazine and MLT compounds efficiently inhibit MALT1, but have not been studied in clinical trials (129-131). The first-in-human MALT1 inhibitor safimaltib (JNJ-6785663) demonstrated safety and clinical activity in various B-cell malignancies, including DLBCL (132). Next to inhibition of MALT1 protease activity, our studies are relevant for the development of novel therapeutic compounds aimed at downstream effectors in the BCR-MALT1- NF- $\kappa$ B pathway, including TRAF6, TAK1 or IKK (66).

In addition to inhibitors of BCR signaling, pre-clinical studies suggest that *MYD88*-mutated lymphomas can be targeted by IRAK1/4 kinase inhibitors (133, 134). Emavusertib (CA-4948), an oral inhibitor of IRAK4, was evaluated for efficacy and safety in patients with relapsed or refractory hematologic malignancies (ClinicalTrials.gov identifier: NCT03328078). Moreover, the immunomodulatory oligonucleotide (IMO)-8400, a selective antagonist of TLRs 7, 8 and 9, has been demonstrated to inhibit tumor growth in *MYD88* mutant cell line models (135). Two dose-escalation studies using IMO-8400 were performed in 5 WM and 6 DLBCL patients with mutant *MYD88* (ClinicalTrials.gov identifier: NCT02252146, NCT02092909). Also targeting *MYD88* itself by blocking *MYD88* TIR domain dimerization inhibits NF- $\kappa$ B signaling and tumor cell survival of *MYD88* mutated cells (136, 137). In addition, the SRC family tyrosine kinase HCK was identified as a key driver of mutated *MYD88* pro-survival signaling, highlighting the potential of targeting this molecule in MCD DLBCL (56). Our studies demonstrated that HCK also functions as a pro-survival kinase in *MYD88*-wildtype MCL cell lines (57). Interestingly, ibrutinib does not only inhibit BTK, but also inhibits HCK activity through a low-affinity, non-covalent interaction (138). More potent inhibition of HCK activity was observed with A419259, a pre-clinical, pan- SRC family kinase inhibitor. In pre-clinical studies, A419259 strongly induced apoptosis in *MYD88*-mutated WM and ABC DLBCL cell lines (56). The even more potent dual HCK/BTK inhibitor KIN-8194 strongly suppressed the growth and survival of *MYD88*-mutated cell lines and markedly reduced tumor growth in ibrutinib-resistant tumor models (139). Altogether, these findings underline the importance of pursuing clinical trials using inhibitors of TLRs, IRAK 1/4, HCK, or *MYD88* itself.

### Targeted combination therapies

Aggressive (extranodal) B-cell lymphomas depend on a multitude of oncogenic signaling pathways, which all cooperate to promote tumor cell proliferation and survival. Simultaneous inhibition of multiple survival pathways can lead to synergistic tumor cell killing as well as prevent or overcome resistance to existing therapeutic agents. High-throughput drug combinatorial screenings demonstrated that ibrutinib synergistically killed ABC DLBCL cell lines when combined with various PI3K/AKT/mTOR pathway inhibitors, BCL2 family inhibitors, BET bromodomain inhibitors and IRAK4 inhibitors (140, 141). Other pre-clinical studies showed that also inhibitors of JAK1 and PKC synergized with ibrutinib to kill ABC DLBCL cells (142, 143). Figure 3 summarizes the most important signaling pathways for the survival and proliferation of (MCD) DLBCL and the different inhibitors targeting intermediates of these pathways. Although many pre-clinical studies are promising, only a few combination therapies have been evaluated in clinical trials. Combined therapy of ibrutinib and the BCL2 inhibitor venetoclax showed promising safety and efficacy in non-GCB DLBCL patients with BCL2 overexpression (144). Also the triple combination of ibrutinib, lenalidomide, and rituximab demonstrated promising activity and little toxicity in non-GCB DLBCL patients (145). Clinical trials examining

ibrutinib-based combination therapies for extranodal (MCD) DLBCL are mostly limited to small cohorts of PCNSL patients. In 6 PCNSL patients, combination of ibrutinib with the pan-PI3K inhibitor copanlisib showed clinical responses in 67% of PCNSL patients (146). Lenalinomide combined with the new-generation BTK inhibitor orelabrutinib, rituximab, high-dose methotrexate and temozolomide showed an ORR of 87% and a CR rate of 73% in a cohort of 15 PCNSL patients (147).

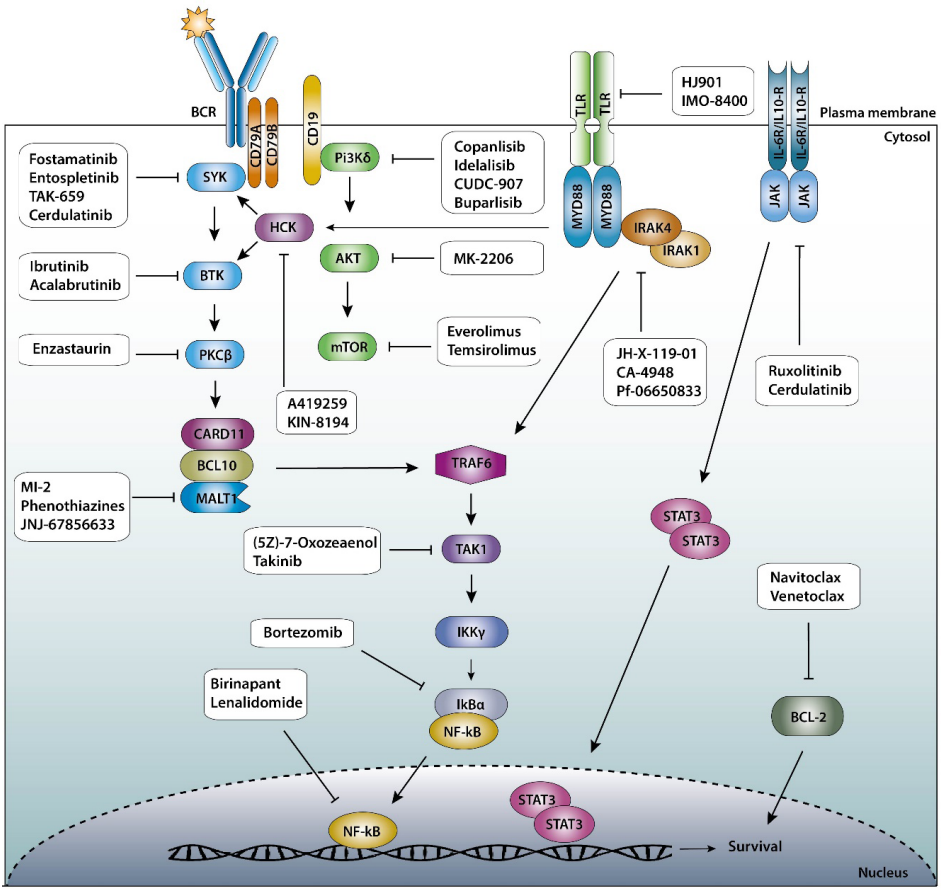


**Figure 3. The most important signaling pathways and potential therapeutic targets in (MCD) DLBCL.** Abbreviations: SYK, spleen tyrosine kinase; BTK, Bruton's tyrosine kinase; PKC $\beta$ , Protein kinase  $\beta$ ; CARD11, Caspase activation and recruitment domain 11; BCL10, B-cell lymphoma 10; MALT1, Mucosa-associated lymphoid tissue lymphoma translocation protein 1; HCK, hematopoietic cell kinase; TLR, toll-like receptor; MYD88, myeloid differentiation primary response 88; IRAK4/1, interleukin-1 receptor (IL-1R) associated kinase 4/1; TRAF6, TNF receptor associated factor 6; TAB1/2, TGF- $\beta$ -activated kinase 1 binding protein 1/2; TAK1, TGF- $\beta$ -activated kinase 1; IKK $\alpha$ / $\beta$ / $\gamma$ , I $\kappa$ B kinase  $\alpha$ / $\beta$ / $\gamma$ ; I $\kappa$ B $\alpha$ , Inhibitor kappa B- $\alpha$ ; IL6/10-R, interleukin 6/10 receptor; JAK, Janus kinase; STAT3, signal transducer and activator of transcription 3; BCL-2, B-cell lymphoma 2;

## CONCLUSIONS AND FUTURE PERSPECTIVES

In this chapter, we shed light on different immune evasion mechanisms and oncogenic TLR/BCR signaling in the pathogenesis of immune-privileged site associated DLBCL. We discussed that these lymphomas hardly employ the PD-1/PD-L1 checkpoint, but use loss of MHC class I and II as primary mechanism of immune evasion. At these extranodal sites, MYD88 L265P mutations co-exist with mutations in CD79A/B ITAM domains at a much higher frequency than expected by chance, implying that these pathways likely cooperate to further drive lymphomagenesis. In PCNSL, self-reactivity towards CNS-associated auto-antigens can partially explain the striking co-occurrence of MYD88 and CD79B mutations as well as the unique affinity of these cells for the CNS microenvironment. Patients with lymphomas harboring MYD88 L265P and CD79A/B mutations can benefit from BCR signalosome inhibitors, such as the BTK inhibitor ibrutinib, but this strategy is largely inefficient in patients that exclusively carry the MYD88 L265P mutation. These patients will presumably benefit from TLR/MYD88/IRAK pathway inhibitors, which are currently in clinical development and evaluated in soon-to-be clinical trials. Moreover, since single drugs are rarely effective in accomplishing complete, long-term remissions, future clinical trials should focus on combining targeted therapies to combat these aggressive lymphomas.

## REFERENCES

1. Wright GW, Huang DW, Phelan JD, Coulibaly ZA, Roulland S, Young RM, et al. A Probabilistic Classification Tool for Genetic Subtypes of Diffuse Large B Cell Lymphoma with Therapeutic Implications. *Cancer Cell*. 2020;37(4):551-68 e14.
2. Nosrati A, Monabati A, Sadeghipour A, Radmanesh F, Safaei A, Movahedinia S. MYC, BCL2, and BCL6 rearrangements in primary central nervous system lymphoma of large B cell type. *Ann Hematol*. 2019;98(1):169-73.
3. Minderman M, Amir A, Kraan W, Schilder-Tol EJM, Oud M, Scheepstra CG, et al. Immune evasion in primary testicular and central nervous system lymphomas: HLA loss rather than 9p24.1/PD-L1/PD-L2 alterations. *Blood*. 2021;138(13):1194-7.
4. Kraan W, Horlings HM, van Keimpema M, Schilder-Tol EJ, Oud ME, Scheepstra C, et al. High prevalence of oncogenic MYD88 and CD79B mutations in diffuse large B-cell lymphomas presenting at immune-privileged sites. *Blood Cancer J*. 2013;3:e139.
5. Chapuy B, Roemer MG, Stewart C, Tan Y, Abo RP, Zhang L, et al. Targetable genetic features of primary testicular and primary central nervous system lymphomas. *Blood*. 2016;127(7):869-81.
6. Schmitz R, Wright GW, Huang DW, Johnson CA, Phelan JD, Wang JQ, et al. Genetics and Pathogenesis of Diffuse Large B-Cell Lymphoma. *N Engl J Med*. 2018;378(15):1396-407.
7. Zolyniak A, Komar D, Debek S, Garbicz F, Pawlak M, Juszczynski P. PIM1 Point Mutations Increase Migration of Diffuse Large B-Cell Lymphoma (DLBCL) Cells. *Blood*. 2023;142:2772.
8. Kraan W, van Keimpema M, Horlings HM, Schilder-Tol EJ, Oud ME, Noorduyn LA, et al. High prevalence of oncogenic MYD88 and CD79B mutations in primary testicular diffuse large B-cell lymphoma. *Leukemia*. 2014;28(3):719-20.
9. Bonzheim I, Sander P, Salmeron-Villalobos J, Susskind D, Szurman P, Gekeler F, et al. The molecular hallmarks of primary and secondary vitreoretinal lymphoma. *Blood Adv*. 2022;6(5):1598-607.
10. Kirkegaard MK, Minderman M, Sjo LD, Pals ST, Eriksen PRG, Heegaard S. Prevalence and prognostic value of MYD88 and CD79B mutations in ocular adnexal large B-cell lymphoma: a reclassification of ocular adnexal large B-cell lymphoma. *Br J Ophthalmol*. 2021.
11. Eriksen PRG, de Groot F, Clasen-Linde E, de Nully Brown P, de Groen RAL, Melchior LC, et al. Sinonasal diffuse large B-cell lymphoma: molecular profiling identifies subtypes with distinctive prognosis and targetable genetic features *Blood Adv*. 2024 Feb 7: Online ahead of print.
12. Barker CF, Billingham RE. Immunologically privileged sites. *Adv Immunol*. 1977;25:1-54.
13. Streilein JW. Peripheral tolerance induction: lessons from immune privileged sites and tissues. *Transplant Proc*. 1996;28(4):2066-70.
14. Shechter R, London A, Schwartz M. Orchestrated leukocyte recruitment to immune-privileged sites: absolute barriers versus educational gates. *Nat Rev Immunol*. 2013;13(3):206-18.
15. Green MR, Monti S, Rodig SJ, Juszczynski P, Currie T, O'Donnell E, et al. Integrative analysis reveals selective 9p24.1 amplification, increased PD-1 ligand expression, and further induction via JAK2 in nodular sclerosing Hodgkin lymphoma and primary mediastinal large B-cell lymphoma. *Blood*. 2010;116(17):3268-77.
16. Gandhi MK, Hoang T, Law SC, Brosda S, O'Rourke K, Tobin JWD, et al. EBV-associated primary CNS lymphoma occurring after immunosuppression is a distinct immunobiological entity. *Blood*. 2021;137(11):1468-77.
17. Hudson K, Cross N, Jordan-Mahy N, Leyland R. The Extrinsic and Intrinsic Roles of PD-L1 and Its Receptor PD-1: Implications for Immunotherapy Treatment. *Front Immunol*. 2020;11:568931.
18. Ansell SM, Lesokhin AM, Borrello I, Halwani A, Scott EC, Gutierrez M, et al. PD-1 blockade with nivolumab in relapsed or refractory Hodgkin's lymphoma. *N Engl J Med*. 2015;372(4):311-9.
19. Armand P, Rodig S, Melnichenko V, Thieblemont C, Bouabdallah K, Tumen G, et al. Pembrolizumab in Relapsed or Refractory Primary Mediastinal Large B-Cell Lymphoma. *J Clin Oncol*. 2019;37(34):3291-9.
20. Horvath KM, Herbst M, Zhou H, Zhang H, Noah TL, Jaspers I. Nasal lavage natural killer cell function is suppressed in smokers after live attenuated influenza virus. *Respir Res*. 2011;12(1):102.
21. Ning Z, Liu Y, Guo D, Lin WJ, Tang Y. Natural killer cells in the central nervous system. *Cell Commun Signal*. 2023;21(1):341.
22. Weissinger SE, Dugge R, Disch M, Barth TF, Bloehdorn J, Zahn M, et al. Targetable alterations in primary extranodal diffuse large B-cell lymphoma. *EJHaem*. 2022;3(3):688-97.
23. Jordanova ES, Riemersma SA, Philippo K, Schuurin E, Kluin PM. Beta2-microglobulin aberrations in diffuse large B-cell lymphoma of the testis and the central nervous system. *Int J Cancer*. 2003;103(3):393-8.
24. Challa-Malladi M, Lieu YK, Califano O, Holmes AB, Bhagat G, Murty VV, et al. Combined genetic inactivation of beta2-Microglobulin and CD58 reveals frequent escape from immune recognition in diffuse large B cell lymphoma. *Cancer Cell*. 2011;20(6):728-40.
25. Fangazio M, Ladewig E, Gomez K, Garcia-Ibanez L, Kumar R, Teruya-Feldstein J, et al. Genetic mechanisms of HLA-I loss and immune escape in diffuse large B cell lymphoma. *Proc Natl Acad Sci U S A*. 2021;118(22).
26. Alame M, Cornillot E, Cacheux V, Rigau V, Costes-Martineau V, Lacheretz-Szablewski V, Colinge J. The immune

- contexture of primary central nervous system diffuse large B cell lymphoma associates with patient survival and specific cell signaling. *Theranostics*. 2021;11(8):3565-79.
27. Leivonen SK, Pollari M, Bruck O, Pellinen T, Autio M, Karjalainen-Lindsberg ML, et al. T-cell inflamed tumor microenvironment predicts favorable prognosis in primary testicular lymphoma. *Haematologica*. 2019;104(2):338-46.
  28. Riemersma SA, Jordanova ES, Schop RF, Filippo K, Looijenga LH, Schuurung E, Kluin PM. Extensive genetic alterations of the HLA region, including homozygous deletions of HLA class II genes in B-cell lymphomas arising in immune-privileged sites. *Blood*. 2000;96(10):3569-77.
  29. Radke J, Ishaque N, Koll R, Gu Z, Schumann E, Sieverling L, et al. The genomic and transcriptional landscape of primary central nervous system lymphoma. *Nat Commun*. 2022;13(1):2558.
  30. Dubois S, Viailly PJ, Mareschal S, Bohers E, Bertrand P, Ruminy P, et al. Next-Generation Sequencing in Diffuse Large B-Cell Lymphoma Highlights Molecular Divergence and Therapeutic Opportunities: a LYSA Study. *Clin Cancer Res*. 2016;22(12):2919-28.
  31. Rimsza LM, Roberts RA, Miller TP, Unger JM, LeBlanc M, Brazier RM, et al. Loss of MHC class II gene and protein expression in diffuse large B-cell lymphoma is related to decreased tumor immunosurveillance and poor patient survival regardless of other prognostic factors: a follow-up study from the Leukemia and Lymphoma Molecular Profiling Project. *Blood*. 2004;103(11):4251-8.
  32. Van Kaer L, Ashton-Rickardt PG, Ploegh HL, Tonegawa S. TAP1 mutant mice are deficient in antigen presentation, surface class I molecules, and CD4-8+ T cells. *Cell*. 1992;71(7):1205-14.
  33. Koens L, Zoutman WH, Ngarmmlertsirichai P, Przybylski GK, Grabarczyk P, Vermeer MH, et al. Nuclear factor-kappaB pathway-activating gene aberrancies in primary cutaneous large B-cell lymphoma, leg type. *J Invest Dermatol*. 2014;134(1):290-2.
  34. Mareschal S, Pham-Ledard A, Viailly PJ, Dubois S, Bertrand P, Maingonnat C, et al. Identification of Somatic Mutations in Primary Cutaneous Diffuse Large B-Cell Lymphoma, Leg Type by Massive Parallel Sequencing. *Journal of Investigative Dermatology*. 2017;137(9):1984-94.
  35. Zhou XA, Louissaint A, Jr., Wenzel A, Yang J, Martinez-Escala ME, Moy AP, et al. Genomic Analyses Identify Recurrent Alterations in Immune Evasion Genes in Diffuse Large B-Cell Lymphoma, Leg Type. *J Invest Dermatol*. 2018;138(11):2365-76.
  36. Schrader AMR, Jansen PM, Willemze R, Vermeer MH, Cleton-Jansen AM, Somers SF, et al. High prevalence of MYD88 and CD79B mutations in intravascular large B-cell lymphoma. *Blood*. 2018;131(18):2086-9.
  37. Shimada K, Yoshida K, Suzuki Y, Iriyama C, Inoue Y, Sanada M, et al. Frequent genetic alterations in immune checkpoint-related genes in intravascular large B-cell lymphoma. *Blood*. 2021;137(11):1491-502.
  38. Menguy S, Prochazkova-Carlotti M, Beylot-Barry M, Saltel F, Vergier B, Merlio JP, Pham-Ledard A. PD-L1 and PD-L2 Are Differentially Expressed by Macrophages or Tumor Cells in Primary Cutaneous Diffuse Large B-Cell Lymphoma, Leg Type. *Am J Surg Pathol*. 2018;42(3):326-34.
  39. Ou A, Sumrall A, Phuphanich S, Spetzler D, Gatalica Z, Xiu J, et al. Primary CNS lymphoma commonly expresses immune response biomarkers. *Neurooncol Adv*. 2020;2(1):vdaa018.
  40. Xu-Monette ZY, Li J, Xia Y, Crossley B, Bremel RD, Miao Y, et al. Immunoglobulin somatic hypermutation has clinical impact in DLBCL and potential implications for immune checkpoint blockade and neoantigen-based immunotherapies. *J Immunother Cancer*. 2019;7(1):272.
  41. Zorofchian S, El-Achi H, Yan Y, Esquenazi Y, Ballester LY. Characterization of genomic alterations in primary central nervous system lymphomas. *J Neurooncol*. 2018;140(3):509-17.
  42. Cho J, Yoon SE, Kim SJ, Ko YH, Kim WS. Comparison of tumor mutation burden of 300 various non-Hodgkin lymphomas using panel based massively parallel sequencing. *BMC Cancer*. 2021;21(1):972.
  43. Montesinos-Rongen M, Van Roost D, Schaller C, Wiestler OD, Deckert M. Primary diffuse large B-cell lymphomas of the central nervous system are targeted by aberrant somatic hypermutation. *Blood*. 2004;103(5):1869-75.
  44. Deutsch AJA, Agelsreiter A, Staber PB, Beham A, Linkesch W, Guelly C, et al. MALT lymphoma and extranodal diffuse large B-cell lymphoma are targeted by aberrant somatic hypermutation. *Blood*. 2006;109(8):3500-4.
  45. Chen C, Liu S, Jiang X, Huang L, Chen F, Wei X, et al. Tumor mutation burden estimated by a 69-gene-panel is associated with overall survival in patients with diffuse large B-cell lymphoma. *Exp Hematol Oncol*. 2021;10(1):20.
  46. Chapuy B, Stewart C, Dunford AJ, Kim J, Kamburov A, Redd RA, et al. Molecular subtypes of diffuse large B cell lymphoma are associated with distinct pathogenic mechanisms and outcomes. *Nat Med*. 2018;24(5):679-90.
  47. Frick M, Bettstetter M, Bertz S, Schwarz-Furlan S, Hartmann A, Richter T, et al. Mutational frequencies of CD79B and MYD88 vary greatly between primary testicular DLBCL and gastrointestinal DLBCL. *Leuk Lymphoma*. 2018;59(5):1260-3.
  48. Xu Y, Li J, Ouyang J, Li J, Xu J, Zhang Q, et al. Prognostic relevance of protein expression, clinical factors, and MYD88 mutation in primary bone lymphoma. *Oncotarget*. 2017;8(39):65609-19.
  49. de Groen RAL, van Eijk R, Bohringer S, van Wezel T, Raghoo R, Ruano D, et al. Frequent mutated B2M, EZH2, IRF8, and TNFRSF14 in primary bone diffuse large B-cell lymphoma reflect a GCB phenotype. *Blood Adv*.

- 2021;5(19):3760-75.
50. Ngo VN, Young RM, Schmitz R, Jhavar S, Xiao W, Lim KH, et al. Oncogenically active MYD88 mutations in human lymphoma. *Nature*. 2011;470(7332):115-9.
  51. Gachard N, PARRENS M, Soubeyran I, Petit B, Marfak A, Rizzo D, et al. IGHV gene features and MYD88 L265P mutation separate the three marginal zone lymphoma entities and Waldenstrom macroglobulinemia/lymphoplasmacytic lymphomas. *Leukemia*. 2013;27(1):183-9.
  52. Dubois S, Viailly PJ, Bohers E, Bertrand P, Ruminy P, Marchand V, et al. Biological and Clinical Relevance of Associated Genomic Alterations in MYD88 L265P and Non-L265P Mutated Diffuse Large B-Cell Lymphoma: Analysis of 361 Cases. *Blood*. 2016;128(22).
  53. Avbelj M, Wolz OO, Fekonja O, Bencina M, Repic M, Mavri J, et al. Activation of lymphoma-associated MyD88 mutations via allosterically-induced TIR-domain oligomerization. *Blood*. 2014;124(26):3896-904.
  54. Phelan JD, Young RM, Webster DE, Roulland S, Wright GW, Kasbekar M, et al. A multiprotein supercomplex controlling oncogenic signalling in lymphoma. *Nature*. 2018;560(7718):387-91.
  55. Wang JQ, Jeelall YS, Beutler B, Horikawa K, Goodnow CC. Consequences of the recurrent MYD88(L265P) somatic mutation for B cell tolerance. *J Exp Med*. 2014;211(3):413-26.
  56. Yang G, Buhrlage SJ, Tan L, Liu X, Chen J, Xu L, et al. HCK is a survival determinant transactivated by mutated MYD88, and a direct target of ibrutinib. *Blood*. 2016;127(25):3237-52.
  57. Lantermans HC, Minderman M, Kuil A, Kersten MJ, Pals ST, Spaargaren M. Identification of the SRC-family tyrosine kinase HCK as a therapeutic target in mantle cell lymphoma. *Leukemia*. 2021;35(3):881-6.
  58. Davis RE, Ngo VN, Lenz G, Tolar P, Young RM, Romesser PB, et al. Chronic active B-cell-receptor signalling in diffuse large B-cell lymphoma. *Nature*. 2010;463(7277):88-92.
  59. Tolar P, Hanna J, Krueger PD, Pierce SK. The constant region of the membrane immunoglobulin mediates B cell-receptor clustering and signaling in response to membrane antigens. *Immunity*. 2009;30(1):44-55.
  60. Gazumyan A, Reichlin A, Nussenzweig MC. Ig beta tyrosine residues contribute to the control of B cell receptor signaling by regulating receptor internalization. *J Exp Med*. 2006;203(7):1785-94.
  61. Busman-Sahay K, Drake L, Sitaram A, Marks M, Drake JR. Cis and trans regulatory mechanisms control AP2-mediated B cell receptor endocytosis via select tyrosine-based motifs. *PLoS One*. 2013;8(1):e54938.
  62. Chan VW, Meng F, Soriano P, DeFranco AL, Lowell CA. Characterization of the B lymphocyte populations in Lyn-deficient mice and the role of Lyn in signal initiation and down-regulation. *Immunity*. 1997;7(1):69-81.
  63. Ma H, Yankeel TM, Hu J, Asai DJ, Harrison ML, Geahlen RL. Visualization of Syk-antigen receptor interactions using green fluorescent protein: differential roles for Syk and Lyn in the regulation of receptor capping and internalization. *J Immunol*. 2001;166(3):1507-16.
  64. Ferch U, Kloos B, Gewies A, Pfander V, Duwel M, Peschel C, et al. Inhibition of MALT1 protease activity is selectively toxic for activated B cell-like diffuse large B cell lymphoma cells. *J Exp Med*. 2009;206(11):2313-20.
  65. Staal J, Driege Y, Bekaert T, Demeyer A, Muylaert D, Van Damme P, et al. T-cell receptor-induced JNK activation requires proteolytic inactivation of CYLD by MALT1. *EMBO J*. 2011;30(9):1742-52.
  66. Minderman M, Lantermans HC, Gruneberg LJ, Cillessen S, Bende RJ, van Noesel CJM, et al. MALT1-dependent cleavage of CYLD promotes NF-kappaB signaling and growth of aggressive B-cell receptor-dependent lymphomas. *Blood Cancer J*. 2023;13(1):37.
  67. Boone DL, Turer EE, Lee EG, Ahmad RC, Wheeler MT, Tsui C, et al. The ubiquitin-modifying enzyme A20 is required for termination of Toll-like receptor responses. *Nat Immunol*. 2004;5(10):1052-60.
  68. Yoshida H, Jono H, Kai H, Li JD. The tumor suppressor cylindromatosis (CYLD) acts as a negative regulator for toll-like receptor 2 signaling via negative cross-talk with TRAF6 AND TRAF7. *J Biol Chem*. 2005;280(49):41111-21.
  69. Lee BC, Miyata M, Lim JH, Li JD. Deubiquitinase CYLD acts as a negative regulator for bacterium NTHi-induced inflammation by suppressing K63-linked ubiquitination of MyD88. *Proc Natl Acad Sci U S A*. 2016;113(2):E165-71.
  70. Wimberger N, Ober F, Avar G, Grau M, Xu W, Lenz G, et al. Oncogene-induced MALT1 protease activity drives posttranscriptional gene expression in malignant lymphomas. *Blood*. 2023;142(23):1985-2001.
  71. Yang G, Zhou YS, Liu X, Xu L, Cao Y, Manning RJ, et al. A mutation in MYD88 (L265P) supports the survival of lymphoplasmacytic cells by activation of Bruton tyrosine kinase in Waldenstrom macroglobulinemia. *Blood*. 2013;122(7):1222-32.
  72. Munshi M, Liu X, Chen JG, Xu L, Tsakmaklis N, Demos MG, et al. SYK is activated by mutated MYD88 and drives pro-survival signaling in MYD88 driven B-cell lymphomas. *Blood Cancer J*. 2020;10(1):12.
  73. Wilson WH, Young RM, Schmitz R, Yang Y, Pittaluga S, Wright G, et al. Targeting B cell receptor signaling with ibrutinib in diffuse large B cell lymphoma. *Nat Med*. 2015;21(8):922-6.
  74. Munshi M, Liu X, Kofides A, Tsakmaklis N, Guerrero ML, Hunter ZR, et al. A new role for the SRC family kinase HCK as a driver of SYK activation in MYD88 mutated lymphomas. *Blood Adv*. 2022.
  75. Minderman M, Lantermans H, van der Zwaan C, Hoogendijk AJ, van den Biggelaar M, Kersten MJ, et al. The oncogenic human B-cell lymphoma MYD88 L265P mutation genocopies activation by phosphorylation at the Toll/interleukin-1 receptor (TIR) domain. *Blood Cancer J*. 2023;13(1):125.

76. Vyncke L, Bovijn C, Pauwels E, Van Acker T, Ruysinck E, Burg E, et al. Reconstructing the TIR Side of the Myddosome: a Paradigm for TIR-TIR Interactions. *Structure*. 2016;24(3):437-47.
77. Loiarro M, Volpe E, Ruggiero V, Gallo G, Furlan R, Maiorino C, et al. Mutational analysis identifies residues crucial for homodimerization of myeloid differentiation factor 88 (MyD88) and for its function in immune cells. *J Biol Chem*. 2013;288(42):30210-22.
78. Xie L, Liu C, Wang L, Gunawardena HP, Yu Y, Du R, et al. Protein phosphatase 2A catalytic subunit alpha plays a MyD88-dependent, central role in the gene-specific regulation of endotoxin tolerance. *Cell Rep*. 2013;3(3):678-88.
79. Oliver PM, Vass T, Kappler J, Marrack P. Loss of the proapoptotic protein, Bim, breaks B cell energy. *J Exp Med*. 2006;203(3):731-41.
80. Akerlund J, Getahun A, Cambier JC. B cell expression of the SH2-containing inositol 5-phosphatase (SHIP-1) is required to establish energy to high affinity, proteinacious autoantigens. *J Autoimmun*. 2015;62:45-54.
81. Jeelall YS, Wang JQ, Law HD, Domaschek H, Fung HK, Kallies A, et al. Human lymphoma mutations reveal CARD11 as the switch between self-antigen-induced B cell death or proliferation and autoantibody production. *J Exp Med*. 2012;209(11):1907-17.
82. Wang JQ, Jeelall YS, Humburg P, Batchelor EL, Kaya SM, Yoo HM, et al. Synergistic cooperation and crosstalk between MYD88(L265P) and mutations that dysregulate CD79B and surface IgM. *J Exp Med*. 2017;214(9):2759-76.
83. Bell SE, Goodnow CC. A selective defect in IgM antigen receptor synthesis and transport causes loss of cell surface IgM expression on tolerant B lymphocytes. *EMBO J*. 1994;13(4):816-26.
84. Niemann CU, Wiestner A. B-cell receptor signaling as a driver of lymphoma development and evolution. *Semin Cancer Biol*. 2013;23(6):410-21.
85. Young RM, Wu T, Schmitz R, Dawood M, Xiao W, Phelan JD, et al. Survival of human lymphoma cells requires B-cell receptor engagement by self-antigens. *Proc Natl Acad Sci U S A*. 2015;112(44):13447-54.
86. Pugh-Bernard AE, Silverman GJ, Cappione AJ, Villano ME, Ryan DH, Insel RA, Sanz I. Regulation of inherently autoreactive VH4-34 B cells in the maintenance of human B cell tolerance. *J Clin Invest*. 2001;108(7):1061-70.
87. Fais F, Ghiotto F, Hashimoto S, Sellars B, Valetto A, Allen SL, et al. Chronic lymphocytic leukemia B cells express restricted sets of mutated and unmutated antigen receptors. *J Clin Invest*. 1998;102(8):1515-25.
88. Cappione AJ, Pugh-Bernard AE, Anolik JH, Sanz I. Lupus IgG VH4.34 antibodies bind to a 220-kDa glycoform of CD45/B220 on the surface of human B lymphocytes. *J Immunol*. 2004;172(7):4298-307.
89. Sabouri Z, Schofield P, Horikawa K, Spierings E, Kipling D, Randall KL, et al. Redemption of autoantibodies on anergic B cells by variable-region glycosylation and mutation away from self-reactivity. *Proc Natl Acad Sci U S A*. 2014;111(25):E2567-75.
90. Montesinos-Rongen M, Kuppers R, Schluter D, Spieker T, Van Roost D, Schaller C, et al. Primary central nervous system lymphomas are derived from germinal-center B cells and show a preferential usage of the V4-34 gene segment. *Am J Pathol*. 1999;155(6):2077-86.
91. Montesinos-Rongen M, Purschke F, Kuppers R, Deckert M. Immunoglobulin repertoire of primary lymphomas of the central nervous system. *J Neuropathol Exp Neurol*. 2014;73(12):1116-25.
92. Montesinos-Rongen M, Purschke FG, Brunn A, May C, Nordhoff E, Marcus K, Deckert M. Primary Central Nervous System (CNS) Lymphoma B Cell Receptors Recognize CNS Proteins. *J Immunol*. 2015;195(3):1312-9.
93. Spies E, Fichtner M, Muller F, Krasemann S, Illerhaus G, Glatzel M, et al. Comment on "Primary Central Nervous System (CNS) Lymphoma B Cell Receptors Recognize CNS Proteins". *J Immunol*. 2015;195(10):4549-50.
94. Thurner L, Preuss KD, Bewarder M, Kemele M, Fadle N, Regitz E, et al. Hyper-N-glycosylated SAMD14 and neurabin-I as driver autoantigens of primary central nervous system lymphoma. *Blood*. 2018;132(26):2744-53.
95. Montesinos-Rongen M, Terrao M, May C, Marcus K, Blumcke I, Hellmich M, et al. The process of somatic hypermutation increases polyreactivity for central nervous system antigens in primary central nervous system lymphoma. *Haematologica*. 2021;106(3):708-17.
96. Belhouachi N, Xochelli A, Boudjoghra M, Lesty C, Cassoux N, Fardeau C, et al. Primary vitreoretinal lymphomas display a remarkably restricted immunoglobulin gene repertoire. *Blood Adv*. 2020;4(7):1357-66.
97. Coupland SE, Hummel M, Muller HH, Stein H. Molecular analysis of immunoglobulin genes in primary intraocular lymphoma. *Invest Ophthalmol Vis Sci*. 2005;46(10):3507-14.
98. Coiffier B, Lepage E, Briere J, Herbrecht R, Tilly H, Bouabdallah R, et al. CHOP chemotherapy plus rituximab compared with CHOP alone in elderly patients with diffuse large-B-cell lymphoma. *N Engl J Med*. 2002;346(4):235-42.
99. Byrd JC, Furman RR, Coutre SE, Flinn IW, Burger JA, Blum KA, et al. Targeting BTK with ibrutinib in relapsed chronic lymphocytic leukemia. *N Engl J Med*. 2013;369(1):32-42.
100. Wang ML, Rule S, Martin P, Goy A, Auer R, Kahl BS, et al. Targeting BTK with ibrutinib in relapsed or refractory mantle-cell lymphoma. *N Engl J Med*. 2013;369(6):507-16.
101. Treon SP, Tripsas CK, Meid K, Warren D, Varma G, Green R, et al. Ibrutinib in previously treated Waldenstrom's

- macroglobulinemia. *N Engl J Med.* 2015;372(15):1430-40.
102. Lionakis MS, Dunleavy K, Roschewski M, Widemann BC, Butman JA, Schmitz R, et al. Inhibition of B Cell Receptor Signaling by Ibrutinib in Primary CNS Lymphoma. *Cancer Cell.* 2017;31(6):833-43 e5.
  103. Deng AL, Kim YR, Lichtenstein EA, O'Connor OA, Deng C. Combination of ibrutinib and chemotherapy produced a durable remission in multiply relapsed diffuse large B-cell lymphoma leg type with mutant MYD88 and wildtype CD79. *Haematologica.* 2017;102(7):e275-e7.
  104. Grommes C, Pastore A, Palaskas N, Tang SS, Campos C, Schartz D, et al. Ibrutinib Unmasks Critical Role of Bruton Tyrosine Kinase in Primary CNS Lymphoma. *Cancer Discov.* 2017;7(9):1018-29.
  105. Grommes C, Tang SS, Wolfe J, Kaley TJ, Daras M, Pentsova EI, et al. Phase 1b trial of an ibrutinib-based combination therapy in recurrent/refractory CNS lymphoma. *Blood.* 2019;133(5):436-45.
  106. Choquet S, Houillier C, Bijou F, Houot R, Boyle E, Gressin R, et al. Ibrutinib Monotherapy in Relapse or Refractory Primary CNS Lymphoma (PCNSL) and Primary Vitreo-Retinal Lymphoma (PVRL). Result of the Interim Analysis of the iLOC Phase II Study from the Lysa and the French LOC Network. *Blood.* 2016;128(22):784-.
  107. Younes A, Sehn LH, Johnson P, Zinzani PL, Hong X, Zhu J, et al. Randomized Phase III Trial of Ibrutinib and Rituximab Plus Cyclophosphamide, Doxorubicin, Vincristine, and Prednisone in Non-Germinal Center B-Cell Diffuse Large B-Cell Lymphoma. *J Clin Oncol.* 2019;37(15):1285-95.
  108. Wilson WH, Wright GW, Huang DW, Hodkinson B, Balasubramanian S, Fan Y, et al. Effect of ibrutinib with R-CHOP chemotherapy in genetic subtypes of DLBCL. *Cancer Cell.* 2021;39(12):1643-53 e3.
  109. Zhang MC, Tian S, Fu D, Wang L, Cheng S, Yi HM, et al. Genetic subtype-guided immunochemotherapy in diffuse large B cell lymphoma: The randomized GUIDANCE-01 trial. *Cancer Cell.* 2023;41(10):1705-16 e5.
  110. Grommes C, Younes A. Ibrutinib in PCNSL: The Curious Cases of Clinical Responses and Aspergillosis. *Cancer Cell.* 2017;31(6):731-3.
  111. Roschewski M, Melani C, Lakhotia R, Pittaluga S, Phelan JD, Peer C, et al. Phase 1 Study of Escalating Doses of Ibrutinib and Temozolomide, Etoposide, Liposomal Doxorubicin, Dexamethasone, Rituximab (TEDDI-R) with Isavuconazole for Relapsed and Refractory Primary CNS Lymphoma. *Blood.* 2020;136(Supplement 1):12-3.
  112. Byrd JC, Harrington B, O'Brien S, Jones JA, Schuh A, Devereux S, et al. Acabrutinib (ACP-196) in Relapsed Chronic Lymphocytic Leukemia. *N Engl J Med.* 2016;374(4):323-32.
  113. Girard J, Reneau J, Devata S, Wilcox RA, Kaminski MS, Mercer J, et al. Evaluating Acabrutinib In The Treatment Of Mantle Cell Lymphoma: Design, Development, And Place In Therapy. *Onco Targets Ther.* 2019;12:8003-14.
  114. Yang H, Xiang B, Song Y, Zhang H, Zhao W, Zou D, et al. Zanubrutinib monotherapy for relapsed or refractory non-germinal center diffuse large B-cell lymphoma. *Blood Adv.* 2022;6(6):1629-36.
  115. Narita Y, Nagane M, Mishima K, Terui Y, Arakawa Y, Yonezawa H, et al. Phase I/II study of tirabrutinib, a second-generation Bruton's tyrosine kinase inhibitor, in relapsed/refractory primary central nervous system lymphoma. *Neuro Oncol.* 2021;23(1):122-33.
  116. Yang Q, Modi P, Newcomb T, Queva C, Gandhi V. Idelalisib: First-in-Class PI3K Delta Inhibitor for the Treatment of Chronic Lymphocytic Leukemia, Small Lymphocytic Leukemia, and Follicular Lymphoma. *Clin Cancer Res.* 2015;21(7):1537-42.
  117. Fjorden K, Ekberg S, Kuric N, Smedby KE, Lagerlof I, Larsen TS, et al. Idelalisib in relapsed/refractory diffuse large B-cell lymphoma: results from a Nordic Lymphoma Group phase II trial. *Br J Haematol.* 2022;196(2):437-40.
  118. Cheah CY, Nastoupil LJ, Neelapu SS, Forbes SG, Oki Y, Fowler NH. Lenalidomide, idelalisib, and rituximab are unacceptably toxic in patients with relapsed/refractory indolent lymphoma. *Blood.* 2015;125(21):3357-9.
  119. Barr PM, Saylor GB, Spurgeon SE, Cheson BD, Greenwald DR, O'Brien SM, et al. Phase 2 study of idelalisib and entospletinib: pneumonitis limits combination therapy in relapsed refractory CLL and NHL. *Blood.* 2016;127(20):2411-5.
  120. Erdmann T, Kleiner P, Lynch JT, Grau M, Vockova P, Molinsky J, et al. Sensitivity to PI3K and AKT inhibitors is mediated by divergent molecular mechanisms in subtypes of DLBCL. *Blood.* 2017;130(3):310-22.
  121. Paul J, Soujon M, Wengner AM, Zitzmann-Kolbe S, Sturz A, Haik K, et al. Simultaneous Inhibition of PI3Kdelta and PI3Kalpha Induces ABC-DLBCL Regression by Blocking BCR-Dependent and -Independent Activation of NF-kappaB and AKT. *Cancer Cell.* 2017;31(1):64-78.
  122. Lenz G, Hawkes E, Verhoef G, Haioun C, Thyve Lim S, Seog Heo D, et al. Single-agent activity of phosphatidylinositol 3-kinase inhibition with copanlisib in patients with molecularly defined relapsed or refractory diffuse large B-cell lymphoma. *Leukemia.* 2020;34(8):2184-97.
  123. Witzig TE, Reeder CB, LaPlant BR, Gupta M, Johnston PB, Micallef IN, et al. A phase II trial of the oral mTOR inhibitor everolimus in relapsed aggressive lymphoma. *Leukemia.* 2011;25(2):341-7.
  124. Korfel A, Schlegel U, Herrlinger U, Dreyling M, Schmidt C, von Baumgarten L, et al. Phase II Trial of Temsirolimus for Relapsed/Refractory Primary CNS Lymphoma. *J Clin Oncol.* 2016;34(15):1757-63.
  125. Jiang VC, Liu Y, Lian J, Huang S, Jordan A, Cai Q, et al. Cotargeting of BTK and MALT1 overcomes resistance to BTK inhibitors in mantle cell lymphoma. *J Clin Invest.* 2023;133(3).
  126. Saba NS, Wong DH, Tanios G, Iyer JR, Lobelle-Rich P, Dadashian EL, et al. MALT1 Inhibition Is Efficacious in

- Both Naive and Ibrutinib-Resistant Chronic Lymphocytic Leukemia. *Cancer Res.* 2017;77(24):7038-48.
127. Fontan L, Yang C, Kabaleeswaran V, Volpon L, Osborne MJ, Beltran E, et al. MALT1 small molecule inhibitors specifically suppress ABC-DLBCL in vitro and in vivo. *Cancer Cell.* 2012;22(6):812-24.
  128. O'Neill TJ, Tofaute MJ, Krappmann D. Function and targeting of MALT1 paracaspase in cancer. *Cancer Treat Rev.* 2023;117:102568.
  129. Nagel D, Spranger S, Vincendeau M, Grau M, Raffeggerst S, Kloos B, et al. Pharmacologic inhibition of MALT1 protease by phenothiazines as a therapeutic approach for the treatment of aggressive ABC-DLBCL. *Cancer Cell.* 2012;22(6):825-37.
  130. Martin K, Junker U, Tritto E, Sutter E, Rubic-Schneider T, Morgan H, et al. Pharmacological Inhibition of MALT1 Protease Leads to a Progressive IPEX-Like Pathology. *Front Immunol.* 2020;11:745.
  131. Pissot Soldermann C, Simic O, Renatus M, Erbel P, Melkko S, Wartmann M, et al. Discovery of Potent, Highly Selective, and In Vivo Efficacious, Allosteric MALT1 Inhibitors by Iterative Scaffold Morphing. *J Med Chem.* 2020;63(23):14576-93.
  132. Kalac M, Hertzberg M, Cheah C, Ribrag V, Abrisquet Acosta P, Opat S, et al. P624: PHASE 1 STUDY OF JNJ-67856633, A FIRST-IN-HUMAN HIGHLY SELECTIVE MALT1 INHIBITOR, IN RELAPSED/REFRACTORY (R/R) B-CELL NON-HODGKIN LYMPHOMA (B-NHL) AND CHRONIC LYMPHOCYTIC LEUKEMIA (CLL). LID - e60782b9. (2572-9241 (Electronic)).
  133. Scott JS, Degorce SL, Anjum R, Culshaw J, Davies RDM, Davies NL, et al. Discovery and Optimization of Pyrrolopyrimidine Inhibitors of Interleukin-1 Receptor Associated Kinase 4 (IRAK4) for the Treatment of Mutant MYD88(L265P) Diffuse Large B-Cell Lymphoma. *J Med Chem.* 2017;60(24):10071-91.
  134. Kelly PN, Romero DL, Yang Y, Shaffer AL, 3rd, Chaudhary D, Robinson S, et al. Selective interleukin-1 receptor-associated kinase 4 inhibitors for the treatment of autoimmune disorders and lymphoid malignancy. *J Exp Med.* 2015;212(13):2189-201.
  135. Bhagat L, Wang D, Jiang W, Agrawal S. Abstract 2570: IMO-8400, a selective antagonist of TLRs 7, 8 and 9, inhibits MYD88 L265P mutation-driven signaling and cell survival: A potential novel approach for treatment of B-cell lymphomas harboring MYD88 L265P mutation. *Cancer Research.* 2014;74(19\_Supplement):2570-.
  136. Wang X, Tan Y, Huang Z, Huang N, Gao M, Zhou F, et al. Disrupting myddosome assembly in diffuse large Bcell lymphoma cells using the MYD88 dimerization inhibitor ST2825. *Oncol Rep.* 2019;42(5):1755-66.
  137. Loiarro M, Capolunghi F, Fanto N, Gallo G, Campo S, Arseni B, et al. Pivotal Advance: Inhibition of MyD88 dimerization and recruitment of IRAK1 and IRAK4 by a novel peptidomimetic compound. *J Leukoc Biol.* 2007;82(4):801-10.
  138. Honigberg LA, Smith AM, Sirisawad M, Verner E, Loury D, Chang B, et al. The Bruton tyrosine kinase inhibitor PCI-32765 blocks B-cell activation and is efficacious in models of autoimmune disease and B-cell malignancy. *Proc Natl Acad Sci U S A.* 2010;107(29):13075-80.
  139. Yang G, Wang J, Tan L, Munshi M, Liu X, Kofides A, et al. The HCK/BTK inhibitor KIN-8194 is active in MYD88-driven lymphomas and overcomes mutated BTKCys481 ibrutinib resistance. *Blood.* 2021;138(20):1966-79.
  140. Schaffer M, Chaturvedi S, Davis C, Aquino R, Stepanchick E, Versele M, et al. Identification of potential ibrutinib combinations in hematological malignancies using a combination high-throughput screen. *Leuk Lymphoma.* 2018;59(4):931-40.
  141. Mathews Griner LA, Guha R, Shinn P, Young RM, Keller JM, Liu D, et al. High-throughput combinatorial screening identifies drugs that cooperate with ibrutinib to kill activated B-cell-like diffuse large B-cell lymphoma cells. *Proc Natl Acad Sci U S A.* 2014;111(6):2349-54.
  142. Rui L, Drennan AC, Ceribelli M, Zhu F, Wright GW, Huang DW, et al. Epigenetic gene regulation by Janus kinase 1 in diffuse large B-cell lymphoma. *Proc Natl Acad Sci U S A.* 2016;113(46):E7260-E7.
  143. He Y, Li J, Ding N, Wang X, Deng L, Xie Y, et al. Combination of Enzastaurin and Ibrutinib synergistically induces anti-tumor effects in diffuse large B cell lymphoma. *J Exp Clin Cancer Res.* 2019;38(1):86.
  144. Zhou Z, Zhang L, Wang X, Li X, Li L, Fu X, et al. Ibrutinib combined with venetoclax for the treatment of relapsed/refractory diffuse large B cell lymphoma. *Ann Hematol.* 2021;100(6):1509-16.
  145. Goy A, Ramchandren R, Ghosh N, Munoz J, Morgan DS, Dang NH, et al. Ibrutinib plus lenalidomide and rituximab has promising activity in relapsed/refractory non-germinal center B-cell-like DLBCL. *Blood.* 2019;134(13):1024-36.
  146. Grommes C, Gavrilovic I, Miller AM, Stone JB, Kaley T, Madzsar JT, et al. Phase Ib of Copanlisib in Combination with Ibrutinib in Recurrent/Refractory Primary CNS Lymphoma (PCNSL). *Blood.* 2019;134(Supplement\_1):1598-.
  147. Yang C, Cui Y, Ren X, Li M, Yu K, Shen S, et al. Orelabrutinib Combined With Lenalidomide and Immunochemotherapy for Relapsed/Refractory Primary Central Nervous System Lymphoma: A Retrospective Analysis of Case Series. *Front Oncol.* 2022;12:901797.
  148. Martinez-Trillos A, Pinyol N, Navarro A, Aymerich M, Jares P, Juan M, et al. Mutations in TLR/MYD88 pathway identify a subset of young chronic lymphocytic leukemia patients with favorable outcome. *Blood.* 2014;123(24):3790-6.
  149. Jeromin S, Weissmann S, Haferlach C, Dicker F, Bayer K, Grossmann V, et al. SF3B1 mutations correlated to cytogenetics and mutations in NOTCH1, FBXW7, MYD88, XPO1 and TP53 in 1160 untreated CLL patients. *Leukemia.* 2014;28(1):108-17.

150. Puente XS, Pinyol M, Quesada V, Conde L, Ordóñez GR, Villamor N, et al. Whole-genome sequencing identifies recurrent mutations in chronic lymphocytic leukaemia. *Nature*. 2011;475(7354):101-5.
151. Xu L, Hunter ZR, Yang G, Zhou Y, Cao Y, Liu X, et al. MYD88 L265P in Waldenstrom macroglobulinemia, immunoglobulin M monoclonal gammopathy, and other B-cell lymphoproliferative disorders using conventional and quantitative allele-specific polymerase chain reaction. *Blood*. 2013;121(11):2051-8.
152. Poulain S, Roumier C, Decambron A, Renneville A, Herbaux C, Bertrand E, et al. MYD88 L265P mutation in Waldenstrom macroglobulinemia. *Blood*. 2013;121(22):4504-11.
153. Bea S, Valdes-Mas R, Navarro A, Salaverria I, Martin-Garcia D, Jares P, et al. Landscape of somatic mutations and clonal evolution in mantle cell lymphoma. *Proc Natl Acad Sci U S A*. 2013;110(45):18250-5.
154. Varettoni M, Arcaini L, Zibellini S, Boveri E, Rattotti S, Riboni R, et al. Prevalence and clinical significance of the MYD88 (L265P) somatic mutation in Waldenstrom's macroglobulinemia and related lymphoid neoplasms. *Blood*. 2013;121(13):2522-8.
155. Jimenez C, Sebastian E, Chillon MC, Giraldo P, Mariano Hernandez J, Escalante F, et al. MYD88 L265P is a marker highly characteristic of, but not restricted to, Waldenstrom's macroglobulinemia. *Leukemia*. 2013;27(8):1722-8.
156. Bohers E, Mareschal S, Bouzefen A, Marchand V, Ruminy P, Maingonnat C, et al. Targetable activating mutations are very frequent in GCB and ABC diffuse large B-cell lymphoma. *Genes Chromosomes Cancer*. 2014;53(2):144-53.
157. Choi JW, Kim Y, Lee JH, Kim YS. MYD88 expression and L265P mutation in diffuse large B-cell lymphoma. *Hum Pathol*. 2013;44(7):1375-81.
158. Fernandez-Rodriguez C, Bellosillo B, Garcia-Garcia M, Sanchez-Gonzalez B, Gimeno E, Vela MC, et al. MYD88 (L265P) mutation is an independent prognostic factor for outcome in patients with diffuse large B-cell lymphoma. *Leukemia*. 2014;28(10):2104-6.
159. Rovira J, Karube K, Valera A, Colomer D, Enjuanes A, Colomo L, et al. MYD88 L265P Mutations, But No Other Variants, Identify a Subpopulation of DLBCL Patients of Activated B-cell Origin, Extranodal Involvement, and Poor Outcome. *Clin Cancer Res*. 2016;22(11):2755-64.
160. Pasqualucci L, Trifonov V, Fabbri G, Ma J, Rossi D, Chiarenza A, et al. Analysis of the coding genome of diffuse large B-cell lymphoma. *Nat Genet*. 2011;43(9):830-7.
161. Treon SP, Xu L, Yang G, Zhou Y, Liu X, Cao Y, et al. MYD88 L265P somatic mutation in Waldenstrom's macroglobulinemia. *N Engl J Med*. 2012;367(9):826-33.
162. Chen Z, Zou Y, Liu W, Guan P, Tao Q, Xiang C, et al. Morphologic Patterns and the Correlation With MYD88 L265P, CD79B Mutations in Primary Adrenal Diffuse Large B-Cell Lymphoma. *Am J Surg Pathol*. 2020;44(4):444-55.
163. Taniguchi K, Takata K, Chuang SS, Miyata-Takata T, Sato Y, Satou A, et al. Frequent MYD88 L265P and CD79B Mutations in Primary Breast Diffuse Large B-Cell Lymphoma. *Am J Surg Pathol*. 2016;40(3):324-34.
164. Mareschal S, Pham-Ledard A, Vially PJ, Dubois S, Bertrand P, Maingonnat C, et al. Identification of Somatic Mutations in Primary Cutaneous Diffuse Large B-Cell Lymphoma, Leg Type by Massive Parallel Sequencing. *J Invest Dermatol*. 2017;137(9):1984-94.
165. Suehara Y, Sakata-Yanagimoto M, Hattori K, Nanmoku T, Itoh T, Kaji D, et al. Liquid biopsy for the identification of intravascular large B-cell lymphoma. *Haematologica*. 2018;103(6):e241-e4.
166. Cao XX, Li J, Cai H, Zhang W, Duan MH, Zhou DB. Patients with primary breast and primary female genital tract diffuse large B cell lymphoma have a high frequency of MYD88 and CD79B mutations. *Ann Hematol*. 2017;96(11):1867-71.
167. Fontanilles M, Marguet F, Bohers E, Vially PJ, Dubois S, Bertrand P, et al. Non-invasive detection of somatic mutations using next-generation sequencing in primary central nervous system lymphoma. *Oncotarget*. 2017;8(29):48157-68.
168. Nakamura T, Tateishi K, Niwa T, Matsushita Y, Tamura K, Kinoshita M, et al. Recurrent mutations of CD79B and MYD88 are the hallmark of primary central nervous system lymphomas. *Neuropathol Appl Neurobiol*. 2016;42(3):279-90.
169. Bruno A, Boisselier B, Labreche K, Marie Y, Polivka M, Jouve A, et al. Mutational analysis of primary central nervous system lymphoma. *Oncotarget*. 2014;5(13):5065-75.
170. Braggio E, Van Wier S, Ojha J, McPhail E, Asmann YW, Egan J, et al. Genome-Wide Analysis Uncovers Novel Recurrent Alterations in Primary Central Nervous System Lymphomas. *Clin Cancer Res*. 2015;21(17):3986-94.
171. Yonese I, Takase H, Yoshimori M, Onozawa E, Tsuzura A, Miki T, et al. CD79B mutations in primary vitreoretinal lymphoma: Diagnostic and prognostic potential. *Eur J Haematol*. 2019;102(2):191-6.
172. Kwak JJ, Lee KS, Lee J, Kim YJ, Choi EY, Byeon SH, et al. Next-Generation Sequencing of Vitreoretinal Lymphoma by Vitreous Liquid Biopsy: Diagnostic Potential and Genotype/Phenotype Correlation. *Invest Ophthalmol Vis Sci*. 2023;64(14):27.
173. Lee J, Kim B, Lee H, Park H, Ho Byeon S, Choi JR, et al. Whole exome sequencing identifies mutational signatures of vitreoretinal lymphoma. *Haematologica*. 2020;105(9):e458-60.

# SUPPLEMENTARY MATERIAL

Supplementary table 1. Frequency of *MYD88* L265P in different types of lymphoma

B-cell malignancy	Method	<i>MYD88</i> L265P (%)	Reference
CLL	WES, Sanger sequencing	16/587 (3%)	(148)
CLL	NGS, Sanger sequencing	11/969 (1%)	(149)
CLL	WGS	9/310 (3%)	(150)
CLL	AS-PCR	1/26 (4%)	(151)
MCL	Sanger sequencing	0/10 (0%)	(152)
MCL	WES	0/29 (0%)	(153)
BL	Sanger sequencing	1/58 (2%)	(50)
FL	Sanger sequencing	1/23 (4%)	(152)
MZL	AS-PCR	2/20 (10%)	(151)
MZL	AS-PCR	5/84 (6%)	(154)
MZL	Sanger sequencing	6/56 (11%)	(50)
MZL	AS-PCR	3/14 (21%)	(155)
GCB-DLBCL	Sanger sequencing	1/68 (1%)	(50)
GCB-DLBCL	AS-PCR	0/28 (0%)	(155)
GCB-DLBCL	Sanger sequencing	1/62 (2%)	(156)
GCB-DLBCL	Sanger sequencing	1/33 (3%)	(157)
GCB-DLBCL	AS-PCR	5/82 (6%)	(158)
GCB-DLBCL	AS-PCR	10/96 (10%)	(159)
ABC-DLBCL	Sanger sequencing	55/174 (32%)	(50)
ABC-DLBCL	AS-PCR	9/48 (19%)	(155)
ABC-DLBCL	Sanger sequencing	17/77 (22%)	(156)
ABC-DLBCL	Sanger sequencing	17/91 (19%)	(157)
ABC-DLBCL	AS-PCR	12/88 (14%)	(158)
ABC-DLBCL	WES, Sanger sequencing	9/111 (8%)	(160)
ABC-DLBCL	AS-PCR	23/90 (26%)	(159)
WM	AS-PCR	97/104 (93%)	(151)
WM	AS-PCR	58/58 (100%)	(154)
WM	Sanger sequencing	49/54 (91%)	(161)
WM	Sanger sequencing	53/67 (79%)	(152)
WM	AS-PCR	101/117 (86%)	(155)
IgM-MGUS	AS-PCR	13/24 (54%)	(151)
IgM-MGUS	AS-PCR	36/77 (47%)	(154)
IgM-MGUS	Sanger sequencing	2/21 (10%)	(161)
IgM-MGUS	AS-PCR	27/31 (87%)	(155)
MM	AS-PCR	0/14 (0%)	(151)
MM	AS-PCR	0/24 (0%)	(155)

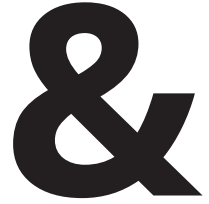
Abbreviations: CLL, chronic lymphocytic leukemia; MCL, mantle cell lymphoma; BL, Burkitt lymphoma; FL, follicular lymphoma; GCB-DLBCL, germinal center B-cell like diffuse large B-cell lymphoma; ABC-DLBCL, activated B-cell like diffuse large B-cell lymphoma; WM, Waldenström macroglobulinemia; IgM-MGUS, IgM monoclonal gammopathy of undetermined significance cases; MM, multiple myeloma; WES, whole exome sequencing; NGS, next generation sequencing; WGS, whole genome sequencing; AS-PCR, Allele-specific polymerase chain reaction.

**Supplementary table 2. Co-occurrence of *CD79A/B* and *MYD88* mutations in ABC DLBCL according to location**

Location	Method	MYD88 L265P mutated (%)	CD79A/B mutations (%)	MYD88 + CD79A/B (%)	Ref
Nodal DLBCL	AS-PCR, Sanger sequencing	5/19 (26%)	2/19 (10%)	2/19 (10%)	(3)
Nodal DLBCL	AS-PCR, Sanger sequencing	6/33 (18%)	1/33 (3%)	1/33 (3%)	(4)
Nodal DLBCL	Targeted NGS	23/81 (28%)	20/81 (25%)	17/81 (21%)	(30)
Nodal DLBCL	NGS, Sanger sequencing	45/155 (29%)	35/155 (23%)	15/155 (10%)	(5)
Gastro-intestinal tract	AS-PCR, Sanger sequencing	2/18 (11%)	1/18 (6%)	0/18 (0%)	(4)
Adrenal	Sanger sequencing	5/25 (20%)	13/25 (52%)	3/25 (12%)	(162)
Breast	Sanger sequencing	9/16 (56%)	3/13 (23%)	2/13 (15%)	(163)
Cutaneous, Leg Type	Sanger sequencing	4/10 (40%)	2/10 (20%)	2/10 (20%)	(33)
Cutaneous, Leg Type	Targeted NGS	15/20 (75%)	8/20 (40%)	7/20 (35%)	(164)
Intravascular	Targeted NGS	5/9 (56%)	6/9 (67%)	3/9 (33%)	(165)
Intravascular	Targeted NGS	10/23 (43%)	6/23 (24%)	4/23 (17%)	(36)
Female genital tract	Sanger sequencing	5/6 (83%)	3/6 (50%)	2/6 (33%)	(166)
Ocular adnexa	AS-PCR, Sanger sequencing	8/16 (50%)	3/16 (19%)	3/16 (19%)	(10)
Sinonasal	Targeted NGS	32/43 (74%)	16/43 (37%)	15/43 (35%)	(11)
CNS	AS-PCR, Sanger sequencing	13/21 (62%)	5/21 (24%)	3/21 (14%)	(3)
CNS	AS-PCR, Sanger sequencing	15/20 (75%)	4/20 (20%)	4/20 (20%)	(4)
CNS	NGS, Sanger sequencing	33/55 (60%)	19/50 (38%)	17/50 (34%)	(5)
CNS	Targeted NGS	20/25 (80%)	7/25 (28%)	6/25 (24%)	(167)
CNS	Targeted NGS, Sanger sequencing	76/106 (72%)	68/106 (64%)	51/106 (48%)	(168)
CNS	NGS, Sanger sequencing	14/37 (38%)	11/37 (30%)	8/37 (22%)	(169)
CNS	NGS, Sanger sequencing	7/10 (70%)	4/10 (40%)	3/10 (30%)	(170)
Testis	AS-PCR, Sanger sequencing	14/19 (74%)	4/19 (21%)	4/19 (21%)	(3)
Testis	AS-PCR, Sanger sequencing	25/37 (68%)	7/37 (19%)	7/37 (19%)	(8)
Testis	NGS, Sanger sequencing	38/49 (78%)	22/45 (49%)	20/45 (44%)	(5)
Vitreoretinal	AS-PCR	12/17 (71%)	6/17 (35%)	3/17 (18%)	(171)
Vitreoretinal	(Targeted) NGS	20/22 (91%)	3/22 (14%)	3/22 (14%)	(172)
Vitreoretinal	NGS	9/9 (100%)	2/9 (22%)	2/9 (22%)	(173)

Abbreviations: CNS, central nervous system; NGS, next generation sequencing; AS-PCR, Allele-specific polymerase chain reaction.





**APPENDIX**

**Summary**

**Nederlandse samenvatting**

**PhD Portfolio**

**Curriculum vitae**

**Publications with author contributions**

**Acknowledgements**

## SUMMARY

B-cell lymphomas can arise from different stages of B-cell development and constitute a clinically and genetically heterogeneous group of malignancies. Diffuse large B-cell lymphoma (DLBCL) and mantle cell lymphoma (MCL) are both mature B-cell malignancies which often display an aggressive clinical course. Aberrant activation of various oncogenic signaling cascades has been implicated in the pathogenesis of DLBCL and MCL. Recognition of an antigen by the B-cell receptor (BCR), a surface-bound immunoglobulin, triggers intracellular signaling pathways that can lead to B cell activation and proliferation. In addition, B cells are able to respond to pathogen and damage associated molecules through Toll-like receptors (TLRs). Dysregulation of BCR and TLR signaling due to mutations or epigenetic events is frequently observed in a large fraction of DLBCL and MCL cases. Primary DLBCLs arising at extranodal, immune-privileged (IP) sites exhibit a remarkably high prevalence of activating *MYD88* and *CD79B* mutations. In addition, these lymphomas often display various mechanisms of immune evasion to evade detection and elimination by the host immune system. Improved understanding of the biology of these lymphomas can help towards development of personalized treatment options for these aggressive subtypes.

In **chapter 2** we demonstrated that low expression of the deubiquitinating enzyme cylindromatosis (*CYLD*) correlates with poor overall survival in both DLBCL and MCL patients. *CYLD* can repress NF- $\kappa$ B activation by removing Lys-63-linked polyubiquitin chains from TAK1, IKK- $\gamma$ , TRAF2 and, to a lesser extent, TRAF6. We showed that chronic BCR signaling controls cleavage-mediated inactivation by the paracaspase MALT1 and subsequent proteosomal degradation of *CYLD* in DLBCL and BCR-dependent MCL cell lines. These findings underline that MALT1 inhibitors could be promising therapeutic agents for B-cell lymphomas that are dependent on chronic BCR signaling.

In **chapter 3** we demonstrated that the SRC-family tyrosine kinase hematopoietic cell kinase (HCK) is aberrantly expressed in MCL, and that high expression of *HCK* is associated with poor overall survival of MCL patients. We showed that, similar to its role in DLBCL, *HCK* is an oncogenic kinase which propagates tumor cell proliferation and survival. In MCL, aberrant *HCK* expression is not driven by mutant *MYD88*, but instead likely depends on local TLR stimulation in the tumor microenvironment. In addition, we demonstrated that *HCK* is involved in integrin-mediated adhesion of MCL cells to the extracellular matrix and stromal cells. Our results help define *HCK* as an important therapeutic target for B-cell malignancies depending on constitutive (wild type or mutant) *MYD88* signaling.

In **chapter 4** we identified an important role for serine 257 phosphorylation in the regulation of MYD88 activation. We showed that MYD88 serine 257 phosphorylation is required for optimal TLR/MYD88-dependent NF- $\kappa$ B activation. In addition, we demonstrate that a MYD88 257D phosphomimetic mutant induces MYD88 aggregation, IRAK1 phosphorylation, NF- $\kappa$ B activity and proliferation in MYD88 wildtype cells to a similar extent as the oncogenic L265P mutant. Finally, we show that MYD88 S257D can rescue MYD88 L265P expressing cells after silencing of endogenous MYD88, implying that these variants indeed exert a similar function.

In **chapter 5** we studied the prevalence and prognostic value of *MYD88* and *CD79B* mutations in ocular adnexal large B-cell lymphoma (OA-LBCL). We demonstrated that *MYD88* mutations are an important driver in a subset of OA-LBCL patients and are associated with reduced progression-free survival. In addition, we showed that *MYD88* mutations frequently co-occur with mutations in *CD79B*. OA-LBCLs without *MYD88* mutations were frequently driven by chromosomal rearrangements and/or aberrant protein expression of the oncogenes *cMYC* and *BCL2* and/or *BCL6*.

In **chapter 6**, we demonstrate that (co-occurring) *MYD88* and *CD79B* mutations are also highly prevalent in a subset of primary sinonasal DLBCL. Moreover, we show that these lymphomas hardly express the immune checkpoint protein programmed death-ligand 1 (PD-L1), but employ loss of MHC class II as their primary mechanism of immune evasion.

In **chapter 7** we confirm that primary testicular lymphomas (PTLs) and primary central nervous system lymphomas (PCNSLs) are characterized by a high prevalence of somatic mutations in *MYD88* and *CD79B*. In addition, we observed a high prevalence of loss of MHC class I and class II expression in PTL and PCNSL. In contrast, we hardly detected PD-L1 expression and 9p24.1/*PD-L1/2* gene rearrangements in our cohort. Altogether, these findings demonstrate that immune evasion strategies are key to the pathogenesis of IP-associated DLBCL, but simultaneously underscore that patients with PTL or PCNSL will likely not benefit from treatment with PD-1/PD-L1 immune checkpoint inhibitors.

## NEDERLANDSE SAMENVATTING

B cel lymfomen kunnen ontstaan tijdens verschillende fasen van de B cel ontwikkeling en vormen een zeer heterogene groep maligniteiten. Diffuus grootcellig B cel lymfoom (DLBCL) en mantelcellilymfoom (MCL) vallen beiden onder de groep van de agressieve non-Hodgkin lymfomen. Aberrante activatie van diverse oncogene signaleringsroutes speelt een belangrijke rol in de pathogenese van zowel DLBCL als MCL. Herkenning van een antigeen door de B-cel receptor (BCR), een membraan gebonden antilichaam, stimuleert intrinsieke signaleringsroutes die zorgen voor B cel activatie en celdeling. Daarnaast brengen B cellen Toll-like receptoren (TLRs) tot expressie waarmee ze potentieel pathogene micro-organismen of lichaamseigen stoffen die bij schade vrijkomen, kunnen herkennen. Verstoorde activatie van zowel BCR als TLR gedreven signaleringsroutes als gevolg van mutaties of epigenetische veranderingen, komt voor bij een groot deel van DLBCL en MCL gevallen. Primaire grootcellige B cel lymfomen die voorkomen op extranodale locaties waar het afweersysteem zeer sterk gereguleerd wordt, worden gekenmerkt door een hoge frequentie van activerende *MYD88* en *CD79B* mutaties. Daarnaast maken deze lymfomen vaak gebruik van verschillende mechanismen om herkenning en eliminatie door het afweersysteem van de gastheer te ontwijken. Het beter begrijpen van de pathobiologie van deze lymfomen kan bijdragen aan de ontwikkeling van specifieke therapieën voor de behandeling van deze agressieve lymfomen.

In **hoofdstuk 2** hebben we laten zien dat lage expressie van het de-ubiquitinerende enzym CYLD gecorreleerd is met een slechte prognose van zowel DLBCL als MCL. CYLD kan NF- $\kappa$ B activatie remmen door het verwijderen van Lys-63-gebonden ubiquitine ketens van de eiwitten TAK1, IKK- $\gamma$ , TRAF2 en, in mindere mate, TRAF6. We hebben gevonden dat chronische signalering via de BCR zorgt voor continue inactivatie van CYLD door het paracaspase MALT1. MALT1 knipt het CYLD eiwit in fragmenten die vervolgens verder worden afgebroken door het proteasoom. Deze resultaten onderstrepen het belang van de ontwikkeling van MALT1 remmers voor de behandeling van B cel lymfomen die afhankelijk zijn van chronische BCR signalering.

In **hoofdstuk 3** hebben we gevonden dat HCK, een kinase dat behoort tot de SRC familie kinases, aberrant tot expressie komt in MCL en dat hoge expressie van HCK geassocieerd is met een slechte prognose. Daarnaast hebben we laten zien dat HCK, net als in DLBCL, een belangrijke rol speelt bij deling en overleving van tumorcellen. Aberrante expressie van HCK in MCL is niet gedreven door mutaties in *MYD88*, maar is waarschijnlijk het gevolg van aanwezigheid van TLR liganden in de tumor micro-omgeving. HCK is ook betrokken bij de adhesie van MCL cellen aan de extracellulaire matrix en stromale cellen. Deze bevindingen onderschrijven dat HCK een interessant

therapeutisch doelwit kan zijn voor de behandeling van B cel lymfomen die afhankelijk zijn van aberrante signalering via het MYD88 eiwit.

In **hoofdstuk 4** hebben we gekeken naar de rol van serine 257 fosforylering bij de activatie van het MYD88 eiwit. We hebben laten zien dat fosforylatie van serine 257 belangrijk is voor optimale activatie van TLR/MYD88-afhankelijke activatie van de NF- $\kappa$ B signaleringsroute. Daarnaast laten we zien dat een mutatie die fosforylatie van deze serine nabootst (MYD88 S257D), zorgt voor meer MYD88 aggregatie, verhoogde fosforylatie van IRAK1, stimulering van NF- $\kappa$ B signalering en verhoogde celdeling. De effecten van de MYD88 S257D mutant komen overeen met de effecten van expressie van de oncogene MYD88 L265P mutant. Daarnaast laten we zien dat de MYD88 S257D mutant de overleving van cellen die voor hun groei afhankelijk zijn van MYD88 L265P kan redden. Samen suggereren deze bevindingen dat beide MYD88 varianten een vergelijkbare functie uitoefenen.

In **hoofdstuk 5** hebben we de frequentie en prognostische waarde van *MYD88* en *CD79B* mutaties in oculair adnexale grootcellig B lymfomen bestudeerd. We laten zien dat *MYD88* mutaties een belangrijke rol spelen in een subset van deze lymfomen en geassocieerd zijn met een slechtere prognose. Daarnaast hebben we laten zien dat mutaties in *MYD88* vaak voorkomen samen met mutaties in *CD79B*. Oculair adnexale lymfomen zonder mutaties in *MYD88* hebben vaak chromosomale herschikkingen en/of aberrante expressie van de oncogene eiwitten cMYC and BCL2 en/of BCL6.

In **hoofdstuk 6** hebben we laten zien dat *MYD88* en *CD79B* mutaties ook vaak (samen) voorkomen in primaire sinonasale B cel lymfomen. Daarnaast demonstreren we dat deze lymfomen vrijwel nooit het immuun checkpoint eiwit PD-L1 tot expressie brengen, maar gebruik maken van verlies van MHC klasse II als belangrijkste mechanisme van immuun evasie.

In **hoofdstuk 7** bevestigen we dat primaire testis lymfomen (PTL) en primaire centraal zenuwstelsel lymfomen (PCNSL) gekenmerkt worden door een hoge frequentie van *MYD88* en *CD79B* mutaties. Daarnaast hebben we gevonden dat deze lymfomen vaak verlies van zowel MHC klasse I als MHC klasse II laten zien. In deze groep lymfomen vonden we nauwelijks expressie van PD-L1 of herschikkingen van de 9p24.1/*PD-L1/2* locus. Deze bevindingen onderschrijven dat immuun evasie mechanismen een belangrijke rol spelen bij de pathogenese van deze lymfomen, maar benadrukken ook dat deze groep patiënten waarschijnlijk geen baat heeft bij behandeling met PD-1/PD-L1 checkpointremmers.

# PHD PORTFOLIO

Name PhD student: Marthe Minderman

PhD period: September 2015 – September 2022

Names of PhD supervisor(s) & co-supervisor(s): Prof. Steven T. Pals, Prof. Marie José Kersten, dr. Marcel Spaargaren

1. PhD training	Year	ECTS
<b>General courses</b>		
- Practical Biostatistics	2019	1.4
<b>Specific courses</b>		
- DNA Technology	2016	2.1
- Computing in R	2021	0.4
<b>Seminars, workshops and master classes</b>		
- OASIS seminars	2015-2016	0.4
- Seminars in pathology	2017-2018	0.6
- Workshop: R2 – Genomics analysis and visualization platform	2017	0.3
- Workshop on Molecular Aspects of Hematological Disorders	2016-2017	1.2
<b>Oral presentation</b>		
- Cancer Center Amsterdam (CCA) conference	2017	0.6
- Dutch Hematology (DHC) conference	2019	0.6
- Dutch Hematology (DHC) conference	2020	0.6
- Dutch Hematology (DHC) conference	2022	0.4
- Cancer Center Amsterdam (CCA) conference	2022	0.6
<b>(Inter)national conferences</b>		
- Tumor Cell Biology meeting	2015-2019	3
- Dutch Hematology (DHC) conference	2016, 2019, 2020, 2022	2.2
- Cancer Center Amsterdam (CCA) conference	2017, 2018, 2022	1.4
- Keystone Symposia Cancer Immunology and Immunotherapy	2017	1.4
<b>Other</b>		
- Weekly LYMMCARE work discussion / journal club	2015-2022	8.4
- Weekly B-cell work discussion	2015-2022	8.4

2. Teaching	Year	ECTS
<b>Supervising</b>		
- Carola López Abad (Bachelor internship)	2018	1.4
- Katja Klooster (Literature thesis)	2018	0.4
- Yasmine Heirouche (Master internship)	2020	2.2

3. Publications	Year
<b>Peer reviewed</b>	
- <b>Minderman M</b> , Lantermans H, van der Zwaan C, Hoogendijk AJ, van den Biggelaar M, Kersten MJ, Spaargaren M, Pals ST. The oncogenic human B-cell lymphoma MYD88 L265P mutation genocopies activation by phosphorylation at the Toll/interleukin-1 receptor (TIR) domain. <i>Blood Cancer J.</i> 2023 Aug 18;13(1):125.	2023
- <b>Minderman M</b> , Lantermans HC, Grüneberg LJ, Cillessen SAGM, Bende RJ, van Noesel CJM, Kersten MJ, Pals ST, Spaargaren M. MALT1-dependent cleavage of CYLD promotes NF-κB signaling and growth of aggressive B-cell receptor-dependent lymphomas. <i>Blood Cancer J.</i> 2023 Mar 15;13(1):37.	2023
- Kirkegaard MK, <b>Minderman M</b> , Sjö LD, Pals ST, Eriksen PRG, Heegaard S. Prevalence and prognostic value of MYD88 and CD79B mutations in ocular adnexal large B-cell lymphoma: a reclassification of ocular adnexal large B-cell lymphoma. <i>Br J Ophthalmol.</i> 2023 Apr;107(4):576-581.	2023
- Lantermans, H. C., <b>Minderman, M.</b> , Kuil, A., Kersten, M. J., Pals, S. T., & Spaargaren, M. (2021). Identification of the SRC-family tyrosine kinase HCK as a therapeutic target in mantle cell lymphoma. <i>Leukemia</i> , 35(3), 881–886.	2021
- <b>Minderman, M.</b> , Amir, A., Kraan, W., Schilder-Tol, E., Oud, M., Scheepstra, C. G., Noorduynd, A. L., Kluin, P. M., Kersten, M. J., Spaargaren, M., & Pals, S. T. Immune evasion in primary testicular and central nervous system lymphomas: HLA loss rather than 9p24.1/PD-L1/PD-L2 alterations. <i>Blood</i> , 138(13), 1194–1197.	2021
- Eriksen, PRG., de Groot, F., Clasen-Linde, E., de Nully Brown, P., de Groen, R., Melchior LC., Maier, AD., <b>Minderman, M.</b> , Vermaat, JSP., von Buchwald, C., Pals, ST., Heegaard, S. Sinonasal diffuse large B-cell lymphoma: molecular profiling identifies subtypes with distinctive prognosis and targetable genetic features. <i>Blood Adv.</i> 2024 Feb 7; <i>Online ahead of print.</i>	2024
<b>Other</b>	
- <b>Minderman, M.</b> , & Pals, S. T. (2020). Towards genomic-based prognostication and precision therapy for diffuse large B-cell lymphoma. <i>Haematologica</i> , 105(9), 2194–2196.	2020

## CURRICULUM VITAE

Marthe Minderman werd geboren op 20 oktober 1990 te Eindhoven. Na het afronden van het Gymnasium aan het Odulphuslyceum in Tilburg, begon zij met haar bachelor Biomedische Wetenschappen aan de Radboud Universiteit Nijmegen. Tijdens haar bachelorstage maakte zij voor het eerst kennis met moleculair biomedisch onderzoek op de afdeling fysiologie van het Radboud Institute for Molecular Life Sciences. Hier deed zij onderzoek naar de rol van het eiwit aquaporine-2 bij het ontstaan van nefrogene diabetes insipidus door het gebruik van lithium onder leiding van Prof. Peter Deen en dr. Anne Sinke. In 2011 startte ze met de master Biomedische Wetenschappen aan de Radboud Universiteit Nijmegen. Tijdens haar master koos ze voor 'Human Pathobiology' als afstudeerrichting (major) met hiernaast een minor in 'Neurosciences'. Als onderdeel van haar major begon zij in 2012 onder leiding van Prof. Gosse Adema en dr. Martijn den Brok aan een onderzoek op de afdeling tumorimmunologie van het Radboud Institute for Molecular Life Sciences. Haar onderzoek hier richtte zich op de werking van het adjuvans saponine op antigeen presentatie door dendritische cellen. Als onderdeel van haar minor 'Neurosciences' deed zij in 2014 onderzoek bij de neuroimmunologie groep van het Montreal Neurological Institute and Hospital in Canada onder leiding van Prof. Jack Antel en dr. Vijay Rao. Hier deed zij onderzoek naar de reactie van astrocyten op (ischemische) stress factoren. De verschillende onderzoeksstages wakkerden haar interesse voor moleculair biomedisch onderzoek verder aan en bevestigden dat zij zich vooral wilde gaan richten op de vakgebieden oncologie en immunologie. In 2015 startte zij als promovendus op de afdeling pathologie van het Amsterdam UMC, locatie AMC, onder begeleiding van Prof. Steven Pals, Prof. Marie José Kersten en dr. Marcel Spaargaren. Haar onderzoek, waarvan de resultaten in dit proefschrift beschreven zijn, richtte zich voornamelijk op oncogene signaleringsroutes en immuun evasie mechanismen van diffuus grootcellig B cel lymfomen en mantelcellymfomen.

## PUBLICATIONS WITH AUTHOR CONTRIBUTIONS

### **MALT1-dependent cleavage of CYLD promotes NF- $\kappa$ B signaling and growth of aggressive B-cell receptor-dependent lymphomas**

Marthe Minderman, Hildo C. Lantermans, Leonie J. Grüneberg, Saskia A. G. M. Cillessen, Richard J. Bende, Carel J. M. van Noesel, Marie José Kersten, Steven T. Pals, Marcel Spaargaren

*Blood Cancer J.* 2023 Mar 15;13(1):37.

Contributions: M.M. designed the research, performed experiments, analyzed the data and wrote the paper; H.C.L. and L.J.G. performed experiments and analyzed the data. S.A.G.M.C., R.J.B. and C.J.M.N. provided patient material. M.K., S.T.P. and M.S. supervised the study, designed the research and analyzed the data. M.S. and S.T.P. wrote the paper.

### **Identification of the SRC-family tyrosine kinase HCK as a therapeutic target in mantle cell lymphoma**

Hildo Lantermans, Marthe Minderman, Annemieke Kuil, Marie-José Kersten, Steven T. Pals, Marcel Spaargaren

*Leukemia.* 2021 Mar;35(3):881-886

Contributions: HCL designed the research, performed experiments, analyzed the data, designed the figures, and wrote the paper; MM and AK performed experiments; MK supervised the study and provided primary patient material; STP and MS supervised the study, designed the research, analyzed the data, and wrote the paper.

### **The oncogenic human B-cell lymphoma MYD88 L265P mutation genocopies activation by phosphorylation at the Toll/interleukin-1 receptor (TIR) domain**

Marthe Minderman, Hildo Lantermans, Carmen van der Zwaan, Arjan J. Hoogendijk, Maartje van den Biggelaar, Marie José Kersten, Marcel Spaargaren, Steven T. Pals

*Blood Cancer J.* 2023 Aug 18;13(1):125.

Contributions: M.M. designed the research, performed experiments, analyzed the data and wrote the paper; H.C.L., C.Z., A.J.H. performed experiments and analyzed the data. M.B., M.K., S.T.P. and M.S. supervised the study, designed the research and analyzed the data. M.S. and S.T.P. wrote the paper.

**Prevalence and prognostic value of MYD88 and CD79B mutations in ocular adnexal large B-cell lymphoma: a reclassification of ocular adnexal large B-cell lymphoma**

Marina Knudsen Kirkegaard, Marthe Minderman, Lene Dissing Sjø, Steven T Pals, Patrick R G Eriksen, Steffen Heegaard

*Br J Ophthalmol.* 2023 Apr;107(4):576-581

Contributions: Study concept and design: MKK, LDS, STP, SH. Acquisition, analysis, or interpretation of data: MKK, MM, PRGE. Drafting of the manuscript: MKK. Critical revision of the manuscript for important intellectual content: MM, LDS, STP, PRGE, SH. Statistical analysis: MKK. Obtained funding: MKK, MM, STP. Study supervision: LDS, STP, SH. Guarantor: SH.

**Sinonasal diffuse large B-cell lymphoma: molecular profiling identifies subtypes with distinctive prognosis and targetable genetic features**

Patrick RG Eriksen, Fleur de Groot, Erik Clasen-Linde, Peter de Nully Brown, Ruben de Groen, Linea C. Melchior, Andrea D Maier, Marthe Minderman, Joost S. P. Vermaat, Christian von Buchwald, Steven T. Pals, Steffen Heegaard

*Blood Adv.* 2024 Feb 7; *Online ahead of print.*

Contributions: PRGE: established cohort and extracted data, COO analyses, statistical calculations, diagrams and figures, and wrote the paper. FdG: performed NGS and analyzed data. EC-L: validated diagnoses and analyzed markers of immune evasion. PdNB: designed the research and provided data. RdG: NGS and genetic subclassification. LCM: analyses. ADM: analyses. MM: performed experiments. JV: supervision of analyses and wrote manuscript. CvB: designed the study, supervised. STP: designed the research and analysis, supervised, data analysis, interpretation of analyses, and wrote manuscript. SH: designed the study, supervised.

**Immune evasion in primary testicular and central nervous system lymphomas: HLA I and II loss rather than 9p24.1/PD-L1/PD-L2 alterations**

Marthe Minderman, Avital Amir, Willem Kraan, Esther J. M. Schilder-Tol, Monique E. C. M. Oud, Cornelis G. Scheepstra, Arnold L. Noorduynd, Philip M. Kluin, Marie José Kersten, Marcel Spaargaren, and Steven T. Pals

*Blood.* 2021 Sep 30;138(13):1194-1197.

Contributions: M.M. performed experiments, analyzed the data and wrote the paper, A.A. designed the research, supervised the study and analyzed the data., W.K. performed experiments and analyzed the data, E.S. and M.O. performed experiments, C.S. A.N. and P.K. provided patient material, M.J.K., M.S. and S.T.P. designed the research, supervised the study, analyzed the data, and wrote the paper.

## ACKNOWLEDGEMENTS

Allereerst wil ik graag mijn promotoren Steven Pals en Marie José Kersten bedanken. Dankzij jullie kon ik in 2015 aan dit mooie door Lymph&Co gefinancierde onderzoeksproject beginnen. Jullie hebben me door de jaren heen ondersteund met waardevolle discussies, suggesties en feedback. Steven, je enthousiasme en persoonlijke interesse voor wetenschappelijk onderzoek werkte zeer aanstekelijk en motiverend. Marie José, ondanks het feit dat je meer vanaf de zijlijn betrokken was, was je altijd bereikbaar voor vragen en feedback en waren je suggesties en commentaren steevast scherp en zinvol. Daarnaast wil ik graag mijn copromotor Marcel Spaargaren bedanken voor de betrokken begeleiding tijdens dit traject. Hoewel ik soms kon balen van alweer een extra experiment (bestaat er echt zoiets als het laatste experiment.. ;-)) of revisie, hebben al je suggesties het onderzoek zonder twijfel naar een hoger niveau getild.

Dan wil ik natuurlijk alle mensen van het lab van de afdeling pathologie ontzettend bedanken voor al jullie hulp en gezelligheid! De goede sfeer op het lab zorgde er voor dat mislukte experimenten snel vergeten waren (meestal dan). Ik wil hierbij graag als eerste Annemieke en Nike bedanken. Jullie waren voortdurend druk bezig om de werkzaamheden van iedereen op het lab in goede banen te leiden (en dit was vaak ook hard nodig ;-)), maar stonden altijd open voor vragen of gewoon een gezellig kopje koffie. Ook Willem en Leonie wil ik ontzettend bedanken; zonder jullie hulp zou dit boekje niet tot stand zijn gekomen. Leonie, bedankt voor je tomeloze inzet voor hoofdstuk 2 en Willem, bedankt voor je keiharde werk aan hoofdstuk 7! Daarnaast zijn jullie hele lieve en fijne collega's die me hebben ondersteund en op weg hebben geholpen toen ik als groentje op het lab binnenkwam. Hildo, je kwam tegelijk met me binnen op het lab en bent een steunpilaar geweest tijdens dit hele traject. Hoewel we best verschillend zijn en elkaar in het 'normale' leven misschien niet snel zouden zijn tegengekomen (o.a. iets met Ajax en PSV), heb ik met veel plezier met je samengewerkt. Bedankt voor je motiverende woorden (vooral tijdens borrels) en het feit dat je altijd klaar stond om anderen te helpen (ook als je zelf net 12 platen of gelen in ging pipetteren). Martin (jongûh!) bedankt voor het brengen van een stukje Brabant naar Amsterdam; ik voelde me meteen een beetje meer thuis met jou in de buurt. Naast het brengen van gezelligheid, sta je voor al je collega's klaar met je betrokkenheid en onuitputtelijke bron van kennis. Timon, jij was de eerste die me op dag één welkom heette in de AIO-kamer en me een beetje op weg hielp. Bedankt dat je altijd tijd had om mee te denken en natuurlijk bedankt voor het regelen van goede koffie (op de AIO-kamer, tijdens het kerstdiner en zelfs voor iedereen thuis!). Bedankt Guus voor het gezamenlijk klagen op de muziek op radio in het (kweek)lab (dit maakte zelfs luisteren naar Suzan & Freek een stukje draaglijker). Sander en Richard, bedankt dat ik altijd kon meegenieten van jullie geouwehoer aan de andere kant van de kartonnen 'muur' (en ook een beetje voor het feit dat jullie als oudgedienden van de afdeling pathologie een

hele hoop vragen konden beantwoorden). Linda, mijn overbuur in de AIO-kamer, altijd gezellig om met je te lunchen of koffie te drinken, of de gesprekken nou gingen over het weekend of over DLBCL cellijnen zie zich gek gedroegen. Maria, thanks for sitting back-to-back with me in the AIO-room, and always being up for a chat about PhD related troubles. Carel en Jeroen, bedankt voor jullie nuttige vragen en input tijdens de woensdagochtend werkbijeenkomsten. Saskia, bedankt voor het vergaren van DLBCL patiëntmateriaal en je steunende blikken af en toe tijdens werkbijeenkomsten met Marcel. Ook bedankt voor alle gezelligheid aan alle andere (oud)kameraden: Tijmen, Zemin, Linda S., Yuxin, Mahnoush en Donner (respect dat je de eeuwige rotzooi in onze kamer hebt kunnen doorstaan ;-)). Dit geldt natuurlijk ook voor de collega's aan de andere kant van de muur; Fangxue, Ryan en Jerry, ook jullie bedankt voor alle gesprekken en ondersteuning! Ryan, ontzettend jammer dat ik je IGF paper niet meer heb kunnen afronden, maar het was fijn om met iemand over DLBCL cellijnen te kunnen sparren. Jerry, ik heb niet heel veel met je samengewerkt, maar het was altijd gezellig met je te borrelen en ik zal je gigantische Excelsheets tijdens de werkbijeenkomsten niet snel vergeten. Fangxue, you went from newest to almost most experienced member of the Spaargaren-lab in a really short time; best of luck with your projects! Nog niet genoemd, omdat ze op het lab of elders op de afdeling zaten, maar ook Avital, Chiel, Thera, Loes, Roy, Robert, Djera, Alessandra, Anna en Jan wil ik bedanken voor de gezellige gesprekken, goede suggesties of hulp op het lab.

Natuurlijk wil ik hier ook mijn paranimfen Yvonne en Nathalie bedanken! Jullie hebben me niet alleen geholpen tijdens de laatste loodjes voor de verdediging, maar ook ontzettend gesteund door alle jaren heen. Alle gezellige lunchmomenten waren een heerlijke afleiding tijdens het werk en daarnaast kon ik met alles bij jullie terecht, zowel op werk als op persoonlijk vlak. Super mooi dat jullie me als atypische Brabander zelfs zo ver hebben gekregen om nog een keer carnaval mee te gaan vieren in Uden. Bedankt Yvonne dat je tijdens je PhD tijd nog in Utrecht woonde, zodat je me op redelijk schappelijke tijden in de trein naar huis kon begeleiden na alle borrels. Jammer dat je inmiddels weer bent vertrokken naar het zonnige Zuiden (nee hoor, alle goeds voor jullie in jullie super mooie huis in Rosmalen). Nathalie, ook bedankt voor alle gezellige momenten tijdens borrels en congressen; ik ben nog altijd jaloers op je geweldige Cell Signaling handdoek! Jammer dat je er de laatste periode niet meer bij was, maar ik ben super trots op je hoe je je hebt herpakt en je plek hebt gevonden. Jullie hebben mijn PhD tijd echt een heel stuk mooier gemaakt en ik hoop dat we elkaar nog regelmatig blijven zien.

Bedankt lieve Odulpus-maatjes; Chris, Johan, Kirstin, Loes en Tim. Wat leuk dat we na de middelbare school op zo'n regelmatige basis contact zijn blijven houden. Chris, bedankt dat je me meerdere keren door de modder hebt geholpen, letterlijk en figuurlijk. Ik hoop dat we nog veel spelletjes mogen spelen en gesprekken over het leven mogen voeren. Johan, bedankt voor alle tot in de puntjes verzorgde hapjes en drankjes, altijd een groot

plezier om bij jou langs te komen (ik zal proberen in de toekomst de telefoon vaker op te nemen ;-)). Kirstin, jij snapte als één van de weinigen hoe het was om als PhD student op een lab te werken, dus het was heerlijk om af en toe even te kunnen ventileren wat er nu weer allemaal fout was gegaan. Alle escape rooms, etentjes, spelletjesmiddagen en andere activiteiten met jullie allemaal boden hele fijne afleiding tijdens de weekenden. Wie organiseert het volgende ijskart-pubquiz-boulder-karaoke-uitje?

Ook veel dank aan de Socioloogjes; Eline, Inge, Mariska, Lisanne, Roos, Niels, Robin, Anouk en Selina. Ik hoop dat jullie na het zien/lezen van dit proefschrift eindelijk inzien dat ik toch echt geen socioloog ben ;-). Ondanks het feit dat we elkaar natuurlijk niet meer zoveel zien als in Nijmegen, vind ik alle activiteiten en weekendjes met jullie nog steeds heel fijn en gezellig. Jullie hebben me altijd gesteund in dit traject (ook al durfden jullie op een gegeven moment niet meer te vragen hoe het ging en wanneer ik ging afronden). Niels en Robin, ik kijk uit naar onze volgende Smash date (behalve als Robin weer kiest voor Jigglypuff..)! Anouk, ondanks alles wat er is gebeurd, was dit proefschrift er zonder jouw jarenlange steun niet geweest, heel veel dank daarvoor. Roos, ik heb je natuurlijk leren kennen lang voordat je socioloog werd (samen in een dramaworkshop worden ingedeeld, schept zichtbaar een diepe band). Bedankt voor je vriendschap en steun door de jaren heen; ik heb veel mooie (en een paar hele gekke ;) herinneringen aan onze momenten samen en hoop dat er nog veel bij mogen komen. Ik kijk uit naar nog meer sociologenweekendjes en natuurlijk naar de grote sociologenreis over een aantal jaar!

Bedankt lieve en leuke boulderbuddies, Charlotte, Katharina en Joanna. Bedankt voor het introduceren van een nieuwe hobby (verslaving?) in mijn leven. Ik heb heel veel zin om met jullie te blijven boulderen en andere activiteiten te ondernemen. Gaan we volgend jaar boulderen in Fontainebleau? Lieve Joanna, ik heb je tijdens een ingewikkelde periode in mijn leven ontmoet, maar ben ontzettend blij dat ik je in korte tijd zo goed heb leren kennen. Je hebt natuurlijk alleen het staartje van dit traject meegekregen (misschien maar goed ook?), maar hebt me enorm gesteund tijdens de zware laatste loodjes. Ik heb genoten van de afgelopen tijd en kijk uit naar de toekomst met jou (en Ollie natuurlijk!).

Tenslotte wil ik graag mijn familie enorm bedanken. Eerst mijn broertje; Daan, je vindt het waarschijnlijk onzin dat je hier genoemd wordt, maar ik wil je bedanken voor de gezellige afleiding in de vorm van eindeloze potjes Mario Kart (op een dag zal ik je innemen). En als laatste natuurlijk mijn ouders; Bedankt dat jullie in me zijn blijven geloven, me altijd gesteund hebben (binnen en buiten dit traject) en altijd voor me klaar staan.